THE UNIVERSITY *of* EDINBURGH

Identification of KLF1-E325K as a loss-of-function mutation in iPSC-derived macrophages

THE UNIVERSITY *of* EDINBURGH

Alisha May

Thesis submitted for the degree of Doctor of Philosophy, College of Medicine and Veterinary Medicine

2022

Declaration

I declare that all the work presented in this thesis has been generated by myself, except where clearly stated in the text. This work has not been submitted for any other degree or professional qualification.

Alisha May

2022

“Life, although it may only be an accumulation of anguish, is dear to me, and I will defend it.”

- Mary Shelley, Frankenstein.

Abstract

With over two million red blood cells produced every second, erythropoiesis is one of the bodies most demanding processes. It is therefore unsurprising that multiple hereditary and acquired red blood cell disorders arise from such a complex system. Existing treatments are effective in managing some of these conditions, but few offer long-term cures. Finding new treatments relies on the full understanding of the cellular and molecular interactions associated with the development of red blood cells, which predominantly occurs within erythroblastic islands. Patients with congenital dyserythropoietic anemia type IV (CDA), caused by mutations in the transcription factor KLF1, present with a large number of nucleated erythrocytes in their peripheral blood. Erythroblastic island macrophages play a vital role in promoting red blood cell enucleation, and therefore a contribution of erythroblastic island macrophages to the defective enucleation observed in these patients was investigated. The use of patient-derived induced pluripotent stem cells, often termed 'Disease-in-a-Dish' approaches, was an attractive option in this study due to the rarity of the disease and therefore limited availability of primary cells.

A CDA type IV patient-derived iPSC line that has a mutation in KLF1 (E325K) was obtained and used to generate erythroid cells to confirm that CDA erythroid pathology could be recapitulated *in vitro*. Key erythroid genes such as *GYPA, TFRC, SLC4A1, HBA1* and *ICAM4* were downregulated in cells generated from CDA patient iPSCs compared to control iPSCs, in agreement with previously a published study. The CDA patient iPSC line was then used to generate macrophages *in vitro*, however, I found that iPSC-derived macrophages generated from CDA patient and control iPSCs expressed very low levels of *KLF1*. Based on previous studies, I would expect KLF1 levels to be high in erythroblastic island macrophages, therefore I concluded that the CDA patient iPSC-derived macrophages were not a good model for CDA patient erythroblastic island macrophages.

Activation of wild-type KLF1 in iPSC-derived macrophages had been previously demonstrated to induce a more 'erythroblastic island macrophage-like' phenotype. Therefore, I generated a KLF1-E325K inducible activation system in iPSCs. As proof of

principle, I generated cells under erythroid differentiation conditions from two inducible KLF1-E325K iPSC lines. These cells recapitulated CDA erythroid cell pathology, with a reduction in populations of $CD235a^+$ cells and $CD71^+$ cells upon KLF1-E325K activation.

I applied the inducible KLF1-E325K activation system to generate macrophages and investigate their phenotype and function. I found that the E325K mutation prevents KLF1-induced macrophage maturation. In an *in vitro* model of the erythroblastic island, I observed reduced maturation and enucleation of erythroid cells in co-culture with KLF1-E325K macrophages compared to KLF1-WT macrophages. I hypothesised that the reduced function of KLF1-E325K macrophages to promote erythroid cell maturation and enucleation was the result of dysregulation of key erythroblastic island macrophage genes. The KLF1-E325K mutation had been identified to dysregulate several genes in erythroid cells, but whether there was any transcriptional dysregulation in CDA patient macrophages had not yet been investigated. Therefore, to investigate this hypothesis, I generated a transcriptomic dataset.

RNA sequencing of KLF1-E325K macrophages revealed that KLF1-E325K does not induce expression of the same target genes as KLF1-WT, including genes encoding secreted factors previously identified to promote erythroid cell maturation and enucleation such as *ANGPTL7*. In fact, the transcriptome of KLF1-E325K macrophages was most comparable to macrophages generated from their parental line which express almost no *KLF1*. In combination with KLF1-E325K macrophages reduced function within the EBI, these data identified KLF1-E325K as a loss-of-function mutation in iPSC-derived macrophages.

Collectively, these findings demonstrate that genetically modified iPSCs can be a valuable tool to study RBC disorders. Additionally, the inducible-activation strategy utilised here could be applied to model and investigate a contribution of EBI macrophages to other RBC disorders, with the goal of finding new druggable targets.

Lay Summary

Red blood cell disorders are a group of conditions that affect red blood cells, the cells that deliver oxygen to all parts of the body. These disorders can be very common, for example iron deficiency anemia, or very rare. Rare red blood cell disorders often have far fewer effective treatment options. One such rare disorder is called congenital dyserythropoietic anemia type IV, in which patients have a defect in red blood cell development due to a specific mutation. I wanted to study this disease with the goal of identifying new targets for treatment. Due to the rarity of this disease, obtaining sufficient numbers of cells from patients to study was difficult. Instead, I used induced pluripotent stem cells that were made from a few patient cells to generate different cell types that have the disease-causing mutation. I made two cell types from these stem cells, red blood cells and macrophages.

Red blood cell development is supported by a specific kind of cell called an erythroblastic island macrophage. I found that macrophages made from the patient-derived stem cells did not express sufficient levels of the disease-causing mutation. Therefore, I genetically modified stem cells to switch on the disease-causing mutation in macrophages. I found that these macrophages were unable to mature as much as their healthy counterparts, and also had a reduced ability to support red blood cell development.

Sequencing technology revealed that the disease-causing mutation in macrophages was able to regulate the expression of far fewer genes than the healthy counterpart. This included genes that encode for proteins that are secreted by macrophages and support red blood cell development. This study showed that genetically modified stem cells can be used to model rare blood cell disorders, and also revealed possible targets for future treatment of patients with congenital dyserythropoietic anemia type IV.

Acknowledgements

To my Tissue Repair girls, Emma, Leslie and Niamh. If the only thing I achieve with the rest of my life is getting to watch you all live yours, I will know that I lived a richer life than most. Sharing this PhD journey with you all has been a joy and an honour.

I would like to thank my supervisor, Professor Lesley Forrester. Thank you for all of your support on this project. You have always made the time to discuss data and ideas and provided invaluable feedback on this thesis.

To Misty Peterson, my first supervisor. Now that I am finishing up a PhD myself, I appreciate more than ever the time and the effort that you took to supervise me. I have used what you taught me every day.

To Antonella, it has been an honour to learn from you. You are one of the smartest people I have ever met, and also one of the kindest, which is incredibly rare. To Telma, I am so glad that we got to do our PhDs together. There is absolutely no one better I could have shared this experience with. We struggled but we made it! To Helen Taylor, thank you for everything you taught me about cell culture. I never took for granted your willingness to listen to me about anything and everything.

To Donia, Switzerland used to have a single Wagamamas, I believe it has since closed down. We will have to find a new place.

To Valerie, your friendship has been a true highlight of the past couple of years.

To my favourite flat boyfriends, Craig, Stephen and Tom. Thank you for loving and supporting some of my favourite people in the world. I am endlessly grateful that they did not bring someone terrible into our lives.

To Jonas, on the eve of something that ought to last. I have been looking for you for a very long time. I am glad we finally met.

For my brother, Alexander. We grew up together, and now we are grown. I love you.

Table of Contents

List of Figures

List of Abbreviations

AGM Aorta-gonad mesonephros
ANGPTL7 Angiopoietin-related protein 7
BasoE Basophilic erythroblast
BEL-A Bristol erythroid cell line adult
BFU-E Burst-forming unit erythroid
BMP4 Bone morphogenetic protein
BSA Bovine serum albumin
CA Calcium
CDA Congenital dyserythropoietic anemia
CFU-E Colony-forming unit erythroid
CMP Common myeloid progenitor
DTR Diphtheria toxin receptor
EB embryoid body
EBI Erythroblastic island
EKLF1 Erythroid krüppel-like factor 1
EMP Erythromyeloid progenitor
EMP/MAEA Erythrocyte macrophage protein/macrophage erythroid attacher
EpCAM Epithelial cell adhesion molecule
EPO Erythropoietin
EryP Primitive erythroid cells
EryP-CFC Erythroid colony-forming progenitors
ESC Embryonic stem cells
FGF Fibroblast growth factor
FMO Fluorescence minus one
Gas6 Growth arrest specific 6
GM-CSF Granulocyte-macrophage colony stimulating factor
GMP Good manufacturing practise
GDF15 Growth-differentiation factor 15
Hb Hemoglobin
HBA Hemoglobin A, adult hemoglobin
HBA1 Hemoglobin subunit alpha 1
HBF Hemoglobin F, fetal hemoglobin
HC hydrocortisone
HCFC Haematopoietic cell forming complex
HIF Hypoxia-inducible transcription factor
HPSC Human pluripotent stem cell
HSC Haematopoietic stem cell
HSPCs Haematopoietic stem and progenitor cell
ICAM-4 Intercellular adhesion molecule-4
iCDA4 Inducible congenital dyserythropoietic anemia type 4
IGFBP IGF-binding protein
IL-3 Interleukin 3
IL-33 Interleukin 33
IL-6 Interleukin 6
IL-11 Interleukin 11

IOP Intraocular pressure
iPSC Induced pluripotent stem cell
iPSC-DM Induced pluripotent stem cell derived macrophage
KLF1 Krüppel-like factor 1
Lab Laboratory
M-CSF Macrophage-colony stimulation factor
MDM Monocyte-derived macrophage
MDS Multidimensional scaling
MEP Megakaryocyte-erythroid progenitor
MFI Mean fluorescence intensity
Mg Magnesium
Nan Neonatal anemia mouse
NC Negative control
OrthoE Orthochromatic erythroblast
PB peripheral blood
PBMC Peripheral blood mononuclear cell
PBS Phosphate buffered saline
PC Positive control
PCA Principal component analysis
PCR Polymerase chain reaction
PMA Phorbol-12-myristate-13-acetate
PNH Paroxysmal nocturnal hemoglobinuria
PolyE Polychromatophilic erythroblast
PPP1R12C Protein phosphate 1 regulatory subunit 12C
ProE Proerythroblast
PSC Pluripotent stem cell
qRT-PCR Real-Time Quantitative Reverse Transcription PCR
RBC Red blood cell
Retic Reticulocyte
RIN RNA integrity number
RNA-seq RNA sequencing
RPM Red pulp macrophage
SCF Stem cell factor
SEP Stress erythroid progenitor
SEM Standard error mean
SERPINB2 Serpin family B member 2
SIRPα Signal regulatory protein alpha
TF Transferrin
TGF-α Transforming growth factor alpha
TPO Thrombopoietin
UCB Umbilical Cord Blood
VCAM-1 Vascular cell adhesion molecule
VEGF Vascular endothelial growth factor

Chapter 1: Introduction

1.1 Haematopoiesis

The earliest observation of blood cells can be attributed to Frenchman Pierre Borel, physician to King Louis XIV, who described a type of 'worm' observed in human blood in 1656 (1). In 1657, Jesuit priest and German scientist Athanasius Kircher made a similar observation when examining blood from plague victims (1). In the following year, 1658, Dutch Biologist Jan Swammerdam described 'red blood corpuscles', the first recorded observation of red blood cells (RBCs) (1). Swammerdam's acquaintance Antoni van Leeuwenhoek later rendered the first illustrations of RBCs from several species (Figure 1.1) (2). In the hundreds of years that followed these observations, an extensive and detailed knowledge about the structure, development and function of blood cells has been gained.

Haematopoiesis is the process of blood cell generation and arises in three overlapping waves during embryonic development. Haematopoiesis is most well studied in the mouse (Figure 1.2). The first two waves of haematopoiesis are haematopoietic stem cell (HSC)-independent, and the third wave is HSC-dependent. The first wave of haematopoiesis is characterised by the emergence of primitive erythroid cells as cell aggregates, termed blood islands, in the yolk sac of human, mice and avian embryos (3, 4, 5). In mice, the first wave begins at E7 and also generates some primitive/embryonic macrophages and megakaryocytes (6). The second wave of haematopoiesis is characterised by the emergence of erythro-myeloid progenitors (EMPs) from haemogenic endothelium in the yolk sac (7). EMPs give rise to definitive erythroid and myeloid cells (8, 9, 10). In the third wave of haematopoiesis HSCs emerge from haemogenic endothelium in the aorta-gonad mesonephros (AGM) region of the dorsal aorta during the endothelial to hematopoietic transition (11, 12, 13). This hemogenic endothelium is distinct from the hemogenic endothelium that gives rise to EMPs (14). These HSCs migrate initially to the fetal liver, and subsequently to the adult bone marrow where they can differentiate into all cell types constituting the blood system (15, 16).

Figure 1.1 Erythrocytes in fish blood. Drawn by Antoni van Leeuwenhoek. Adapted from Davis et al (2).

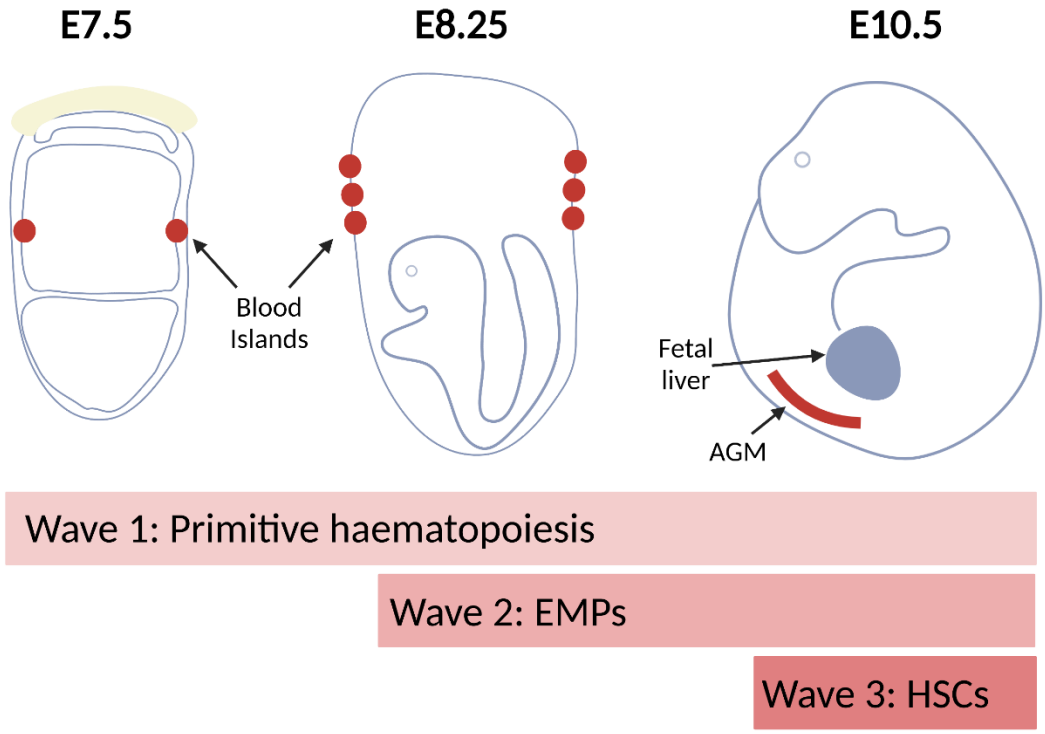

Figure 1.2 The three waves of haematopoiesis illustrated in mice. During the first wave, primate erythroid progenitors, macrophages and megakaryocytes emerge in the yolk sac. In the second wave erythromyeloid progenitors (EMPs) arise from hemogenic endothelium in the blood islands region of the yolk sac. In the third wave, haematopoietic stem cells (HSCs) arise from hemogenic endothelium in the AGM region of the embryo before colonising the fetal liver. Figure created with biorender.com.

1.2 Erythropoiesis

RBCs, the most abundant cell type in humans, are generated through a process called erythropoiesis. The main function of RBCs is the delivery of oxygen loaded onto hemoglobin in the lungs and offloaded into tissues, and the clearance of carbon dioxide from tissues to the lungs for exhalation (17). In human adult RBCs, hemoglobin A (HbA, adult hemoglobin) accounts for approximately 97% of the protein molecules, and hemoglobin F (HbF, fetal hemoglobin) accounts for 1% (18). In addition to platelets and the lens fiber cells of the eye, RBCs are enucleated cells in humans, with the final stage of RBC development being the ejection of the nucleus (enucleation). RBCs need to be robust and flexible enough during their 120 day lifespan to allow them to deform and travel through capillaries which are only a few micrometres in diameter (17). This deformability is conferred by RBC membrane proteins. The RBC membrane consists of proteins such as spectrin, actin, protein 4.1R and ankyrin, which provide the RBC with the ability to deform (17).

Erythropoiesis in mammals can be divided into primitive and definitive erythropoiesis (19). Primitive erythropoiesis generates the primitive RBCs of the embryo, and definitive erythropoiesis generates the definitive RBCs of the embryo and the adult (19).

1.2.1 Primitive erythropoiesis

Primitive erythropoiesis takes place in the yolk sac and is responsible for the production of the first blood cells in the mammalian embryo (Figure 1.3) (19). In mice, shortly after the onset of gastrulation at E7, mesoderm cells give rise to hemangioblasts, which then differentiate into erythroid colony-forming progenitors (EryP-CFC) (7, 19). EryP-CFCs differentiate through the erythroid precursors proerythroblast, basophilic erythroblast, polychromatic erythroblast, and orthochromatic erythroblast, to give rise to a wave of primitive erythroid cells (EryP) (20). After several days in circulation EryPs enucleate (21). This enucleation generates a transient population of pyrenocytes, which consist of the extruded nucleus surrounded by a thin layer of cytoplasm and a lipid bilayer (22). EryPs were noted to bind to fetal liver macrophages, forming erythroblastic islands (EBIs), which engulf

the extruded nuclei (23). Enucleated EryPs have been observed in the circulation of mice for several days post birth (21, 24).

Primitive erythropoiesis has been most extensively studied in the mouse. Due to ethical concerns and the inaccessibility of the early embryo, relatively little is known about human primitive erythropoiesis. Ethical concerns surrounding human embryo research are often rooted in the belief that life begins at fertilisation, and that the destruction of these embryos once they have been used for research is preventing their normal development and birth (25). Human embryo research is restricted to 14 days in several countries, at which timeframe it is unlikely that women will both know that they are pregnant and be able to donate embryos for research. Therefore, most embryos for research are sourced from assisted reproductive technologies such as *in vitro* fertilisation (25). Embryos donated for research should be high quality, and because embryos generated from assisted reproductive technologies are either implanted or preserved for future transplantation, access to these embryos is limited. In humans, blood islands and their primitive erythroid cells first arise between days 18-20 of gestation and are the only circulating erythroid cells for the first 3 to 6 weeks of gestation (19). Nucleated primitive erythroid cells have been identified in the circulation of human embryos throughout the first trimester (19). As in the mouse system, human primitive erythroblasts enucleate (26).

1.2.2 Definitive erythropoiesis

Definitive erythroid cells are generated during the second and third waves of haematopoiesis (Figure 1.3). The second wave of haematopoiesis generates the first definitive erythroid cells in the mouse embryo from EMPs. In mice, EMPs arise at E8.25 and colonise the fetal liver by E10.5 (7). Definitive erythroid cells are distinct from their primitive erythroid counterparts and can be characterised by their smaller size, expression of adult globin genes and their maturation in circulation (27, 28, 29).

The third wave of haematopoiesis generates HSC-derived definitive erythroid cells. HSC-dependent erythropoiesis occurs initially in the fetal liver, before migrating to the bone marrow which is the main site for erythropoiesis throughout adult life. Definitive erythropoiesis occurs in three distinct stages. In the first stage, HSCs sequentially differentiate to common myeloid progenitors (CMP), megakaryocyte-

erythroid progenitors (MEP), burst-forming unit erythroid (BFU-E) progenitors, and colony-forming unit erythroid (CFU-E) progenitor (30, 31, 32, 33). BFU-Es and CFU-Es are traditionally defined by their ability to form colonies of maturing erythroid cells in *in vitro* colony assays (32, 33, 34, 35). BFU-Es have low numbers of EPO receptors, but as they mature into CFU-Es they become dependent on EPO for their ability to generate erythroid colonies and their survival, and this is concurrent with an increase in EPO receptors (section 1.2.4.1) (36, 37). While useful in the staging of erythroblasts, it is important to note that phenotypic characterisations of cells, such as morphology, and functional observations of cells, such as colony formation assays, may overlap.

In the second stage, CFU-E progenitors differentiate through the erythroid precursors proerythroblast, basophilic erythroblast, polychromatic erythroblast, and orthochromatic erythroblast (38, 39). As the differentiating erythroblasts progress through this second stage of development, chromatin is condensed, and the cell undergoes extensive cytoskeletal remodelling in preparation for the expulsion of the nucleus (40, 41). This second stage of erythropoiesis occurs within a specialised microenvironment called the erythroblastic island (EBI), which will be described in subsequent sections.

During the third stage of definitive erythropoiesis, also termed terminal differentiation, the nucleus is expelled from the orthochromatic erythroblast as a pyrenocyte (42). The resulting reticulocyte expels any remaining organelles and enters circulation (40). Considerable membrane remodelling then takes place to generate the fully mature, biconcave erythrocyte (41, 43, 44).

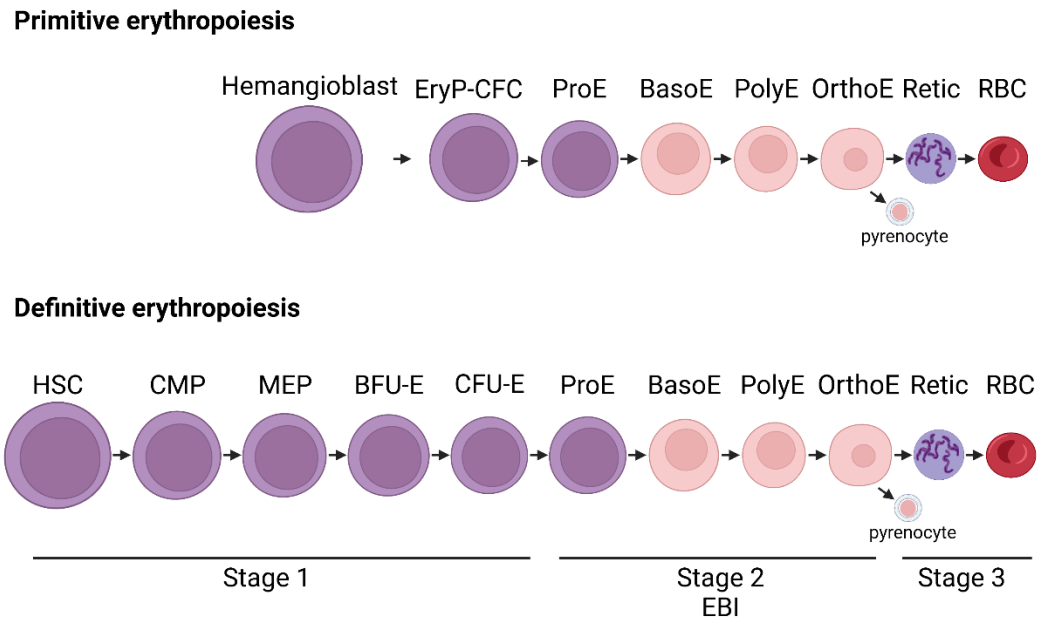

Figure 1.3 Primitive and definitive erythropoiesis. During both primitive and definitive erythropoiesis, erythroid progenitors give rise to erythroid precursors: proerythroblasts (ProE), basophilic erythroblasts (BasoE), polychromatophilic erythroblasts (PolyE), orthochromatic erythroblasts (OrthoE). OrthoEs enucleate to form a pyrenocyte and a reticulocyte (Retic) that gives rise to RBCs. The second stage of definitive erythropoiesis takes place within erythroblastic islands (EBI). Figure created with biorender.com.

1.2.3 Stress erythropoiesis

Steady-state erythropoiesis can be defined as the production of new RBCs at a consistent rate in the bone marrow to replace old and damaged RBCs (45). In contrast to steady-state erythropoiesis is stress erythropoiesis, a process in which RBC production increases up to 10-fold in response to anemia and hypoxia (46). During stress erythropoiesis, extramedullary sites such as the liver and spleen become sites of erythroid development in addition to the bone marrow (45, 47). This leads to expansion of the erythroid progenitor pool in the form of stress erythroid progenitors (SEPs) (47). As with steady-state erythropoiesis, stress erythropoiesis is largely regulated by EPO, and during severe hypoxia, EPO production can be increased up to 1,000-fold (47, 48).

As well as regulating expression of the transcription factors GATA1 and KLF1, which regulate erythropoiesis, the BMP4/Smad5 pathway has a significant role in stress

erythropoiesis (49, 50, 51). The demand for RBCs in stress erythropoiesis is similar to the demand for RBCs in a rapidly growing embryo (49). Indeed, BMP4/Smad5 dependent stress erythropoiesis was identified to be required for the expansion of erythroid progenitors in the fetal liver during embryonic development (49).

1.2.4 Regulation of erythropoiesis

Erythropoiesis is regulated at multiple levels both intrinsically via transcription factors and microRNAs, and extrinsically via erythropoietin and cytokines (52). The most well studied regulators of erythropoiesis are described in this section.

1.2.4.1 Cytokines

Erythropoietin (EPO) is a 34 kDa glycoprotein hormone primarily, but not exclusively, produced by the kidneys which account for approximately 80% of EPO production in adults (53, 54). During fetal development, EPO is produced mainly in the fetal liver (55). Erythropoietin is one of the main drivers of erythropoiesis and prevents erythroid progenitor cell and primitive erythroblast apoptosis (55, 56, 57). EPO and EPOR null mice die at E13.5 with a lack of definitive erythrocytes (57). Erythropoietin is secreted by cells of the kidney in response to hypoxia through the activity of the hypoxia-inducible transcription factor (HIF) (55). Decreased oxygen delivery to the kidneys causes an increase in EPO expression and secretion, which stimulates the survival, proliferation, and differentiation of CFU-E erythroid progenitors (48, 52).

Mutations in HIF pathway proteins have been identified to cause erythrocytosis, the excessive production of RBCs, in humans. For example, patients with polycythemia vera, a disease characterised by this excessive production of RBCs, carry a gain-of-function mutation in *Jak2* (*Jak2*^{V617F}) which causes hypersensitivity of erythroid progenitors to EPO (58, 59, 60).

The earliest erythroid progenitors are responsive to cytokines including thrombopoietin (TPO), granulocyte-macrophage colony stimulating factor (GM-CSF), interleukin 3 (IL-3), interleukin 11 (IL-11), and stem cell factor (SCF) (61). SCF is present in both soluble and membrane-bound form, with membrane-bound SCF demonstrated to have a role in erythropoiesis in addition to its soluble form by experiments utilising the *Steel-Dickie* mutant mouse (62, 63). *Steel-Dickie* mice carry

a deletion of exon 6 from the *Scf* gene which results in the production of soluble SCF and no membrane bound SCF, which causes impaired erythropoiesis and anemia in these mice (62). IL-3 and GM-CSF enhance BFU-E growth, with no effect on CFU-E growth (64). Insulin-like growth factor I enhances CFU-E growth (in the absence of insulin) (64). BFU-E cells also respond to glucocorticoids, and interleukin 6 (IL-6) (52).

1.2.4.2 Transcription factor KLF1 (EKLF)

Several transcription factors have been identified with a role in erythropoiesis, including EKLF1/KLF1, GATA1 and BCL11a, with KLF1 being the most studied transcriptional regulator of erythropoiesis (52, 61). Erythroid Krüppel-like factor (EKLF1) was first identified in 1992 and named as such due to its observed erythroid restricted expression and its likeness to the fruit fly pattern-determining protein Krüppel (65). *EKLF1* was isolated by enriching for genes expressed in a mouse erythroleukemia cell line but not expressed in a mouse monocyte-macrophage cell line and was predicted to encode a 38 kDA protein with three zinc fingers (65). EKLF1 protein was identified to bind to the motif 5'-CCACACCCT-3', an essential element of the beta-globin promotor, and its expression was initially found to be limited to erythroid and mast cell lines (65). Subsequently, seventeen Krüppel-like factors have been identified and its nomenclature was changed to KLF1 to reflect the order of discovery within this gene family (66). Since its identification, KLF1 has be found to be highly expressed in MEPs and its expression has been shown to inhibit the formation of megakaryocytes while stimulating erythroid differentiation (67). KLF1 has also been shown to be expressed in the supportive macrophages of the EBI niche (68).

During early mammalian development, *KLF1* expression is regulated by the BMP4 pathway, particularly via Smad5 (50, 51, 69). *KLF1* expression is initiated prior to erythroid commitment during hematopoiesis, and is likely first activated in a progenitor population that has erythroid-megakaryocytic potential (51). In murine development, *Klf1* mRNA is first expressed at the neural plate stage E7.5 within primitive erythroid cells, followed by the fetal liver at E9 where it remains highly expressed and the sole source of *Klf1* mRNA at E14.5 (70). KLF1 protein is expressed

in primitive erythroid cells and the fetal liver (71). KLF1 detection in the embryo coincides with the emergence of primitive erythroid progenitors (7).

Following its discovery, several studies demonstrated that KLF1 is essential for erythropoiesis and beta-globin expression (72, 73). KLF1$^{-/-}$ mice are normal during the yolk sac stage of erythropoiesis, suggesting that KLF1 is not required for yolk sac primitive erythropoiesis (72, 73). Conversely, nucleated erythroid cells generated in the fetal liver of KLF1$^{-/-}$ mice lack the proper amount of hemoglobin, resulting in anemia and lethality at embryonic day 14-15, implicating KLF1 in definitive erythropoiesis (72, 73). This embryonic lethality was initially attributed to beta-globin deficiency, however the phenotype was not rescued upon correction of the globin chain imbalance (74). It was speculated that deficiency of KLF1 target genes is a contributor to this embryonic lethality, implicating KLF1 in the regulation of other key erythroid genes. This has since been confirmed by transcriptome analyses of KLF1 null erythroid cells (75, 76). KLF1-dependent genes have been identified with roles in hemoglobin synthesis, membrane stability, and cell cycle regulation (75, 77, 78, 79). Comparison of KLF1-null erythroid cells with control, wild type cells has also identified downregulation of several genes involved in the terminal stage of erythroid differentiation in the absence of KLF1 (75, 80, 81, 82, 83, 84).

While KLF1$^{-/-}$ mice appear normal during the yolk sac stage of erythropoiesis, several studies have identified a role for KLF1 in EryPs by regulating embryonic globin gene expression, cytoskeleton, and maintaining membrane stability (75, 79, 80, 85).

In humans, the first reported loss-of-function mutations in KLF1 were identified as the basis of the rare blood group In(Lu) (inhibitor of Lutheran antigen expression) phenotype (86). Gene expression profiling identified over 650 putative KLF1 target genes, including the blood group antigens CD44 and BCAM which are suppressed in In(Lu) individuals (86). Haploinsufficiency for KLF1, in addition to several KLF1 mutations have been identified to cause hereditary persistence of fetal hemoglobin in adults (87, 88). KLF1 was also identified as a key regulator of the *Bcl11a* gene, which encodes a suppressor of fetal hemoglobin expression (87). KLF1 regulates *Bcl11a* in mice and humans, and is therefore a regulator of globin switching in erythroid cells (89).

1.3 Red blood cell disorders

RBC disorders represent a broad spectrum of conditions with mild to fatal clinical outcomes (90, 91, 92, 93, 94). Disorders range from inherited disorders such as sickle cell anemia and thalassemia, to acquired disorders such as paroxysmal nocturnal hemoglobinuria (PNH) and polycythemia vera (90, 91, 92, 93). Outcomes of these disorders can be mild, for example iron-deficiency anemia, or severe, such as poor growth and skeletal abnormalities which occur in a subgroup of beta-thalassemia (94, 95). Anemia represents the most prevalent group of RBC disorders, crudely defined as a condition in patients who lack adequate numbers of healthy RBCs and diagnosed by a low blood hemoglobin (Hb) concentration (96). Anemias affect approximately 1.62 billion people worldwide, which accounts for 8.8% of the total worldwide disease burden (97, 98).

The most common treatments for RBC disorders include blood transfusions, iron supplements for iron-deficiency anemia, and iron chelation therapy to counteract iron accumulation in patients requiring repeated transfusions (95, 99). In severe cases of beta-thalassemia, transfusions can be required as often as every two weeks (95). Several erythropoiesis stimulating drugs, such as erythropoietin (EPO), have been approved as treatments and are routinely used to treat anemias associated with chronic kidney disease and cancer (100, 101, 102).

There are fewer effective treatment options for rarer RBC disorders, and these are often prohibitively expensive. For example, PNH is a rare disorder characterised by hemolysis, the rupture and destruction of RBCs (91).Eculizumab is a monoclonal antibody against terminal complement protein C5 that is used to reduce hemolysis and stabilise hemoglobin levels in PNH patients (103). Eculizumab is widely reported as one of the world's most expensive drugs at a cost of around $400,000 per year of treatment, but only 20% of patients reach normal hemoglobin values and 40% remain anemic (103, 104). Some rare RBC disorders, including PNH and acquired aplastic anemia, can be effectively cured by bone marrow transplantation (105, 106). However, due to the requirement for preconditioning which ablates the hematopoiesis of the host, bone marrow transplants are associated with significant morbidity and mortality rates (106, 107).

1.3.1 Congenital dyserythropoietic anemias

Congenital dyserythropoietic anemias (CDAs) are a group of inherited RBC disorders that are characterised by ineffective erythropoiesis and classified into four types: CDA types I, II and III, and transcription-factor-related CDAs (108). CDAs are classified based on distinct morphological, clinical and genetic features (108).

1.3.1.1 Congenital dyserythropoietic anemias type I, II and III

Approximately 90% of CDA type I cases are caused by bi-allelic mutations in either *CDAN1* or *CD15orf41*, and to date over 50 causative mutations have been documented (109, 110, 111). CDA type II is caused by bi-allelic mutations in *SEC23B* (112). CDA type III is a dominant disorder caused by the P916R mutation in kinesin family member, *KIF23* (113). Morphologically, CDA type I is characterised by the presence of internuclear chromatin bridges between the nuclei of erythroblasts, type II by the presence of binucleate erythroblasts, and type III by the presence of large multinucleate erythroblasts (108).

1.3.1.2 Congenital dyserythropoietic anemia type IV

Congenital dyserythropoietic anemia type IV (CDA type IV) is in the transcription factor-related subgroup of CDAs (114, 115). The identification of a single-point mutation in KLF1 associated with dyserythropoietic anemia was the first association of this transcription factor with human disease (114, 116). A male patient presented at birth with anemia, deficiency of the erythroid proteins CD44 and Aquaporin 1, high HbF levels, and a large number of nucleated RBCs in peripheral blood (116). Ultrastructural abnormalities were identified in these nucleated cells, particularly abnormal cytoplasmic inclusions and enlarged nuclear pores (116). A female patient studied extensively in the 1990's also presented at birth with severe anemia, high HbF levels, and deficiency of the erythroid proteins CD44 and Aquaporin 1 (117, 118, 119). Examination of the coding sequence of *KLF1* in both patients and comparison with unaffected relatives identified a point mutation in one allele, c.973G>A (114, 116).

CDA type IV is an autosomal dominant disease (116). The c.973G>A mutation results in the substitution of the glutamate 325 reside with a lysine residue (E325K) in the second zinc finger of KLF1 (116). Glutamate 325 is predicted to contact DNA and is

located on a helix directed toward the DNA backbone, according to a modelling structure of KLF1-DNA binding (116, 120). The substitution of glutamate for lysine found in patients reverses the side-chain charge from negative to positive and extends the side-chain towards the negatively charged DNA backbone. This charge-reversal enhances the interaction between KLF1 and DNA and has the potential to create a novel hydrogen bond, and so the E325K variant of KLF1 was predicted to stabilise the binding of KLF1 to DNA (116).

To date, nine patients worldwide have been reported with CDA type IV, with six of these carrying the E325K mutation in KLF1 (114, 116, 117, 118, 121, 122, 123, 124, 125, 126). One other patient carries a novel KLF1 mutation (p.Ser323Leu, S323L), and genotypes are not available for the remaining two patients (122, 123, 127). CDA type IV patients have been reported to present with a range of symptoms including the persistence of nucleated RBCs in peripheral blood, abnormalities in bone marrow erythroblasts, elevated fetal hemoglobin, and iron overload (Figure 1.4) (116, 121). Iron overload is reported as the most frequent complication of CDAs and has been most well studied in CDAII patients, in which increased levels of the hormone erythroferrone lead to impairment of iron regulation by reducing expression of hepcidin, a master regulatory of iron homeostasis (108). The cause of iron overload in CDA type IV patients is less clear, but could also result from alterations in erythroferrone and hepcidin expression, in addition to dysregulation of genes involved in iron metabolism, and repeat blood transfusions.

The most comparable mouse model for CDA type IV is the neonatal anemia mouse (nan). This spontaneous mouse mutant carries a mutation in KLF1, KLF1-E339D, which is at the corresponding position in the second zinc finger domain of KLF1 to KLF1-E325K in humans (128). However, this results in a substitution of glutamate 339 for aspartic acid, and the phenotype of nan mutant mouse erythroid cells is very different to CDA type IV patient erythroid cells (116, 129). Nan mouse erythroid cells exhibit present spherocytosis, where RBCs have a spherical shape and are more fragile, but normal enucleation (129).

The molecular mechanisms of the KLF1-E325K mutation in erythroid cells have been well studied (130, 131). These studies demonstrated that the KLF1-E325K mutation

induces cell cycle arrest in erythroid cells, in addition to dysregulation of key erythroid genes involved in iron-utilisation, membrane protein expression and cell-cycle regulation (130, 131).

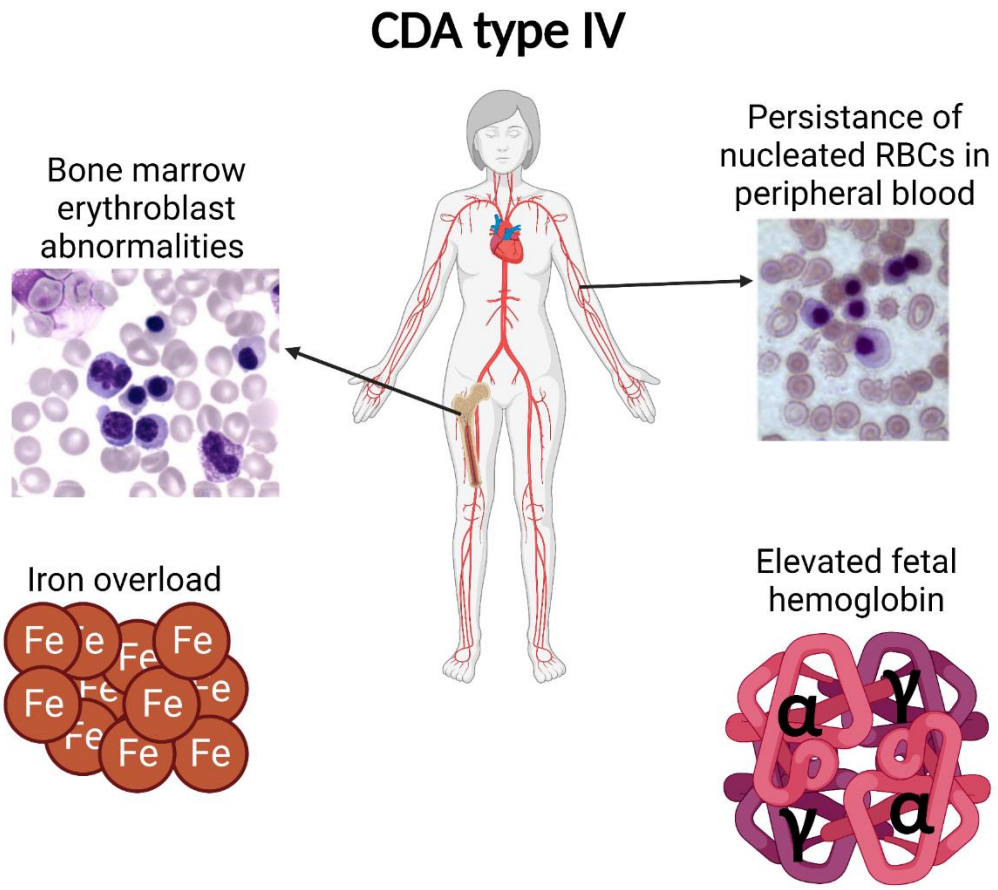

Figure 1.4 Symptoms of congenital dyserythropoietic anemia type IV. Patients with CDA type IV have been reported with bone marrow erythroblast abnormalities such as multinucleated erythroblasts, persistence of nucleated RBCs in peripheral blood, iron overload and elevated fetal hemoglobin. Bone marrow and peripheral blood smears adapted from Arnaud et al (116). Figure created with biorender.com.

1.4 Therapeutic potential of *in vitro* generated RBCs

Blood transfusions are an essential and life-saving procedure during surgeries, cancer treatment, chronic illnesses and traumatic injuries (132). Patients can receive RBCs, platelets or plasma (132). In 2019 in the United States alone, over 10 million RBC units were transfused, which equates to approximately 29,000 units of RBCs per day (133). Compared to the 5,000 units of platelets and 6,500 units of plasma transfused daily, RBCs are the most widely transfused blood component (132).

While the majority of blood transfusions are safe and effective, there are several limitations that could be addressed by the transfusion of laboratory (lab)-grown cells (134, 135). Currently, all blood transfusions come from volunteer donors and are therefore susceptible to supply issues. Estimates indicate that only 3% of age-eligible people donate blood yearly (132). In October 2022, NHS Blood and Transplant UK issued an amber alert as blood stocks fell below a two-day supply, meaning that hospitals would be asked to put management plans in place to protect blood stocks (136).

Acute haemolytic transfusion reactions occur in cases of transfusion with ABO incompatible RBCs, mostly against rare RhD, RhC or RhE antigens, and the interaction of recipients antibodies with donor RBC antigens results in the immediate destruction of transfused RBCs (134). These reactions result in kidney damage and account for a significant proportion of all transfusion-related deaths (137). If RBCs were to be generated from recipient-derived cell, this would eliminate the risk of immune incompatibility. Although extensive blood-screening technologies for known pathogens are in place, blood transfusions still carry a risk of transmission of blood-borne infections. Recent estimates place the risk of catching human immunodeficiency virus from a blood transfusion at 1 in 2 million, hepatitis B at 1 in 300,000, hepatitis C at 1 in 1.5 million, and West Nile Virus at 1 in 350,000 (132).

The transfusion of *in vitro* derived RBCs presents an especially attractive treatment option for patients in which finding a well-matched donor is difficult, for example patients with rare blood types and diseases such as sickle cell disease and beta-thalassemia who require regular transfusions (95, 138). An estimated 300,000 babies

are born with sickle cell anemia each year and require repeated blood transfusions throughout their lives (138).

In 2011, RBCs generated from peripheral blood $CD34^+$ haematopoietic stem and progenitor cells (HSPCs) were successfully injected into one human recipient and persisted in circulation for several weeks, establishing proof of principle for the transfusion of *in vitro* generated RBCs (139). In November of 2022, researchers from The University of Cambridge in collaboration with NHS Blood and Transplant UK began the first clinical trial of the transfusion of lab-generated RBCs into another person (140). RBCs were generated from $CD34^+$ HSPCs, and approximately 24 litres of nutrient media were required to generate one to two tablespoons of RBCs. Whilst this is an exciting progression in the field, progress still needs to be made to generate a more cost-effective method to generate RBCs with a higher yield.

Extensive work has been undertaken to generate RBCs from $CD34^+$ haematopoietic stem and progenitor cells (HSPCs), pluripotent stem cells (PSCs), and immortalised erythroid cell lines.

1.4.1 $CD34^+$ HSPC-derived RBCs

HSPCs express the cell surface marker CD34 and can be isolated from both peripheral blood (PB) and umbilical cord blood (UCB) using flow cytometry or magnetic sorting (141, 142, 143, 144, 145, 146). The Duoay group was the first to produce human RBCs *in vitro* from isolated $CD34^+$ cells (141). $CD34^+$ UCB-derived HSPCs were cultured with SCF, IL-3, and EPO before co-culture with murine stromal cells (MS5). RBC enucleation rates were observed at over 90%, and interestingly elimination of the contact between erythroid cells and stromal cells using a transwell reduced enucleation to approximately 2% (141). Erythroid cells generated using this protocol expressed adult hemoglobin, fetal hemoglobin, and were able to bind and release oxygen (141). The main limitation to the scaling-up and clinical application of this protocol is the complexity associated with the co-culture. In an attempt to overcome this limitation, RBCs were generated in the same cytokine cocktail but without co-culture and with the addition of vascular endothelial growth factor (VEGF) and insulin-like growth factor II (142). As observed by the Duoay lab, there were very low RBC enucleation rates (142). Human RBCs were also differentiated from $CD34^+$ UCB-derived HSPCs co-

cultured with human CD34$^+$ UCB derived macrophages where 99.4% of erythroblasts enucleated (143). Protocols for generating UCB CD34$^+$ HSPC-derived RBCs in the absence of supporting cells with higher enucleation rates have since been developed (144, 145). Several studies have shown that these *in vitro* generated RBCs survive and continue to mature and enucleate when transplanted into mice *in vivo* (144, 147).

Traditionally, RBC yields from PB-derived CD34$^+$ cells are lower than those from UCB and have a lower expansion potential (146). Following work generating CD34$^+$ UCB-derived RBCs, a protocol for efficient expansion and differentiation of PB-derived CD34$^+$ cells to RBCs without co-culture was described (146). Cells were cultured with transferrin, insulin, and hydrocortisone in addition to SCF, IL-3, and EPO, and this achieved an enucleation rate of 45% (146). Subsequently, RBCs generated from PB-derived CD34$^+$ cells under good manufacturing practise conditions (GMP) were successfully injected into one human recipient and persisted in circulation for several weeks (139).

The main limitations to generating RBCs from CD34$^+$ HSPCs is that, like blood transfusion, these cells are donor dependent. They are also a rare cell population with reports that they constitute approximately 1.33% of human UCB cells (148). CD34$^+$ cells can be mobilised to peripheral blood, but even then the mean percentage of CD34$^+$ cells in the leukocyte fraction obtained has been reported at 0.2-0.5% (149).

1.4.2 Immortalised erythroid cell lines

RBCs have also been generated from immortalised human erythroid cell lines (150, 151). Immortalised cell lines have been established from erythroid progenitor cells differentiated from iPSCs, ESCs or CD34$^+$ UCB-derived HSPCs (152, 153, 154). Unlike RBCs generated *in vivo* from definitive erythropoiesis, RBCs generated from these immortalised cell lines express fetal and embryonic globin and have terminal differentiation deficiencies (152, 153, 154). To address these limitations, an immortalised erythroid cell line (Bristol Erythroid Line Adult; BEL-A) was established from adult human erythroid cells (150). BEL-A cells were demonstrated to be able to generate erythroid cells that enucleate to generate mature reticulocytes and have similar survival rates to adult donor RBCs *in vivo* (150).

The use of immortalised erythroid cell lines to generate RBCs have several advantages. Unlike RBCs obtained from traditional donation, these lines are able to generate RBCs that are donor-independent once the lines have been established from the initial donor cells. They are also inexpensive to grow and easy to acquire. However, enucleation rates in immortalised erythroid cell lines are still not high enough for transfusion into patients.

1.4.3 PSC-derived RBCs

Human PSCs, including embryonic stem cells (ESCs) and induced pluripotent stem cells (iPSCs), are self-renewing cells that can be differentiated to the three embryonic lineages: ectoderm, mesoderm and endoderm (155). Several studies demonstrated that RBCs can be generated from human ESCs, however these are subject to both ethical and legislative challenges (156, 157, 158, 159).

In 2006 and 2007, two ground-breaking studies from Takahashi and Yamanaka reported that iPSCs could be generated from both mouse and human fibroblasts by transiently expressing four transcription factors: OCT4, SOX2, C-MYC, and KLF4 (160, 161). Since then, a wide range of cell types have been generated from iPSCs, including cells of the neural lineage, hepatocytes, and of course, RBCs (162, 163). RBCs can be generated from iPSCs irrespective of donor cell type of origin and are subject to fewer of the ethical and legislative challenges that ESC-derived cells are (164, 165, 166, 167).

One of the biggest advantages to generating RBCs from iPSCs is that iPSCs can be subjected to a vast array of techniques for genetic manipulation, including zinc finger nucleases, TALENS, lentiviral vectors, and CRISPR-Cas9 (168, 169, 170, 171, 172, 173). iPSC technology has even been used to generate disease-corrected patient-specific blood cells. Fibroblasts taken from patients with Fanconi anemia, the most commonly inherited bone marrow failure syndrome, were corrected with lentiviral vectors and iPSCs were generated (174). It was observed that uncorrected fibroblasts could be reprogrammed to iPSCs but could not be maintained past the third passage in culture, therefore correction of patient cells was a pre-requisite for iPSC generation (174). These corrected iPSCs were demonstrated to generate phenotypically normal $CD34^+$ haematopoietic progenitors capable of differentiation into cells of myeloid and

erythroid lineages (174). The therapeutic potential of such corrected patient-specific cells is vast.

Protocols for the generation of RBCs from human PSCs can be divided into feeder cell-dependent or feeder cell-independent. The most commonly used feeder cells in feeder cell-dependent protocols are the OP9 murine bone marrow cell line, however human mesenchymal cell lines and human primary stromal cells from fetal liver have also been used with the aim of preventing xenogenic contamination (175, 176). Enucleation rates using these protocols is low, with between 2-10% enucleation observed, and the RBCs express predominantly fetal and embryonic globins (176). Feeder-free protocols include the production of 3-dimensional structures known as embryoid bodies (EB) and erythroid cells produced in this way have been reported to express high levels of embryonic and fetal globins, with low enucleation rates (177). More recently, feeder-free protocols with an EB step have been reported to generate erythroid cells with up to 60% enucleation rates (165).

Serum- and feeder-free protocols for the generation of RBCs from PSCs were subsequently developed to be GMP compliant (159, 178). These protocols are complex and expensive, requiring careful modulation of an extensive array of cytokines including BMP4, VEGF, SCF, and IL3 (159, 178). Using these protocols, a single PSC can produce up to 200,000 erythroid cells in 31 days, but these erythroid cells express predominantly fetal globins and, as observed in feeder cell-dependent and feeder-free protocols, less than 10% of cells enucleate (159).

One of the main limitations to the generation of RBCs from iPSC cells is their low enucleation rates, typically only 2-10% of erythroid cells generated from iPSCs enucleate (159, 176). Additionally, embryonic globins are expressed at high levels, with almost no expression of adult globins (159, 172, 176, 177). Comparison of the dynamics of the gene expression program between iPSC-, PB $CD34^+$ HSPC-, and UCB $CD34^+$ HSPC -derived erythroid progenitors indicated that iPSC-derived erythroid cells may be more primitive and suggested several mechanisms to explain the low enucleation of these cells (179). For example, TRIM58, a protein that facilitates erythroblast enucleation, was identified to be downregulated in iPSC-derived erythroid cells (179).

Proteomic comparisons performed on erythroid cells derived from three iPSC lines and PB $CD34^+$ HSPC-derived erythroid cells quantified 1989 proteins (180). Of the 1989 proteins quantified, less 3% of these differed in expression levels (2-fold or more) between erythroid cells generated from the three iPSC lines (180). When compared to PB $CD34^+$ HSPC-derived erythroid cells, 11% of the proteins quantified differed in levels of expression (180). Cytoskeletal proteins were identified in the pool of differentially expressed proteins and this was suggested to, in part, explain the low enucleation rates of iPSC-derived erythroid cells (180).

1.5 The Erythroblastic island

The proerythroblast to orthochromatic stages of definitive erythropoiesis in mammals occur within erythroblastic islands (EBIs) (Figure 1.3). First visualised by Marcel Bessis in 1958, EBIs are specialised microcompartments consisting of a central macrophage surrounded by erythroblasts at varying stages of differentiation (181, 182). EBIs have been identified in all sites of mammalian definitive erythropoiesis, including the fetal liver, bone marrow, and spleen in rodents and humans (183, 184).

EBIs are predominantly situated in the bone marrow during steady-state erythropoiesis but can expand into the liver and spleen during stress erythropoiesis (47, 181, 185, 186). EBIs are not spatially restricted within the bone marrow, and their composition is altered depending on their proximity to sinusoids. EBIs adjacent to sinusoids are enriched for orthochromatophilic erythroblasts, while nonadjacent EBIs are enriched in proerythroblasts (187). This suggests either a mechanism in which the entire island migrates closer to sinusoids or a mechanism in which erythroblasts detach and re-attach to EBIs situated closer to sinusoids as their differentiation progresses.

The composition of EBIs varies across mammalian species, with rat EBIs consistently containing around 10 erythroblasts per island, compared to human EBIs which are variable with between 5-30 erythroblasts surround the central macrophage (188, 189). To date, EBIs have not been identified in non-mammalian vertebrate species (birds, reptiles, amphibians, and fish) and it has been hypothesised that this is due to the fact that the erythrocytes of these species do not enucleate (190). An interesting

exception to this is the enucleated erythrocytes identified in some salamander and one teleost fish species (191, 192). In salamanders, enucleation is speculated to have evolved as a response to problems associated with the circulation of large RBCs through small capillaries, which is a theory shared for the emergence of enucleated RBCs in mammals (193).

Compared with extensive studies into the HSC bone marrow niche microenvironment, the EBI niche has been the focus of a relatively small number of research groups (194, 195, 196). Most of these studies into the EBI have been performed in mice. While there are a vast array of cell types implicated in the HSC niche, the EBI niche appears to be comparatively simple consisting primarily of the central macrophage and developing erythroblasts (16). A recent study suggested a role for the EBI in granulopoiesis in parallel with erythropoiesis (197). Within the HSC bone marrow niche, macrophages function to maintain HSC retention and self-renewal and their depletion mobilises HSCs to the blood stream (198). In contrast, central macrophages in the EBI promote the differentiation of erythroblasts into mature and enucleated RBCs that enter the blood stream.

1.5.1 Erythroblastic island macrophages

Erythroblastic island macrophages were first hypothesised to supply ferritin to the developing erythroblasts for hemoglobin synthesis, and since then several additional functions of the central macrophage have been elucidated (199). EBI macrophages support erythroblast differentiation by several mechanisms including cell-cell contact, secretion of supportive factors, phagocytosis of extruded nuclei, and providing a source of iron (Figure 1.5) (199, 200, 201, 202, 203, 204).

Cell surface markers associated with EBI macrophages in mice and rats include vascular cell adhesion molecule 1 (Vcam-1), F4/80, EPOR, CD163, and CD169 (205, 206, 207, 208). To date, human EBI macrophages have been found to express the following cell surface markers: FcRI, FcRII, FcRIII, CD4, CD13, CD14, CD16, CD18, CD31, CD32, CD11a, CD11c, EPOR, and and HLA-DR (183, 188, 209). Intact EBIs isolated from different haematopoietic tissues in mice and rats and analysed for known EBI macrophage cell surface markers showed them to be a heterogenous macrophage population (205, 210). For example, in mouse bone marrow Vcam1 and CD169 are

broadly expressed by EBI macrophages, while only a proportion of EBI macrophages express CD163 (210). No markers have yet been identified to be exclusive to EBI macrophages.

1.5.1.1 Cell-Cell contact

The association of erythroblasts with macrophages promotes erythroid cell proliferation, maturation, and enucleation, with cultured erythroblasts proliferating 3-fold more when in contact with macrophages (211, 212). The proteins that facilitate these attachments are critical for EBI integrity and are highly expressed in proerythroblasts, with expression progressively lost by the orthochromatic erythroblast stage (39). The most studied macrophage-erythroblast attachment proteins are described below, however the precise role of most macrophage-erythroblast attachments is not completely understood.

1.5.1.1.1 Erythroblast α4β1 integrin binds macrophage VCAM1

One of the first erythroblast-macrophage attachment proteins identified was α4β1 integrin. Expressed by erythroblasts, α4β1 integrin binds to VCAM-1 expressed by macrophages (207). Blocking of either receptor using monoclonal antibodies was demonstrated to significantly impair EBI formation *in vitro* (207).

1.5.1.1.2 Erythrocyte macrophage protein

Erythrocyte macrophage protein, also known as macrophage erythroid attacher (MAEA), is a 36kDa transmembrane protein expressed by both macrophages and erythroblasts that is important for enucleation (211, 213). Erythrocyte macrophage protein will be referred to as EMP/MAEA to prevent confusion with erythromyeloid progenitors (EMPs). EMP/MAEA null embryos die shortly after birth and present with an increased number of nucleated, immature erythrocytes in their peripheral blood (214, 215). Very few EBIs were observed in the fetal liver of EMP/MAEA null mice (214). EMP/MAEA expressed by macrophages, but not by erythroblasts has been demonstrated to maintain adult EBIs (216). EMP/MAEA was deleted in macrophages using $Maea^{Csf1r\text{-}Cre}$ and $Maea^{CD169\text{-}Cre}$ mice and deleted in erythroid cells using $Maea^{Epor\text{-}Cre}$ mice (216). EMP/MAEA deletion in macrophages significantly reduced bone marrow macrophages, erythroblasts and *in vivo* EBI formation, while deletion in erythroid cells had no phenotype (216). The authors suggested that this points to

the presence of a currently unidentified macrophage EMP/MAEA receptor on erythroid cells (216).

EMP/MAEA has also been implicated in the phagocytosis of extruded nuclei by EBI macrophages. As the nucleus is expelled, EMP/MAEA expressed on erythroblasts partitions predominantly to the plasma membrane surrounding the extruded nucleus (pyrenocyte) rather than the reticulocyte (217). This would allow binding of the pyrenocyte to the EBI macrophage, facilitating its uptake (183, 217).

1.5.1.1.3 Erythroblast ICAM-4 binds macrophage αv integrins

In vitro antibody inhibition studies identified that intercellular adhesion molecule-4 (ICAM-4), a member of the intercellular adhesion molecule family expressed in erythroid cells, binds to α4 β1integrin and αv integrins (218). The subsequent observation that EBIs are defective in *Icam-4* null mice and the demonstration that it interacts with αv integrins on macrophages confirmed its involvement in maintaining EBI integrity (219). A significant decrease in EBI formation was observed in *Icam-4* null mice compared to WT mice both *in vivo* and *in vitro* through reconstitution studies (219). The transcription factor KLF1 directly activates *Icam4* in erythroid cells, and ICAM4 levels mirror KLF1 during both primitive and definitive erythropoiesis (68, 220).

1.5.1.1.4 Other attachment proteins

Several other macrophage proteins have been implicated with a role in erythroblast attachment, however these are much less studied. Rat CD163 is a receptor for hemoglobin-haptoglobin complexes, contributing to the clearance of free hemoglobin. CD163 was identified as an erythroblast adhesion receptor, and in rats was demonstrated to stimulate erythroid expansion, with no significant effects on erythroid maturation (221). CD169, also known as Siglec1, is extensively expressed by EBI macrophages and has been shown to localise to sites of macrophage-erythroblast contact in EBIs (222).

Palladin, an actin cytoskeleton-associated protein, has also been implicated with a role in macrophage-erythroblast attachment (223, 224). *Palladin*$^{-/-}$ mouse embryos were observed to have a significant defect in definitive erythropoiesis, with a

reduction in fetal liver erythroid cells accompanied by increased apoptosis and partial stalling of erythroid differentiation (224). There was no observed defect in primitive erythropoiesis, which suggested a defect in the erythropoietic microenvironment, the EBI. As expected, *Palladin*$^{-/-}$ fetal liver cells failed to form EBIs *in vitro*. WT macrophages could form EBIs with either WT or PALLADIN-null erythroblasts, whereas PALLADIN-null macrophages were unable to bind WT or PALLADIN-null erythroblasts, supporting the idea that PALLADIN is a critical component of the microenvironment where erythroid cells mature (224).

1.5.1.2 Secreted factors

In addition to attachment protein interactions, EBI macrophages support erythroid cell proliferation and maturation through contact-independent mechanisms. Co-cultures of human peripheral blood mononuclear cell (PBMC) derived macrophages and erythroblasts increased the proliferation of erythroid cells when compared to erythroblasts cultured alone. When contact between these MDMs and erythroblasts was prevented in trans-well culture experiments, the increase in erythroid cell proliferation was reduced by about 75% (209). In a study conducted by the Forrester lab, co-culture of iPSC-derived macrophages and CD34^{+} umbilical cord blood (UCB) derived erythroblasts increased the production of mature, enucleated erythroid cells when compared to erythroblasts cultured alone (201). This increase in mature enucleated erythroid cells was partially retained when contact between macrophages and erythroblasts was prevented in trans-well experiments (201). Together, these studies demonstrate that both cell-cell contact and mechanisms that are not contact-dependent are involved in erythroid development within the EBI (201, 209).

It has been reported that macrophages secrete factors that are able to act as positive regulators of erythropoiesis (211, 225). For example, macrophages secrete insulin-like growth factor 1 stimulates erythroid proliferation and cell survival (64, 226). EPO is one of the key regulators of erythropoiesis, driving erythroid proliferation and differentiation and preventing apoptosis (55, 56, 57). Subsets of both mouse and human EBI macrophages express EPOR (210). Over 90% of mouse EBI macrophages analysed were EPOR^{+}, while approximately 27% of CD163^{+} human fetal liver

macrophages (which enriches for EBI macrophages) were $EPOR^+$ (210). Pre-treatment of macrophages with EPO significantly increased the number of erythroblasts attached to macrophages in an *in vitro* model of the EBI, providing evidence for the hypothesis that EPO plays a role in EBI formation by acting on EPO-responsive macrophages (210). EPO mRNA expression has been identified in EBI macrophages, and co-culture of erythroblasts with macrophages has been shown to prevent erythroblast apoptosis, however it remains unclear whether EPO is one of the factors secreted by EBI macrophages (213, 227).

There is also some evidence that EBI macrophages secrete factors that act as negative regulators of erythropoiesis (225). Bone marrow macrophages secrete soluble receptor binding cancer antigen expressed in Siso cells which activates proapoptotic capases-8 and -3 in immature erythrocytes (228).

Erythroblasts themselves also secrete factors that act as positive and negative regulators of erythropoiesis, including growth arrest specific 6 (Gas6), vascular endothelial growth factor A, and placenta growth factor (229, 230). Binding of Gas6 to its erythroblast receptor decreases macrophage secretion of the inhibitory factors IL-10, IL-13, IL-1α, IL-1β, IL-6, and TNF-α within the EBI (229). Erythroblasts have no receptors for vascular endothelial growth factor A or placenta growth factor, while macrophages do, suggesting that these factors may be mediators of cross-talk between erythroblasts and macrophages within the EBI (225, 230).

1.5.1.3 Phagocytosis of extruded nuclei

EBI macrophages have been demonstrated to be highly phagocytic, phagocytosing the extruded nuclei of erythroblasts within the EBI (201, 231, 232). This phagocytic ability is selective, phagocytosing only the extruded nuclei and not the remaining reticulocyte. The mechanism for this selectivity has not been fully elucidated but could be due in part to the partitioning of erythroblast membrane proteins such as EMP/MAEA to the pyrenocyte and not the reticulocyte (217). Enucleation is one of the final steps of erythropoiesis, in which the nucleus is expelled from an erythroblast as a pyrenocyte (42). Pyrenocytes are engulfed by macrophages via a MerTK-protein S-dependent mechanism in which protein S binds to phosphatidylserine on pyrenocytes and MerTK on macrophages (233, 234). Once ingested, DnaseII breaks

down the nuclei. This is supported by observations *in vivo* showing that the fetal liver macrophages of mice lacking DnaseII become enlarged with several ingested but not digested nuclei (235). Interferon-β mRNA was detected in EBI macrophages with a build-up of undigested nuclei, resulting in a severe defect in erythropoiesis and embryonic lethal anemia. (236).

1.5.1.4 Iron source

Observations of ferritin molecules in the human EBI, which are incorporated into erythroblasts, led to speculation that EBI macrophages act as a source of iron (199, 202). Macrophages were later demonstrated to support erythroid cell growth in the absence of transferrin in culture, and this was shown to be via ferritin synthesised and secreted by macrophages (204, 237). In macrophage-erythroblast co-culture studies, macrophages were identified to synthesise and secrete ferritin via endocytosis, which is subsequently taken up by erythroblasts. Iron is then released from ferritin by acidification and proteolysis and used for heme synthesis (204). However, the transfer of iron from EBI macrophages to erythroblasts has not yet been conclusively proven *in vivo.*

1.5.1.5 EBI macrophages in stress and disease

One hallmark of stress erythropoiesis in the mouse is the generation of stress erythroid progenitors (SEPs), and the extension of RBC production from the bone marrow to extramedullary sites such as the liver and the spleen (47, 49, 238, 239). During healthy erythropoiesis a population of tissue-resident macrophages in the spleen, red pulp macrophages (RPM), function to phagocytose senescent erythrocytes and recycle their iron and degrade heme (240). In times of erythropoietic stress following bone marrow transplantation and myeloablation, RPMs have been observed to form EBIs (241). The role of EBI macrophages during stress erythropoiesis has been demonstrated by macrophage depletion studies (209, 242). Using a CL2MDP-liposome strategy splenic RPMs were depleted, and this resulted in a 5-day delay in splenic erythropoiesis and suppression of erythropoiesis at the CFU-E level (242). $F4/80^{+}$ macrophages emerged from day 6 and this coincided with a recovery of erythropoietic activity (242). Macrophages were also depleted using a CD169-DTR mouse strain in which the human diphtheria toxin receptor (DTR)

is expressed under the control of the endogenous *Siglec-1 (CD169)* promotor (243). Bone marrow CD169^{+} macrophage depletion significantly impaired erythropoietic recovery in murine models of hemolytic anemia, acute blood loss and myeloablation, causing a significant delay in hematocrit and reticulocytosis recovery (209). A further study showed that during recovery from anemia, monocytes are recruited to the spleen where they differentiate into RPMs and associate with SEPs to form EBIs (244). These data suggest a model in which RPMs, both resident and monocyte-derived, form EBIs with SEPs to promote their expansion and differentiation, thus contributing to erythropoietic recovery during stress erythropoiesis (209, 242, 244).

As well as their contribution to stress erythropoiesis, macrophages have been implicated in the pathological progression of two RBC disorders, polycythemia vera and beta-thalassemia (209, 245). In a murine model of polycythemia vera, a disease in which a point mutation in *Jak2* (*Jak2*^{V617F}) causes excessive production of erythroid cells, blood hematocrit was normalised following depletion of CD169^{+} macrophages (59, 60, 209). Using the *Jak2*$^{V617F/+}$ murine model of polycythemia vera, clodronate-mediated macrophage depletion also normalised RBC numbers (58, 245). Clodronate-mediated macrophage depletion also improved the phenotype of a mouse model of beta-thalassemia, increasing hemoglobin and RBC numbers (245, 246). It is important to note that while these models deplete CD169^{+} EBI macrophages, they do not exclusively deplete EBI macrophages. It is unclear what contribution, if any, the depletion of other subsets of macrophages has on erythropoiesis.

1.5.1.6 KLF1 in erythroblastic island macrophages

Aside from the well-defined intrinsic role of KLF1 in erythroid cells, KLF1 has been identified to have an extrinsic role on erythropoiesis within the macrophage compartment of the EBI (68). KLF1 was identified in EBI macrophages isolated from E13.5 fetal livers, and these KLF1^{+} macrophages expressed more *DNase2* and *Vcam1* compared to KLF1^{-} macrophages (68). Approximately 30% of KLF1^{+} macrophages were shown to express VCAM1 on their surface, and this in combination with studies showing VCAM1 levels are decreased in total liver cell RNA from KLF1-null embryos suggests that KLF1 regulates VCAM1 (68, 84). *DNaseII*, which is required for

degradation of ingested nuclei in macrophages, is also a KLF1 target (200). KLF1 expressed in EBI macrophages was shown to bind and activate the promotor of *DnaseII* (200). $EPOR^{+}$ macrophages, which have been annotated as EBI macrophages, were also identified to express KLF1 (210).

There is some evidence indicating that KLF1 expression in EBI macrophages could also have a role in stress erythropoiesis. The BMP4/Smad5 pathway both regulates KLF1 expression and stress erythropoiesis (49, 50, 51). Macrophage depletion has been shown to lead to a reduction in BMP4 activity, and it has been considered that compromised KLF1 levels could be contributing to the low erythroid numbers observed after stress induction (68, 209).

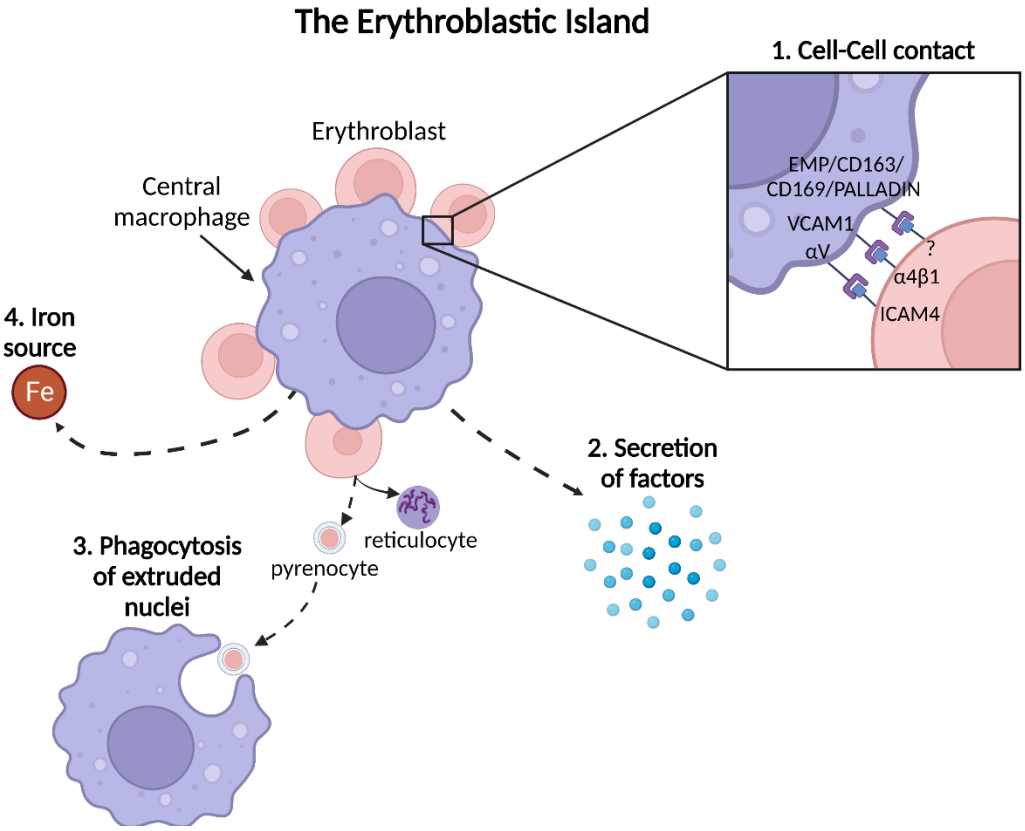

Figure 1.5 EBI macrophages support erythropoiesis via several mechanisms. **1:** Cell-cell contact. Cultured erythroblasts proliferate 3-fold more when in contact with macrophages. EMP, CD163, CD169, PALLADIN, VCAM-1, αv, α4β1, and ICAM4 have been identified as membrane proteins involved in the attachment of erythroblasts and macrophages. **2:** EBI macrophages secrete factors that promote erythroid cell maturation and enucleation. **3:** EBI macrophages phagocytose the extruded nuclei of erythroblasts. **4:** EBI macrophages have been shown to act as a source of iron for erythroblasts *in vitro*.

1.5.2 *In vitro* modelling of the erythroblastic Island

The vast majority of studies into the EBI have been performed in mice, using techniques such as the isolation of intact EBIs, reconstitution of islands *in vitro*, *in vivo* macrophage depletion studies, and gene targeting studies to model and study the EBI (212, 214, 216, 219, 224, 235, 245).

The isolation of intact EBIs from rodent bone marrow were the first models utilised in the study of EBIs, allowing for morphological analyses via microscopy and characterisation of cells by antibody staining (181, 208, 247). Studies employing reconstituted EBIs were used to observe that macrophage contact with erythroblasts supports their proliferation and differentiation, and later to identify proteins involved

in this macrophage-erythroblast attachment, including erythroblast α4β1 integrin and macrophage VCAM-1 (207, 211, 212). The reconstitution of EBIs *in vitro* through the co-culture of erythroblasts and macrophages was first proposed in 1979 and is now a method widely employed (22, 212, 219, 224, 248).

Gene targeting studies have been used to interrogate genes speculated to have an important role in EBIs and strengthen observations made in previous *in vitro* studies. Antibody inhibition studies *in vitro* identified that ICAM-4 binds to α4 β1integrin and αv integrins (218). The subsequent isolation of intact EBIs from ICAM-4 null mice confirmed that its interaction with αv integrins on macrophages is involved in maintaining EBI integrity (219). Additionally, both targeted gene inactivation using a gene trapping approach and macrophage-specific condition gene deletion confirmed the *in vivo* function of EMP/MAEA as critical for island integrity, which had been previously implicated as an important mediator of erythroblast-macrophage attachment and enucleation (211, 213, 214, 216).

Stress erythropoiesis has been shown to be particularly sensitive to modifications in the EBI niche, and gene targeting studies in the mouse have been used to assess the role of specific genes in this process (47). Growth-differentiation factor 15 (Gdf15), is an essential regulator of stress, but not steady-state, erythropoiesis in both mice and humans (249, 250). *Gdf15*$^{-/-}$ mice exhibited a reduced expansion of the splenic stress erythropoiesis niche from monocyte recruitment, resulting in an impaired proliferation of SEPs (250). Macrophage depletion studies have been used to identify a role for EBI macrophage in the pathological progression of two RBC disorders, beta-thalassemia and polycythemia vera (209, 245).

Mouse models have contributed significantly to our understanding of the murine EBI niche (184). However, it unclear whether these models precisely mimic the human EBI niche. Models of the human EBI niche are required to enable a full understanding of the processes involved in erythropoiesis within the human EBI. Due to their inaccessibility in the bone marrow, human EBIs are difficult to obtain and as a result rarely studied (188). Therefore, the majority of studies into the human EBI niche have relied upon *in vitro* modelling. To model the human EBI, EBIs have been generated *in vitro* from CD34^{+} HSPCs, PBMCs, and iPSCs (201, 204, 231, 251). These models could

also be applied to modelling the EBI niche in RBC disorders, enabling the identification of new therapeutic targets.

1.5.2.1 CD34$^+$ HSPC-derived EBIs

Human EBIs can be generated *in vitro* from CD34$^+$ HSPCs that differentiate into both macrophages and erythroid cells and form EBIs. Gene expression and proteomic studies on *in vitro* CD34$^+$ cell derived EBIs generated in an Mpl-based Cell Growth Switch system identified expression of common EBI proteins such as EMP, ICAM-4, CD163, and DNASE2 (251, 252). These EBIs were able to support the maturation of erythroid cells, with 78% of the erythroblasts in contact with macrophages reaching the pre-reticulocyte stage (251).

One major advantage to CD34$^+$ HSPC-derived EBIs is that the macrophages and erythroid cells develop in concert with each other. While the ontogeny of EBI macrophages remains unknown, studies have demonstrated that during stress erythropoiesis macrophages and erythroid cells mature in concert with each other within the EBI (244). Therefore, this system may most accurately reflect the developmental ontogeny of EBIs. This is also a limitation however, especially in the context of disease EBI modelling for which the culture of healthy and diseased cells of the EBI niche together could allow for dissection of their individual contributions to disease pathology.

1.5.2.2 PBMC-derived EBIs

Human EBIs can also be generated in *vitro* from PBMCs that differentiate into both macrophages and erythroid cells (204). These cells can be independently generated using specific differentiation conditions, then subsequently co-cultured to form EBIs. In one study, this strategy was used to demonstrate that macrophages can function as a ferritin source for erythroblasts (204). The addition of glucocorticoids to monocytes isolated from PBMCs induced their differentiation to a more 'EBI macrophage' like phenotype and function, in which EBIs are formed and erythroid cells enucleate within these EBIs (231).

1.5.2.3 iPSC-derived EBIs

Human EBIs have been generated *in vitro* through the co-culture of iPSC-derived macrophages (iPSC-DMs) and $CD34^+$ HSPCs (201). There are several advantages to the use of iPSC-DMs over other human macrophage sources to model the EBI *in vitro*. One of the main advantages is that they are genetically manipulatable. In a study from the Forrester lab, a 4OH-tamoxifen-ER^{T2} expression system was used in which the transcription factor KLF1 was expressed under the control of a constitutive CAG promoter and translocates to the nucleus upon 4OH-tamoxifen addition. 4-hydroxytamoxifen (4OH-tamoxifen) is generated in the liver *in vivo* and is one of the active metabolites of tamoxifen. Therefore, *in vitro* experiments use this active compound, 4OH-tamoxifen, directly. Nuclear translocation, and therefore activation, of KLF1 in iPSC-DMs led to the generation of macrophages with an 'EBI macrophage' like phenotype and function. KLF1-activated iPSC-DMs were highly phagocytic, expressed EBI macrophage markers, and were better able to promote erythroblast maturation and enucleation compared to WT control macrophages (201). The use of this *in vitro* EBI model enabled the identification of three KLF1-regulated secreted factors, interleukin-33 (IL-33), serpin family B member 2 (SERPINB2), and angiopoietin-related protein 7 (ANGPTL7), that were demonstrated to be important for promoting erythropoiesis (201).

Unlike EBIs generated from $CD34^+$ HSPCs and PBMCs, iPSC-DMs are not reliant upon repeated donations. Of course, a fully iPSC-derived EBI would reduce this reliance on donations even further. However, replacing $CD34^+$ HSPCs with iPSC-derived erythroid cells has its own challenges. iPSC-derived RBCs have very low enucleation rates, and enucleation is one of the defining stages of erythropoiesis within the EBI (159, 176, 183)

1.6 Macrophages

Macrophages, first identified by the Russian zoologist Élie Metchnikoff, are often described as the most plastic cells of the haematopoietic system. In adult mammals, macrophages can be found in the majority of tissues, where have they a diverse range of functions and are able to alter their phenotype rapidly upon environmental cues (253, 254, 255, 256). Macrophages are often named based on the tissue in which they

reside, for example 'Kupffer cells' in the liver, 'Microglia' in the brain, and 'Erythroblastic Island Macrophages' in the bone marrow (183, 257, 258, 259). Metchnikoff suggested that macrophages have a role in the maintenance of tissue integrity and homeostasis, for which he was awarded a Nobel Prize, and for which we now have a wealth of studies (253).

1.6.1 Developmental origin

It was initially assumed that all macrophages are derived from HSCs during the third wave of haematopoiesis. However, observations that bone marrow transplantation leads to inefficient replacement of tissue-resident macrophages coupled with observations of macrophages in embryos before the emergence of HSCs prompted further investigation into the developmental origins of macrophages (6, 260, 261). The identification of the transcription factor Myb as indispensable for the development of HSCs, $CD11b^{high}$ monocytes and macrophages, but dispensable for yolk sac macrophages allowed for the identification of tissue-resident macrophages as an HSC-independent population (6). Several studies have identified macrophages that arise with EryPs during the first wave of haematopoiesis, some of which persist as tissue-resident macrophages (262, 263). Tissue-resident macrophages also derive from EMPs generated during the second wave of haematopoiesis (264). The generation of a *Cx3cr1*-GFP mouse reporter line, which marks yolk sac derived macrophages in mice and humans, allowed for *in vivo* observations of macrophage colonisation of embryonic tissues, predominantly via intravascular trafficking (262). Depending on the tissue, these yolk sac derived tissue-resident macrophages either persist or are gradually replaced by circulating HSC-derived monocytes (263, 264, 265, 266, 267, 268).

While the exact developmental origins of EBI macrophages have not yet been elucidated, it is thought that they arise from yolk sac-derived EMPs, thus sharing ontogeny with tissue-resident macrophages (6, 269). This EMP population arises in the E8.25 yolk sac before seeding the fetal liver by E11.5. Observations that single cells derived from EBs can give rise to EBIs has also been speculated as evidence for EMP-derived EBI macrophages and EBIs (68). Of course, what differentiates EBI macrophages from other tissue-resident macrophage populations is their situation in

the bone marrow, which is also the site of HSC-dependent haematopoiesis. Whether the EBIs observed in the fetal liver associated with EryPs migrate and colonise the bone marrow remains to be seen (23). It is possible that similar to tissue-resident macrophages in serous cavities and the intestine, EBI macrophages are initially yolk sac derived and are replaced by HSC-derived macrophages either neonatally or progressively with age (265, 266). Equally, any yolk sac-derived contribution to EBI macrophages could be replaced by HSC-derived macrophages during the late embryonic and neonatal stages, as observed in the salivary gland (268).

HSC-dependent macrophages emerge during the third wave of haematopoiesis and are replaced continually from a macrophage and dendritic cell progenitor (270, 271). HSC-derived macrophages are transcription factor Myb and Run1xc dependent (261).

1.6.2 Heterogeneity of function

Historically, macrophages have been classified as immune cells whose main function is immune surveillance. As described in section 1.5.1, macrophages play a vital role in the development of RBCs within EBIs during steady-state and stress erythropoiesis, and these EBI macrophages have been implicated in the pathological progression of two RBC disorders. Macrophages are now known to have a vast array of functions during development, homeostasis, disease and tissue repair, in addition to the immune system (253). The varied roles of macrophages have been the subject of extensive reviews, in this section only the role of macrophages within the immune system and disease are discussed.

1.6.2.1 Macrophages within the immune system

The main function of inflammation is to restore tissue homeostasis through the removal of damaged tissue or infectious agents (272, 273). Inflammation, in response to tissue damage or infection, utilises both HSC-dependent and HSC-independent tissue-resident macrophages (273). Stressed, damaged or dying cells produce damage-associated molecular patterns that interact with pattern recognition receptors and activate the innate immune system (274, 275). Tissue-resident macrophages express a large range of pattern recognition receptors, therefore contributing to the activation of the innate immune system in response to tissue damage (276). One of the most important processes during activation of the innate

immune system is the recruitment of monocytes to the site of inflammation (273). HSC-dependent macrophages differentiate from these monocytes. These monocyte-derived macrophages promote the resolution of inflammation in various ways, including the secretion of anti-inflammatory cytokines and the phagocytosis of pathogens (277).

1.6.2.2 Macrophages in disease

In addition to the role of macrophages in the pathological progression of beta-thalassemia and polycythemia vera discussed in section 1.5.1.5, macrophages have been implicated with a role in several other diseases such as cancer and rheumatoid arthritis (209, 245, 268, 278, 279, 280).

At the point of tumour initiation, macrophages generate an inflammatory environment (278). During tumour progression, macrophages promote malignant progression by stimulating angiogenesis, enhancing tumour cell migration and invasion, and suppressing anti-tumour immunity (278). The majority of these tumour associated macrophages arise from HSC-dependent monocytes (278, 281). Aside from their role in cancer initiation and tumour progression, macrophages have been identified to have a role in tissue repair after cancer treatment. Radiation therapy is a common treatment for cancers, including head and neck cancer where it carries the side effect of damaging salivary glands and drastically reducing saliva production (282). Using a *Mafb*$^{Cre/+}$*:Cx3cr1*$^{LSL\text{-}DTR/+}$ mouse strain in which macrophages can be depleted through the addition of diphtheria toxin, a study demonstrated that submandibular salivary gland tissue-resident macrophages are essential for supporting tissue repair following irradiation injury (268).

There is often an interplay in disease in which MDMs contribute to disease progression, while a tissue-resident macrophage population proceeds to aid in the resolution of disease and restoration of tissue homeostasis. Rheumatoid arthritis is a good example of these opposing macrophage roles. Rheumatoid arthritis is an autoimmune and inflammatory disease characterised by disordered adaptive immune responses against host cells and cytokine dysregulation that causes the synovium of a joint to become inflamed (283). During active rheumatoid arthritis there is an influx of monocytes into synovial tissue, which then differentiate into pro-

inflammatory macrophages and secrete TNF(279). In contrast, two synovial tissue-resident macrophage subsets have been identified to promote the restoration and maintenance of synovial homeostasis (280).

1.6.3 *In vitro* macrophage models

Therapeutic modulation and targeting of macrophage subpopulations have been proposed as a potential treatment for diseases including rheumatoid arthritis, beta-thalassemia, and polycythemia vera, and also as a method of promoting tissue repair following radiotherapy (209, 245, 268, 280). Indeed, therapies targeting tumour-associated macrophages have already been clinically validated (284). Tumour cells commonly overexpress CD47, often called the 'don't eat me' signal, which binds to signal-regulatory protein alpha (SIRPα) on macrophages and prevents their phagocytosis (284). Targeting the 'don't eat me' signalling pathway by blocking this CD47-SIRPα interaction between tumour cells and macrophages has been demonstrated to enhance phagocytosis of tumour cells leading to impaired tumour growth, inhibition of metastasis and tumour regression (284, 285).

Understanding the molecular mechanisms associated with macrophage function in disease is therefore crucial to the identification of novel therapeutic targets and strategies. The elucidation of these molecular mechanisms relies upon *in vivo* and *in vitro* modelling of human macrophage subpopulations in disease. *In vivo* studies of macrophages, traditionally in mice, have employed the use of techniques such as macrophage depletion, *in vivo* tracing, and the generation of genetic deletion strains (209, 245, 262). As with the techniques used to model the mouse EBI niche, these tools to study macrophages *in vivo* cannot be applied to the human system. Additionally, the study of macrophages within the human embryo are limited due to ethical and legislative challenges, with a 14-day limit imposed on human embryo research (286). Therefore, *in vitro*-derived macrophage models prove especially useful for the study of human macrophages. Macrophages can be derived for study *in vitro* from peripheral blood monocytes, immortalised monocytic cell lines, and PSCs.

1.6.3.1 Monocyte-derived macrophages

Human macrophage studies have relied heavily on MDMs generated from peripheral blood monocytes. Monocytes are mainly sourced from peripheral blood (287). Monocyte isolation protocols from peripheral blood have high purity and yields and involve the separation of PBMCs from either whole blood or buffy coats by density centrifugation (288, 289). Monocytes can then be isolated from PBMCs using several methods, however the method most often employed is magnetic bead cell-enrichment and this results in the highest cell viability, reported at over 95% (288, 290). Macrophages are then derived from monocytes using differentiation conditions that include macrophage-colony stimulating factor (M-CSF), and these macrophages also have high reported viability (90%) (288).

One of the main advantages associated with MDMs is that they more closely resemble *in vivo* macrophages when compared to macrophages derived from monocytic cell lines. In the context of macrophages for cell-based therapies, MDMs have successfully been generated in a GMP-compliant protocol (288, 291). Macrophages generated from this protocol expressed high levels of mature macrophage markers such as 25F9 and CD206, had an effective phagocytic capacity, and were functionally viable for up to 48 hours (291).

One of the main disadvantages associated with MDMs, as with $CD34^+$ HSPC-derived RBCs is availability, as collection of peripheral blood is donor dependent. This is especially challenging for studying macrophages in rare diseases, for which there may be limited donors. Additionally, the phenotype of macrophages is significantly impacted by the monocyte isolation technique used. A study comparing MDMs from monocytes isolated using three common techniques (plastic adhesion, negative selection and $CD14^+$ selection) identified differential expression of macrophage markers including CD163 on the resulting MDMs (292). To date, PB monocytes have not been successfully expanded *in vitro* and this therefore restricts the yields of MDMs.

1.6.3.2 Immortalised monocytic cell lines

Immortalised human monocyte cell lines such as U-937, Mono Mac 6, and THP-1 can also generate macrophages (293). The U-937 line was derived from tissue from a

male adult donor with generalised histiocytic lymphoma (294). U-937 cells can be differentiated into macrophages through the addition of phorbol-12-myristate-13-acetate (PMA), interferon-gamma, or vitamin D3 (295, 296). The Mono Mac 6 line was derived from the peripheral blood of a male adult patient with monoblastic leukaemia and cells can be differentiated into macrophages through the addition of PMA or LPS (297).

Currently, the most widely used immortalised cell line for macrophage generation is the THP-1 line, derived from the peripheral blood of a 1-year old leukemic child (298). THP-1 cells can be differentiated into macrophages through the addition of PMA or M-CSF (299). PMA treatment is described as the most effective and induces a macrophage morphology (flat, elongated, and adherent cells), an increase in the expression of macrophage markers and a decrease in the expression of the monocyte marker CD14 (299, 300, 301).

Immortalised monocytic cell lines share the same advantages as immortalised erythroid cell lines discussed in section 1.4.3, namely that once established these lines are donor-independent, inexpensive to grow, and easy to acquire. Additionally, while PB monocytes to date have not been successfully expanded *in vitro,* THP-1 and U397 monocytic cells can be expanded indefinitely and quickly, significantly increasing the numbers of macrophages able to be generated (299). THP-1 macrophages have been demonstrated to be comparable to MDMs as a model to study bacterial infection (302). In an *in vitro* model of *Mycobacterium tuberculosis* infection, THP-1 macrophage and MDM response to infection was found to be comparable, with similar bacterial uptake, viability and host response to drug-susceptible and drug-resistant infections (302).

Immortalised monocytic cell lines have been derived from cancer cells. This raises the question of how 'normal' these cells are and how well they recapitulate features of *in vivo* cells. Indeed, THP-1 cells have been identified to be karyotypically abnormal (303). When compared to their physiological counterparts PB monocytes, THP-1 cells express low levels of CD14 amongst other differences (304).

1.6.3.3 iPSC-derived macrophages

Macrophages have been successfully generated from both human ESC and iPSC lines. However, due to the ethical and legislative challenges associated with human ESC research, iPSC-derived macrophages are focussed on here (158).

Macrophages have been generated from human iPSCs using several different protocols. Protocols that are serum- and feeder-free are more adaptable to GMP compliant procedures, have proven to be reproducible, and generate high and pure yields of macrophages (303, 305). In these serum and feeder-free protocols iPSCs are mechanically dissociated and cultured in low adherence plates, and mesodermally primed with the addition of the cytokines bone morphogenetic protein (BMP4), SCF and VEGF (303, 305). This results in the formation of EBs that are plated onto an adherent surface and cultured with the addition of IL-3 to support haematopoietic progenitors, and M-CSF to drive myeloid cell-fate specification. These EBs produce monocyte-like suspension cells, characterised by expression of the monocyte-marker CD93, that are terminally differentiated into macrophages by additional culture with M-CSF.

iPSC-DMs are Myb-independent, and therefore resemble the developmental ontology of tissue-resident macrophages (6, 269). In addition, iPSC-DMs express high levels of CD163, with is a macrophage-specific marker highly expressed on tissue-resident macrophages and lowly expressed by MDMs (201, 254, 305, 306). It has been speculated that iPSC-derived macrophages would best model tissue-resident macrophages, and this has been the subject of much discussion within the field (307). The inaccessibility of tissue-resident macrophages has presented challenges to the study of these macrophages, therefore their generation from iPSCs allows for their study.

iPSC-DMs share the advantages of immortalised monocytic cell lines, namely that once established these lines are donor-independent and easy to acquire. However, the costs associated with iPSC cell culture are much higher than monocytic cell lines. iPSC-DMs can be harvested repeatedly from cultures, which greatly increases the available yield of macrophages compared MDMs (305).

In macrophage therapies, the generation of macrophages from recipient-derived iPSCs would reduce the risks associated with immune rejections and open a route for personalised treatments (308). Several iPSC lines have been established from patients with a variety of diseases, including Parkinson's disease, Huntington disease and both Duchenne and Becker muscular dystrophy (309). iPSCs have also been successfully used to model disease-specific pathologies. Motor neurons generated from iPSCs reprogrammed from the fibroblasts of a child with spinal muscular atrophy contained far fewer nuclear gems compared with WT-iPSC-derived motor neurons (nuclear aggregate structures containing survival motor neuron protein) (310). Nuclear gems are reduced in spinal muscular atrophy patient motor neurons.

One of the main advantages of iPSC-DMs, shared with the iPSC-derived RBCs described in section 1.4.4, is that iPSCs can be subjected to genetic manipulation (168, 169, 170, 171, 172, 173). Indeed, genetically modified iPSCs have been used to model specific macrophage subsets (201). Genetic manipulation of iPSCs to generate KLF1-activated iPSC-DMs (described in section 1.5.2.3) generated an *in vitro* model for EBI macrophages and were utilised to identified factors that promote erythropoiesis (168, 201). iPSC technology also allows for the development of often termed 'disease-in-a-dish' approaches in which patient-derived iPSCs can be used to model cell types and investigate the pathogenesis of diseases (311). This would prove useful not only for diseases in which a role of macrophages in pathogenesis has been well defined, but to investigate a possible contribution of macrophages to other diseases.

1.7 Rationale and hypothesis

Existing treatments for RBC disorders are often effective in managing these conditions, while offering no long-term cures (95, 99). The establishment of new treatments for RBC disorders relies on the full understanding of the cellular and molecular interactions associated with the production and maturation of RBCs. Considering that the majority of erythropoiesis occurs in the EBI niche, little is understood about the contribution of the niche to RBC disorders. The elucidation of processes associated with the EBI niche both in health, stress erythropoiesis and disease has relied upon *in vivo* modelling and reconstitution of the EBI in animal

models, with complexities dissected using *in vitro* systems. Recent progress in the field has utilised state of the art stem cell and gene editing technology, enabling a more detailed study of the human EBI niche. I speculated that this technology could be applied to modelling the EBI niche in RBC disorders, specifically CDA type IV. Furthermore, these models could aid in research into the manufacturing of RBCs *in vitro* to replace donor blood transfusions, which is the most common treatment of blood disorders.

I applied iPSC technology to the study of the EBI niche in CDA type IV. The intrinsic effect of the KLF1-E325K mutation in RBCs has been well defined, but it had not been investigated in macrophages (116, 131). To address this, Iused iPSCs derived from a CDA type IV patient and developed a novel iPSC line where the KLF1-E325K mutant protein could be activated in an inducible manner.

I hypothesised that the KLF1-E325K mutation affects the macrophage compartment of the EBI niche, reducing their ability to mature and enucleate RBCs.

1.8 Aims

1. Assess the effect of the KLF1-E325K mutation on the phenotype and function of iPSC-DMs derived from a CDA patient iPSC line.

2. Establish a novel iPSC line where the mutant KLF1-E325K protein can be activated by the addition of 4OH-tamoxifen.

3. Assess the effect of KLF1-E325K activation on the phenotype and function of iPSC-DMs.

4. Characterise the transcriptome of KLF1-E325K iPSC-DMs to investigate whether any genes are differentially regulated by KLF1-WT and KLF1-E325K.

Chapter 2: Materials and Methods

2.1 Cell culture

2.1.1 Production of iPSCs

The SFCi55 human iPSC line was generated by Roslin Cells from fibroblasts obtained from the skin of an O Rhesus negative individual (R Biomedical Ltd, Edinburgh, UK under REC 1/AL/0020 ethical approval). Fibroblasts were reprogrammed to iPSCs using an episomal strategy with four transcription factors, OCT4, KLF4, SOX2 and cMYC (160). The BM2.3 and CDA type IV patient iPSC lines were generated by ReachBio LLC #0200-100 and provided to us by the James Bieker lab at Mount Sinai, New York. Fibroblasts obtained from a skin biopsy were reprogrammed to iPSCs using the CytoTune-iPS Sendai Reprogramming Kit (Invitrogen).

2.1.2 iPSC Maintenance

2.1.2.1 Culture of iPSCs

Human iPSC lines were maintained in StemPro™ hESC SFM media (A1000701, Gibco) supplemented with 20 ng/ml human basic FGF (R&D) on either CELLstart™ Substrate (A1014201, Gibco) or Vitronectin (A31804, Gibco) coated wells. To coat CELLstart™ Substrate on plates, the original stock of CELLstart™ was diluted with DPBS containing Ca^{2+} and Mg^{2+} at a ratio of 1:50. To coat Vitronectin on plates, 6 ul vitronectin stock was diluted in PBS (10010023, Gibco) at a ratio of 1:10. StemPro™ hESC SFM was compromised of 500 ml DMEM/F-12 with Glutamax™ media (10565-018, Gibco) supplemented with 40 ml 25% BSA (A10208-01, Gibco), 10 ml StemPro supplement (A10006-01, Gibco) and 1 ml of 50 mM β-Mercaptoethanol (31350010, Gibco). Media was changed daily.

2.1.2.2 Passage of iPSCs

iPSCs were passaged when wells reached approximately 70-80% confluency. Culture media was exchanged on a confluent well with fresh StemPro™ hESC SFM media approximately 1 hour before passaging. The cell colonies were then cut into small squares using a StemPro EZPassage™ Disposable Stem Cell Passaging Tool (23181010, Gibco). These small squares in suspension were then transferred to new CELLstart™ or Vitronectin coated wells in fresh StemPro™ hESC SFM media at a ratio of 1:4.

2.1.2.3 Cryopreservation of iPSCs

StemPro™ hESC SFM media supplemented with 10 uM ROCK inhibitor (Y-27632, MERCK) was changed on cells of 70-80% confluent well 1 hour prior to cryopreservation. Cells were cut with a StemPro EZPassage™ tool and centrifuged at 300 g for 5 minutes. Colonies were resuspended in 1 ml of cold CryoStor® cell cryopreservation media (C2874, Sigma-Aldrich) and divided into two labelled cryovials. Cryovials were cooled at a rate of approximately 1°C per minute in a Mr Frosty™ Freezing Container (5100-0001, ThermoFisher Scientific) in a -80°C freezer overnight before moving to long-term storage in a -150°C freezer.

2.1.2.4 Thawing of iPSCs

A cryovial of iPSCs was thawed at 37°C in a bead bath before cells were washed with warm StemPro™ media and centrifuged at 300 g for 5 minutes. Cell colonies were resuspended in 1.5 ml StemPro™ supplemented with 10 uM ROCK inhibitor and transferred to 1 CELLstart™ or Vitronectin coated well. ROCK inhibitor was removed after 24 hours.

2.1.3 Differentiation of iPSCs under erythroid differentiation conditions

2.1.3.1 Step 1: Generation of EBs

One 70-80% confluent iPSC well was cut using the StemPro EZPassage™ tool into 3 ml of StemPro Mix 1 media. Cell colonies were split into 2 wells of 6-well plate with Cell-Repellent Surface (657970, Greiner Bio-One Inc). Cell colonies were maintained for 4 days to induce EB formation, with a top-up of cytokines on day 2.

StemPro Mix 1: StemPro™ hESC SFM media (Gibco) supplemented with 50 ng/ml Recombinant human BMP4-CF (Bio-Techne Ltd), 50 ng/ml Recombinant Human VEGF165 (Bio-Techne Ltd) and 20 ng/ml SCF (C-Kit Ligand) Recombinant Human Protein (PHC2111, Life Technologies).

2.1.3.2 Step 2: Maintenance of EBs

10-15 EBs per well were transferred to a 0.1% gelatin coated 6-well tissue culture treated plate (Greiner Bio-One Inc) with 3 ml SFD media per well supplemented with 100 ng/mL SCF (PHC2111, Life Technologies), 3 U/ml Recombinant Human Erythropoietin (EPO) (287-TC, R&D Systems), and 5 ng/mL IL-3 (200-03-10uG,

Peprotech EC Ltd). SFD media was changed on EB plates every 7 days. EB plates start to produce haematopoietic suspension cells after approximately 2-3 weeks.

SFD media: 500 ml IMDM media (12440053, Gibco) supplemented with 167 ml Ham's F12 Nutrient Mix (11765054, Gibco), 5 ml N-2 Supplement 100X (17502048, Gibco), 10 ml B-27™ 50X serum free (17504044, Gibco), 5 mg/ml Ascorbic Acid (A4544, Sigma-Aldrich), 2.5 ml GlutaMAX™ Supplement 100X (35050038, Gibco), 19.5 ul MTG 11.5M (M6145, Sigma-Aldrich), 2.5 ml Human serum albumin and 50 mg/ul holo-Transferrin human (T0665, Sigma-Aldrich).

2.1.3.3 Step 3: Collection of suspension cells

Suspension cells were harvested from EB plates once every 7 days and analysed at the point of harvest. All suspension cells were collected for analysis, with yields varying between 5 x 10^5 to 5 x 10^6 cells per 6-well plate of EBs.

2.1.4 Differentiation of iPSCs to macrophages

2.1.4.1 Step 1: Generation of EBs

One 70-80% confluent iPSC well was cut using the StemPro EZPassage™ tool into 3 ml of StemPro Mix 1 media. Cell colonies were split into 2 wells of 6-well plate with Cell-Repellent Surface (657970, Greiner Bio-One Inc). Cell colonies were maintained for 4 days to induce embryoid body (EB) formation, with a top-up of cytokines on day 2.

StemPro Mix 1: StemPro™ hESC SFM media (Gibco) supplemented with 50 ng/ml Recombinant human BMP4, CF (314-BP-010/CF, Bio-Techne Ltd), 50 ng/ml Recombinant Human VEGF165 (293-VE-010, Bio-Techne Ltd) and 20 ng/ml SCF (PHC2111, Life Technologies).

2.1.4.2 Step 2: Maintenance of EBs

10-15 EBs per well were transferred to a 6-well tissue culture treated plate (Greiner Bio-One Inc) coated with 0.1% gelatin (brand) with 3 ml Mix 2. Mix 2 media was changed on EB plates every 3-4 days. EB plates start to produce macrophage precursor cells after approximately 2 weeks.

Mix 2: Lonza XVivo 15 with Gentamycin and PR media (LZBE02-060Q, Scientific Laboratory Supplies Ltd) supplemented with 100 ng/ml Recombinant Human M-CSF carrier-free protein (574806, Biolegend), 25 ng/ml Human IL-3 (200-03-10uG, Peprotech EC Ltd), 1% Penicillin-Streptomycin (brand), 2 mM GlutaMAX supplement (35050038, Life Technologies), and 0.55 mM β-Mercaptoethanol.

2.1.4.3 Step 3: Maintenance of suspension cells (macrophages)

Macrophage precursor cells were harvested every 3-4 days into 6-well tissue culture treated plates (Greiner Bio-One Inc) with 3 ml Mix 3 per well. Suspension cells were maintained in Mix 3 for 9-11 days to allow maturation into macrophages. For KLF1-E325K and KLF1-WT activation experiments, 100 nM 4-hydroxy4OH-tamoxifen (H6278, Sigma-Aldrich) was added to the cultures on days 8 and 10.

Mix 3: Lonza X-VIVO^{TM} 15 Serum-free Hematopoietic Cell Medium with Gentamycin (BE02-060F, Scientific Laboratory Supplies Ltd) supplemented with 100 ng/ml Recombinant Human M-CSF carrier-free protein (574804, Biolegend), 1% Penicillin-Streptomycin (15140122, Gibco), and 2 mM GlutaMAX supplement (35050061, Gibco).

2.1.5 Transfection of cells

The SFCi55 iPSC line was transfected with either the pZDonor-AAVS1-Puromycin-CAG-HA-KLF1E325K-ER^{T2}-PA plasmid or the CAG-PURO-GFP control plasmid using Xfect^{TM} Transfection Reagent (631317, Takara Bio) following the manufacturer's instructions. Briefly, plasmid was mixed with Xfect buffer and Xfect polymer, vortexed thoroughly and incubated for 10-20 minutes at room temperature. 1 million iPSCs in single suspension were added to a CELLstart^{TM} or Vitronectin coated 10 cm tissue culture dish, and the Xfect mixture was added in a drop-wise manner. Cells were incubated overnight, and media was changed in the morning to remove Xfect reagents. Cells were maintained in StemPro^{TM} hESC SFM media that was changed daily. Puromycin selection was started at 2 ug/ml two days post transfection and increased to 4 ug/ml 4 days post transfection. Surviving colonies were picked approximately 2 weeks post transfection and grown into a 6-well plate format for genomic DNA extraction and PCR screening.

2.1.6 Thawing, expansion and cryopreservation of human UCB CD34$^+$ cells

A vial of 10 x^6 CD34$^+$ cells isolated from UBC (70008, STEMCELL Technologies) was thawed at 37°C in a bead bath. Cells were washed with warm IMDM Mix 0 media and resuspended in 18 ml of IMDM Mix 1 media and transferred to 6-wells of a 6-well plate. A complete media change of IMDM Mix 1 was carried out on days 2 and 4. On day 6, cells were frozen at a density of 5 x^5 cells per vial in 0.5 ml of IMDM Mix 0 and 0.5 ml of 60% KnockOut™ Serum Replacement (10828028, Gibco), 20% DMSO (D12345, Invitrogen) and 20% IMDM Mix 0. Cryovials were cooled at a rate of approximately 1°C per minute in a Mr Frosty™ Freezing Container in a -80°C freezer overnight before moving to long-term storage in a -150°C freezer.

IMDM Mix 0: IMDM media (Gibco) supplemented with 5% Human Serum (H4522, Sigma-Aldrich), 3 U/ml Heparin sodium salt from porcine intestinal mucosa (H3149, Sigma-Aldrich), 10 ug/ml Insulin (I9278, Sigma-Aldrich), and 200 ug/ml holo-Transferrin human (T0665, Sigma-Aldrich).

IMDM Mix 1: IMDM Mix 0 supplemented with 60 ng/ml SCF (PHC2111, Life Technologies), 5 ng/ml Human IL-3 (200-03-10uG, Peprotech EC Ltd), 3 U/ml Recombinant Human Erythropoietin (EPO) (287-TC, R&D Systems) and 1 uM hydrocortisone (74142, STEMCELL technologies).

2.1.7 *In vitro* assays

2.1.7.1 Methylcellulose assay

Suspension cells harvested from differentiations of iPSCs under erythroid differentiation conditions were counted and 1 x10^4 cells were resuspended in SFD media. Cells were seeded into 2 ml of MethoCult™ H4435 Enriched Methylcellulose-based media (04435, STEMCELL Technologies). Cells were incubated at 37°C for 14 days.

2.1.7.2 Cell cycle analysis

1 x 10^5 cells per sample were resuspended in PBS with 1% BSA (A2153, Sigma-Aldrich) and 5 mM EDTA (15575020, Invitrogen). Samples were kept on ice until DAPI staining and data collection using the LSR Fortessa (BD Biosciences) and BD FACSDIVA™ software. DAPI (D9542, Sigma-Aldrich) was added to samples for 1 minute prior to

data collection at 1:1000. Data was analysed using FlowJo 10.8.1 software (Figure 2.1). Flow cytometry plots were gated for single cells, and segregated into cycling and non-cycling cells (Figure 2.1).

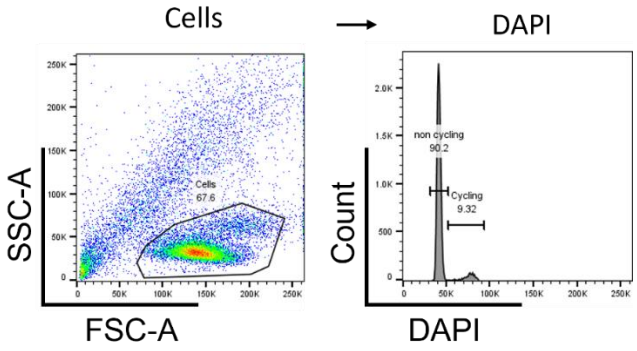

Figure 2.1 Flow cytometry gating strategy for cell cycle analyses. Cells were gated, and non-cycling and cycling cells were segregated in a histogram.

2.1.7.3 Erythroid cell maturation and enucleation assay (*in vitro* EBI model)

A vial of frozen day 6 expanded CD34$^+$ cells was thawed at 37°C in a bead bath. Cells were washed with warm IMDM Mix 0 media and resuspended into 18 ml of warm IMDM Mix 1 media (Section 2.1.6) and cultured in 6 wells of a 6-well plate.

On day 8, expanded CD34$^+$ cells were resuspended into IMDM Mix 2 media in a 12-well plate at a density of 50 10 x^4 cells per well. For the *in vitro* erythroblastic island model, iPSC-derived macrophages were added at a ratio of 1:3 (expanded CD34$^+$cells: macrophages). For KLF1-E325K and KLF1-WT activation experiments, 100 nM 4-hydroxy4OH-tamoxifen (H6278, Sigma-Aldrich) was added every other day for the duration of the culture. For investigations into IGFBP-6, IGFBP-6 was added every other day for a final concentration of 100 or 200 nM during the duration of the culture. Cytokines were topped up on day 10.

IMDM Mix 2: IMDM Mix 0 supplemented with 60 ng/ml SCF (PHC2111, Life Technologies), 3 U/ml EPO (R&D Systems), 1 uM hydrocortisone (74142, STEMCELL technologies) and 300 ug/ml holo-Transferrin human (T4778, Sigma-Aldrich).

On day 11, suspension cells were adjusted to a density of 1 x^6 cells per well in IMDM Mix 3 media. Cytokines were topped up on days 13, 17 and 20. Full media changes

were conducted on days 15 and 18. For the *in vitro* erythroblastic island model, a top up of 150,000 macrophages were added on day 15. Suspension cells are analysed via cytospin and flow cytometry on days 11, 14, 18 and 21.

IMDM Mix 3: IMDM Mix 0 supplemented with 3 U/ml EPO (R&D Systems) and 300 ug/ml holo-Transferrin human (Sigma-Aldrich).

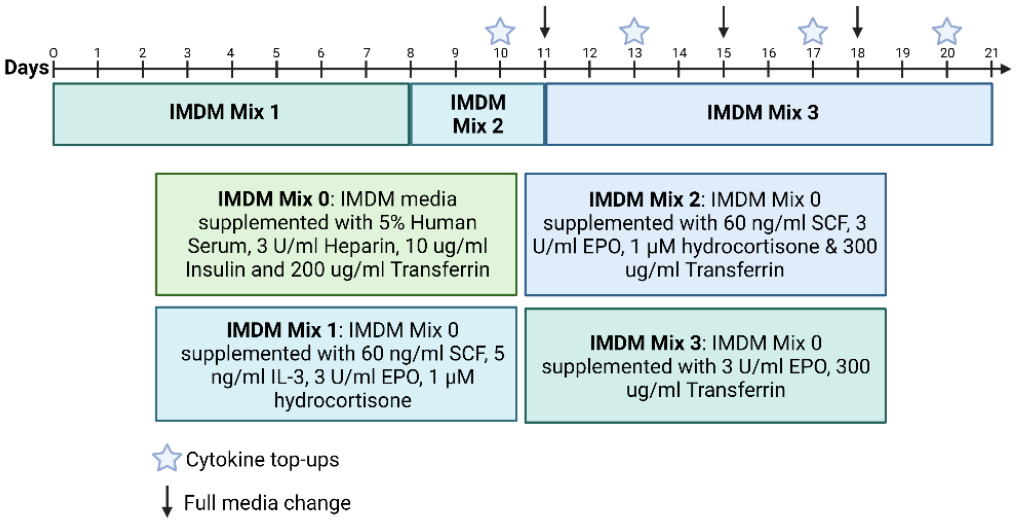

Figure 2.2 Erythroid cell maturation and enucleation assay. Cytokines are topped up on days 10, 13, 17 and 20. Full media changes are conducted on days 11, 15 and 18. Cells are cultured in IMDM Mix 1 from days 0-8, IMDM Mix 2 from days 8-11, and IMDM Mix 3 from days 11 to 21.

2.2 Molecular Biology Techniques

2.2.1 Restriction enzyme digestions

Restriction enzyme digests were carried out at 37 °C for 1 hour with 1 µg plasmid and 1 unit per restriction enzyme (EcoRI R010S, HindIII R0104S, New England Biolabs) in the provided CutSmart Buffer. Digestion reactions were run on a 1% agarose gel with 1:10,000 GelRed (41003, Biotium) for 45 minutes at 110V.

2.2.2 Ligation reactions

Ligation reactions were performed using the Quick Ligation™ Kit (M2200S, New England Biolabs) for 5 minutes at room temperature following the manufacturer's instructions.

2.2.3 Site-directed mutagenesis

Site-directed mutagenesis on the pBR332-KLF1 subcloning plasmid was performed using the Q5® Site-Directed Mutagenesis Kit (E0554S, New England BioLabs) following the manufacturer's instructions. The forward KLF1 SDM NEB_FW (CGGGTCAGCTTGTCCGAGCGC) and reverse KLF1 SDM NEB_RV (CCACTACCGGAAACACACGGG) primers were used.

2.2.4 Sanger sequencing

Samples for sequencing of KLF1 around the KLF1-E325K mutation locus were sent to Source Bioscience for sequencing using the KLF1FW2 primer (CACTTTGTTCATCCTAGTCCCA) .

2.2.5 Transformation of competent cells

50 ul of competent cells were thawed on ice. 2 ul of either a ligation reaction or a plasmid was added to the competent cells, mixed gently by flicking the tube, and incubated on ice for 20 minutes. Cells were then heat-shocked at 42°C for 45 seconds, before being allowed to recover on ice for 2 minutes. Cells were mixed with 1 ml room temperature LB media and incubated at 37°C with shaking at 200 rpm for 1-2 hours. After incubation, 150 ul culture was spread onto agar plates with 50 ug/ml ampicillin (A5354, Sigma-Aldrich). Plates were incubated overnight at 37°C and kept at 4°C for short-term storage.

2.2.6 Plasmid purification

One colony of bacteria was picked and expanded in 5 ml LB media with 50 ug/ul ampicillin (A5354, Sigma-Aldrich) at 37°C with shaking at 200 rpm overnight. Plasmid was then extracted using the QIAprep Spin Miniprep Kit (27106, QIAGEN) following manufacturer's instructions. Plasmid was eluted into nuclease-free water (129114, QIAGEN) and stored at -20°C. For long term storage of plasmids, bacterial glycerol stocks were generated as follows. One colony of bacteria was expanded in 5 ml LB media with 50 ug/ul ampicillin (A5354, Sigma-Aldrich) at 37°C with shaking at 200 rpm overnight. 500 ul of overnight culture was added to 500 ul 50% glycerol (G5516, Sigma-Aldrich), gently mixed, and stored at -80°C.

2.2.7 Gel extraction

DNA was extracted from 1% agarose gels using the QIAquick Gel Extraction Kit (28704, QIAGEN) following the manufacturer's instructions.

2.2.8 Genomic DNA extraction

Genomic DNA was extracted from a pellet of approximately 1 x10^6 cells using the MasterPure^{TM} Complete DNA and RNA Purification Kit (MC85200, EpicentreBio) following the Total Nucleic Acids Purification Protocol. RNA was removed from samples by incubation with RNase A (MRNA092, EpicentreBio). Genomic DNA was resuspended in nuclease-free water (129114, QIAGEN) and kept at -20°C for short-term storage (<1 month) and -80°C for long-term storage (>1 month).

2.2.9 PCR

Polymerase chain reactions (PCR) were performed on genomic DNA extracted from iPSC clones transfected with a pZDonor-AAVS1-CAG-HA-KLF1-E325K-ER^{T2}-PolyA plasmid to screen for correct integration. 100 ng genomic DNA was added to 25 ul PrimeSTAR Max Premix (2X) (R045A, TakaraBio), 0.2 uM of forward and reverse primers (Table 2.1) and sterile distilled water for a total reaction volume of 50 ul. Reactions were carried out on the following programme for 30 cycles: 98°C for 10 seconds, 55°C for 5 seconds, and 72°C for 5 seconds.

PCR primer name	Sequence
KLF1_FW	GAGGATCCAGGTGTGATAGCCGAGA
ERT2_RV	CTTCATGCTGTACAGATGCTCCATG
pZDonor_FW	CCGTCGACGCTCTCTAGAGCTAG
Int_RV	CCGTCGACGCTCTCTAGAGCTAG
5'aavs1_FW	CGGAACTCTGCCCTCTAACGCTGCCG
5'aavs1_RV	CTGCCAGATCTCTCGAGGCCCTGTGG
Ext_RV	ACAGCCCCAGGTGGAGAAACTG

Table 2.1 Primers used for PCR screening of clones.

2.3 Cell Surface Marker Analyses

2.3.1 Flow cytometry analysis of cells generated under erythroid differentiation conditions

Cells were resuspended in PBS with 1% BSA (A2153, Sigma-Aldrich) and 5 mM EDTA (15575020, Invitrogen). 1 x 10^5 cells per sample were stained with the appropriate antibodies for 15 minutes at room temperature (Table 2.2). For panel 1, DAPI (D9542,

Sigma-Aldrich) was added to samples immediately prior to data collection at 1:1000 as a marker to gate out dead cells (Figure 2.3A). For panel 2, LIVE/DEAD™ Fixable Near-IR Stain Kit (L10119, Invitrogen) was included in the antibody stain to allow gating of live cells (Figure 2.3B). Samples were kept on ice until data collection using the LSR Fortessa (BD Biosciences) and BD FACSDIVA™ software. Data was analysed using FlowJo 10.8.1 software. Flow cytometry plots were gated using fluorescence minus one (FMO) controls. Briefly, single and live cells were gated, and then FMO controls were used to distinguish populations positive and negative for a specific marker (Figure 2.3).

Cell Surface Marker	Conjugated Fluorochrome	Manufacturer	Dilution
CD43	APC	17-0439-42, Invitrogen	1:100
EpCAM	PE	324205, Biolegend	1:100
CD235a	FITC	349104, Biolegend	1:200
CD71	APC	17-0719-42, Invitrogen	1:200

Table 2.2 Antibodies used for flow cytometry analysis of cells generated under erythroid differentiation conditions.

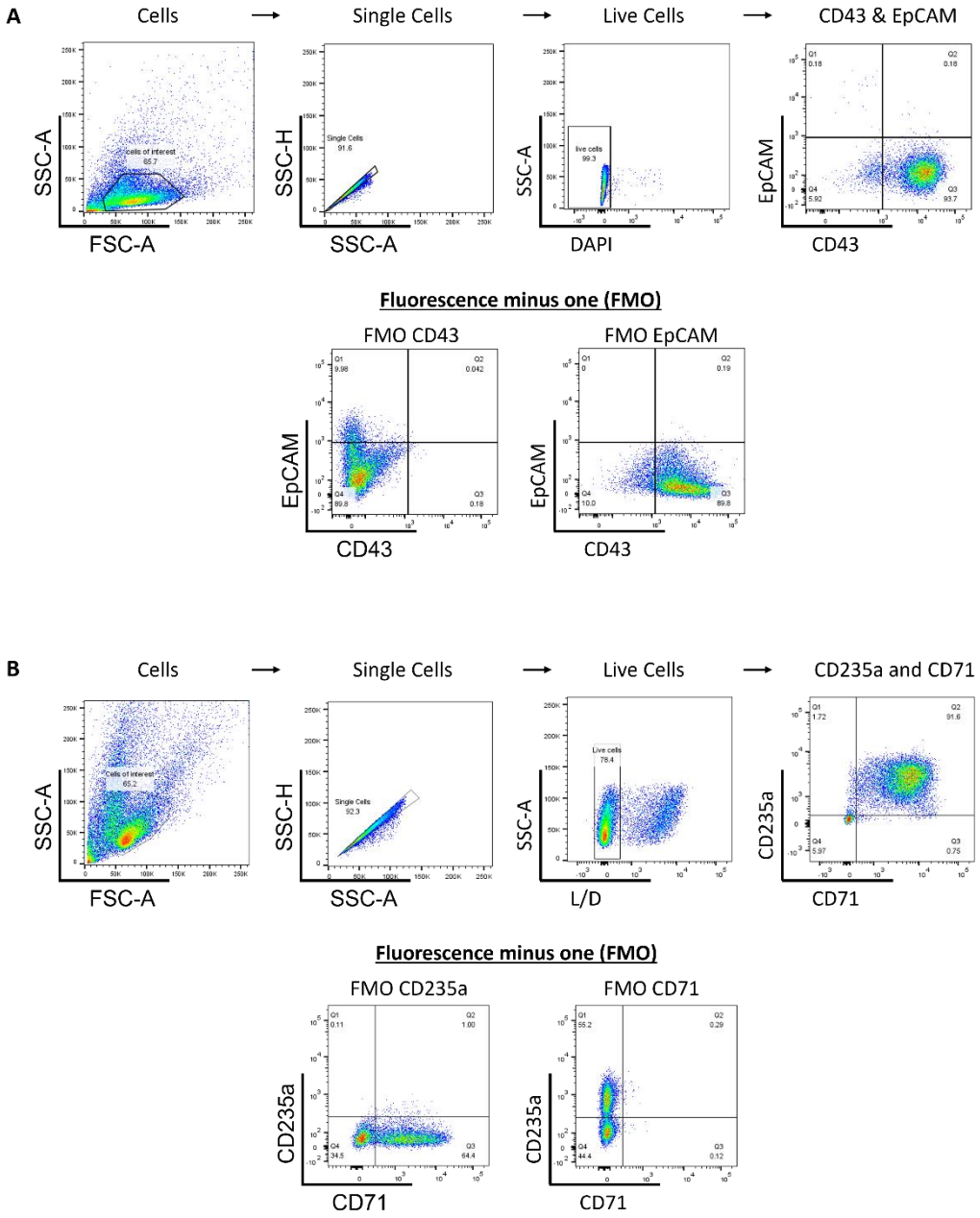

Figure 2.3 Flow cytometry gating analyses of cells generated under erythroid differentiation conditions. Single, live cells were gated and analysed for the expression of the cell surface markers CD43, EpCAM, CD235a and CD71 in two panels: **.** A: CD43 and EpCAM. B: CD235a and CD71. FMO controls were used to gate and quantify the percentage of cells expressing each marker. Representative plots shown.

2.3.2 Flow cytometry analysis of iPSC-derived macrophages

Single cell suspensions were prepared by incubating macrophages with either Cell Dissociation Buffer (13151014, Gibco) or StemPro™ Accutase™ Cell Dissociation Reagent (A1110501, Gibco) for 5 minutes at room temperature or 37 °C, respectively. Cells were resuspended in PBS with 1% BSA (A2153, Sigma-Aldrich) and 5 mM EDTA

(15575020, Invitrogen). 1 x 10^5 cells per sample were stained with the appropriate antibodies for 10 minutes at room temperature (Table 2.3). Samples were kept on ice until data collection using the LSR Fortessa (BD Biosciences) and BD FACSDIVA™ software. DAPI (D9542, Sigma-Aldrich) was added to samples immediately prior to data collection at 1:1000 as a marker to gate out dead cells. Data was analysed using FlowJo 10.8.1 software. Flow cytometry plots were gated using FMO controls. Briefly, single and live cells were gated, and then FMO controls were used to distinguish populations positive and negative for a specific marker (Figure 2.4).

Cell Surface Marker	Conjugated Fluorochrome	Manufacturer	Dilution
CD45	APC	15577936, Ebioscience	1:100
CD93	PE	10804637, Ebioscience	1:200
25F9	E-FLUOR-660	15599866, Ebioscience	1:20
CD163	PE-CY7	333614, Biolegend	1:25
CD169	APC	346007, Biolegend	1:25

Table 2.3 Antibodies used for flow cytometry analysis of iPSC-derived macrophages.

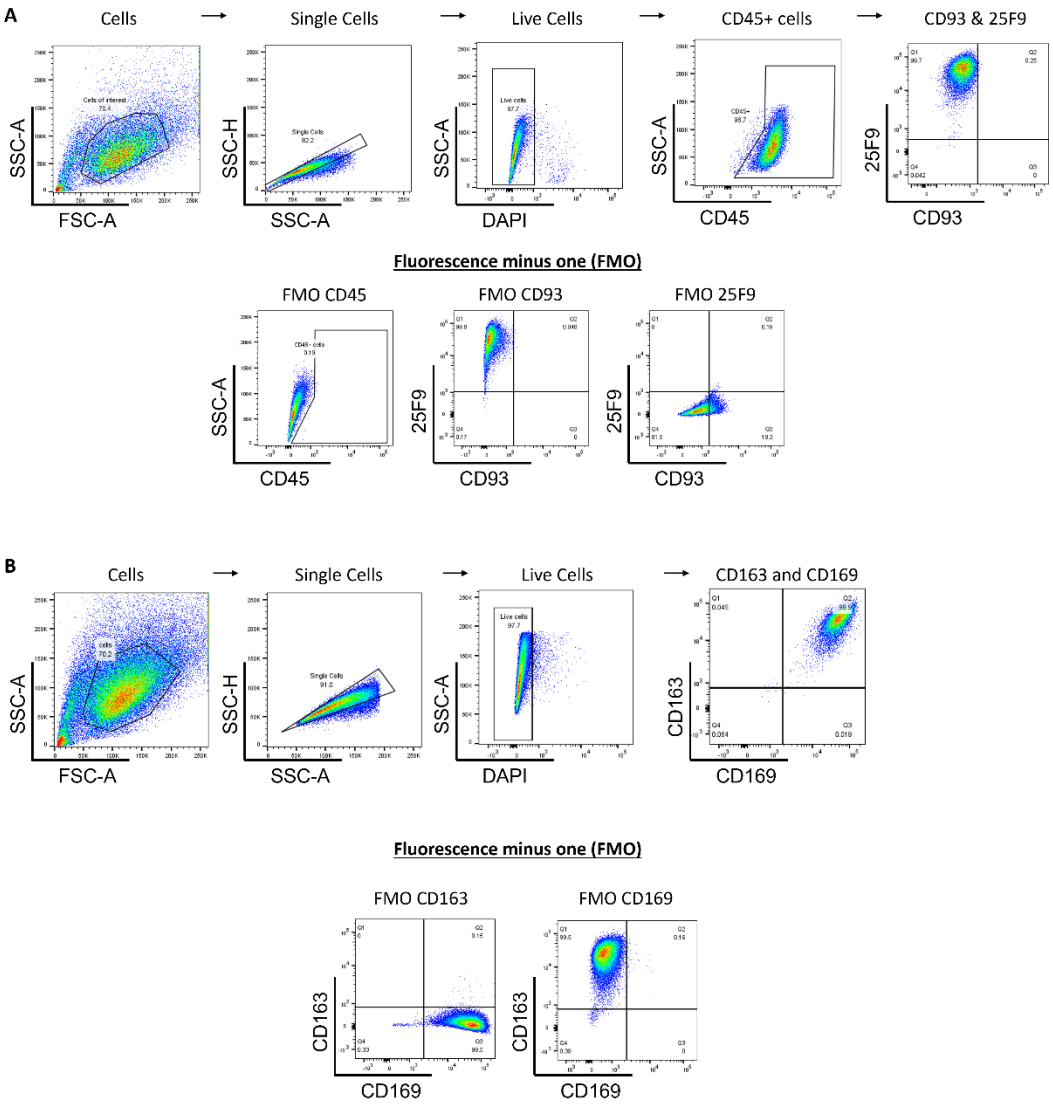

Figure 2.4 Flow cytometry gating analyses of iPSC-derived macrophages. Single, live cells were gated and analysed for the expression of the cell surface markers CD45, CD93, 25F9, CD163 and CD169 in two panels: **.** A: CD45, CD93 and 25F9. B: CD163 and CD169. FMO controls were used to gate and quantify the percentage of cells expressing each marker. Representative plots shown.

2.3.3 Flow cytometry analysis of suspension cells generated from the erythroid cell maturation and enucleation assay

Cells were resuspended in PBS with 1% BSA (A2153, Sigma-Aldrich) and 5 mM EDTA (15575020, Invitrogen). 1 x 10^5 cells per sample were stained with Hoechst 33342 (R37605, Invitrogen) for 5 minutes at room temperature. Cells were then further stained with CD235a, CD71 and LIVE/DEAD™ Fixable Near-IR Stain Kit (L10119, Invitrogen) for 15 minutes at room temperature. Samples were kept on ice until data collection using the LSR Fortessa (BD Biosciences) and BD FACSDIVA™ software. Data

was analysed using FlowJo 10.8.1 software. low cytometry plots were gated using FMO controls. Briefly, single and live cells were gated, and then FMO controls were used to distinguish populations positive and negative for a specific marker (Figure 2.5).

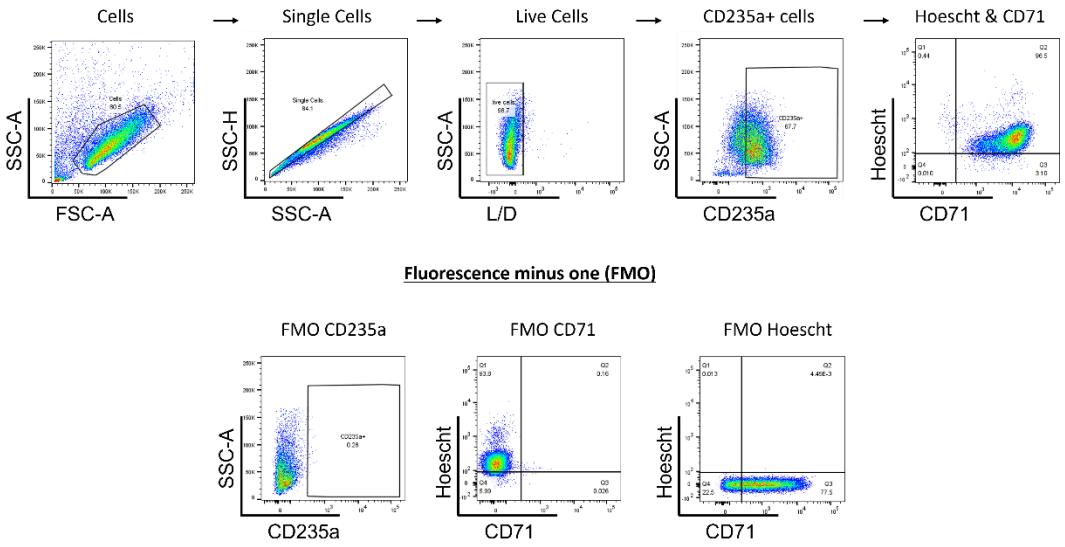

Figure 2.5 Flow cytometry gating analyses of suspension cells generated from the erythroid cell maturation and enucleation assay. Single, live cells were gated and analysed for the expression of the cell surface markers CD235a and CD71, and the nuclear dye Hoechst.

2.4 Imaging

2.4.1 Cytospins

Cells for cytospins were suspended at a density of 3 x 10^5 cells in 200 ul PBS. Cells were cyto-centrifuged onto polysine slides at 500 rpm for 5 minutes in a Thermo Shandon Cytospin 4 and allowed to air-dry for 4-12 hours. Cells were fixed and stained using the Shandon™ Kwik-Diff™ Staining Kit (9990702, Thermo Fisher Scientific) containing 3 solutions: Reagent 1, a fixative; Reagent 2, Eosin; Reagent 3, Methylene Blue. Air-dried slides were first dipped into Reagent 1 for 20 seconds, immediately transferred into Reagent 2 for 40 seconds, immediately transferred into Reagent 3 for 30 seconds, and were then rinsed in water and air-dried.

2.4.2 Immunohistochemistry

Cells were fixed into 96-well glass bottom plates (6055302, Perkin Elmer) in 4 % Formaldehyde (10231622, Fisher Scientific) for 15 minutes at room temperature. Cells were washed thrice with PBS and then permeabilised in PBS with 1 % BSA (A2153, Sigma-Aldrich) and 0.5 % Triton X-100 (X100, Sigma-Alrich) for 1 hour at room temperature. Cells were washed thrice with PBS before overnight incubation at 4°C in PBS with 1% donkey serum (ab7475, Abcam) and 1:200 Anti-EKLF/KLF1 antibody (ab2483, Abcam). Cells were then washed thrice with PBS and incubated for 1 hour at room temperature in PBS with 1 % donkey serum (ab7475, Abcam) and 1:1000 Donkey anti-Goat IgG (H+L) Cross-Absorbed Secondary Antibody, Alexa Fluor 647 (A-21447, Invitrogen). Cells were washed once with PBS and incubated with 1:1000 DAPI (D9542, Sigma-Aldrich) for 5 minutes at room temperature. Cells were washed twice with PBS and stored in PBS at 4 °C before imaging. Cells were imaged at 40X on the Opera Phenix® Plus High-Content Screening System and processed with Fiji software. All images had their contrast enhanced by 0.3%.

2.5 Gene Expression Analyses

2.5.1 RNA extraction

RNA extraction was performed using the RNAeasy Mini Kit (74106, QIAGEN). 1 x 10^6 cells were collected into 500 ul of RLT buffer supplemented with 1% β-Mercaptoethanol. 500 ul 70% ethanol was added to the columns and mixed well before 700 ul was transferred to an RNAeasy spin column. Columns were centrifuged for 15 seconds at 10,000 RPM, supernatant was discarded and the column was washed with 350 ul RW1 buffer. DNA was removed from samples using the RNase-free DNase Set (79254, QIAGEN). 80 ul DNase 1 mix (10 ul DNase1 and 70 ul RDD buffer) was added to the spin column, and columns were incubated at room temperature for 15 minutes. Columns were washed with 350 ul RW1 buffer, followed by 500 ul of RPE buffer. Columns were placed into collection tubes, 35 ul RNase-free water was added, and RNA was eluted by centrifuging for 1 minute at 10,000 RPM. RNA samples were stored at -80°C.

2.5.2 cDNA synthesis

cDNA was generated from 500 ng of RNA per sample using the High-Capacity cDNA Reverse Transcription Kit (4368814, Thermo Fisher Scientific). 500 ng RNA in a total volume of 10 ul RNase free water was added to 10 ul of High-Capacity cDNA Reverse Transcription Kit Mix containing: 10X RT Buffer, 25X dNTP Mix (100mM), 10X RT Random Primers, and MultiScribe Reverse Transcriptase. These 20 ul reactions were carried out on the following programme: 25°C for 5 minutes, 37°C for 2 hours, 85°C for 5 minutes before cooling to 4°C. cDNA samples were kept at -20°C for short-term storage (<1 month) and -80°C for long-term storage (>1 month).

2.5.3 qRT-PCR analysis

Real-Time Quantitative Reverse Transcription polymerase chain reaction (qRT-PCR) reactions were performed on the Roche LightCycler® 480 Instrument. 2 ng of cDNA was amplified per reaction in a 364-well plate (4729749001, Roche) with LightCycler® 480 SYBR Green I Master (4887352001, Roche) according to the manufacturer's instructions. All reactions were performed with 3 biological and 3 technical replicates. Primers used are listed in Table 2.4.

Amplification reactions were carried out using the following programme: 95°C for 5 minutes (pre-incubation, 1 cycle), 95°C for 10 seconds, 54°C for 10 seconds and 72°C for 10 seconds (Amplification, 45 cycles), 95°C for 5 seconds, 65°C for 1 minute and 97°C for 1 minute (Melting curve, 1 cycle). CT values were normalised to the reference gene GAPDH or the mean of the reference genes GAPDH and β-Actin. These housekeeping genes were selected as their expression remained consistent across cell lines, and differentiation of cell lines into different cell types. Data was analysed using the 2–ΔΔCt method. Graphs were generated and statistical analysis was performed using GraphPad Prism 8 software. To analyse data relative to GAPDH, the following equation was used: (2^GAPDH CT value)/(2^CT value gene of interest).

Gene	Forward primer sequence	Reverse primer sequence
CD163	GAAGATGCTGGCGTGACA	GCTGCCTCCACCTCTAAG
CD169	GGATCATCCAACACCTCACTC	GGTGATGGTGACACCTGGA
CD11B	GGCATCCGCAAAGTGGTA	GGATCTTAAAGGCATTCTTTCG
CD64	GACCCCATACAGCTGGAAATC	ACCTCAAGGCCAGAGGTTCT
TNF-α	CAGCCTCTTCTCCTTCCTGAT	GCCAGAGGGCTGATTAGAGA
PECAM-1	GCAACACAGTCCAGATAGTCGT	GACCTCAAACTGGGCATCAT
VCAM1	TGCACAGTGACTTGTGGACAT	CCACTCATCTCGATTTCTGGA
EMP	AAGAGACTGGACGCTGTGAGA	GTCCAGCTGGCTCCCTTC
ITGAV	AAGCTGAGCTCATCGTTTCC	GCACAGGAAAGTCTTGCTAAGG
CD68	GTCCACCTCGACCTGCTCT	CACTGGGGCAGGAGAAACT
KLF1-WT	ACACCAAGAGCTCCCACCT	GTAGTGGCGGGTCAGCTC
KLF1-WT + KLF1-E325K	ACACCAAGAGCTCCCACCT	GTAGTGGCGGGTCAGCT
CMAF	GTACAAGGAGAAATACGAGAAG	TATGAAAAACTCGGGAGA
CD11a	CCAGAAGTGAGAGCAGGCTATT	GAGGCCAGCAACGAAGTCT
IL33	CCACCAAAAGGCCTTCACT	AAGGCAAAGCACTCCACAGT
IGFBP6	CACAGGATGTGAACCGCAGAGA	CACTGAGTCCAGATGTCTACGG
GYPA	ATATGCAGCCACTCCTAGAGCTC	CTGGTTCAGAGAAATGATGGGCA
TFRC	ATCGGTTGGTGCCACTGAATGG	ACAACAGTGGGCTGGCAGAAAC
SLC4A1	CTGCTGGTGTTTGAGGAAGCCT	CACCAGCAGGATGAGCCAGAAG
ICAM4	GGCACCCATTACACTGATGCTC	AGGCACTTGCATAGGTACGCAG
HBA1	GACCCGGTCAACTTCAAGC	AGAAGCCAGGAACTTGTCCA

Table 2.4 Primers used for qRT-PCR gene expression analyses.

2.5.4 Transcriptomic analyses (RNA-sequencing)

RNA extraction was performed using the RNAeasy Mini Kit (QIAGEN) following the manufacturer's instructions. DNA was removed from samples using the RNase-free DNase Set (QIAGEN). RNA quantity and quality was assessed using the Agilent 2100 Bioanalyser in conjuction with the RNA 6000 PicoLabChip Kit following manufacturer's instructions. 35 automated TruSeq stranded mRNA-seq libraries from total RNA samples were generated by Edinburgh genomics and sequenced using NovaSeq 100PE. Reads were trimmed using Cutadapt (version cutadapt-1.18-venv) (312). Reads were trimmed for quality at the 3' end using a quality threshold of 30 for adaptor sequences of the TruSeq DNA kit (AGATCGGAAGAGC). Reads after trimming were required to have a minimum length of 50. The reference used for mapping was the Homo sapiens (GRCh38) genome from Ensembl. The annotation used for counting was the standard GTF-format annotation for that reference (annotation version 104). Reads were aligned to the reference genome using STAR

(version 2.7.3a) specifying paired-end reads and the option --outSAMtype BAM Unsorted (313). All other parameters were left at default. Resulting BAM files were analysed using the DeSEQ2 package by myself in R-4.2.1 for Windows. Genes were filtered and only genes with a count of 10 or higher in at least 2 samples were kept. Principal component analysis and multidimensional scaling were undertaken on normalised and filtered expression data. For differential gene expression analyses, genes were filtered to include only genes with an adjusted p-value below 0.05.

2.6 Statistical analyses

Statistical analyses were performed using GraphPad Prism 8 software. Error bars are expressed as mean ± standard error mean (SEM). p-values less than 0.05 were considered statistically significant (*$p < 0.05$, **$p < 0.01$, ***$p < 0.001$, ****$p < 0.0001$).

The following statistical analyses were used:

1. One-way ANOVA to compare one factor across multiple groups.
2. Unpaired t-test to compare one factor across two groups.

Chapter 3: Characterisation of Erythroid Progenitors and Macrophages Generated from a CDA type IV Patient-Derived iPSC Line

3.1 Introduction

In recent decades, erythroblastic island (EBI) macrophages have been implicated in the pathological progression of two RBC disorders, polycythemia vera and beta-thalassemia (209, 245). Polycythemia vera is a disease characterised by excessive erythrocyte production (erythrocytosis) as a result of a gain-of-function mutation in *Jak2* (*Jak2*^{V617F}) (314). Using mouse models of polycythemia vera, the Frenette and Rivella lab independently demonstrated that macrophage depletion normalised the erythroid compartment of these mice, reducing erythrocytosis (209, 245). Beta-thalassemia is a blood disorder that reduces hemoglobin production (95). Macrophage depletion improved the phenotype of a mouse model of beta-thalassemia, with increased hemoglobin production observed in macrophage depleted mice (245). Considering this data, and the critical role that EBI macrophages play in RBC development, I speculated that EBI macrophages could be contributing to the pathological progression of other RBC disorders. One such disorder is congenital dyserthropoietic anemia type IV (CDA type IV).

Patients with CDA type IV can present with a range of symptoms, including a large number of nucleated RBCs in their peripheral blood, abnormalities in bone marrow erythroblasts, elevated fetal hemoglobin, and iron overload (116, 121). CDA type IV is caused by mutations in the transcription factor KLF1. Of the nine patients world-wide that have been reported with CDA type IV, six carry the mutation KLF1-E325K, which has been associated with genetic disarray and cell cycle arrest in erythroid cells (116, 121, 122, 123, 124, 125, 126, 127, 130, 131, 315). Genotypes are not available for two of the nine patients, and the remaining patient has a novel KLF1 mutation (p.Ser323Leu, S323L) (122, 123, 127).

A possible contribution of EBI macrophages to the erythroid pathologies observed in CDA type IV patients is supported by the following observations:

1. EBI macrophages promote and support the enucleation of developing erythroblasts before they enter circulation. It is therefore interesting to speculate that a disease in which there is a defect in enucleation could in part be associated with a deficiency in EBI macrophages (200, 235).

2. CDA type IV is the result of mutations in KLF1. Aside from the well-defined intrinsic role of KLF1 within the erythroid lineage, an extrinsic role of KLF1 has also been identified within the EBI niche (68). KLF1 has been shown to regulate genes associated with island integrity in EBI macrophages, and island integrity is adversely affected in KLF1-null mouse embryos (68, 201).

CDA type IV is a rare disease, with only 9 reported cases worldwide (116, 117, 118, 121, 122, 123, 124, 125, 126, 315). This makes sourcing any primary cells for investigation very difficult. While careful flushing of bone marrow with divalent-ion containing media has been successfully employed to isolate intact mouse EBIs, this is not a method that has been employed using human bone (205). Intact human EBIs have been isolated from human rib specimens resected during surgery, however there are no recent reports of this technique in the literature (188). The production of cell types associated with the EBI niche from patient-derived iPSCs provides a powerful alternative to model the diseased EBI niche *in vitro*.

The *in vitro* modelling of the human EBI niche is also especially useful for diseases in which animal models do not exactly recapitulate the human disease. This is the case for CDA type IV in which the nan mutant mouse is currently the closest available mouse model. The neonatal anemia mouse carries a mutation in KLF1 (KLF1-E339D) homologous to the KLF1-E325K mutation that is observed in patients, but the phenotype is very different (116, 129). These KLF1-E339D mice present with spherocytosis, in which the erythrocytes have a spherical shape, but do not have any defects in enucleation.

I hypothesised that macrophages generated from a CDA type IV patient-derived iPSC line, and therefore carrying the E325K mutation, could be used to model the diseased EBI niche *in vitro*. This could prove especially useful when dissecting the contribution and interaction of the different cell types in the EBI niche to the disease. For example, patient iPSC-derived macrophages could be cultured with healthy erythroid cells and vice versa to assess both the extrinsic and intrinsic effects of the KLF1 mutation. A fuller understanding of how the KLF1-E325K mutation in EBI macrophages contributes to the patient pathology will also determine whether targeting the niche might be a therapeutic option.

3.2 Aims and Approaches

1. The first aim of the experiments presented in this chapter was to confirm that the disease phenotype in erythroid cells could be recapitulated by cells generated from the CDA type IV patient-derived iPSC line (CDA patient line). To do this, a published iPSC erythroid differentiation protocol was adapted, and the production and phenotype of cells generated were compared (165).

2. The second aim of this chapter was to generate macrophages from the CDA patient line and characterise their phenotype compared to macrophages generated from control iPSC lines.

3. The third aim of this chapter was to assess the function of CDA patient iPSC-derived macrophages in an *in vitro* model of the EBI niche by comparing their ability to support the erythroid differentiation, maturation and enucleation of UCB $CD34^+$ cells to control iPSC-derived macrophages. UCB $CD34^+$ cell-derived erythroid cells have a much higher enucleation rate *in vitro* compared to iPSC-derived erythroid cells, with reported enucleation ranging from 44.20-67.50% (144, 316). This makes UCB $CD34^+$ cell-derived erythroid cells a better option than iPSC-derived erythroid cells to use in an *in vitro* model of the EBI where the output assessed is enucleation.

3.3 Results

3.3.1 Cells generated from CDA patient iPSCs under erythroid differentiation conditions recapitulate disease pathology

3.3.1.1 Establishing an adapted iPSC erythroid differentiation culture system

To establish a protocol for erythroid differentiation from iPSCs, a published protocol from the Dorn lab was adapted (Section 2.1.3) (165). This protocol reported high rates of enucleation for iPSC-derived erythroid cells, up to 60%, through the generation of an intermediate which they termed a 'haematopoietic cell forming complex' (HCFC). This is speculated to roughly mimic the physiological niche of definitive erythropoiesis and therefore in part recapitulates the second stage of erythropoiesis (Figure 3.1A). From these HCFCs, $CD43^+$ haematopoietic progenitors and $CD36^+$ erythroid precursors emerge and are continually released into suspension and collected repeatedly for several weeks. The authors noted that the progenitors released had high erythroid colony-forming potential.

Briefly, the protocol to generate erythroid cells from iPSCs consists of two steps (Figure 3.1). In the Dorn lab protocol, EBs were generated from iPSCs without the addition of cytokines, and these EBs were plated with the addition of SCF, IL-3 and EPO to generate erythroid cells (Figure 3.1B). In adapted protocol, EBs were generated from iPSCs with the addition of BMP4, VEGF, and SCF, and plated with the addition of SCF, IL-3 and EPO (Figure 3.1C). Suspension cells were harvested every seven days for eight weeks and were analysed on the day that they were harvested.

The Dorn lab protocol included a third step of the culture in which harvested suspension cells undergo further erythroid differentiation into mature erythroid cells, and up to 60% undergo enucleation. This was attempted in the adapted protocol however cells did not remain viable 1-2 days post-harvest (Data not shown).

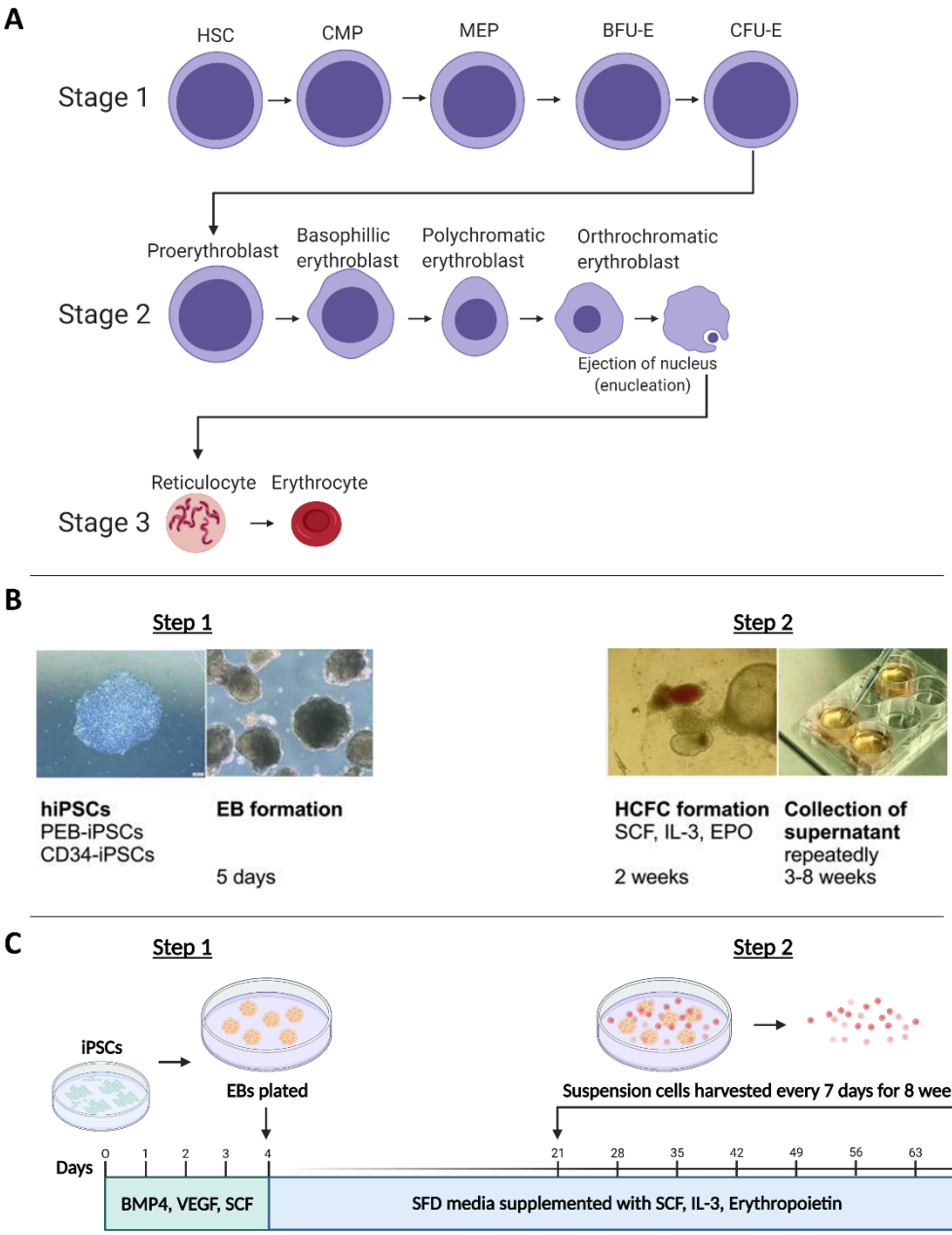

Figure 3.1 Establishment of an erythroid differentiation culture system.
A: A schematic diagram of the three stages of definitive erythropoiesis.
B: The Dorn lab protocol. In step 1, EBs are generated from iPSCs derived from $CD36^+$ erythroblasts (PEB-iPSCs) or umbilical cord blood derived $CD34^+$ cells (CD34-iPSCs) without the addition of cytokines. In step 2, EBs are plated with the addition of SCF, IL-3 and EPO to form HCFCs from which haematopoietic cells emerge. Adapted from Bernecker et al (165).
C: A schematic diagram of the adapted erythroid differentiation culture system. In step 1, EBs are generated from iPSCs derived from fibroblasts, with the addition of BMP4, VEGF, and SCF. In step 2, EBs are plated with the addition of SCF, IL-3 and EPO to generate haematopoietic cells.

3.3.1.2 Cells generated from CDA patient and control iPSCs under erythroid differentiation conditions are morphologically comparable

Cells were generated from the CDA patient iPSC line and two control iPSC lines that possess a wildtype KLF1 genotype (SFCi55 and BM2.3) under erythroid differentiation conditions. Cells generated from the CDA patient iPSC line are morphologically comparable to cells generated from the control iPSC lines (Figure 3.2). Interestingly, macrophages are generated in differentiations from all iPSC lines. These macrophages are in contact with other cells and can be identified by their larger size and the presence of large vesicles throughout the cytoplasm lines (Figure 3.2). This is consistent with previous reports that observed that macrophages were generated in erythroid differentiation conditions from murine embryonic stem cells, and these macrophages were observed to be in contact with erythroid cells (68).

The remaining cells generated from all iPSC lines, which in the Dorn lab protocol consist of haematopoietic progenitors and erythroid precursors, have a spherical shape and range between approximately 10-20 µm in size. This cell size, in combination with the cell morphology and contact with macrophages, suggests that a large proportion of these cells are erythroblasts (40).

This stage of the differentiation protocol recapitulates the second stage of erythropoiesis, and as such the majority of erythroid cells are still nucleated (Figure 3.2). It is therefore not possible to assess whether these CDA patient iPSC-derived erythroid cells have the same defect in enucleation observed in the peripheral blood of CDA patients at this stage (116).

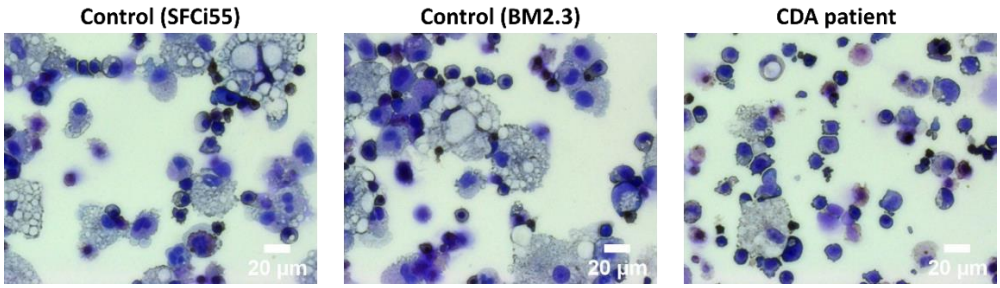

Figure 3.2 Cells generated from CDA patient and control iPSCs under erythroid differentiation conditions are morphologically comparable. Representative Kwik-Diff stained cytospins of suspension cells generated under erythroid differentiations from two control KLF1-WT iPSC lines (SFCi55 and BM2.3) and a CDA type IV patient-derived iPSC line. Cytospins were performed on the day that suspension cells were harvested. 20x magnification. 20 µm scale bar.

3.3.1.3 Significantly fewer CD235a$^+$ cells and CD71$^+$ cells are generated from CDA patient iPSCs compared to control iPSCs under erythroid differentiation conditions

Harvested suspension cells generated under erythroid differentiation conditions from CDA patient iPSCs were assessed for the expression of several cell surface markers and compared to cells generated from control iPSCs.

- CD43: A pan hematopoietic marker, also known as leukosialin or sialophorin. CD43 identifies early progenitors committed to hematopoietic development, before expression of CD45 (317). In hESC culture, the first-appearing CD34$^+$CD43$^+$CD235a$^+$CD41a$^{+/-}$CD45$^-$ cells are representative of precommitted erythro-megakaryocytic progenitors, and CD43$^+$ cells have been identified as the cell population of origin for *in vitro* erythropoiesis (317, 318).
- Epithelial cell adhesion molecule (EpCAM): Also known as CD326. Bone marrow erythroid progenitor cells have been shown to express EpCAM (319, 320). EpCAM is also a marker of erythroid-committed progenitors in *in vitro* differentiations of human PSCs to HSPCs (321). Therefore, EpCAM is an appropriate marker to identify erythroid-committed progenitors in *in vitro* differentiations.
- Glycophorin A (CD235a): CD235a is a transmembrane protein expressed by human erythroid precursors and erythrocytes both *in vivo* and *in vitro* (322).
- Transferrin receptor 1 (CD71): CD71 is a transferrin receptor highly expressed by developing erythroblasts that mediates the uptake of transferrin-iron (323). The vast majority of mature erythrocytes lack CD71 expression, thus making CD71 in combination with CD235a a good marker to distinguish immature and mature erythrocytes (39, 324, 325).

Flow cytometry plots were gated as described (Chapter 2 Section 2.3.1). A comparable percentage of cells generated under erythroid differentiation conditions from all iPSC lines were CD43$^+$ and EpCAM$^+$, with no significant difference observed in the numbers of cells positive for either marker between iPSC lines (Figure 3.3).

There were significantly fewer CD235a$^+$ cells generated from CDA patient iPSCs compared to control iPSCs (Figure 3.3). The percentage of CD235a$^+$ cells generated

under erythroid differentiation conditions, averaged across harvests: control (SFCi55) 68.26%$^{+}$, control (BM2.3) 72.31%$^{+}$, and CDA patient 8.24%$^{+}$.

There were also significantly fewer CD71^{+} cells generated from CDA patient iPSCs compared to control iPSCs (Figure 3.3). The percentage of CD71^{+} cells generated under erythroid differentiation conditions, averaged across harvests: control (SFCi55) 70.56%$^{+}$, control (BM2.3) 47.05%$^{+}$, and CDA patient 17.38%$^{+}$.

These data are consistent with previously published RNA-sequencing data that analysed erythroid cells generated from healthy donor and CDA type IV patient-derived PBMCs and showed a downregulation of the genes encoding for CD235a and CD71 in CDA patient cells (131).

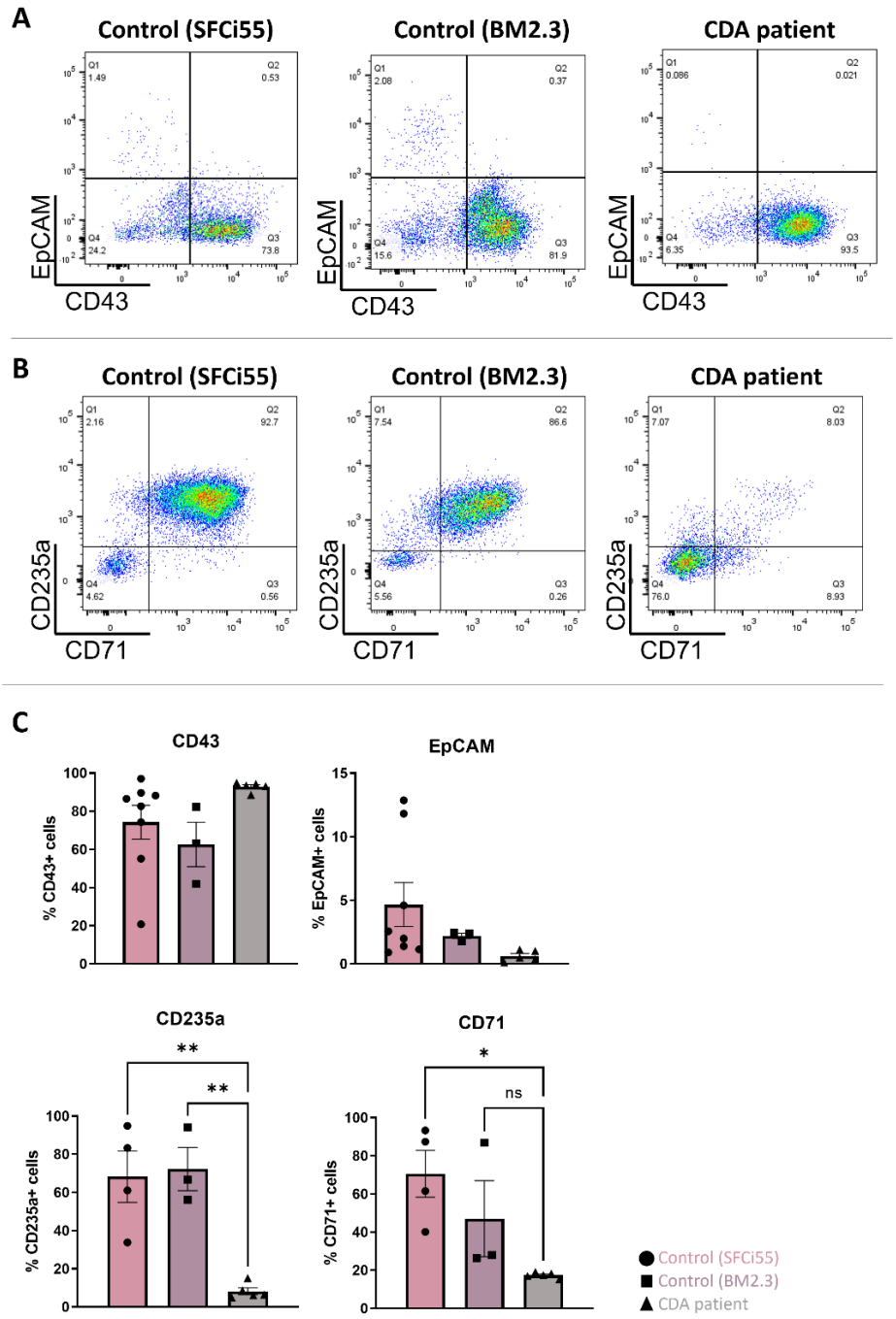

Figure 3.3 Significantly fewer CD235a$^+$ cells and CD71$^+$ cells are generated from CDA patient iPSCs under erythroid differentiation conditions. Flow cytometry analyses were performed on suspension cells generated under erythroid differentiation conditions from two control iPSC lines (SFCi55 and BM2.3) and a CDA type IV patient-derived iPSC line. Suspension cells were assessed on the day that they were harvested. **A:** Representative flow cytometry plots of suspension cells generated under erythroid differentiation conditions assayed for expression of CD43 and EpCAM. **B:** Representative flow cytometry plots of suspension cells generated under erythroid differentiation conditions assayed for expression of CD235a and CD71. **C:** Quantification of flow cytometry analyses of the percentage of cells expressing each marker. Datapoints represent individual suspension cell harvests. Error bars represent SEM. One-way ANOVA with Tukey post-test. *$p < 0.05$, **$p < 0.01$.

3.3.1.4 *GYPA, TFRC, SLC4A1, HBA1 and ICAM4* are downregulated in cells generated from CDA patient iPSCs compared to control iPSCs under erythroid differentiation conditions

Harvested suspension cells generated under erythroid differentiation conditions from CDA patient iPSCs were assessed for the expression of several erythroid genes that were previously identified as being expressed at lower levels in cells generated from CDA type IV patient PBMCs compared to the appropriate control cells (131).

- *GYPA*: Encodes for CD235a, a transmembrane protein expressed on human erythrocytes with a poorly characterised molecular function (326, 327).
- *TFRC*: Encodes for CD71, a transferrin receptor mediates the uptake of transferrin-iron (323).
- *SLC4A1*: Encodes for BAND 3, a membrane transport protein that also comprises part of the ankyrin complex that anchors the RBC cytoskeleton to its cell membrane (328, 329).
- *HBA1*: Encodes for the alpha chain of adult hemoglobin. Shortly after birth, there is a switch from fetal to adult hemoglobins (330). CDA type IV patients have been reported to present with elevated and high levels of fetal hemoglobin (116, 118, 121, 124, 125, 331).
- *KLF1*: Total *KLF1* expression was previously identified to be lower in CDA erythroid cells (131).
- *ICAM4:* Also known as Landstein-Wiener blood group antigen. A KLF1-regulated adhesion molecule that binds to αV integrin expressed by EBI macrophages and therefore EBI integrity (219).

Consistent with previously published data, *GYPA, TFRC, SLC4A1, HBA1* and *ICAM4* were downregulated in cells generated from the CDA patient iPSCs compared to control iPSCs (131) (Figure 3.4). KLF1 expression in cells generated from CDA patient iPSCs was comparable to cells generated from control iPSCs (Figure 3.4).

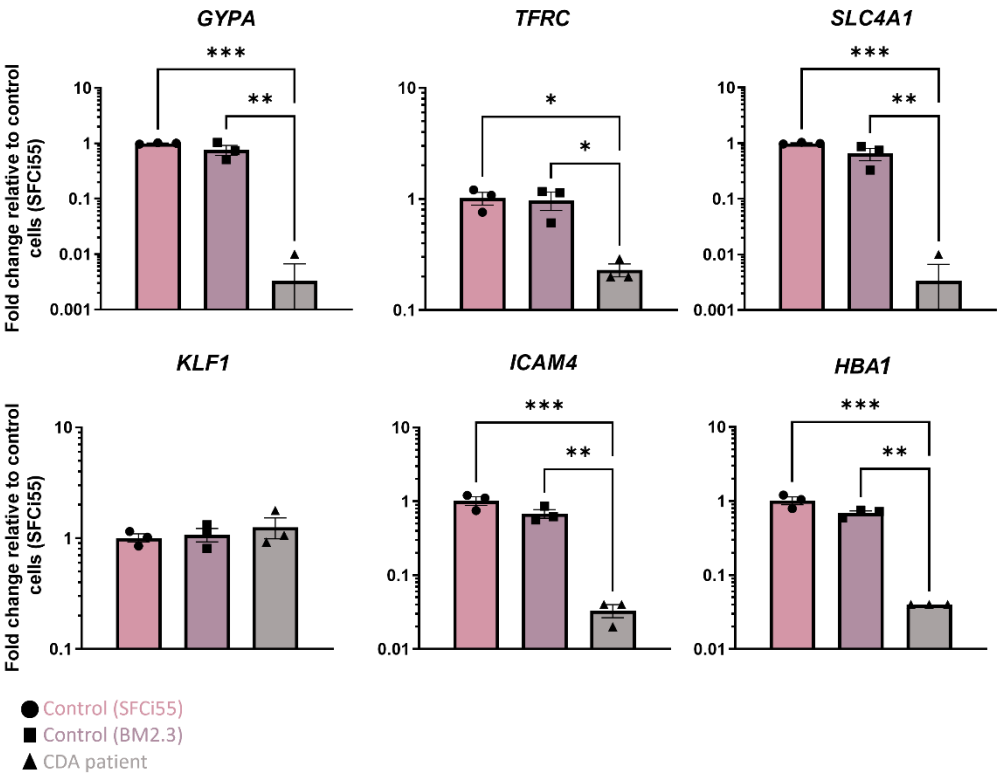

Figure 3.4 *GYPA*, *TFRC*, *SLC4A1*, *HBA1* and *ICAM4* are downregulated in cells generated from CDA patient iPSCs under erythroid differentiation conditions. qRT-PCR of RNA extracted from suspension cells generated under erythroid differentiation conditions from two control iPSC lines (SFCi55 and BM2.3) and a CDA patient iPSC line. RNA was taken on the day that suspension cells were harvested. Datapoints represent individual suspension cell harvests Fold change analysed relative to cells generated from SFCi55 iPSCs under erythroid differentiation conditions. Error bars represent SEM. One-way ANOVA with Tukey post-test. *p < 0.05, **p < 0.01**,** *** p <0.001.

3.3.1.5 Characterisation of erythroid differentiation hematopoietic output by methylcellulose assay

In an attempt to characterise the haematopoietic output of suspension cells generated under erythroid differentiation conditions, methylcellulose assays were attempted on suspension cells on the day that they were harvested. However, no colonies were formed from cells generated under erythroid differentiation conditions from all cell lines.

3.3.2 CDA patient iPSC-DMs are comparable to control iPSC-DMs

Macrophages were generated from the CDA patient iPSC line and two control iPSC lines (SFCi55 and BM2.3) in a three-step protocol (Figure 3.5) (305). In Step 1, iPSCs were mesodermally primed with the addition of BMP4, VEGF, and SCF, and formed EBs. In Step 2, EBs were plated with the addition of IL-3 and M-CSF to induce the release of macrophage precursors into suspension. In the third step, macrophage precursors were harvested from suspension twice per week and terminally differentiated into mature macrophages with M-CSF for 11 days. Macrophages were analysed after 11 days of terminal maturation.

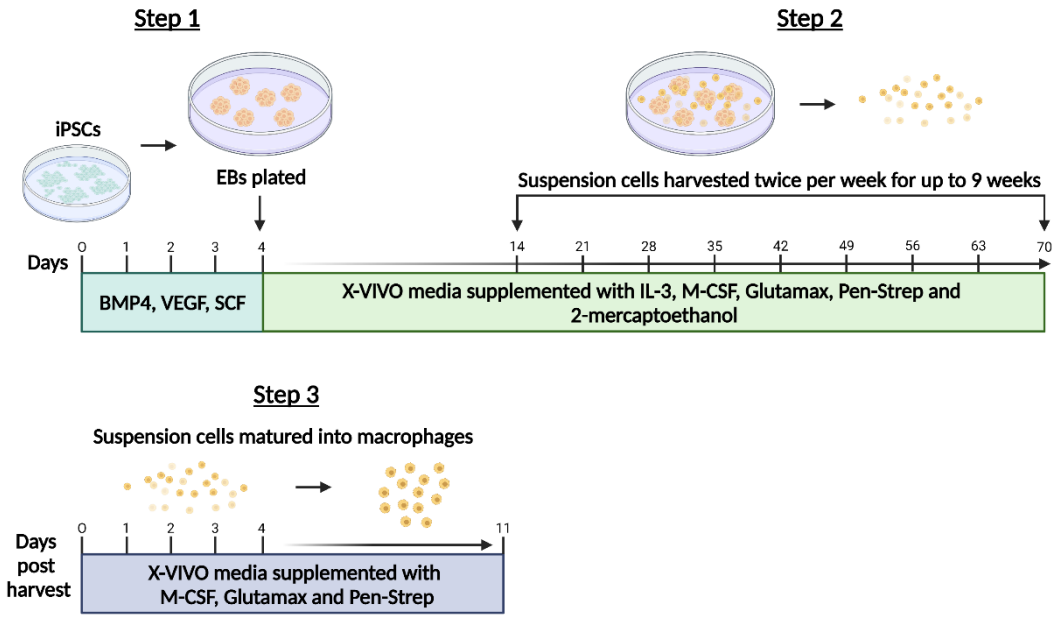

Figure 3.5 iPSC-derived macrophage differentiation protocol (305)**.** In step 1 of the differentiation, iPSCs are mesodermally primed with BMP4, VEGF, and SCF, and form EBs. In step 2, EBs are plated and cultured with IL-3 and M-CSF and after 2 weeks release macrophage precursors into suspension. In the third step, these macrophage precursors are harvested and terminally differentiated into mature macrophages with the addition of M-CSF.

3.3.2.1 CDA patient iPSC-DMs are comparable to control iPSC-DMs in terms of morphology

Macrophages were generated from CDA patient iPSCs (CDA patient iPSC-DMs) and had a comparable morphology to macrophages generated from control iPSCs (control iPSC-DMs) (Figure 3.6). Macrophages generated from all iPSC lines ranged between 20-40 µm in size, with a small nucleus and numerous large vesicles throughout the cytoplasm (Figure 3.6). This morphology is characteristic of *in vitro* PSC-derived macrophages (201, 254, 303, 305). In contrast to cells generated under erythroid differentiation conditions in which both erythroid cells and macrophages were observed (Figure 3.2), macrophage differentiation conditions generated a pure macrophage population (Figure 3.6).

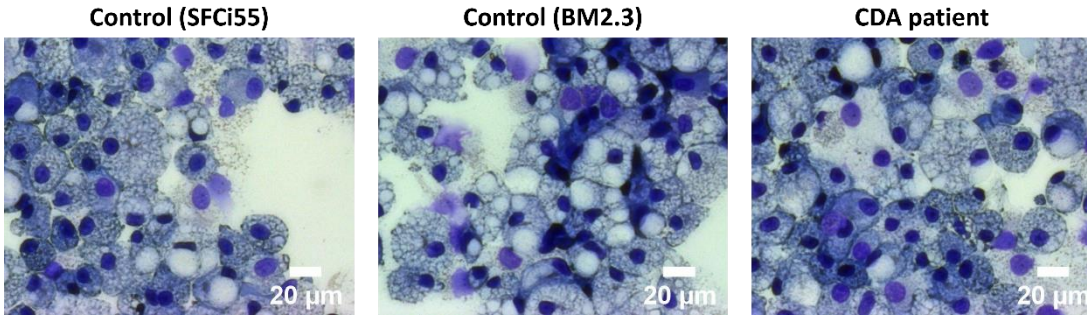

Figure 3.6 CDA patient iPSC-DMs are comparable to control iPSC-DMs in terms of morphology. Representative Kwik-Diff stained cytospins of macrophages generated from two control iPSC lines (SFCi55 and BM2.3) and a CDA type IV patient-derived iPSC line. 20x magnification. 20 µm scale bar.

3.3.2.2 CDA patient iPSC-DMs are comparable to control iPSC-DMs in terms of cell surface marker expression

CDA patient iPSC-DMs were assessed for expression of several cell surface markers to assess their haematopoietic lineage commitment and maturation in comparison to control iPSC-DMs:

- CD45: A pan leukocyte marker. CD45 is expressed on all nucleated haematopoietic cells (332).
- CD93: A highly glycosylated transmembrane protein expressed on monocytes, endothelial cells, neutrophils and stem cells (333). CD93 is not expressed by mature macrophages (334).

- 25F9: The 25F9 monoclonal antibody recognises an uncharacterised protein specifically expressed on the surface of mature human macrophages (334). Expression is not found on monocytes or immature macrophages, thus making 25F9 in combination with CD93 a good marker to distinguish immature and mature macrophages.
- CD163: Exclusively expressed by monocytes and macrophages, CD163 is a receptor that scavenges haemoglobin by mediating endocytosis of hemoglobin-haptoglobin complexes (335, 336, 337). CD163 has also been identified as erythroblast adhesion receptor within the EBI (221).
- CD169: Also known as Siglec-1, CD169 is expressed on different macrophage subpopulations including iPSC-derived macrophages, bone marrow macrophages and Kupffer cells (305, 338). CD169 is also heterogeneously expressed on EBI macrophages (205).

Flow cytometry plots were gated as described (Chapter 2 Section 2.3.2). Haematopoietic commitment was assessed using the marker CD45, and a comparable percentage of iPSC-DMs from all iPSC lines were $CD45^+$ (Figure 3.7). Macrophage maturity was assessed using the markers CD93 and 25F9. Mature macrophages are negative for the monocyte marker CD93, and positive for the mature macrophage marker 25F9. A comparable percentage of iPSC-DMs from all iPSC lines are $CD93^+$ and $25F9^+$ (Figure 3.7). CD163 and CD169 were selected to assess cell surface expression of markers expressed by EBI macrophages. A comparable percentage of iPSC-DMs from all iPSC lines were $CD163^+$ and $CD169^+$ (Figure 3.7).

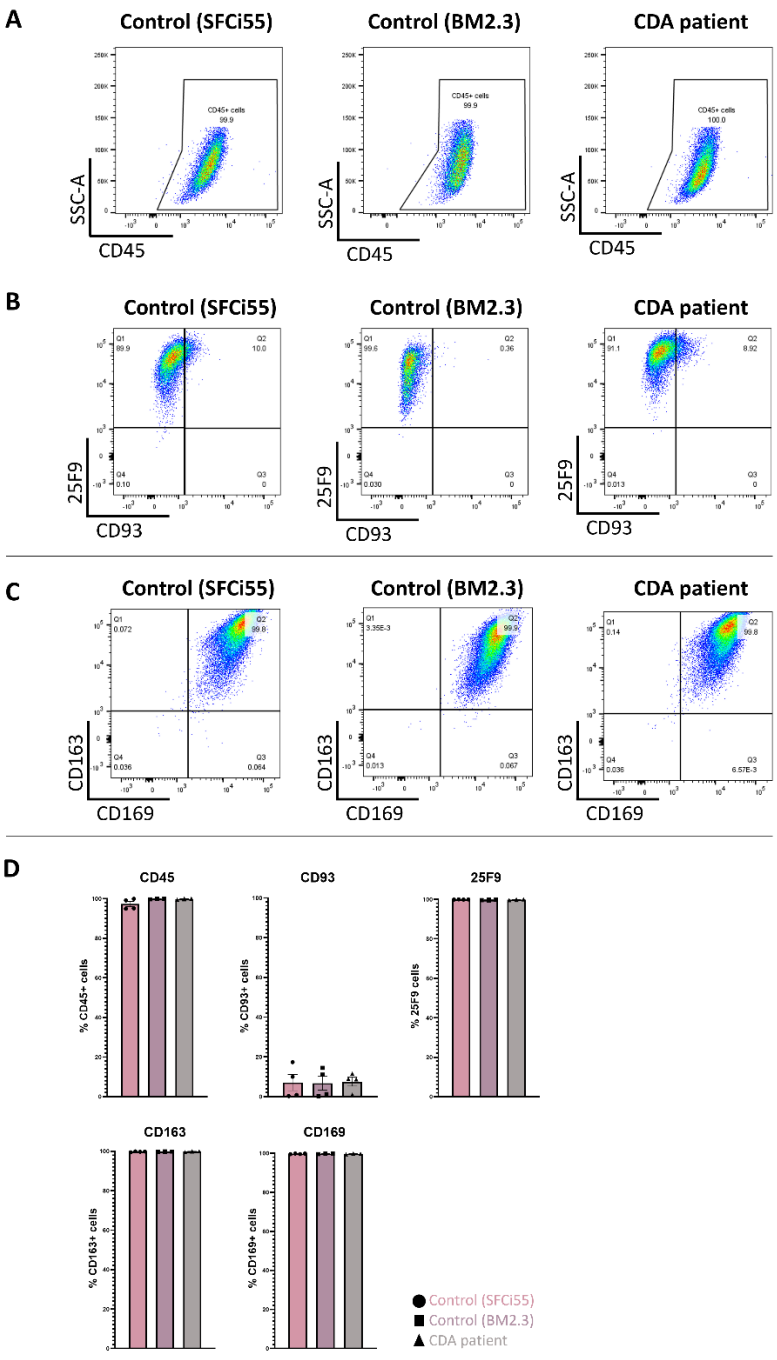

Figure 3.7 CDA patient iPSC-DMs are comparable to control iPSC-DMs in terms of cell surface marker expression. Flow cytometry analyses were performed on iPSC-DMs generated from two control iPSC lines (SFCi55 and BM2.3) and a CDA type IV patient-derived iPSC line.

A: Representative flow cytometry plots of iPSC-DMs assayed for expression of CD45.

B: Representative flow cytometry plots of iPSC-DMs assayed for expression of CD93 and 25F9.

C: Representative flow cytometry plots of iPSC-DMs assayed for expression of CD163 and CD169.

D: Quantification of flow cytometry analyses of the percentage of cells expressing each marker. Datapoints represent individual macrophage harvests. Error bars represent SEM. One-way ANOVA with Tukey post-test generated no statistically significant p-values.

3.3.2.3 CDA patient iPSC-DMs are comparable to control iPSC-DMs in terms of gene expression

CDA patient iPSC-DMs were assessed for expression of the following EBI macrophage associated genes: *TNF-α, CMAF, PECAM-1, ITGAV, CD11a, CD11b, EMP/MAEA, VCAM1, CD68, CD163, CD169,* and *CD64.* CDA patient iPSC-DMs expressed comparable levels of all genes compared to control iPSC-DMs (Figure 3.8).

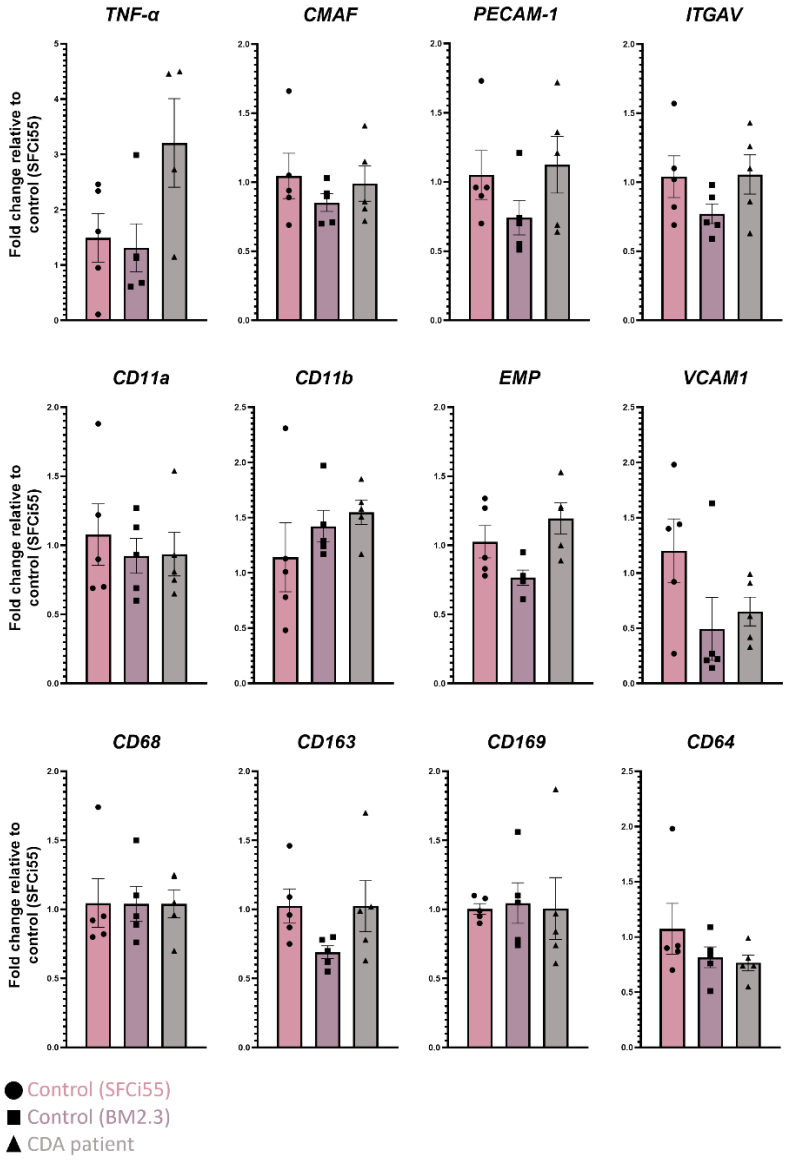

Figure 3.8 CDA patient iPSC-DMs are comparable to control iPSC-DMs in terms of gene expression. qRT-PCR of RNA extracted from macrophages generated from two control iPSC lines (SFCi55 and BM2.3) and a CDA patient iPSC line. Datapoints represent individual macrophage harvests. Error bars represent SEM. One-way ANOVA with Tukey post-test generated no statistically significant p-values.

3.3.2.4 CDA patient iPSC-DMs are functionally comparable to control iPSC-DMs in a model of the erythroblastic island niche

The majority of patients with CDA type IV have a KLF1-E325K mutation and present with a large number of nucleated RBCs in their peripheral blood (116, 121, 122, 123, 124, 125, 126, 127, 131, 315). The enucleation step of erythropoiesis takes place within the EBI, supported and promoted by EBI macrophages. It was therefore hypothesised that KLF1-E325K might affect the macrophage compartment of the EBI niche in CDA type IV patients, reducing macrophages ability to support and promote erythroblast enucleation, contributing to the disease pathology.

To assess whether KLF1-E325K affects the function of EBI macrophages, CDA patient iPSC-DMs were used in an *in vitro* model of the EBI niche. In this model, iPSC-DMs were co-cultured with UCB-derived $CD34^+$ cells under erythroid differentiation cell culture conditions (Figure 3.9). Erythroid differentiation efficiency was measured by assessing the proportion of mature enucleated erythroid cells in the culture by flow cytometry on days 11, 14 , 18 and 21. Macrophages predominantly remain adherent in the culture, therefore analysis of only the suspension cell population enriches for differentiating UCB-derived $CD34^+$ cells. Flow cytometry plots were gated as described (Chapter 2 Section 2.3.3).

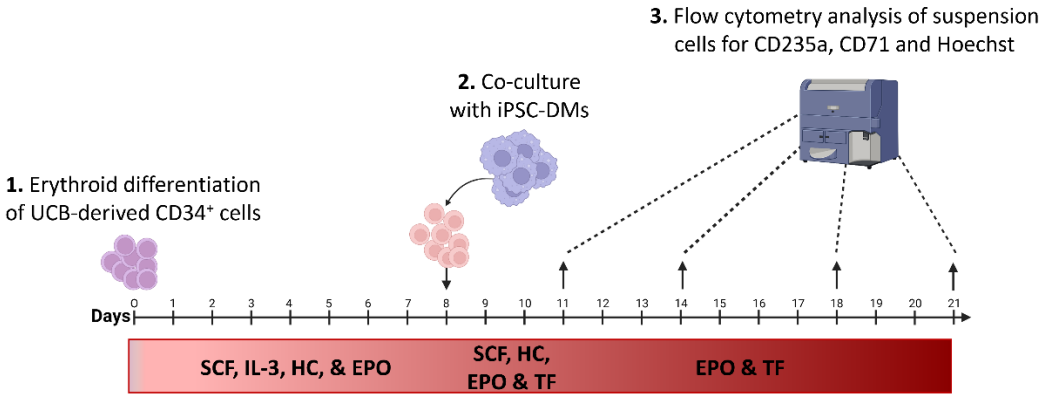

Figure 3.9 *In vitro* erythroblastic island model protocol. Day 0-8: UCB-derived $CD34^+$ cells were cultured with SCF, IL-3, hydrocortisone (HC) and EPO. Day 8-11: iPSC-DMs were added and cultured with the erythroid progenitors with SCF, HC, EPO and transferrin (TF). Day 11-21: Co-cultures were cultured with EPO and TF. At days 11, 14, 18 and 21 suspension cells were analysed by flow cytometry for expression of CD235a, CD71 and Hoechst.

Based on cytospin analyses of suspension cells sampled at each timepoint, which were not quantified, cells cultured with iPSC-DMs were observed to form EBI structures in which the differentiating erythroblasts attach to the macrophages (Figure 3.10). Flow cytometry analyses showed that from day 11 to day 21, the suspension cells decreased in size, as shown by forward scatter (Figure 3.10). There was a corresponding increase in the percentage of $CD235a^+$ cells and a decrease in $CD71^+$ cells indicating the maturing of erythrocytes (Figure 3.10). Loss of CD71 expression coincided with the loss of Hoechst staining, a DNA/nuclear marker (Figure 3.10). The loss of this nuclear marker is an indication that the erythroid cell has ejected its nucleus and can be referred to as enucleated. Therefore, a mature and enucleated erythrocyte is marked by positive expression of CD235a, and negative expression of CD71 and Hoechst ($CD235a^+CD71^-Hoechst^-$).

There was a progressive increase in the percentage of $CD235a^+$ suspension cells in the cultures, and by day 21 over 96% of suspension cells in all conditions were $CD235a^+$ (Figure 3.10). In agreement with previous studies, the presence of macrophages in the culture significantly increased erythroblast maturation and enucleation (Figure 3.10) (201, 211, 212). Averaged across cell lines, the percentage of mature enucleated erythroid cells increased from around 20% when cells were cultured alone to around 55-60% when cells were cultured in the presence of iPSC-DMs (Figure 3.10).

CDA patient iPSC-DMs supported erythroid cell maturation and enucleation at comparable levels to control iPSC-DMs. The percentage of $Hoechst^-CD71^-$ cells in cultures with CDA patient iPSC-DMs comparable to the percentage of $Hoechst^-CD71^-$ cells in cultures with control iPSC-DMs at each timepoint (Figure 3.10).

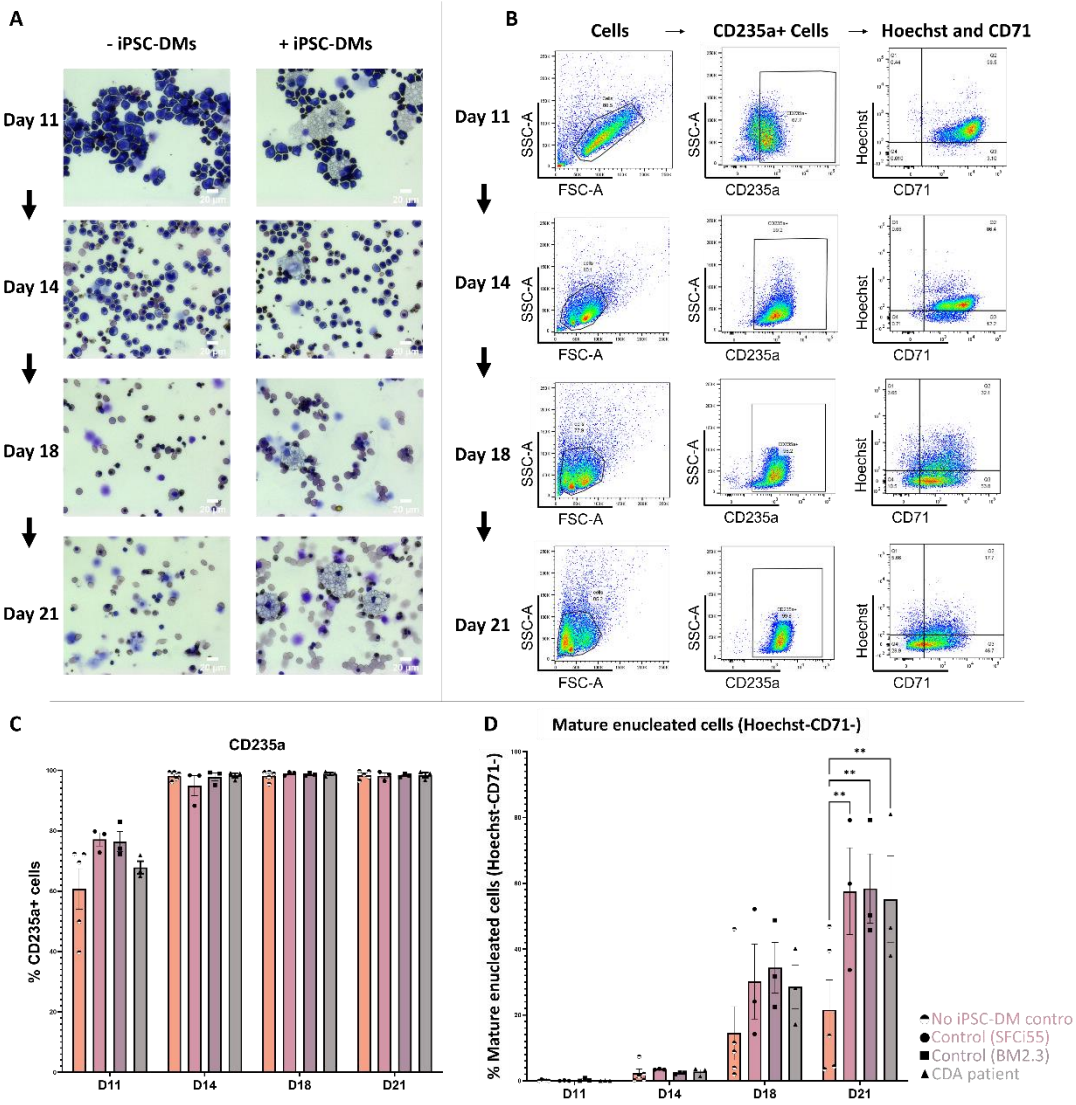

Figure 3.10 CDA patient iPSC-DMs are functionally comparable to control iPSC-DMs in an *in vitro* EBI model.

A: Representative Kwik-Diff stained cytospins of $CD34^+$ cells cultured in the presence or absence of iPSC-DMs on days 11, 14, 18 and 21 of the culture.

B: Representative flow cytometry plots of suspension cells assayed for CD235a, CD71 and Hoechst for days 11, 14, 18 and 21 of the culture.

C: Quantification of flow cytometry analyses of the percentage of suspension cells expressing CD235a for days 11, 14, 18 and 21 of the culture. Datapoints represent individual experiments. Error bars represent SEM. One-way ANOVA with Tukey post-test generated no statistically significant p-values.

D: Quantification of flow cytometry analyses of the percentage of Hoechst-CD71- suspension cells for days 11, 14, 18 and 21 of the culture. Datapoints represent individual experiments. Error bars represent SEM. One-way ANOVA with Tukey post-test. *$p < 0.05$, **$p < 0.01$.

3.3.2.5 iPSC-DMs express low levels of KLF1

A previous study observed that KLF1 is expressed at very low levels in iPSC-DMs (201). To investigate KLF1 expression levels, in both control and CDA patient iPSC-DMs, CT values of genes analysed previously in section 3.3.2.3 were compared to the CT values of the reference gene GAPDH. This allowed for comparison of relative expression between KLF1 and other genes. Compared to other genes in this analysis, KLF1 was expressed at the lowest level (Figure 3.11). CT values for KLF1 were consistently high in macrophages generated from all iPSC lines indicating low expression levels. Based on previous studies,I would expect KLF1 levels to be higher in EBI macrophages, therefore I concluded that the CDA patient iPSC-derived macrophages characterised in this chapter may not represent a good model of an EBI macrophage (68, 201).

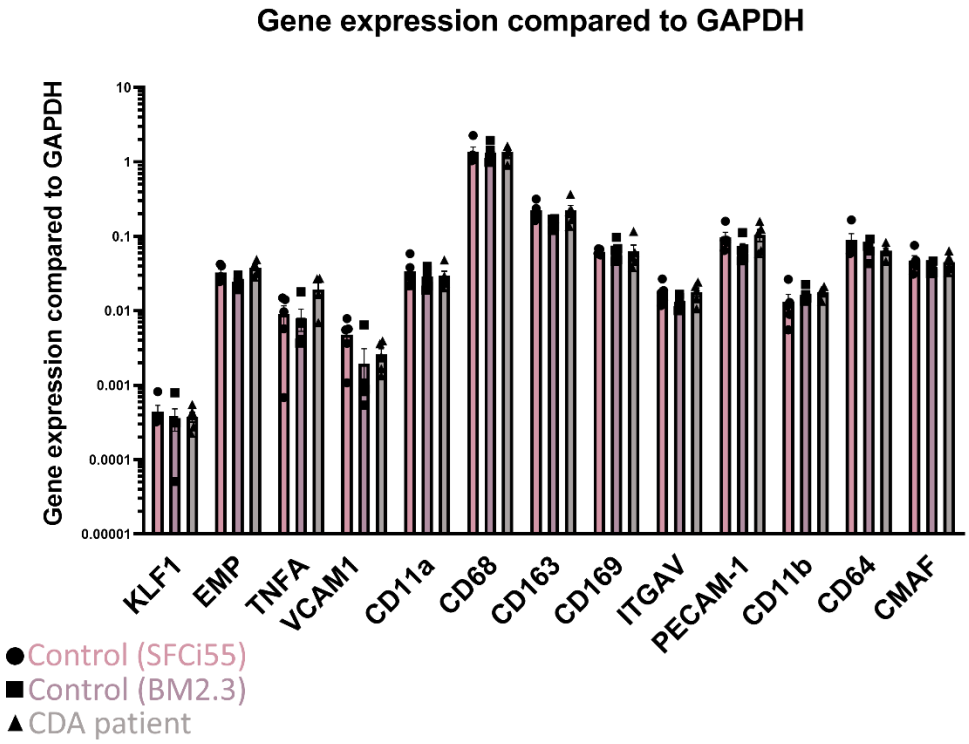

Figure 3.11 iPSC-DMs express low levels of *KLF1*. qRT-PCR of RNA extracted from macrophages generated from two control iPSC lines (SFCi55 and BM2.3) and a CDA patient iPSC line. Datapoints represent individual macrophage harvests. Gene expression was analysed compared to GAPDH. Error bars represent SEM.

3.4 Discussion

I have shown that cells generated from CDA patient iPSCs under erythroid differentiation conditions recapitulate the disease phenotype. There is a significant decrease in the populations of $CD235a^+$ cells and $CD71^+$ cells generated from CDA patient iPSCs compared to those derived from control iPSCs. Additionally, *GYPA, TFRC, SLC4A1, HBA1* and *ICAM4* are expressed at a lower level in cells derived from CDA patient iPSCs cells compared to controls, consistent with findings in a previous study (131). Macrophages generated from CDA patient iPSCs have comparable morphology, cell surface marker expression and gene expression to macrophages generated from control iPSC lines. CDA patient iPSC-DMs function within the EBI niche at comparable levels to control iPSC-DMs, and iPSC-DMs from all iPSC lines express low levels of *KLF1*.

3.4.1 iPSC erythroid differentiation culture system

One of main advantages to the erythroid differentiation culture system used in this chapter compared to other protocols is that it is a harvestable system. Suspension cells can be harvested from plates once every 7 days, and these harvests are the only media changes made throughout the culture. This system was adapted from a protocol that uses low numbers of supporting cytokines and is therefore much more cost effective than other published protocols in which the addition of over 10 cytokines can be required (159, 165, 178). Additionally, these protocols require careful modulation of these cytokines, whereas in this system IL-3, SFC and EPO are added only once every 7 days when the media is changed and is therefore a much simpler culture system (159, 165, 178). This protocol therefore consumes less media, is less complex, and has a high output of cells compared to other published protocols (159, 165, 178).

The Dorn lab reported that CD43 expression is progressively gained in the first three weeks of culture, and therefore suspension cells were only harvested and analysed in my system three weeks after the plating of EBs (165). The Dorn lab protocol reported that over 90% of suspension cells were $CD43^+$ which is higher than my system in which 77% of cells generated from all iPSC lines were $CD43^+$. The Dorn lab used CD36 as a marker for erythroid progenitors and reported that approximately

80% of suspension cells were $CD36^+$ (165). In this study I used the human erythroid cell marker CD235a, and approximately 60% of suspension cells generated from control WT iPSC lines were $CD235a^+$, which was lower than the published protocol.

It is interesting to note that the protocol published by the Dorn lab used human iPSC lines generated from both cord blood $CD34^+$ cells and $CD36^+$ erythroblasts (165). The iPSC lines used in this chapter were generated from fibroblasts. Persistent donor cell-specific gene expression patterns have been identified in human iPSCs produced from different cell types, which suggests an influence of the cell type of origin on the resulting iPSC (339). Additionally, the cell type of origin has been identified to affect differentiation of human iPSCs, for example iPSCs generated from endothelial cells were better able to differentiate into endothelial cells than iPSCs generated from fibroblasts and cardiac progenitor cells (340). This could explain why more haematopoietic and erythroid progenitors were generated in the published protocol compared to those reported in this chapter. In contrast, a previous report has shown that erythroid differentiation of human iPSCs was independent of the donor cell type of origin, however this used a different erythroid differential protocol and did not include fibroblasts as a cell type of origin (167).

The Dorn lab culture system harvested suspension cells for a further 18 days in a three-phase erythropoiesis assay (167). Suspension cells generated in this chapter using the adapted protocol were put in the same further erythroid differentiation cultures, however cells did not remain viable 1-2 days post-harvest (Data not shown). It is possible that this is caused by the replacement of the STEMdiff media (STEMCELL Technologies) used in the published protocol with the SFD media used in this adapted protocol. SFD media is more cost effective, and EBs cultured in SFD with EPO, SCF and IL-3 were able to generate erythroid progenitors. The composition of STEMdiff media is proprietary information, therefore it can only be speculated that the media contains a factor that promotes erythroid progenitor viability allowing them to be terminal differentiated. The composition of media for the further erythroid culture in both the published and adapted protocol were the same.

In a single-cell RNA sequencing dataset generated on human HSPCs derived at day 10 of iPSC differentiation, *EpCAM* was predominantly expressed throughout the

erythroid annotated clusters (321). Therefore, EpCAM was selected as a marker to identify HSPCs that had committed to the erythroid lineage in the erythroid differentiation protocol used in this study. However, I noted that *EpCAM* was expressed on only a very small minority of cells generated in the differentiation of all iPSC lines suggesting that at the stage of differentiation tested, the cells had matured beyond this erythroid commitment step and had lost expression of this marker. Consistent with this interpretation, the morphology of the cells generated from both the control and CDA patient iPSC lines indicated that they had progressed to an erythroblast stage of erythropoiesis and that it is likely that these populations of cells contain few erythroid committed HSPCs i.e., $EpCAM^{+}$ cells.

3.4.2 Assessment of CDA disease pathology in cells generated from CDA patient iPSCs under erythroid differentiation conditions

iPSCs have been reported to be able to successfully model disease-specific pathologies, for example motor neurons generated from iPSCs reprogrammed from a child with spinal muscular atrophy displayed features of the disease (310). In this study, cells generated from CDA patient iPSCs under erythroid differentiation conditions recapitulated features of CDA erythroid cells, including downregulation of *GYPA*, *TFRC*, *SLC4A1*, *HBA1* and *ICAM4* (131).

The low viability of harvested suspension cells prevented further erythroid culture, and therefore it could not be assessed whether the cells generated from CDA patient iPSCs recapitulated the low enucleation rates observed in CDA patient erythroid cells. However, while the erythroid cell enucleation rates reported using the Dorn lab protocol are high for iPSC-erythroid differentiations, up to 60%, this is still low compared to *in vivo* RBCs (165). Therefore, iPSC-derived erythroid cells are limited as models for RBC disorders in which defective enucleation is a feature, such as CDA type IV (116, 121).

3.4.3 iPSC-DMs express low levels of KLF1

Expression of the *KLF1* gene is very low in both CDA patient iPSC-DMs and control iPSC-DMs. A previous report in the Forrester lab demonstrated that iPSC-DMs that carried a transgene that increases *KLF1* expression 60-fold were more 'EBI macrophage-like', with increased expression of EBI-related macrophage genes and

an increased functional effect on erythroid cell maturation and enucleation (201). Thus, as a result of their low KLF1 expression, the iPSC-DMs generated from control and patient iPSCs may not be an accurate model of an EBI macrophage. This might explain why no functional differences on UCB $CD34^{+}$-derived erythroid cell maturation and enucleation were observed between control and CDA patient iPSC-DMs. Any transcriptional dysregulation or functional defect in CDA patient EBI macrophages as a result of the mutation may not be revealed because KLF1 expression is so low.

Chapter 4: Generation and Validation of an Inducible KLF1-E325K Activation System

4.1 Introduction

A human iPSC line expressing a 4OH-tamoxifen inducible KLF1 fusion protein (KLF1-ER^{T2}) was previously generated in the Forrester lab (172). In this system, the KLF1 expression vector (pZDonor-AAVS1-CAG-HA-KLF1-ER^{T2}-PolyA) was targeted into the AAVS1 'safe-harbor' locus of the SFCi55 human iPSC line. The AAVS1 locus, in intron 1 of PPP1R12C (protein phosphate 1 regulatory subunit 12C), has been reported as a 'safe harbor' because integration of sequences into this locus are not subject to silencing and do not have adverse effects on the cell (169, 341). The CAG promotor used here was previously identified to drive high levels of transgene expression during stem cell differentiation towards mesoderm and is therefore appropriate for use in experiments in this and the subsequent chapter in which erythroid cells and macrophages are generated from mesodermally primed EBs (342). The pZDonor-AAVS1-puromycin vector was used as the back-bone vector. The resulting inducible KLF1-WT iPSC line (iKLF1-WT) constitutively expressed KLF1 protein in the cytoplasm of the cell. The ER^{T2} domain sequesters KLF1 in the cytoplasm via association with the HSP90 chaperone (343). Upon 4OH-tamoxifen addition, the KLF1-ER^{T2} fusion protein dissociates from HSP90 and translocates to the nucleus, where it can function as a transcription factor and is therefore active.

iPSCs from the iKLF1-WT line were differentiated into macrophages and incorporated into the *in vitro* model of the EBI niche described in the previous chapter. Activation of KLF1-WT in iPSC-DMs, via 4OH-tamoxifen addition, induced a more 'EBI macrophage-like' phenotype. KLF1-WT activation in iPSC-DMs increased expression of several EBI-associated genes and cell surface markers such as CD163 and CD11b (201). Within the *in vitro* EBI model, there was an increase in the percentage of mature enucleated erythroid cells in suspension cell populations cultured with KLF1-WT activated macrophages. This increase was identified to be, in part, the result of up-regulation of the secreted factors IL-33, SERPINB2 and ANGPTL7, which were demonstrated to promote erythroid cell maturation and enucleation (201).

Macrophages generated from the CDA patient-derived iPSC line in the previous chapter have a very low level of endogenous KLF1-expression (Figure. 3.10). I therefore hypothesised that macrophages generated from a KLF1-E325K inducible

activation iPSC line (iKLF1-E325K), which would have increased expression of *KLF1-E325K* due to the CAG promotor, would be a more appropriate model for a CDA patient EBI macrophage. In addition to increasing the expression levels of *KLF1-E325K* in iPSC-DMs, this strategy also provides isogenic controls. The effect of KLF1-E325K activation can be assessed by comparing cells in the presence (activation) and absence of 4OH-tamoxifen. As the iKLF1-E325K cell lines were generated from the same parental line as the KLF1-WT cell line (SFCi55) and therefore have the same genetic background, comparison of these lines allows for the assessment of the effect of KLF1-E325K only.

4.2 Aims and Approaches

1. The first aim of this chapter was to generate a pZDonor-AAVS1-CAG-HA-KLF1-E325K-ER^{T2}-PolyA construct by site directed mutagenesis of an existing pZDonor-AAVS1-CAG-HA-KLF1-ER^{T2}-PolyA construct.

2. The second aim was to generate an iPSC line carrying an inducible KLF1-E325K activation system where a pZDonor-AAVS1-CAG-HA-KLF1-E325K-ER^{T2}-PolyA construct was targeted to the *AAVS1* locus.

3. The third aim was to generate erythroid cells from inducible KLF1-E325K iPSC lines and to investigate whether this strategy could recapitulate the CDA disease phenotype in erythroid cells.

4.3 Results

4.3.1 Generation of inducible KLF1-E325K iPSC lines

4.3.1.1 Generation of pZDonor-AAVS1-CAG-HA-KLF1-E325K-ER^{T2}-PolyA plasmid

The KLF1-E325K mutation (c.973G>A) was introduced into an existing pZDonor-AAVS1-CAG-HA-KLF1-ER^{T2} plasmid via site-directed mutagenesis. Due to the GC-rich sequences contained in both the CAG promotor and KLF1 gene, site-directed mutagenesis could not be performed on the whole plasmid. Therefore, the mutation was introduced using a three-part subcloning strategy (Figure 4.1).

1. A fragment of the existing KLF1-WT plasmid was excised using restriction enzymes at EcoRI and HindIII restriction sites. The resulting fragment was subcloned into a pBR332 plasmid at the same restriction sites. This resulted in the generation of a pBR332-KLF1-WT plasmid (Figure 4.1A).

2. Site-directed mutagenesis was performed on the pBR332-KLF1-WT plasmid to introduce the c.973G>A mutation, generating a pBR332-KLF1-E325K plasmid (Chapter 2 Section 2.2.3) (Figure 4.1B).

3. A fragment of this pBR332-KLF1-E325K was excised using restriction enzymes and ligated back into the existing plasmid backbone to generate the pZDonor-AAVS1-CAG-HA-KLF1-E325K-ER^{T2} plasmid (Figure 4.1A).

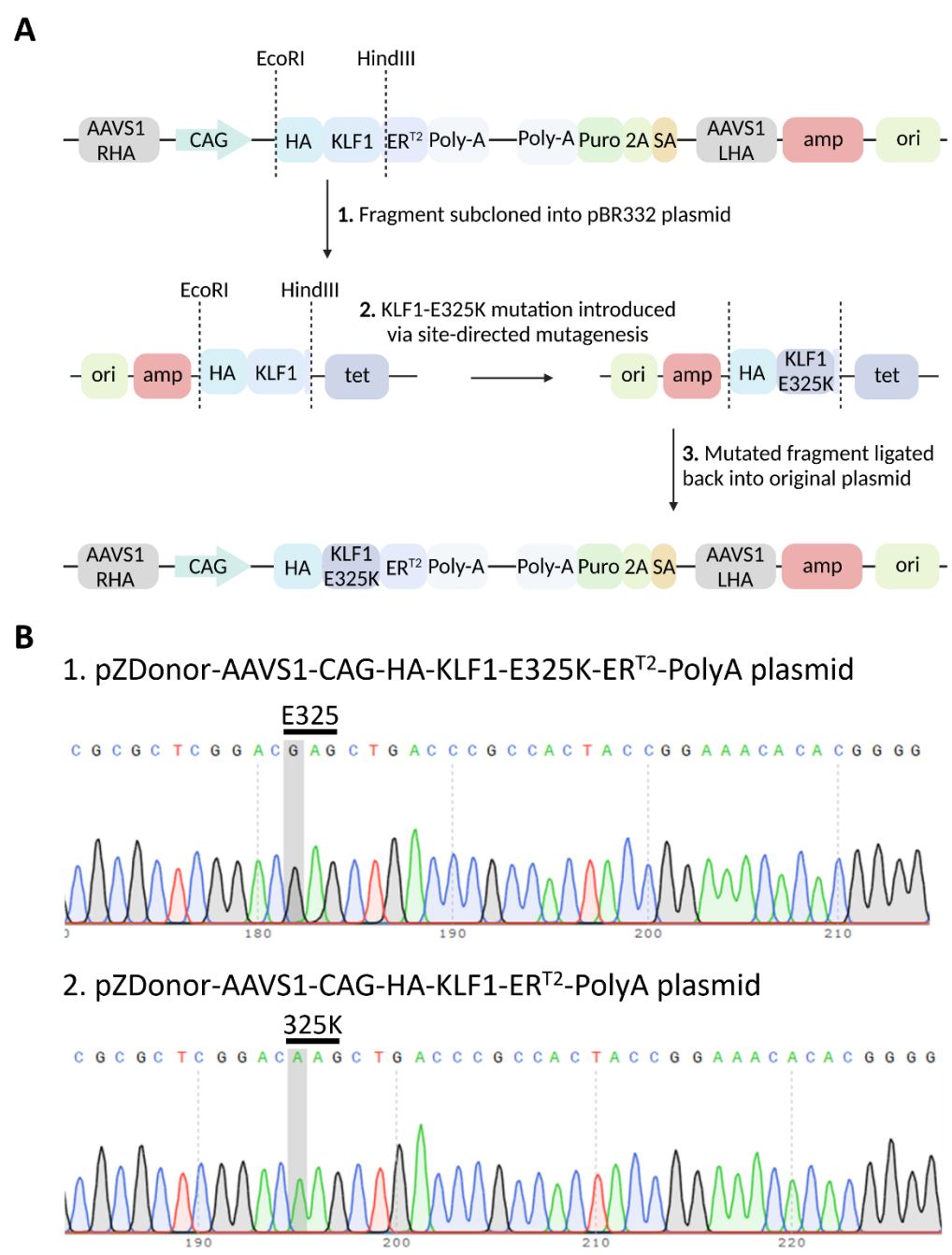

Figure 4.1 Generation of pZDonor-AAVS1-CAG-HA-KLF1-E325K-ER^{T2}-PolyA plasmid. **A:** Schematic diagram of the strategy used to generate the pZDonor-AAVS1-CAG-HA-KLF1-E325K-ERT2-PolyA plasmid.
B: Sanger sequencing of KLF1 around the c.973 site of the c.973G>A mutation showing: 1. The KLF1-WT base in the existing KLF1-WT plasmid and 2. The mutated G>A base in the KLF1-E325K plasmid.

4.3.1.2 Transfection of pZDonor-AAVS1-CAG-HA-KLF1-E325K-ERT2-PolyA plasmid into SFCi55 iPSCs

The SFCi55 iPSC line was selected for transfection with the pZDonor-AAVS1-CAG-HA-KLF1-E325K-ER^{T2}-PolyA plasmid because it is the parental line of the KLF1-WT inducible iPSC line (172). This ensures that any differences observed between the two iPSC lines and derived cells is the result of the KLF1 mutation and not other genetic differences in the genetic background of the cells. Parental iPSCs were transfected with the pZDonor-AAVS1-CAG-HA-KLF1-E325K-ER^{T2}-PolyA plasmid using the Xfect^{TM} Transfection Reagent Protocol (Chapter 2 Section 2.1.5). Following transfection, cells were cultured in maintenance media supplemented with puromycin to select for clones carrying the transfected plasmid.

4.3.1.3 Screening of clones via PCR

Following puromycin selection for 14 days, 23 puromycin resistant colonies were picked and expanded into 6-well plates. The correct integration of the KLF1-E325K-ER^{T2} construct was confirmed by PCR analysis of genomic DNA extracted from these iPSC clones. Genomic DNA from the parental SFCi55 iPSC line and the inducible KLF1-WT iPSC line were used as negative and positive controls respectively. 5 different PCR reactions were used to assess integration. PCR reactions 1-4 used primer pairs that generated specific amplicons used to confirm integration of the intact construct and to confirm correct integration into the *AAVS1* locus (Figure 4.2A). PCR 5 consisted of a primer pair that assessed whether the construct has been integrated into one or both of the *AAVS1* alleles (Figure 4.2B).

- PCR 1: Generates a KLF1-ER^{T2} amplicon
- PCR 2: Generates an amplicon at the right homology arm of the construct
- PCR 3: confirms integration into the 5' *AAVS1* locus
- PCR 4: confirms integration into the 3' *AAVS1* locus
- PCR 5: Generates an amplicon from the unedited *AAVS1* locus. In combination with PCRs 1-4, PCR 5 was used to assess whether clones have integration of the construct into one or both *AASV1* alleles.

Four clones were shown to have successful integration of the entire construct into the *AAVS1* locus: clones 1, 19, 20 and 21 (Figure 4.2A). Of these four clones, three were shown to have heterozygous integration of the construct, i.e. integration into one *AAVS1* allele (1, 19 and 21) and the remaining clone had homozygous integration of the construct, i.e. integration into both *AAVS1* alleles (20) (Figure 4.2B). Clones 1-10 were generated from the first transfection, and clones 11-14 and 15-23 were generated in two separate subsequent transfections. iPSC clones were named iCDA4.1, iCDA4.19, iCDA4.20 and iCDA4.21 respectively, for inducible Congenital Dyserythropoietic Anemia type 4 (iCDA4).

The iKLF1-E325K iPSC lines iCDA4.1 and iCDA4.20 were selected for the experiments presented in this thesis, representative of one heterozygous and one homozygous iPSC line.

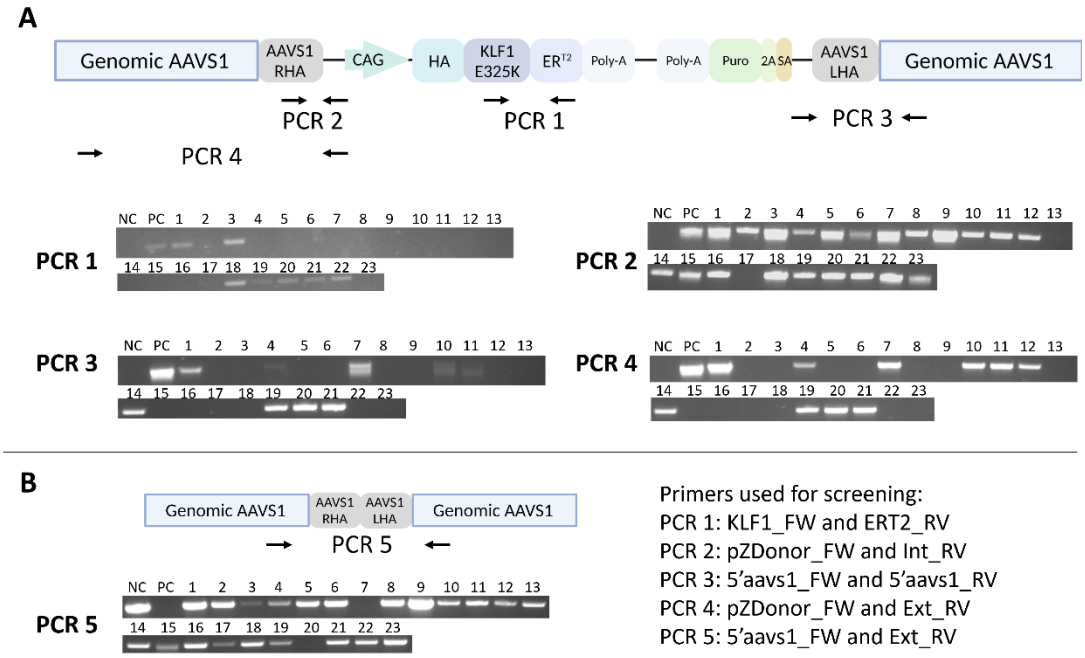

Figure 4.2 PCR screening of iPSC clones for correct integration of the KLF1-E325K-ER^{T2} construct into the AAVS1 locus of SFCi55 iPSCs.
A: A schematic diagram of the KLF1-E325K-ER^{T2} construct targeted into the AAVS1 locus showing the amplicons for PCRs 1-4 and the PCR screening results for clones 1-23. Negative control (NC): SFCi55 iPSCs. Positive control (PC): iKLF1-WT iPSCs.
B: A schematic diagram of the non-targeted AAVS1 locus showing the amplicon for PCR 5 and the PCR screening results for the NC, PC and clones 1-23.

4.3.1.4 Confirmation of *KLF1-E325K* expression in selected clones

qRT-PCR was used to confirm that expression of *KLF1-E325K* was at a level consistent with CAG promotor activity (Figure 4.3A). Both iKLF1-E325K iPSC lines (iCDA4.1 and iCDA4.20) expressed significantly more KLF1 than the parental line (Figure 4.3B). It was previously reported that the iKLF1-WT iPSC line was homozygous with the transgene being integrated into both *AAVS1* alleles (172). The homozygous iKLF1-E325K iPSC line (iCDA4.20) had comparable KLF1 expression to the iKLF1-WT line. As predicted the iKLF1-E325K iPSC line (iCDA4.1), in which the KLF1-E325K-ER^{T2} construct is integrated into only one *AAVS1* allele, expressed less *KLF1* than the two homozygous lines (Figure 4.3B).

Upon the addition of 4OH-tamoxifen, the KLF1-E325K-ER^{T2} fusion protein translocates from the cell cytoplasm to the nucleus. Therefore, I also investigated whether this translocation of KLF1-E325K-ER^{T2} to the nucleus had an effect on endogenous KLF1 expression. To investigate any potential transcriptional feedback loop of KLF1-E325K expression on endogenous KLF1 expression, qRT-PCR was performed using a reverse primer that is complementary to the KLF1-WT sequence and will therefore only amplify KLF1-WT transcript and not KLF1-E325K (Figure 4.3A). iPSCs were either untreated or treated with 100 nM 4OH-tamoxifen for 24 hours prior to fixing and staining. Use of this primer confirmed that there was no significant increase in endogenous KLF1-WT expression in both iKLF1-E325K iPSC lines upon 4OH-tamoxifen induced KLF1-E325K activation (Figure 4.3C).

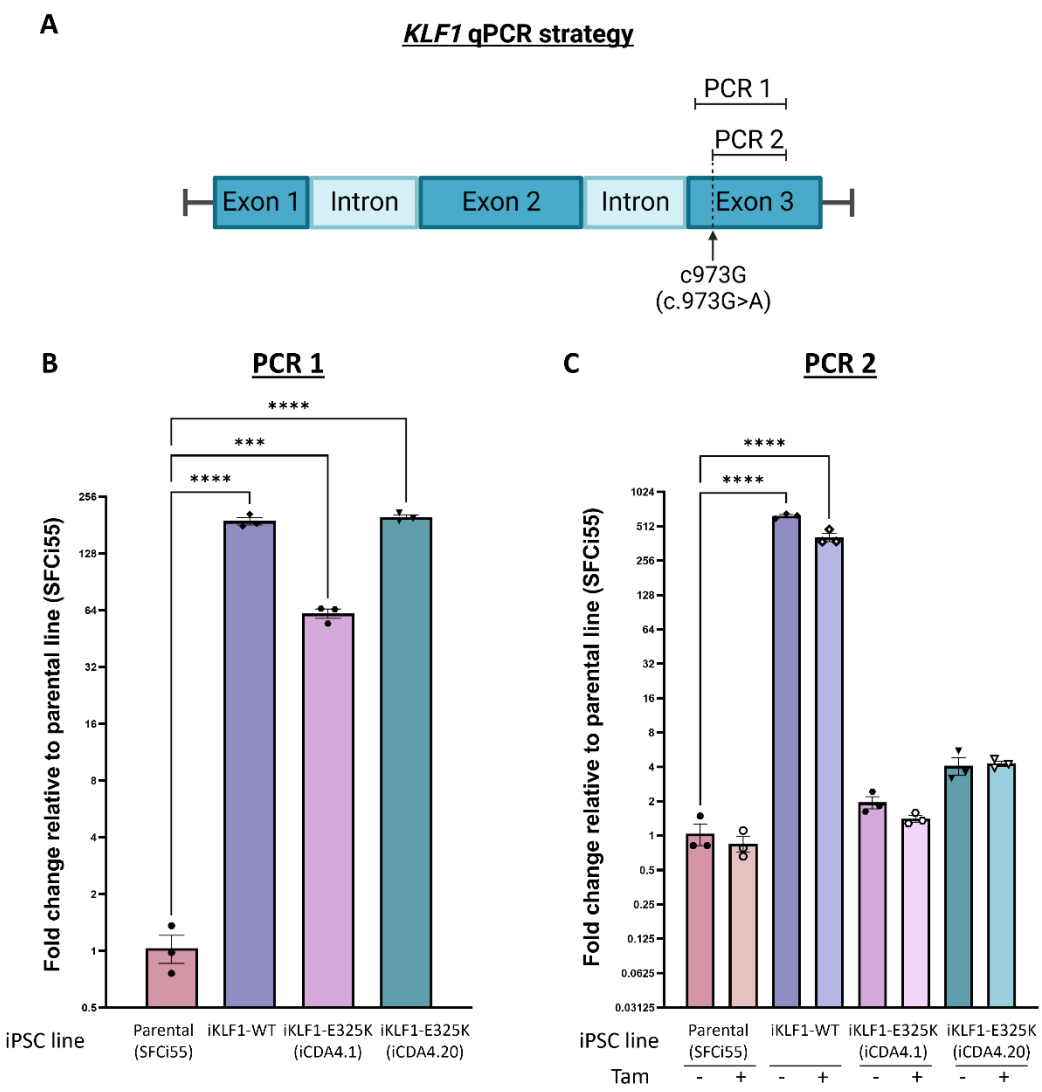

Figure 4.3 Gene expression of KLF1-WT and KLF1-E325K in undifferentiated iPSCs assessed by qRT-PCR.

A: KLF1 qRT-PCR strategy. qRT-PCR 1 amplifies both KLF1-WT and KLF1-E325K transcripts. qRT-PCR 2 amplifies only KLF1-WT transcripts. qRT-PCRs were conducted on RNA extracted from iPSCs from the parental (SFCi55), iKLF1-WT, and both iKLF1-E325K iPSC lines.

B: qRT-PCR for both KLF1-WT and KLF1-E325K. Fold change analysed relative to parental line. Datapoints represent individual iPSC harvests.

C: qRT-PCR for KLF1-WT only. Fold change analysed relative to parental line iPSCs -Tam. Error bars represent SEM. One-way ANOVA with Tukey post-test. *p < 0.05, **p < 0.01, ***p<0.001, ****p<0.0001. Datapoints represent individual iPSC harvests.

4.3.1.5 Confirmation of KLF1-E325K-ER^{T2} fusion protein nuclear translocation

Immunohistochemistry was used to confirm that the KLF1-E325K-ER^{T2} fusion protein translocated to the nucleus upon 4OH-tamoxifen addition, and that the KLF1-E325K mutation does not affect this activity. iPSCs were either untreated or treated with 100 nM 4OH-tamoxifen for 24 hours prior to fixing and staining. iKLF1-WT iPSCs were used as a positive control as translocation of the KLF1-WT-ER^{T2} fusion protein has been previously confirmed (172).

Fixed iPSCs from all inducible iPSC lines (+/- 4OH-tamoxifen) were evaluated by immunofluorescence staining using an anti-KLF1 antibody (Chapter 2 Section 2.4.2). KLF1 was detected in the cytoplasm of iPSCs from the iKLF1-WT and iKLF1-E325K lines (Figure 4.4). There was a noticeable reduction in the intensity of KLF1 staining in the cytoplasm of 4OH-tamoxifen treated cells compared to untreated cells. Also, more intense staining of KLF1 was observed in the nucleus of iPSCs from all lines treated with 100 nM of 4OH-tamoxifen compared to untreated cell. Taken together this demonstrates that the strategy was working as predicted and KLF1-E325K-ER^{T2} fusion protein translocated to the nucleus (Figure 4.4). There was no observable difference between KLF1-WT and KLF1-E325K fusion protein translocation suggesting that the E325K point mutation had no effect on this activity (Figure 4.4). I did observe some staining of KLF1 in the nucleus of untreated cells, showing that there is some nuclear translocation of the KLF1-WT/E325K-ER^{T2} fusion proteins without 4OH-tamoxifen addition.

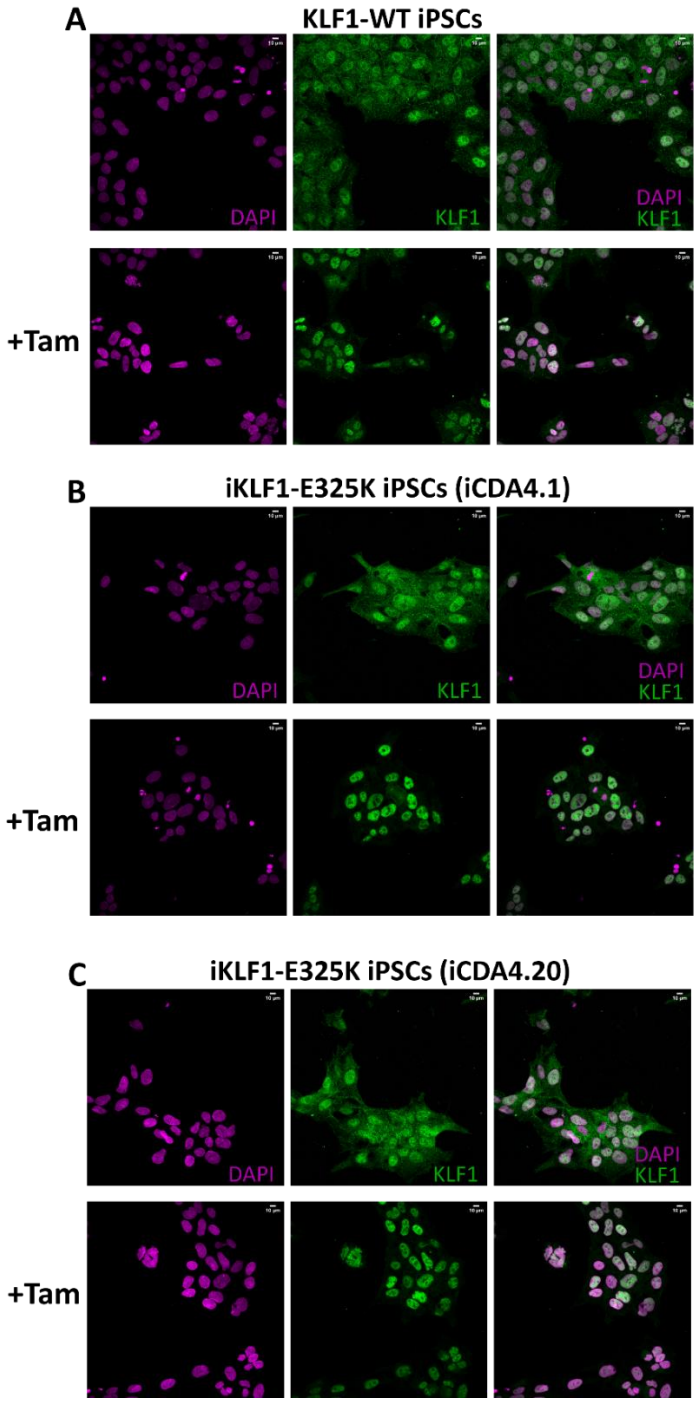

Figure 4.4 KLF1-WT-ER^{T2} and KLF1-E325K- ER^{T2} fusion proteins translocate to the cell nucleus upon 4OH-tamoxifen addition in undifferentiated iPSCs.
A: Representative images of fixed iKLF1-WT iPSCs in the presence and absence of 4OH-tamoxifen using an anti-KLF1 antibody.
B: Representative images of fixed iKLF1-E325K iPSCs from the heterozygous line (iCDA4.1) in the presence and absence of 4OH-tamoxifen using an anti-KLF1 antibody.
C: Representative images of fixed iKLF1-E325K iPSCs from the homozygous line (iCDA4.20) in the presence and absence of 4OH-tamoxifen using an anti-KLF1 antibody. Magenta represents nuclei and green represents KLF1. 40X magnification. 10 µm scale bar.

Together, these data confirm that iKLF1-E325K iPSCs express high levels of transgenic *KLF1-E325K* and that the KLF1-E325K-ER^{T2} fusion protein translocated from the cytoplasm of the cell to the nucleus upon 4OH-tamoxifen addition.

4.3.2 KLF1-E325K activation recapitulates disease pathology in cells generated from iKLF1-E325K iPSCs under erythroid differentiation conditions

With the iKLF1-E325K iPSC cell lines established, it was first assessed whether erythroid cells could be generated from these lines, and whether activation of KLF1-E325K in erythroid cells induced a CDA patient phenotype.

4.3.2.1 KLF1-E325K activation does not alter the morphology of cells generated under erythroid differentiation conditions

Cells were generated under erythroid differentiation conditions from two inducible iKLF1-E325K iPSC lines (iCDA4.1 and iCDA4.20) and one control iKLF1-WT iPSC line (Figure 3.1C). 100 nM 4OH-tamoxifen was added to cultures every 2 days to induce KLF1-E325K activation. Cells generated from the iKLF1-E325K iPSC lines are morphologically comparable to cells generated from control iKLF1-WT iPSCs (Figure 4.5). 4OH-tamoxifen addition alone has no effect on cell morphology (Appendix 3). Macrophages can be observed in suspension cell populations generated under erythroid differentiation conditions from all iKLF1-E325K and iKLF1-WT lines (Figure 4.5). These macrophages are in contact with other cells and can be identified by their larger size and the presence of large vesicles throughout the cytoplasm lines (Figure 4.5).

The remaining cells generated from all iPSC lines, which consist of haematopoietic cells and erythroid precursors, have a spherical shape and range between approximately 10-20 µm in size. This cell size, in combination with the cell morphology and contact with macrophages, suggests that a large proportion of these cells are erythroblasts. Induction of both KLF1-WT and KLF1-E325K activation via the addition of 4OH-tamoxifen appears to have no effect on the morphology of cells generated (Figure 4.5).

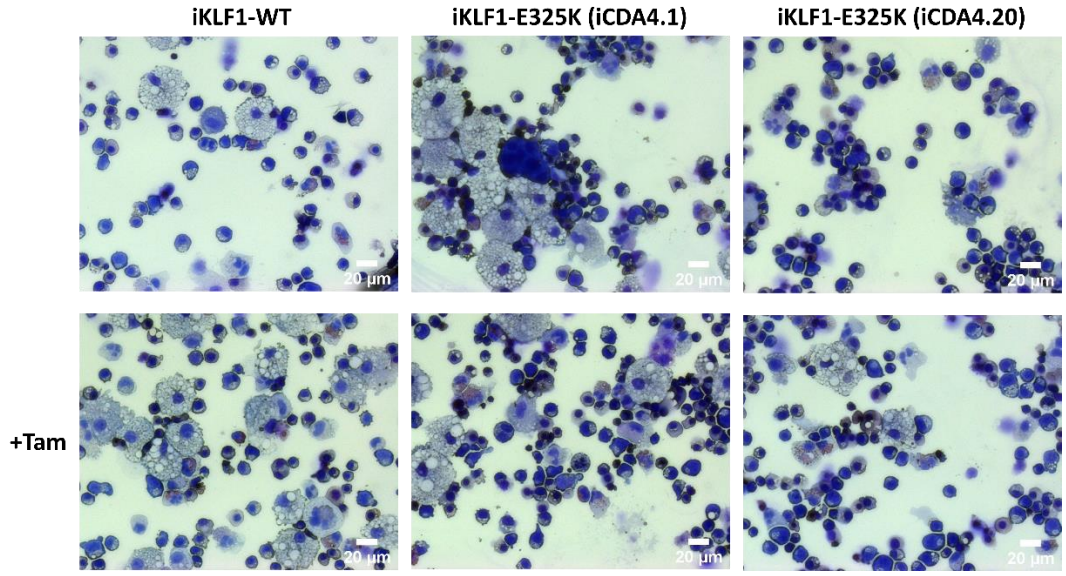

Figure 4.5 KLF1-E325K activation does not alter the morphology of cells generated under erythroid differentiation conditions. Representative Kwik-Diff stained cytospins of cells generated from erythroid differentiations of a KLF1-WT iPSC line and two control iKLF1-E325K iPSC lines (iCDA4.1 and iCDA4.20) in the presence and absence of 4OH-tamoxifen. Cytospins were performed on suspension cells on the day they were harvested. 20x magnification. 20 µm scale bar.

4.3.2.2 KLF1-E325K activation significantly reduces populations of CD235a$^+$ cells and CD71$^+$ cells generated under erythroid differentiation conditions

Cells generated under erythroid differentiation conditions from two inducible iKLF1-E325K iPSC lines (iCDA4.1 and iCDA4.20) were assessed for the expression of the cell surface markers CD43, EpCAM, CD235 and CD71, and compared to cells generated from a control iKLF1-WT iPSC line.

Flow cytometry plots were gated as described (Chapter 2 Section 2.3.1). A comparable percentage of cells generated under erythroid differentiation conditions from all iPSC lines were CD43$^+$ and EpCAM$^+$, with no significant difference observed in the numbers of cells positive for either marker between iPSC lines and 4OH-tamoxifen untreated vs treated cells (Figure 4.6B).

In Chapter 3 I observed that significantly fewer CD235a$^+$ cells and CD71$^+$ cells were generated from CDA patient iPSCs compared to control iPSCs under erythroid differentiation conditions (Chapter 3 Section 3.3.1.2). It was therefore assessed whether KLF1-E325K activation induced this phenotype. KLF1-E325K activation

significantly reduced the populations of CD235a$^+$ cells and CD71$^+$ cells (Figure 4.6C/D). KLF1-E325K activation in both iKLF1-E325K lines reduced the population of CD235a$^+$ cells by approximately 50%, and the population of CD71$^+$ cells by approximately 60%. KLF1-WT activation had no effect on the populations of CD235a$^+$ cells and CD71$^+$ cells generated (Figure 4.6C/D). 4OH-tamoxifen addition alone had no effect on the proportion of cells expressing CD43, EpCAM, CD235a and CD71 (Appendix 3).

There appears to be a KLF1-E325K expression level-dependent effect on the reduction in populations of CD235a$^+$ cells and CD71$^+$ cells. Upon KLF1-E325K activation, there was a significantly lower percentage of CD235$^+$ cells generated from iKLF1-E325K iPSCs from the homozygous line (iCDA4.20) that had two copies of the KLF1-E325K-ER^{T2} transgene, compared to cells generated from iKLF1-E325K iPSCs from the heterozygous line (iCDA4.1) that had one copy (Figure 4.6D). There is a similar trend in CD71$^+$ cells populations. Upon KLF1-E325K activation, there were fewer CD71$^+$ cells generated from iKLF1-E325K iPSCs from the homozygous line (iCDA4.20) compared to cells generated from iKLF1-E325K iPSCs from the heterozygous line (iCDA4.1) (Figure 4.6D).

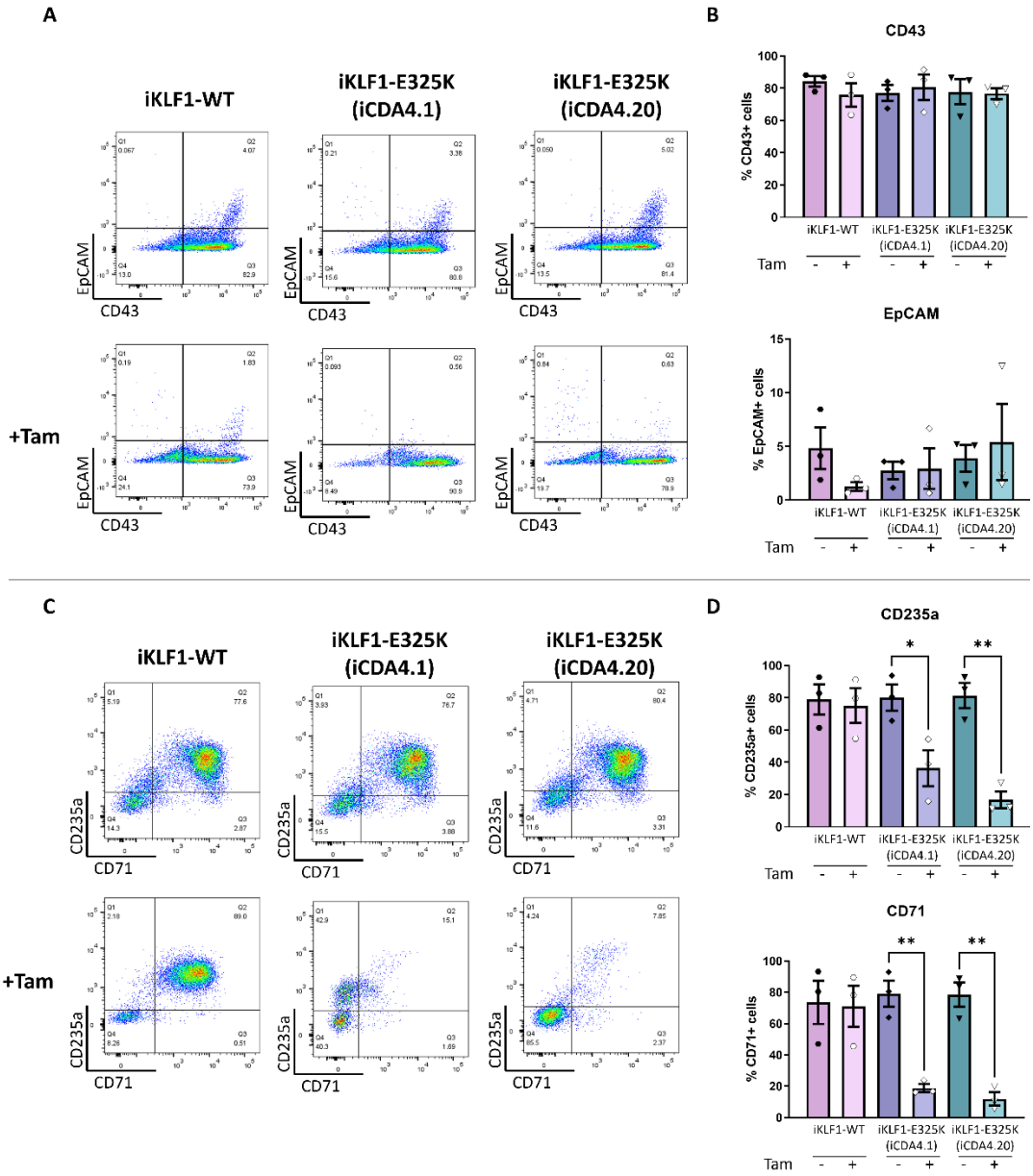

Figure 4.6 KLF1-E325K activation significantly reduces populations of CD235a$^+$ cells and CD71$^+$ cells generated under erythroid differentiation conditions. Flow cytometry analyses were performed on suspension cells generated under erythroid differentiation conditions from two inducible iKLF1-E325K iPSC lines and one control iKLF1-WT iPSC line. Suspension cells were assessed on the day that they were harvested. Datapoints represent individual suspension cell harvests.

A: Representative flow cytometry plots of suspension cells generated in the presence and absence of 4OH-tamoxifen assayed for expression of CD43 or EpCAM.

B: Quantification of flow cytometry analyses of the percentage of cells expressing CD43 or EpCAM. Error bars represent SEM. One-way ANOVA with Tukey post-test generated no statistically significant p-values.

C: Representative flow cytometry plots of suspension cells generated in the presence and absence of 4OH-tamoxifen assayed for expression of CD235a or CD71 Quantification of flow cytometry analyses of the percentage of cells expressing each marker.

D: Quantification of flow cytometry analyses of the percentage of cells expressing CD235 or CD71. Error bars represent SEM. One-way ANOVA with Tukey post-test. *p < 0.05 **p < 0.01.

4.3.3. Tamoxifen treatment alone has no observed effect on cells generated under erythroid differentiation conditions

Untreated and 4OH-tamoxifen treated cells generated under erythroid differentiation conditions from the parental iPSC line (SFCi55) were used to assess any effects as a result of 4OH-tamoxifen treatment only.

4OH-tamoxifen treatment had no effect on the morphology or cell surface marker expression of CD43, EpCAM, CD235a or CD71 of cells generated under erythroid differentiation conditions (Figure 4.7).

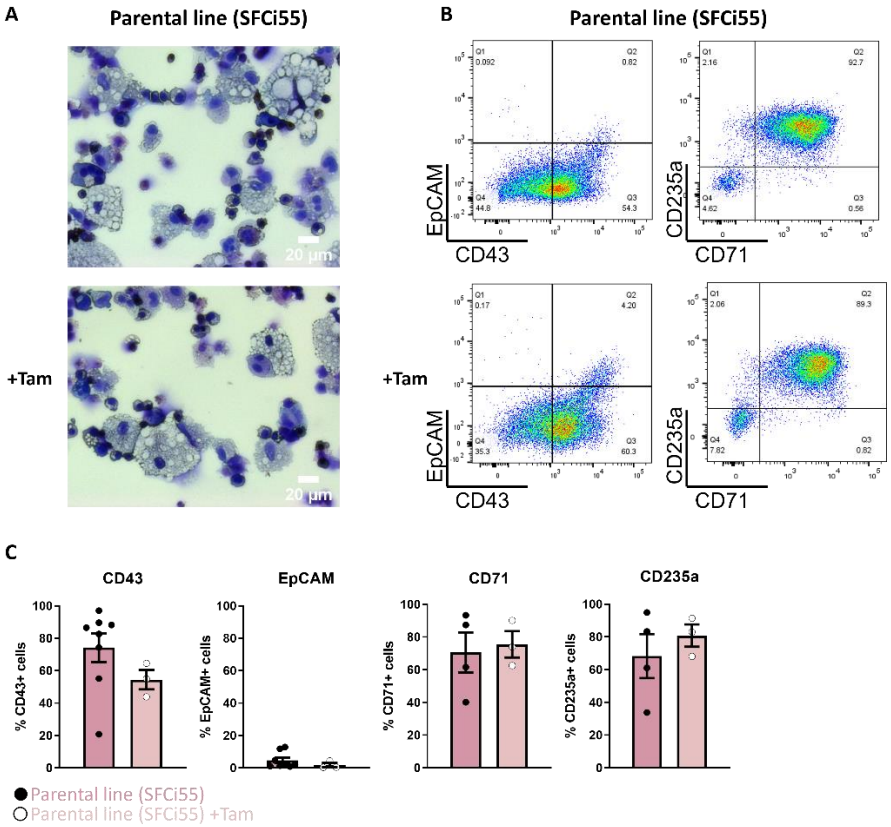

Figure 4.7 4OH-tamoxifen treatment alone has no observed effect on cells generated from parental line iPSCs (SFCi55) under erythroid differentiation conditions. **A:** Representative Kwik-Diff stained cytospins of cells generated under erythroid differentiation conditions from parental line (SFCi55) iPSCs. Cytospins were performed at the point of harvest. 20X magnification. 20 µm scale bar. **B:** Representative flow cytometry plots of suspension cells generated under erythroid differentiation conditions assayed for expression of CD43, EpCAM, CD235a and CD71. **C:** Quantification of flow cytometry analyses of the percentage of cells expressing each marker. Datapoints represent individual suspension cell harvests. Error bars represent SEM. Unpaired t-tests generated no statistically significant p-values.

4.4 Discussion

I generated several iKLF1-E325K iPSC lines in which a KLF1-E325K-ER^{T2} fusion protein was constitutively expressed in the cytoplasm of the cell and translocated to the nucleus upon 4OH-tamoxifen addition. I selected two iKLF1-E325K iPSC lines, with either one (iCDA4.1) or two (iCDA4.20) copies of the KLF1-E325K-ER^{T2} transgene, for experiments. *KLF1-E325K* gene expression levels in both iKLF1-E325K iPSC lines were confirmed to be consistent with CAG promotor activity, and I observed nuclear translocation of the KLF1-E325K-ER^{T2} fusion protein in both lines. I then showed that KLF1-E325K activation in cells generated from both iKLF1-E325K iPSC lines under erythroid differentiation conditions induced the CDA erythroid cell phenotype, with a significant reduction in the percentage of CD235a^{+} cells and CD71^{+} cells generated.

4.4.1 Leakiness of KLF1-E325K-ER^{T2} system

Leakiness of the ER^{T2} system has been previously reported in bone marrow cells, and also in erythroid differentiations of iKLF1-WT iPSCs (172, 344). Both iKLF1-WT and iKLF1-E325K iPSCs do appear to show some leakiness here, with staining of KLF1 observed in the nucleus of iPSCs in the absence of 4OH-tamoxifen. This leakiness was not quantified. In the absence of tamoxifen, I would not expect to observe baseline KLF1 expression as endogenous KLF1 expression is not well detected by immunocytochemistry, therefore I have attributed the KLF1 staining in the nucleus to leakiness. The observation of KLF1 staining, and therefore the KLF1-E325K- ER^{T2} fusion protein, in the nucleus of untreated iKLF1-E325K iPSCs does not appear to have functional consequences in cells generated under erythroid differentiation conditions. Cells generated from both iKLF1-E325K iPSC lines in the absence of 4OH-tamoxifen show no decrease in the percentage of CD235a^{+} cells and CD71^{+} cells compared to cells generated from iKLF1-WT iPSCs.

4.4.2 Assessment of CDA disease pathology in cells generated from iKLF1-E325K iPSCs under erythroid differentiation conditions

A previous study that noted that fewer cells were generated during erythroid differentiations of iKLF1-WT iPSCs compared to a parental control line (172). In agreement with this study, far fewer cells were generated from iKLF1-E325K and iKLF1-WT iPSC lines under erythroid differentiation conditions compared to the CDA

patient and control iPSC lines described in Chapter 3 (Data not shown). As a result, cell yields were sufficient for cytospins and flow cytometry analyses only. No RNA was extracted from cells generated from the iKLF1-WT and iKLF1-E325K iPSC lines and therefore no gene expression analyses could be performed on these cells. This decrease in yields is likely due to the presence of the construct itself, rather than being a KLF1-E325K or KLF1-WT specific effect as there was no significant difference in yields between iKLF1-E325K and iKLF1-WT differentiations.

Additionally, there were technical factors that could have introduced variability between experiments. Erythroid differentiations of CDA patient and control iPSC lines were conducted several months before erythroid differentiations of the iKLF1-E325K and iKLF1-WT lines. During this 6-month period, no EBs were able to be generated. This was due to an unidentified issue with StemPro^{TM} iPSC maintenance media in which iPSCs were either not viable or did not form EBs. This indicated either an issue or change in formulation of the StemPro^{TM} media, which could have impacted upon subsequent differentiations once EBs could be generated again.

There appears to be a KLF1-E325K expression level-dependent effect on the reduction in populations of CD235a^{+} cells and CD71^{+} cells generated under erythroid differentiation conditions when KLF1-E325K is activated. Upon KLF1-E325K activation, there are significantly fewer CD235a^{+} cells generated from homozygous iKLF1-E325K iPSCs that had two copies of the KLF1-E325K-ER^{T2} transgene (iCDA4.20) compared to cells generated from heterozygous iKLF1-E325K iPSCs with one copy (iCDA4.1). There is a similar trend in CD71^{+} cells populations. The percentage of CD235a^{+} cells and CD71^{+} cells generated from both iKLF1-E325K iPSC lines upon KLF1-E325K activation are comparable with the percentage of CD235a^{+} cells and CD71^{+} cells generated under erythroid differentiation conditions from the CDA patient iPSC line (Chapter 3). I would therefore speculate that the KLF1-E325K-ER^{T2} system results in expression of *KLF1-E325K* comparable to that of endogenous *KLF1* expression in CDA patient erythroid cells, however I could not confirm this via qRT-PCR.

There are more CD71^{+} cells than CD235a^{+} cells generated under erythroid differentiation conditions from CDA patient iPSCs. Conversely, there are more CD235a^{+} cells than CD71^{+} cells generated under erythroid differentiation conditions

from both iKLF1-E325K iPSC lines. There are several explanations for this observed trend:

1. More macrophages, which are $CD71^+$, are generated from CDA patient-derived iPSCs than iKLF1-E325K iPSCs under erythroid differentiation conditions. Based on observations of cytospin images of the cells, this does not appear to be the case.

2. Cells generated under erythroid differentiation conditions from iKLF1-E325K iPSCs are more mature than cells generated from CDA patient iPSCs. As erythroid differentiation progresses, expression of CD71 is lost, while expression of CD235a is gained (39). CD235a is expressed by both erythroid precursors and erythrocytes (322). Therefore, $CD235a^+$ $CD71^-$ cells represent mature erythroid cells.

3. The erythroid differentiation presented in Chapter 3 was less efficient than the erythroid generation presented in this chapter. Approximately 70% of cells generated from two iPSC control lines in Chapter 3 are $CD235a^+$, compared to approximately 80% of cells generated from the untreated inducible iPSC lines. This does indeed suggest that the erythroid differentiation in this chapter was more efficient than the previous differentiation and could explain the increase in $CD235a^+$ cells.

One limitation to the generation of erythroid cells from iPSCs, using both the patient-derived iPSCs and the iKLF1-E325K iPSCs used in this chapter, is that expression of KLF1-related structural proteins such as *ICAM4,* tropomodulin *1*, and *BAND 3* are significantly lower in CDA type IV patient erythroid cells (131). Low levels of these proteins in CDA patient erythroid cells have been speculated to contribute to the fragility of patients RBCs (131). One of the existing limitations to the differentiation of RBCs from iPSCs is that the cells produced have a fragile morphology (172). This limitation is therefore amplified when trying to generate erythroid cells from iPSCs that carry a mutation that affects the expression of structural proteins in these cells. As a result, it was very challenging to generate KLF1-E325K erythroid cells robust enough for any additional assays or analyses, and this likely also contributed to the low cell numbers that were able to be harvested. This is therefore a key limitation to using iPSCs to model erythroid cells in RBC disorders.

Chapter 5: The E325K mutation impedes phenotypic and functional changes induced by KLF1

5.1 Introduction

The ability to genetically engineer iPSCs, and therefore any cells derived from them, presents a promising approach to dissect the role of individual genes within the human EBI niche. Indeed, the 4OH-tamoxifen-ER^{T2} system has been particularly useful as it appears to recapitulate endogenous gene expression levels, avoiding the very high non-physiological expression levels often seen in standard transgenic or viral expression systems (172, 201). A KLF1-WT activation strategy was previously shown to induce phenotypic and functional changes in iPSC-DMs, inducing a more EBI-macrophage like phenotype (201). This human iPSC-derived macrophage strategy holds great potential in the context of RBC disorders, where pathogenic gene mutations can be introduced into EBI-like macrophages to investigate whether genetic deficiencies in the niche contribute to disease pathology.

One key limitation of the CDA patient iPSC-derived macrophages that were described and characterised in Chapter 3 is that they expressed very low levels of KLF1 and so might not accurately model *in vivo* EBI macrophages. EBI macrophages in mice have been shown to express KLF1, and the Forrester lab previously demonstrated that increasing the level of *KLF1* resulted in an EBI-like macrophage phenotype in iPSC-DMs (201). I hypothesised that the generation of a faithful model of CDA patient EBI macrophages might also require increased *KLF1-E325K* expression levels. I therefore generated and validated two iPSC lines carrying an activatable form of KLF1-E325K (iKLF1-E325K) (Chapter 4). KLF1-E325K activation in cells generated under erythroid differentiation conditions from both of the iKLF1-E325K iPSC lines mimicked the CDA patient phenotype.

5.2 Aims and Approaches

1. The first aim of this chapter was to generate macrophages from iKLF1-E325K iPSC lines and confirm that *KLF1-E325K* expression levels and translocation of the KLF1-E325K-ER^{T2} fusion protein are comparable to undifferentiated iPSCs.

2. The second aim of this chapter was to characterise and compare the phenotype of iKLF1-E325K iPSC-DMs with iKLF1-WT iPSC-DMs following activation with 4OH-tamoxifen.

3. The third aim of this chapter was to assess the function of iKLF1-E325K iPSC-DMs in an *in vitro* model of the EBI niche by comparing their ability to support the erythroid differentiation, maturation and enucleation of erythroid cells with iKLF1-WT iPSC-DMs.

5.3 Results

5.3.1 Generation and confirmation of inducible KLF1-E325K iPSC-DMs

Macrophages were generated from two inducible iKLF1-E325K iPSC lines (iCDA4.1 & iCDA4.20) and one control iKLF1-WT iPSC line. 4OH-tamoxifen was added during the terminal maturation stage, stage 3, of the iPSC-macrophage differentiations on days 8 and 10 (Figure 3.5).

5.3.1.1 KLF1-E325K activation does not alter macrophage morphology

Macrophages generated from all iPSC lines were large in size, ranging between 20-40 µm, with a small nucleus and numerous cytoplasmic vesicles (Figure 5.1). This is consistent with the morphology of macrophages characterised in Chapter 3. iKLF1-WT iPSC-DMs had a comparable morphology to iKLF1-E325K iPSC-DMs and activation of KLF1-WT or KLF1-E325K via the addition of 4OH-tamoxifen had no obvious effect on macrophage morphology (Figure 5.1).

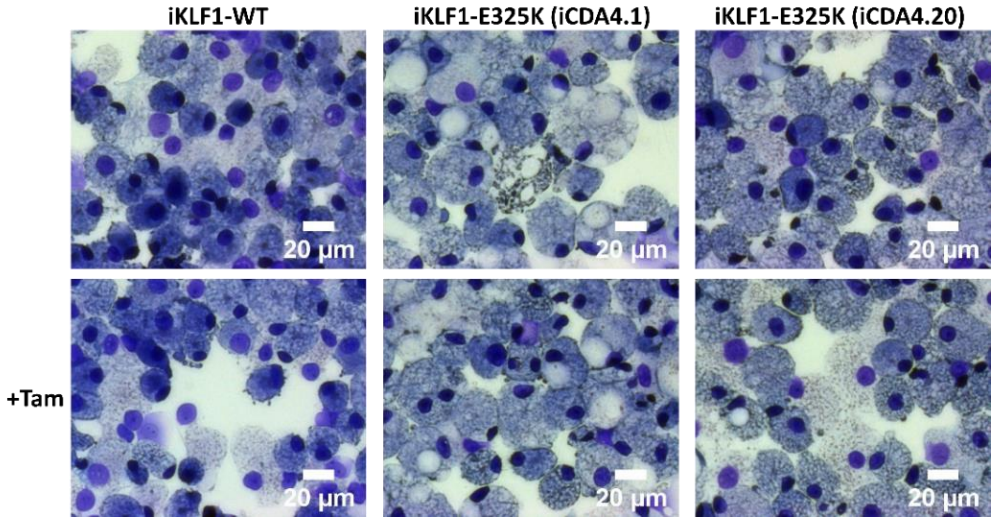

Figure 5.1 The E325K mutation in KLF1 does not alter macrophage morphology. Representative Kwik-Diff stained cytospins of macrophages generated from two inducible iKLF1-E325K iPSC lines (iCDA4.1 & iCDA4.20) and one control iKLF1-WT iPSC line. 20x magnification. 20 µm scale bar.

5.3.1.2 Confirmation of *KLF1-E325K* expression in iKLF1-E325K iPSC-DMs

Using the strategy presented in Chapter 4, qRT-PCR was used to confirm that iKLF1-E325K iPSC-DMs expressed *KLF1-E325K* at a level consistent with CAG promotor activity, and that KLF1-E325K activation did not induce endogenous KLF1-WT expression (Figure 5.2A).

iKLF1-E325K iPSC-DMs generated from both iKLF1-E325K iPSC lines (iCDA4.1 and iCDA4.20) expressed high levels of *KLF1-E325K* (Figure 5.2B). iKLF1-E325K iPSC-DMs generated from the heterozygous line that had one copy of the KLF1-E325K-ER^{T2} transgene (iCDA4.1) expressed a lower level of *KLF1-E325K* than iPSC-DMs generated from the homozygous line that had two copies (iCDA4.20) (Figure 5.2B). KLF1-E325K activation did not significantly affect endogenous KLF1-WT expression in iKLF1-E325K iPSC-DMs from both lines (Figure 5.2C). 4OH-tamoxifen addition alone had no effect on the expression level of KLF1 (Appendix 3).

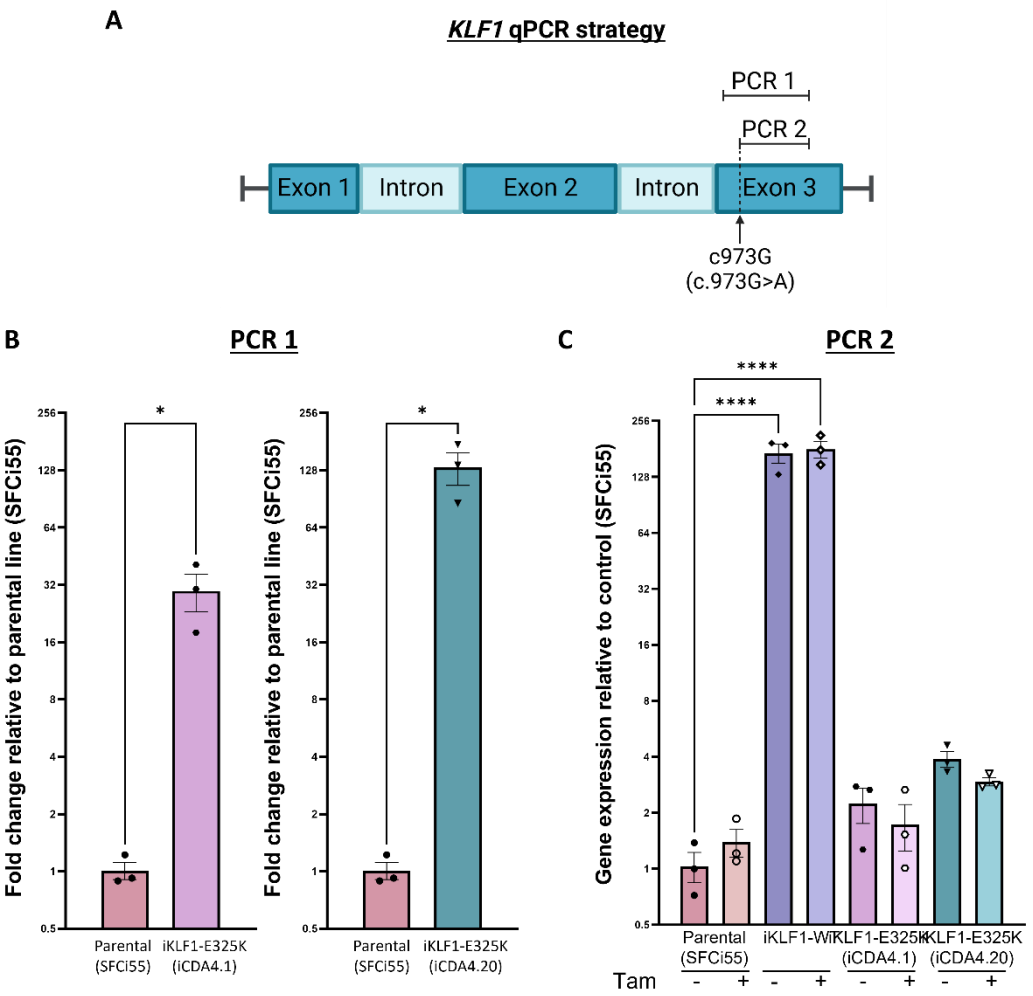

Figure 5.2 Gene expression of KLF1-WT and KLF1-E325K in iPSC-DMs assessed by qRT-PCR. A: KLF1 qRT-PCR strategy. qRT-PCR 1 amplifies both KLF1-WT and KLF1-E325K transcripts. qRT-PCR 2 amplifies only KLF1-WT transcripts. qRT-PCRs were conducted on RNA extracted from iPSC-DMs generated from the parental (SFCi55), iKLF1-WT, and both iKLF1-E325K iPSC lines.

B: qRT-PCR1 to detect KLF1-WT and KLF1-E325K. Fold change analysed relative to parental line iPSCs. Error bars represent SEM. Unpaired t-test. *p < 0.05. Datapoints represent individual macrophage harvests.

C: qRT-PCR to detect KLF1-WT only. Fold change analysed relative to parental line iPSCs - Tam. Error bars represent SEM. One-way ANOVA with Tukey post-test. *p < 0.05, **p < 0.01, ***p<0.001, ****p<0.0001. Datapoints represent individual macrophage harvests.

5.3.1.3 Confirmation of KLF1-E325K-ER^{T2} fusion protein nuclear translocation in iKLF1-E325K iPSC-DMs

As presented in Chapter 4, the KLF1-E325K-ER^{T2} fusion protein translocated to the nucleus upon 4OH-tamoxifen addition in undifferentiated iPSCs (Figure 4.4). The same immunofluorescence staining protocol was used to confirm that this translocation activity was retained in differentiated macrophages generated from iKLF1-E325K iPSC lines.

iKLF1-E325K iPSC-DMs were either untreated or treated with 100 nM 4OH-tamoxifen for 24 hours prior to fixing and staining. iKLF1-WT iPSC-DMs were used as a positive control.

Fixed iPSC-DMs from all inducible iPSC lines (+/- 4OH-tamoxifen) were evaluated by immunofluorescence staining using an anti-KLF1 antibody (Chapter 2 Section 2.4.2). KLF1 was detected in the cytoplasm of iPSC-DMs from the iKLF1-E325K and iKLF1-WT lines (Figure 5.3). As observed in undifferentiated iPSCs, there was a noticeable reduction in the intensity of KLF1 staining in the cytoplasm of 4OH-tamoxifen treated cells compared to untreated cells. More intense staining of KLF1 was observed in the nucleus of iPSC-DMs generated from all lines treated with 100 nM of 4OH-tamoxifen compared to untreated iPSC-DMs. Taken together, this demonstrates that the KLF1-E325K-ER^{T2} fusion protein retained its ability to translocate to the nucleus upon 4OH-tamoxifen addition in iKLF1-E325K iPSC-DMs (Figure 5.3).

As observed in undifferentiated iPSCs, I see staining of KLF1 in the nucleus of untreated cells, showing that there is nuclear translocation of the KLF1-WT/E325K-ER^{T2} fusion proteins without 4OH-tamoxifen addition (Figure 5.3). The nuclear KLF1 staining observed in untreated iPSC-DMs appears much brighter than the nuclear KLF1 staining observed in undifferentiated iPSCs (Figure 4.4, Figure 5.3). This was not quantified. This suggests that the system is 'leakier' in iPSC-DMs, meaning that there is more translocation of the fusion proteins without 4OH-tamoxifen addition in iPSC-DMs compared to undifferentiated iPSCs.

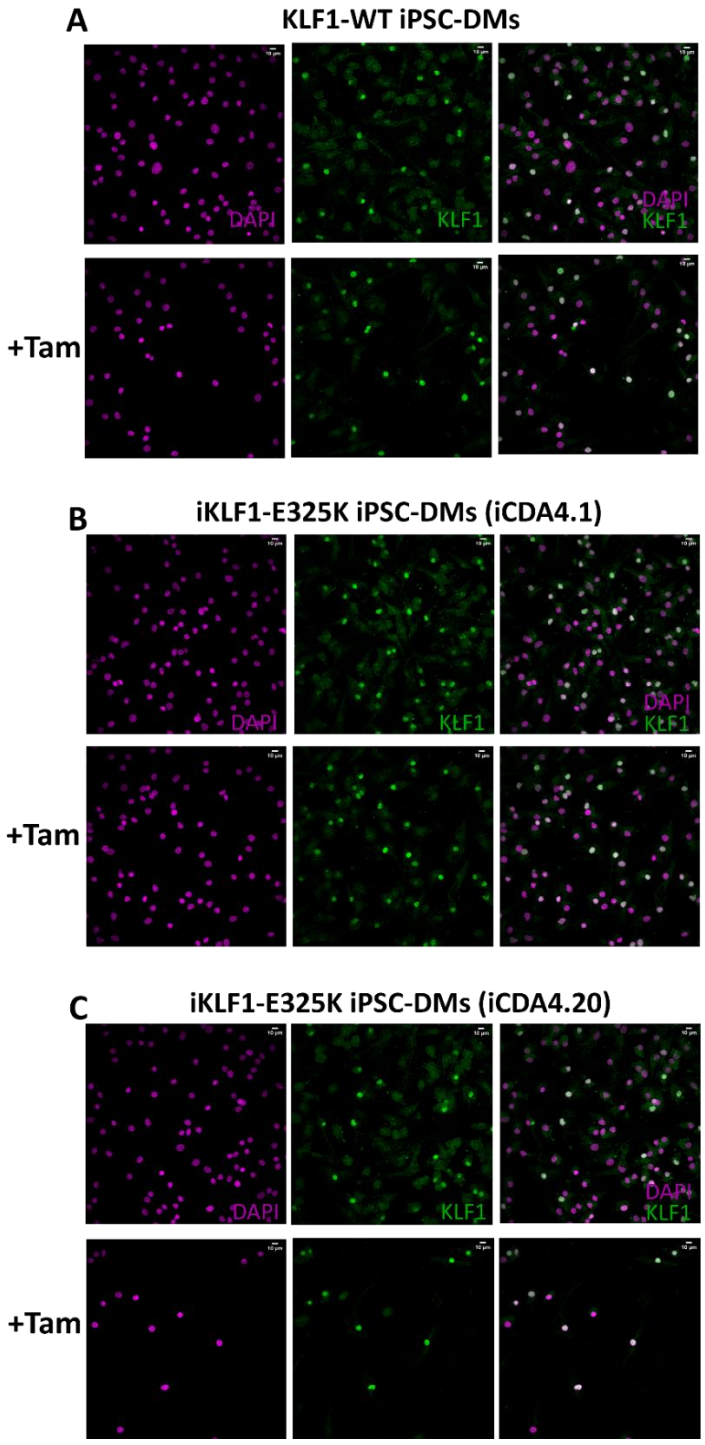

Figure 5.3 KLF1-WT-ER^{T2} and KLF1-E325K- ER^{T2} fusion proteins translocate to the cell nucleus upon 4OH-tamoxifen addition in iPSC-DMs.

A: Representative images of fixed iKLF1-WT iPSC-DMs in the presence and absence of 4OH-tamoxifen using an anti-KLF1 antibody.

B: Representative images of fixed iKLF1-E325K iPSC-DMs from the heterozygous line (iCDA4.1) in the presence and absence of 4OH-tamoxifen using an anti-KLF1 antibody.

C: Representative images of fixed iKLF1-E325K iPSC-DMs from the homozygous line (iCDA4.20) in the presence and absence of 4OH-tamoxifen using an anti-KLF1 antibody. Magenta represents nuclei and green represents KLF1. 20X magnification. 10 µm scale bar.

5.3.2 The E325K mutation impedes the loss of CD93 induced by KLF1

Flow cytometry analyses of cells generated from iKLF1-E325K iPSCs under erythroid differentiation conditions confirmed that KLF1-E325K activation could induce a CDA patient phenotype. Therefore, iKLF1-E325K iPSCs were phenotypically characterised by flow cytometry to assess the effects of KLF1-E325K activation on the expression of cell surface markers in iPSC-DMs. iKLF1-E325K iPSC-DMs were assessed for expression of the following cell surface markers to assess the effect of KLF1-E325K activation on haematopoietic lineage commitment and maturation: CD45, CD93, 25F9, CD163 and CD169.

Flow cytometry plots were gated as described in the methods (Chapter 2 Section 2.3.2) and representative plots for iPSC-DMs generated from each inducible iPSC line are shown (Figure 5.4). KLF1-E325K activation had no effect on the haematopoietic commitment of iKLF1-E325K iPSC-DMs, with a comparable percentage of $CD45^+$ cells observed between untreated and 4OH-tamoxifen treated iKLF1-E325K iPSC-DMs (Figure 5.4). KLF1-E325K activation also had no effect on the expression of the EBI macrophage markers CD163 and CD169, with a comparable percentage of $CD163^+$ and $CD169^+$ cells observed between untreated and 4OH-tamoxifen treated iKLF1-E325K iPSC-DMs (Figure 5.4). There was a comparable percentage of $CD45^+$, $CD163^+$ and $CD169^+$ cells between iKLF1-E325K and iKLF1-WT iPSC-DMs. 4OH-tamoxifen addition alone had no effect on expression of CD45, CD163 and CD169 (Appendix 3).

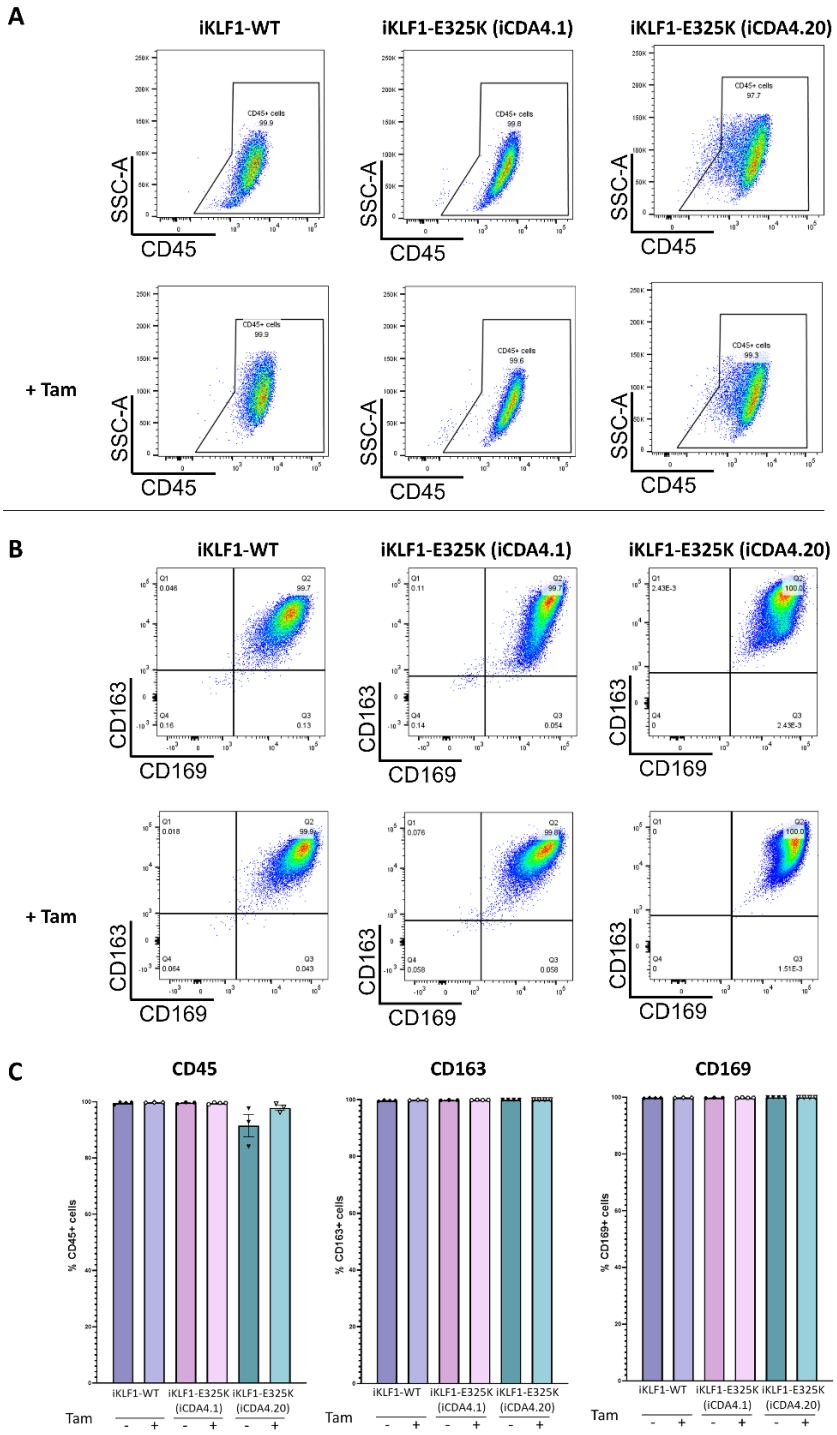

Figure 5.4 The E325K mutation in KLF1 has no effect on cell surface expression of CD45, CD163 and CD169. Flow cytometry analyses were performed on iPSC-DMs generated from two inducible iKLF1-E325K iPSC lines (iCDA4.1 and iCDA4.20) and one control iKLF1-WT iPSC line.

A: Representative flow cytometry plots of iPSC-DMs assayed for expression of CD45.

B: Representative flow cytometry plots of iPSC-DMs assayed for expression of CD163 and CD169.

C: Quantification of flow cytometry analyses of the percentage of cells expressing each marker. Datapoints represent individual macrophage harvests. Error bars represent SEM. One-way ANOVA with Tukey post-test generated no statistically significant p-values.

KLF1-E325K activation had no discernible effect on the expression of the mature macrophage marker 25F9, with a comparable percentage of $25F9^+$ cells observed between untreated and 4OH-tamoxifen treated iKLF1-E325K iPSC-DMs (Figure 5.5).

As iPSC-DMs mature, they lose expression of the monocyte marker CD93 (334). In agreement with a previous study in which KLF1-WT activation significantly increased cell surface expression of the mature macrophage marker CD206 (201), KLF1-WT activation reduced the percentage of immature $CD93^+$ iPSC-DMs (Figure 5.5). This suggests that KLF1-WT activation promotes iPSC-DM maturation. In contrast, KLF1-E325K activation increased the percentage of immature $CD93^+$ iPSC-DMs generated from both the heterozygous and homozygous iPSC lines (Figure 5.5). This suggests that the presence of the E325K mutation in KLF1 impedes its ability to induce the maturation of macrophages. In fact, activation of the KLF1-E325K protein in macrophages appears to inhibit macrophage maturation resulting in an increase in the proportion of cells expressing CD93.

Interestingly, there were significantly more $CD93^+$ iKLF1-E325K iPSC-DMs from untreated iPSC-DMs generated from the homozygous (iCDA4.20) iPSC line compared to untreated iKLF1-WT iPSC-DMs (Figure 5.5). This shows that there was a phenotypic effect to the leakiness of the KLF1-E325K-ER^{T2} system within iPSC-DMs, with observation of KLF1 staining and therefore the KLF1-E325K-ER^{T2} fusion protein in the nucleus of untreated macrophages (Figure 5.3).

Further evidence that the inhibition of macrophage maturation is associated with the KLF1-E325K mutation is provided by the observation that the increase in the proportion of $CD93^+$ cells is correlated with the level of expression of KLF1-E325K. There were significantly more immature $CD93^+$ iKLF1-E325K iPSC-DMs generated from the homozygous line (iCDA4.20) in which there are two copies of the KLF1-E325K-ER^{T2} transgene, compared to iKLF1-E325K iPSC-DMs generated from the heterozygous line (iCDA4.1) that only had one copy (Figure 5.5).

4OH-tamoxifen addition alone has no effect on expression of 25F9 and CD93 (Appendix 3).

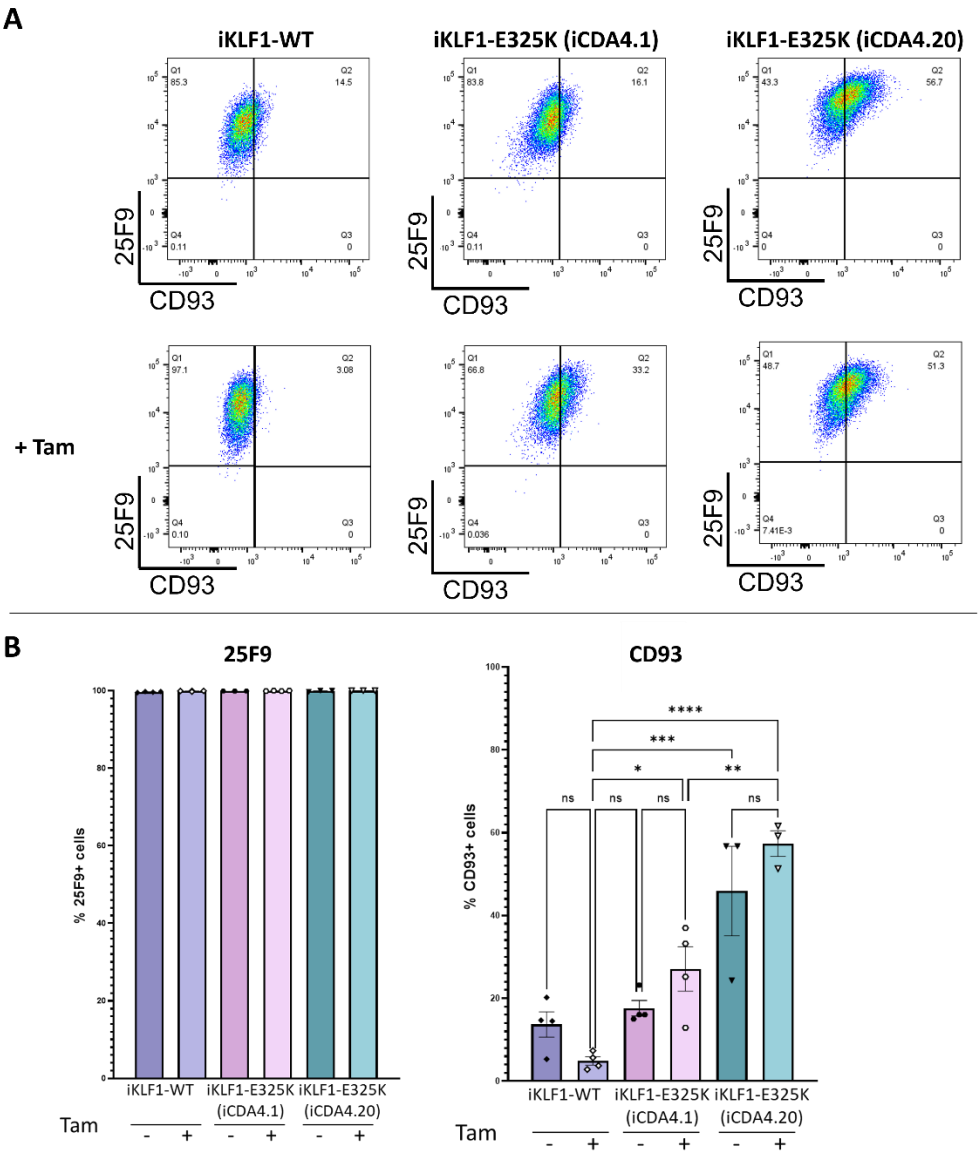

Figure 5.5 The E325K mutation in KLF1 impedes its ability to induce the maturation of macrophages. Flow cytometry analyses were performed on iPSC-DMs generated from two inducible iKLF1-E325K iPSC lines (iCDA4.1 and iCDA4.20) and one control iKLF1-WT iPSC line.

A: Representative flow cytometry plots of iPSC-DMs assayed for expression of 25F9 and CD93.

B: Quantification of flow cytometry analyses of the percentage of cells expressing each marker. Datapoints represent individual macrophage harvests. Error bars represent SEM. One-way ANOVA with Tukey post-test. *p < 0.05, **p < 0.01, ***p<0.001, ****p<0.0001.

5.3.3 Reduced maturation and enucleation of erythroid cells in co-culture with iKLF1-E325K iPSC-DMs compared to iKLF1-WT iPSC-DMs

I observed that the presence of the E325K mutation induced a phenotypic effect in iKLF1-E325K iPSCs, showing that KLF1-E325K impedes the loss of the monocyte marker CD93 from iKLF1-E325K iPSC-DMs (Figure 5.5). I next wanted to assess whether this phenotypic change in macrophage marker expression has any functional consequences. I hypothesised that iKLF1-E325K iPSC-DMs would be a more appropriate model for a CDA patient EBI macrophage due to their increased KLF1-E325K expression levels. Therefore, I assessed whether KLF1-E325K affected the function of EBI macrophages, specifically their supportive role in erythroid cell maturation. iKLF1-E325K iPSC-DMs were used in an *in vitro* model of the EBI niche described in chapter 3. Briefly iPSC-DMs were co-cultured with UCB-derived $CD34^+$ cells under erythroid differentiation cell culture conditions (Figure 3.9). Erythroid differentiation efficiency was measured by assessing the proportion of mature enucleated erythroid cells in the culture by flow cytometry on days 11, 14 , 18 and 21. Flow cytometry plots were gated as described in the methods (Chapter 2 Section 2.3.3).

The effect of co-culture with iKLF1-E325K iPSC-DMs was compared to the effect of iKLF1-WT iPSC-DMs as activation of KLF1 was previously shown to increase the percentage of mature enucleated erythroid cells produced from differentiating UCB-derived $CD34^+$ cells (201).

In agreement with results presented in Chapter 3, there was a progressive increase in the percentage of $CD235a^+$ suspension cells in all cultures, and by day 21 over 98% of cells in all conditions expressed CD235a (Figure 5.6B) . This result indicates that the E325K mutation in KLF1 had no significant effect on erythroid lineage commitment. In agreement with previous studies and results presented in Chapter 3, the presence of macrophages in the culture significantly increased erythroid cell maturation and enucleation (Figure 5.6C) (201, 211, 212). Averaged across cell lines, the percentage of mature enucleated erythroid cells increases from around 20% when cells are cultured without macrophages, to around 55-60% in the presence of macrophages (Figure 5.6C).

Interestingly, there was a decrease in the percentage of mature enucleated erythroid cells at both days 18 and 21 when differentiating erythroid cells were co-cultured with iKLF1-E325K iPSC-DMs compared to iKLF1-WT iPSC-DMs irrespective of 4OH-tamoxifen treatment (Figure 5.6C). At day 21, this decrease was approximately 15% (Figure 5.6). Consistent with CD93 expression described in the previous section, there appears to be a KLF1-E325K expression level-dependent effect on the number of mature enucleated cells produced. There was a slightly lower proportion of mature enucleated cells in co-cultures with iCDA4.20 iPSC-DMs that had two copies of the transgene compared to iCDA4.1 iPSC-DM that only had one (Figure 5.6C).

There is a modest increase in the percentage of mature enucleated cells in cultures with KLF1-WT activated iPSC-DMs at day 21, however the effect of activation was significantly less than previously observed (Figure 5.6C) (201). In agreement with previous findings there was no non-specific effect of 4OH-tamoxifen on expression of CD235a, or the percentage of mature enucleated cells in cultures when cultured with control iPSC-DMs that did not contain the transgene (Appendix 3).

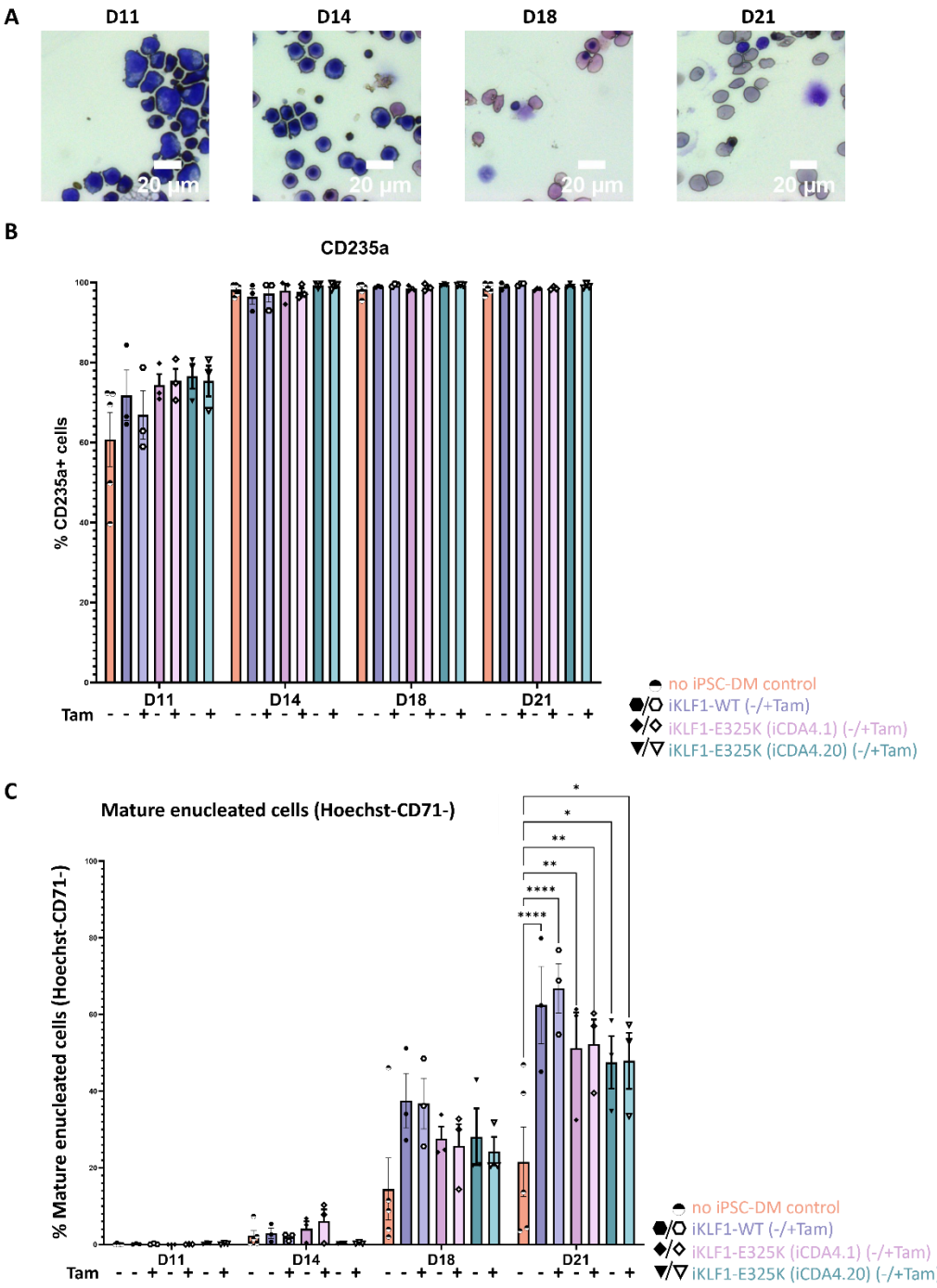

Figure 5.6 Fewer erythroid cells mature and enucleate in co-culture with iKLF1-E325K iPSC-DMs compared to iKLF1-WT iPSC-DMs.

A: Representative Kwik-Diff stained cytospins of UCB CD34$^+$ cells cultured in the presence of inducible line iPSC-DMs for days 11, 14, 18 and 21 of the culture.

B: Quantification of flow cytometry analyses of the percentage of CD235a$^+$ suspension cells for days 11, 14, 18 and 21 of the culture. Error bars represent SEM. One-way ANOVA with Tukey post-test generated no statistically significant p-values. Datapoints represent individual experiments.

C: Quantification of flow cytometry analyses of the percentage of Hoechst$^-$CD71$^-$ suspension cells for days 11, 14, 18 and 21 of the culture. Error bars represent SEM. One-way ANOVA with Tukey post-test. *p < 0.05, **p < 0.01, ***p<0.001, ****p<0.0001. Datapoints represent individual experiments.

5.3.4 Tamoxifen treatment alone has no observed effect on iPSC-derived macrophage phenotype and function within the erythroblastic island

Untreated and 4OH-tamoxifen treated iPSC-DMs from the parental iPSC line (SFCi55) were used to assess any effects as a result of 4OH-tamoxifen treatment only.

4OH-tamoxifen treatment had no effect on iPSC-DM morphology or cell surface marker expression of CD45, CD93, 25F9, CD163 or CD169. 4OH-tamoxifen treatment also had no effect on CD235a expression and the percentage of mature enucleated cells at several timepoints in an *in vitro* model of the EBI (Figure 5.7).

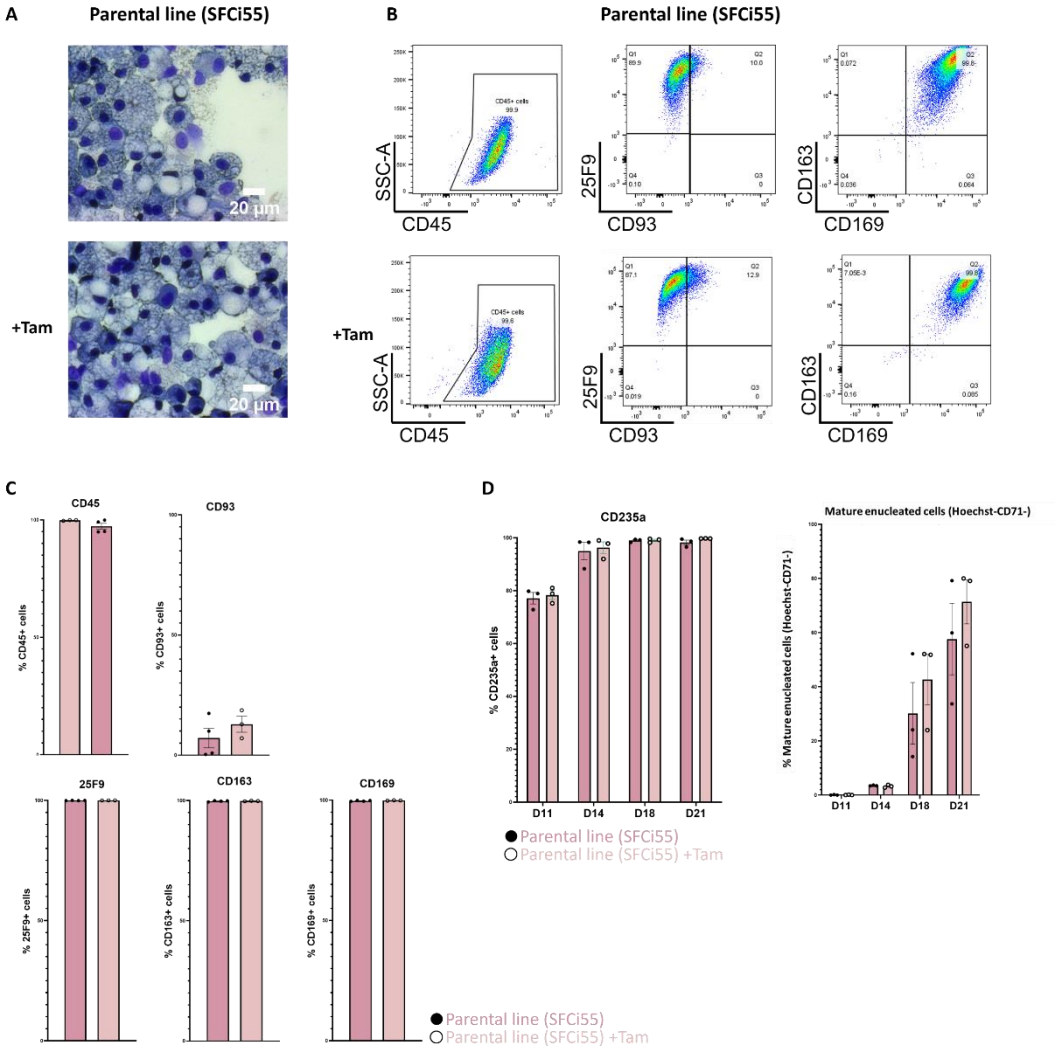

Figure 5.7 4OH-tamoxifen treatment alone has no observed effect on macrophages generated from parental line iPSCs (SFCi55)

A: Representative Kwik-Diff stained cytospins of parental line (SFCi55) iPSC-DMs. 20X magnification. 20 µm scale bar.

B: Representative flow cytometry plots of parental line iPSC-DMs assayed for expression of CD45, CD93, 25F9, CD163 and CD169.

C: Quantification of flow cytometry analyses of the percentage of iPSC-DMs expressing each marker. Datapoints represent individual macrophage harvests. Error bars represent SEM. Unpaired t-tests generated no statistically significant p-values.

D: Quantification of flow cytometry analyses of the percentage of suspension cells expressing CD235a, Hoechst and CD71 for days 11, 14, 18 and 21 of the culture. Datapoints represent individual experiments. Error bars represent SEM. Unpaired t-tests generated no statistically significant p-values.

5.4 Discussion

Macrophages were generated from both the heterozygous and homozygous iKLF1-E325K iPSC lines (iCDA4.1 and iCDA4.20). I have shown that the presence of a E325K mutation in iPSC-DMs impedes the maturation of macrophages assessed using the monocyte marker CD93. Additionally, the E325K mutation reduced the function of iPSC-DMs in an *in vitro* model of the EBI niche. Fewer erythroid cells matured and enucleated in co-culture with iKLF1-E325K iPSC-DMs compared to iKLF1-WT iPSC-DMs.

5.4.1 Leakiness of KLF1-E325K-ER^{T2} system in iPSC-DMs

As observed in undifferentiated iPSCs in Chapter 4, both iKLF1-E325K and iKLF1-WT iPSC-DMs show leakiness, with staining of KLF1 and therefore the KLF1-E325K/WT-ER^{T2} fusion protein, observed in the nucleus of untreated iPSC-DMs. This leakiness was not quantified however comparison of KLF1 staining images presented in this and the previous chapter show that there is more leakiness of the system in iPSC-DMs compared to the undifferentiated iPSCs. This cell-specific effect suggests that either an aspect of the intrinsic biology of macrophages themselves induces translocation of the fusion protein, or an experimental factor in the differentiation of iPSCs to macrophages is inducing translocation. It is possible that one of the media components used in the differentiation and culture of iPSC-DMs contains a 4OH-tamoxifen analogue, and as a result is inducing translocation of the fusion protein. It is difficult to control for changes in purchased media, and as discussed in Chapter 4 an issue or a change in formulation of media could introduce experimental variability.

In contrast to cells generated under erythroid differentiation conditions, the presence of the KLF1-E325K- ER^{T2} fusion protein in the nucleus of untreated iKLF1-E325K iPSC-DMs had a significant phenotypic effect. There were significantly more CD93^{+} iKLF1-E325K iPSC-DMs from untreated iPSC-DMs generated from the homozygous (iCDA4.20) iPSC line compared to untreated iKLF1-WT iPSC-DMs. This shows that there was sufficient translocation of the KLF1-E325K-ER^{T2} fusion protein to the nucleus in untreated macrophages to induce effects of the E325K mutation.

5.4.2 The E325K mutation impedes the loss of CD93 induced by KLF1

As iPSC-DMs mature, they lose expression of the monocyte marker CD93 (334). Activation of KLF1-WT reduced the percentage of $CD93^+$ iPSC-DMs, suggesting that KLF1-WT activation promotes iPSC-DM maturation. This supports previous work showing that activation of KLF1-WT significantly increased the cell surface expression of the mature macrophage marker CD206 (201). In contrast, significantly more macrophages derived from the iKLF1-E325K lines expressed CD93 compared to control macrophages where KLF1-WT was activated. As CD93 is a monocyte marker that is lost in mature macrophages, these data suggest that the presence of the E325K mutation in KLF1 impedes the ability of this transcription factor to induce macrophage maturation.

Over 99% of iPSC-DMs generated from both iKLF1-E325K iPSC lines are positive for the mature macrophage marker 25F9, with over 97% of these already positive for this marker only 3 days after being harvested from EBs (unpublished data). At this early stage of differentiation, most iPSC-DMs express CD93 (unpublished data) and are therefore immature. These mature over the next few days and by 9 days after harvesting from EBs, over 89% lose CD93 expression and are $25F9^+$ $CD93^-$ (unpublished data). Thus, the majority of iKLF1-E325K iPSC-DMs being $25F9^+$ does not implicate them as mature macrophages, only in combination with loss of CD93 are iPSC-DMs considered fully mature.

5.4.3 Fewer erythroid cells matured and enucleated in co-culture with iKLF1-E325K iPSC-DMs compared to iKLF1-WT iPSC-DMs

I observed a lower percentage of mature enucleated erythroid cells at both days 18 and 21 in co-cultures with iKLF1-E325K iPSC-DMs compared to iKLF1-WT iPSC-DMs. At day 21, this decrease was approximately 15%. While this decrease was not statistically significant, it could represent a biologically relevant result. Indeed, several studies caution against dismissing results simply because they do not meet the $p > 0.05$ significance threshold (345, 346). A decrease of 15% in enucleation in human definitive erythropoiesis, in which 2 million RBCs are generated each second, would equate to a decrease of 300,000 mature enucleated RBCs each second (19). Additionally, when compared to cultures with no macrophages, significantly more

erythroid cells mature and enucleate in the presence of iKLF1-WT iPSC-DMs compared to iKLF1-E325K iPSC-DMs.

A previously published study which used iKLF1-WT iPSC-DMs in the same *in vitro* EBI model reported a significant increase in the percentage of mature enucleated erythroid cells in cultures when KLF1-WT was activated in iPSC-DMs (201). In contrast, I observed a modest increase in the percentage of mature enucleated erythroid cells in cultures with 4OH-tamoxifen treated iKLF1-WT iPSC-DMs (KLF1 activation) compared with untreated iKLF1-WT iPSC-DMs. One explanation for the reduced effect of KLF1-WT activation in our EBI model could be due to the leakiness of the system. I observed KLF1 staining, and therefore the KLF1-WT-ER^{T2} fusion protein, in the nucleus of untreated iKLF1-WT macrophages. It is possible that KLF1-WT-ER^{T2} fusion protein was present the in the nucleus of untreated iKLF1-WT iPSC-DMs at levels sufficient to induce expression of KLF1-target genes, for example those previously identified to encode for secreted factors that promote erythroid cell maturation and enucleation (201).

RNA-sequencing analysis of CDA patient erythroid cells identified that the gene encoding for the structural protein ICAM4 is expressed at a lower level in CDA patient erythroid cells compared to cells from a healthy donor (131). ICAM4 on erythroblasts binds to αv integrin on macrophages and is critical for EBI integrity (218, 219). Therefore, it would be very interesting to investigate whether reduced *ICAM4* expression affects EBI integrity *in vitro* using our EBI model. Additionally, it would be interesting to investigate whether EBIs generated from CDA patient erythroid cells cultured with iKLF1-E325K iPSC-DMs have less integrity than EBIs generated from CDA patient erythroid cells cultured with iKLF1-WT iPSC-DMs. Attempts were made to investigate these questions, however due to the low viability of cells generated from both CDA patient and iKLF1-E325K iPSCs under erythroid differentiation conditions, they were unable to survive in such *in vitro* EBI cultures.

Chapter 6: Transcriptional profiling of iPSC-derived macrophages identifies KLF1-E325K as a loss-of-function mutation

6.1 Introduction

RNA-sequencing analysis of CDA patient erythroid cells identified several dysregulated genes in comparison with healthy erythroid cells (131). For example, genes encoding structural proteins such as *ICAM4,* and genes encoding membrane proteins such as *BAND 3*, are downregulated in CDA erythroid cells compared to healthy control cells (131). The intrinsic transcriptional effect of KLF1-E325K within erythroid cells of CDA patients is therefore well defined. However, whether there is a transcriptional effect in patient EBI macrophages had not been investigated. Over 65 mutations in KLF1 have been identified in humans, resulting in a diverse range of phenotypes (347). It is possible that these phenotypes are, in part, the result of mutant KLF1 expression in cell types outside of the erythroid lineage, such as EBI macrophages. I applied the iKLF1-E325K iPSC system to generate macrophages and investigate their phenotype and function. I identified that the KLF1-E325K mutation prevents the loss of CD93 by iPSC-DMs and observed reduced maturation and enucleation of erythroid cells in co-culture with iKLF1-E325K iPSC-DMs compared to co-culture with iKLF1-WT iPSC-DMs (Chapter 5).

I hypothesised that this reduction in the function of iKLF1-E325K iPSC-DMs to support erythroid cell maturation and enucleation within the EBI is due to the dysregulation of key genes involved in EBI macrophage function. To investigate this hypothesis, I generated a transcriptomic dataset. Generating a transcriptomic dataset of iKLF1-E325K macrophages would allow for their comparison with iKLF1-WT macrophages to investigate whether there are any transcriptomic alterations as a result of the KLF1-E325K mutation in macrophages. Characterisation and validation of any dysregulated genes could identify new therapeutic targets for the treatment of CDA within EBI macrophages. Additionally, the dataset could be used to identify factors that can be tested for a role in erythroid cell maturation and enucleation.

6.2 Aims and Approaches

1. The first aim of this chapter was to generate a transcriptomic data set of iKLF1-E325K and iKLF1-WT iPSC-DMs and investigate whether any genes are differentially regulated by KLF1-E325K compared to KLF1-WT. Bulk-RNA sequencing was performed on macrophages generated from the parental (SFCi55), iKLF1-WT and the

heterozygous iKLF1-E325K iPSC line (iCDA4.1) in the presence and absence of 4OH-tamoxifen.

2. The second aim of this chapter was to utilise the transcriptomic dataset to identify factors that could play a role in supporting erythroid cell maturation and enucleation.

6.3 Results

6.3.1 Transcriptome profiling of iPSC-derived macrophages

6.3.1.1 Sample preparation and quality control

I generated macrophages from three iPSC lines: parental line (SFCi55), iKLF1-E325K (iCDA4.1) and iKLF1-WT. Macrophages were either untreated or treated with 100 nM of 4OH-tamoxifen (5 replicates of each). Macrophages were harvested on day 11 of the terminal maturation stage, stage 3, of the iPSC-macrophage differentiation (Figure 3.5). For 4OH-tamoxifen treated samples, 4OH-tamoxifen was added during stage 3 on days 8 and 10. RNA was extracted from these samples and tested for integrity. The integrity of RNA used in an RNA-sequencing (RNA-seq) analysis is the most important factor for obtaining good quality data (348). The integrity of the RNA used for RNA-seq in this analysis was assessed by calculating an RNA Integrity Number (RIN) using a Bioanalyzer (Chapter 2 Section 2.5.4). The use of RIN allows for standardisation of RNA quality control and can be more accurate than using the ratio of 28S:18S to assess RNA quality (349). RIN values above seven are considered suitable for downstream analyses (348). RIN values for each of the samples was above 8, and therefore of good quality (Figure 6.1). TruSeq stranded mRNA-seq libraries were generated from RNA samples by Edinburgh Genomics, who also performed sequence alignments (Chapter 2 Section 2.5.4).

A

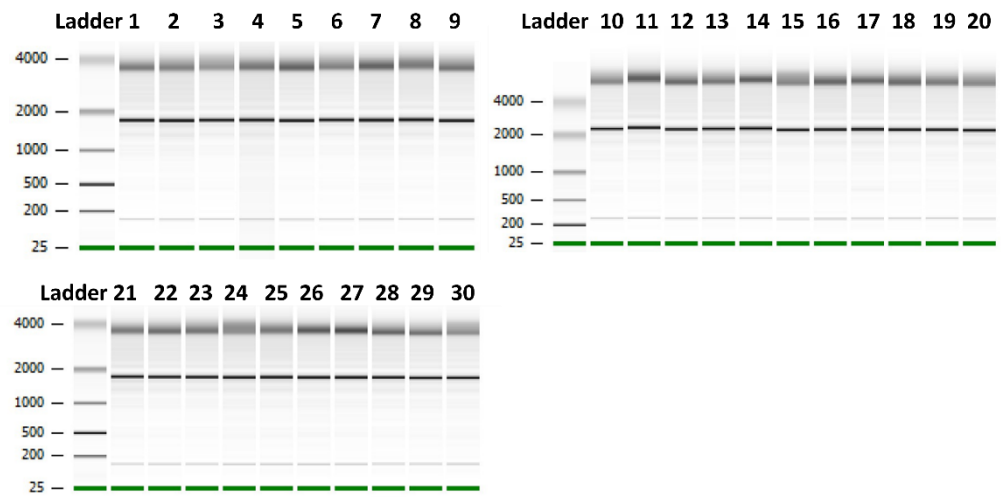

B

Lane	Sample	RIN
1	Parental	9.10
2	Parental	8.30
3	Parental	9.20
4	Parental	9.20
5	Parental	9.40
6	iKLF1-WT	9.30
7	iKLF1-WT	9
8	iKLF1-WT	9.10
9	iKLF1-WT	9.20
10	iKLF1-WT	8.20
11	iKLF1-E325K	8.80
12	iKLF1-E325K	8.70
13	iKLF1-E325K	8.90
14	iKLF1-E325K	8.80
15	iKLF1-E325K	8.90

Lane	Sample	RIN
16	Parental +Tam	9.10
17	Parental +Tam	9
18	Parental +Tam	8.60
19	Parental +Tam	8.50
20	Parental +Tam	8.70
21	iKLF1-WT +Tam	9.30
22	iKLF1-WT +Tam	9.10
23	iKLF1-WT +Tam	8.30
24	iKLF1-WT +Tam	8.80
25	iKLF1-WT +Tam	8.90
26	iKLF1-E325K +Tam	8.80
27	iKLF1-E325K +Tam	8.90
28	iKLF1-E325K +Tam	9.30
29	iKLF1-E325K +Tam	8.70
30	iKLF1-E325K +Tam	8.40

Figure 6.1 Assessment of RNA quality of samples generated for bulk-RNA sequencing. iPSC-DMs were generated from the parental (SFCi55), iKLF1-WT and iKLF1-E325K (iCDA4.1) iPSC lines. RNA was extracted from 10 harvests per cell line, 5 cultured with the addition of 100nM 4OH-tamoxifen for 4 days, and 5 cultured in the absence of 4OH-tamoxifen.
A: Separation profiles for all 30 samples
B: RIN values for each sample.

6.3.1.2 Principal component analyses and clustering

Principal component analyses (PCA) plots were generated for the first and second principal components for all 30 samples. Samples were annotated for the iPSC line that macrophages were generated from, and 4OH-tamoxifen treatment (Figure 6.2A). The main difference between samples was between iKLF1-WT iPSC-DMs and the other samples (iKLF1-WT and parental line iPSC-DMs). iKLF1-E325K iPSC-DMs cluster closely with parental line iPSC-DMs. A multidimensional scaling (MDS) plot was generated for all samples and annotated for the iPSC line macrophages were generated from, and 4OH-tamoxifen treatment (Figure 6.2B). There is a clear segregation between untreated iKLF1-WT iPSC-DMs and 4OH-tamoxifen treated iKLF1-WT iPSC-DMs (Figure 6.2B). PCA and MDS plots are both techniques for dimensionality reduction and visualisation, however they optimise for different parameters. PCA projects directions in the data with the most variance, while MDS projects points where distances are preserved. Samples were also clustered by euclidean distances and again, iKLF1-E325K iPSC-DMs cluster closely with parental line iPSC-DMs (Figure 6.2C).

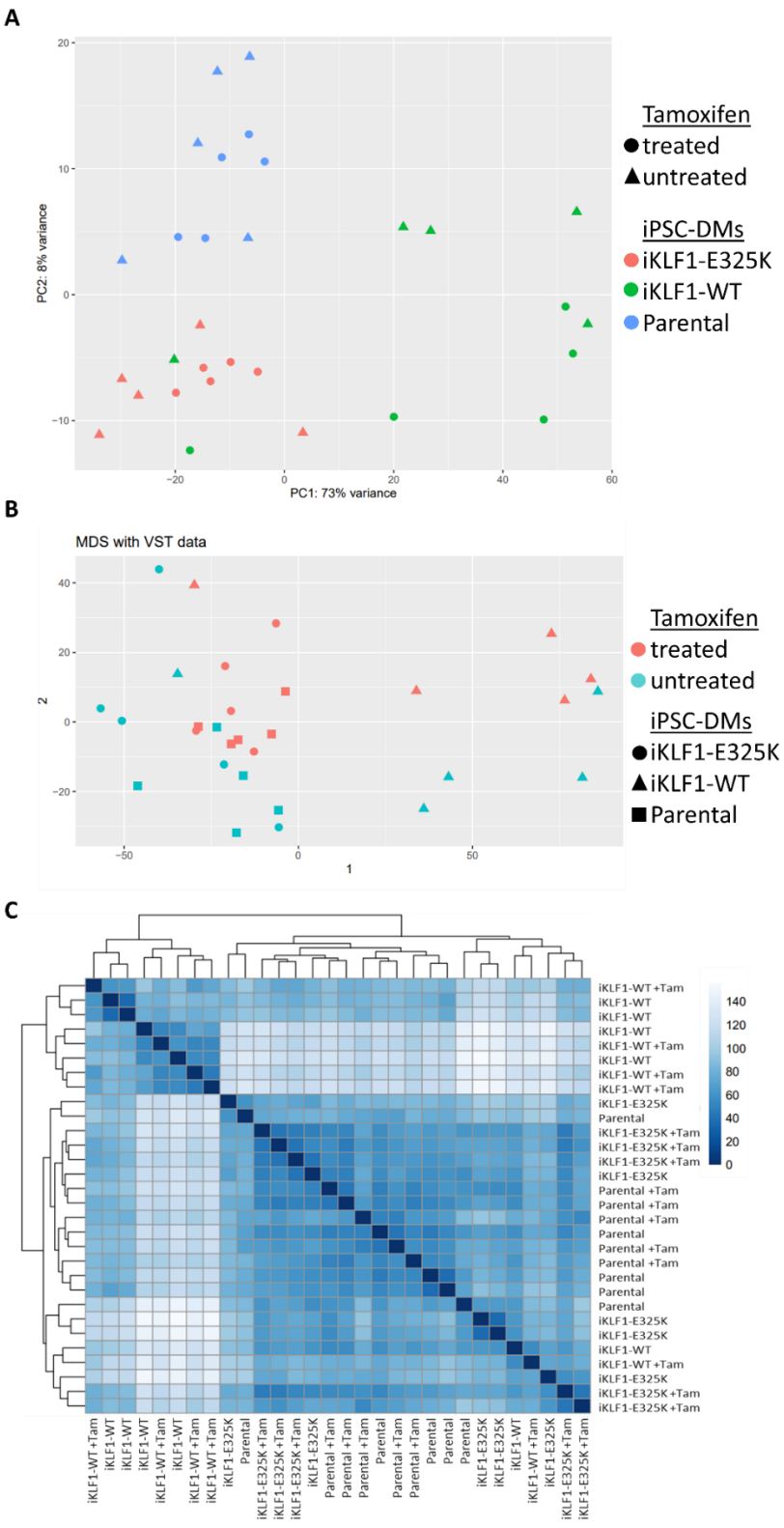

Figure 6.2 iKLF1-E325K iPSC-DMs cluster separately from iKLF1-WT iPSC-DMs and closely to parental line iPSC-DMs Samples were annotated for the iPSC line macrophages were generated from, and 4OH-tamoxifen treatment. Datapoints represent individual samples. **A:** PCA plot of the first and second principal components generated using all 30 samples. **B:** MDS plot generated using all 30 samples.
C: Clustering of all 30 samples based on euclidean distances.

6.3.1.3 Differential gene expression analyses

Differential gene expression analyses were performed using the DESeq2 package (Chapter 2 Section 2.5.4). Genes were filtered for a count of 10 or higher in at least 2 samples, and an adjusted p-value below 0.05. It was anticipated that KLF1-WT would regulate more genes than KLF1-E325K for two reasons. Firstly, 4OH-tamoxifen treatment of iKLF1-WT iPSC-DMs activates KLF1-WT, the fully functional protein that has been previously identified to regulate gene expression in EBI macrophages (68, 201). Secondly, as described in Chapter 4, iKLF1-WT iPSCs have two copies of the KLF1-WT-ER^{T2} transgene, while iKLF1-E325K iPSCs have only one copy of the iKLF1-E325K-ER^{T2} transgene.

Differential expression analysis between untreated and 4OH-tamoxifen treated iKLF1-E325K iPSC-DMs identified 17 up-regulated and 2 down-regulated genes (Figure 6.3A). Differential expression analysis between untreated and 4OH-tamoxifen treated iKLF1-WT iPSC-DMs identified 221 up regulated genes and 203 down-regulated genes (Figure 6.3B). Differential gene expression analysis between untreated and 4OH-tamoxifen treated parental line iPSC-DMs identified 19 up-regulated and 2 down-regulated genes. Of these 4OH-tamoxifen up- and down-regulated genes only *SRPX2*, a proteoglycan over expressed in human cancer, was regulated by either KLF1-WT or KLF1-E325K and was down-regulated upon KLF1-WT activation (350). As such, *SRPX2* is excluded from further analyses presented in this chapter.

KLF1 has been demonstrated to regulate several genes important for integrity of the EBI, and KLF1 activation was previously shown to up-regulate several genes involved within the EBI (68, 201). Because I hypothesised that the reduction in the function of iKLF1-E325K iPSC-DMs to support erythroid cell maturation and enucleation within the EBI presented in the previous chapter is due to the dysregulation of key genes involved in EBI macrophage function, I focussed my analysis on the top up-regulated genes (Figure 6.3C/D). Most strikingly, of the 221 genes up-regulated upon KLF1-activation, only 5 were also up-regulated upon KLF1-E325K activation (Figure 6.3E).

TRG-AS1, PHOSPHO1, SLC11A1, an uncharacterised transcript, and *IL-33* are up-regulated upon activation of both KLF1-WT and KLF1-E325K (Figure 5.3E).

A

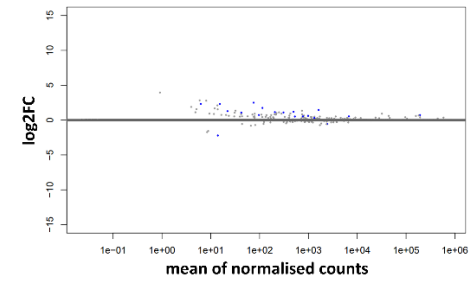

B

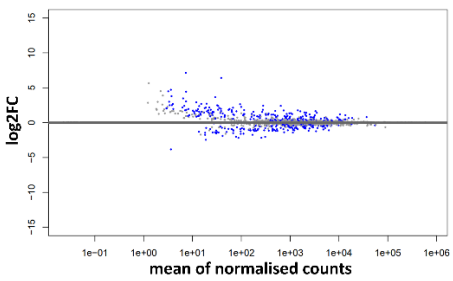

C

Up-regulated genes
iKLF1-E325K vs iKFL1-E325K +Tam

Gene	Log2FC
TMEM168	0.306515
PHC1P1	0.511415
TRG-AS1	0.531043
MT-TP	0.534019
GSE1	0.617724
MT-CYB	0.728561
TDO2	0.734786
SOCS3	1.082487
TGFA	1.094275
DACT3	1.147702
PHOSPHO1	1.198515
SSC5D	1.281377
SLC11A1	1.457926
Uncharacterised transcript	1.74479
TREM1	2.316142
IL33	2.327529
LGALS2	2.499182

D

Top up-regulated genes
iKLF1-WT vs iKFL1-WT +Tam

Gene	Log2FC
IL33	2.179093
CD300E	2.2561
CEACAM3	2.383734
FFAR3	2.396169
RHBDL3	2.409973
FFAR2	2.41574
EPHB6	2.438721
S100A16	2.489859
IL1RL1	2.498954
DSG3	2.502357
RAB27B	2.654442
ANGPTL7	2.677951
GPR42	2.688941
NLRP12	2.719696
AKR1C1	2.914237
RNASE7	2.998179
RXFP1	3.043993
TRABD2B	3.484162
CAV1	3.653689
TUBBP5	3.794367
NGFR	4.440166
MMP28	4.495856
PRRT4	4.718408
FDCSP	6.41501
AADAC	7.144139

E

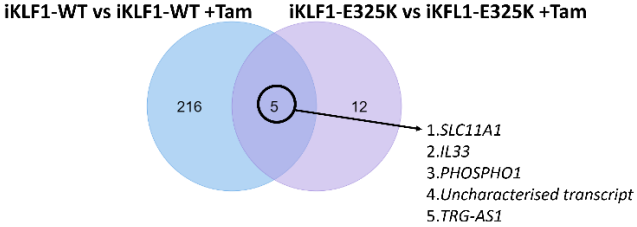

Figure 6.3 Differential gene expression analyses of iKLF1-E325K and iKLF1-WT iPSC-DMs. Genes were filtered for a count of 10 or higher in at least 2 samples, and an adjusted p-value below 0.05.

A/B: Volcano plots for specified contrasts illustrating up-and down-regulated genes by Log2 fold change (Log2FC). Blue dots represent individual genes with an adjusted p-value below 0.05.

C: Table of genes up-regulated in iKLF1-E325K iPSC-DMs treated with 4OH-tamoxifen compared to untreated iKLF1-E325K iPSC-DMs. Genes ordered in ascending Log2FC.

D: Table of genes up-regulated in iKLF1-WT iPSC-DMs treated with 4OH-tamoxifen compared to untreated iKLF1-WT iPSC-DMs. Genes ordered in ascending Log2FC.

E: Venn diagram of genes up-regulated in 4OH-tamoxifen treated iKLF1-WT iPSC-DMs and genes up-regulated in 4OH-tamoxifen treated iKLF1-E325K iPSC-DMs.

This data is consistent with a previous report that identified *IL-33* as a gene up-regulated upon KLF1-WT activation in iPSC-DMs (201). *IL-33* encodes for the secreted factor IL-33, and IL-33 treatment was demonstrated to significantly increase the maturation and enucleation of UCB-derived $CD34^+$ cells under erythroid differentiation conditions when added to cultures in combination with two other secreted factors, ANGPTL7 and SERPBINB2 (201). IL-33 in combination with either ANGPTL7 and/or SERPINB2 was able to increase erythroid cell maturation and enucleation, however IL-33 treatment alone did not (201). In this dataset, *ANGPTL7* is significantly up-regulated upon KLF1-WT activation, but not upon KLF1-E325K activation (Figure 6.3C/D). *SERPINB2* was not identified as an up-regulated gene in this transcriptomic dataset. I observed in the previous chapter that fewer erythroid cells matured and enucleated in co-culture with iKLF1-E325K iPSC-DMs compared to iKLF1-WT iPSC-DMs (Figure 5.6). The loss of *ANGPTL7* expression in iKLF1-E325K iPSC-DMs could be responsible for this reduced function within the EBI niche.

There is no significant increase in *IL-33* counts in parental line iPSC-DMs upon the addition of 4OH-tamoxifen, therefore *IL-33* expression is not up-regulated by 4OH-tamoxifen treatment only (Figure 6.4A). qRT-PCR was used to validate *IL-33* expression in iKLF1-E325K iPSC-DMs from the homozygous line (iCDA4.20) as only the heterozygous iPSC line was included in RNA-sequencing (Figure 6.4B). Both normalised count data and qPCR suggest that up-regulation of *IL-33* is lower in iKLF1-E325K iPSC-DMs compared with iKLF1-WT iPSC-DMs (Figure 6.4A/B). The decrease in *IL-33* up-regulation between iKLF1-WT iPSC-DMs and iKLF1-E325K iPSC-DMs appeared to be correlated with the level of expression of KLF1-E325K. There was a lower up-regulation of *IL-33* in iKLF1-E325K iPSC-DMs generated from the homozygous line (iCDA4.20) in which there are two copies of the KLF1-E325K-ER^{T2} transgene, compared to iKLF1-E325K iPSC-DMs generated from the heterozygous line (iCDA4.1) that only had one copy (Figure 6.4B).

I identified *TGFA* to be the only gene that is differentially regulated by KLF1-E325K compared to KLF1-WT (Figure 6.4C). *TGFA* encodes for the protein transforming growth factor alpha (TGF-α), a member of the epidermal growth factor which activates a signalling pathway for cell proliferation (351). *TGFA* is significantly up-regulated upon KLF1-E325K activation, and in contrast is significantly down-regulated upon KLF1-WT activation (Figure 6.4). Primers to assay *TGFA* expression in iKLF1-E325K iPSC-DMs generated from the homozygous line could not be obtained in time for preparation of this thesis.

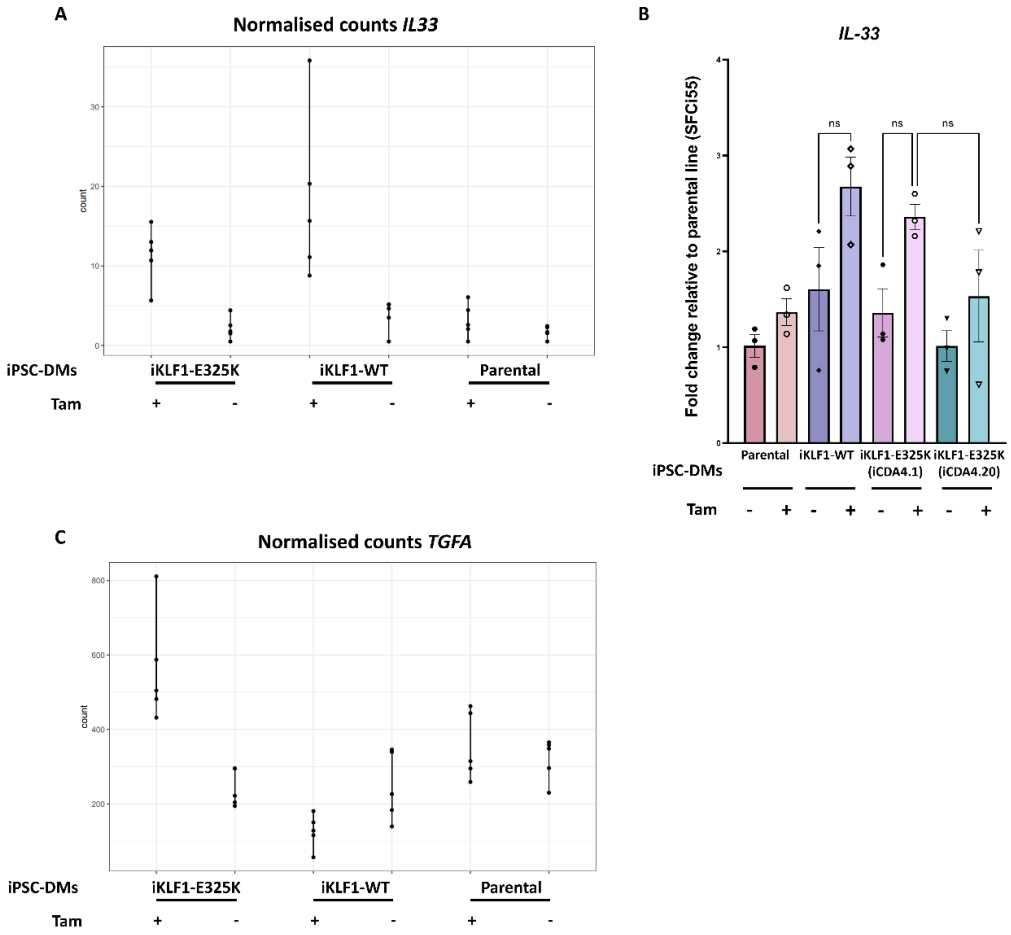

Figure 6.4 Normalised counts and gene expression analyses. Normalised counts shown for all 30 samples sequenced. qRT-PCRs were conducted on RNA extracted from iPSCs from the parental (SFCi55), iKLF1-WT, and both iKLF1-E325K iPSC lines (iCDA4.1 and iCDA4.20).
A: Normalised counts for *IL-33*. Datapoints represent individual samples.
B: Gene expression of *IL-33* assessed by qRT-PCR. Datapoints represent individual harvests. Fold change analysed relative to parental line (SFCi55) iPSC-DMs -tam. Error bars represent SEM. One-way ANOVA with Tukey post-test. *p < 0.05, **p < 0.01.
C: Normalised counts for *TGFA.* Datapoints represent individual samples.

6.3.1.4 Differentially expressed genes encoding secreted factors not identified by differential gene expression analyses

One limitation to the iPSC-DMs used to generate this transcriptomic dataset is that I observed translocation of the KLF1-WT- and KLF1-E325K-ER^{T2} fusion proteins to the nucleus of untreated macrophages (Figure 5.3). This translocation in the absence of 4OH-tamoxifen was shown to be at amounts sufficient enough to induce a phenotypic effect in iKLF1-E325K iPSC- DMs (Figure 5.5). I speculated that this leakiness to the system in iPSC-DMs could hinder the identification of differentially expressed genes. Due to this leakiness, some differentially expressed genes could be up- or down-regulated in untreated iPSC-DMs sufficiently enough that they would not be identified as differentially expressed.

To investigate this, I utilised a previously published dataset of bulk RNA-sequencing of untreated and 4OH-tamoxifen treated iKLF1-WT iPSC-DMs (201). These iKLF1-WT iPSC-DMs demonstrated less nuclear translocation of the KLF1-WT-ER^{T2} fusion protein in untreated macrophages than the macrophages used in this chapter (unpublished data). Differential expression analysis of untreated and 4OH-tamoxifen treated iKLF1-WT iPSC-DMs in the published dataset identified 803 up-regulated and 593 down-regulated genes upon KLF1-WT activation. This is much higher than the 221 up regulated and 203 down-regulated genes identified upon KLF1-WT activation in my dataset (Figure 6.3B). This data suggests that there are a considerable number of KLF1-WT regulated genes not identified in my analyses.

I probed my dataset for expression of the previously validated top-20 most differentially expressed genes encoding secreted factors up-regulated by KLF1-WT activation (201). Ie chose to probe for genes encoding secreted factors because several of these factors were subsequently identified to support erythroid cell maturation and enucleation. 4 of the top-20 genes encoding secreted factors were identified in my differential gene expression analysis as up-regulated upon KLF1-WT activation: *FDCSP*, *ANGPTL7*, *IL-33*, and *ABI3BP* (Figure 6.5A). Probing for the remaining previously identified 16 genes encoding secreted factors up-regulated upon KLF1-WT activation using normalised count data identified one gene that appeared to be up-regulated upon KLF1-WT activation in my dataset, *IGFBP6* (Figure

6.5B). *IGFBP6* has been previously indicated to have a potential role in erythroid cell maturation and enucleation (unpublished data). There is no increase in counts in parental line iPSC-DMs upon the addition of 4OH-tamoxifen, therefore *IGFBP6* expression was not up-regulated by 4OH-tamoxifen treatment only (Figure 6.5B). qRT-PCR was used to investigate whether *IGFBP6* expression was significantly upregulated in 4OH-tamoxifen treated iKLF1-WT iPSC-DMs. qRT-PCR was also used to investigate *IGFBP6* expression in iKLF1-E325K iPSC-DMs from the homozygous line (iCDA4.20). *IGFBP6* is significantly up-regulated upon KLF1-WT activation, but not upon KLF1-E325K activation (Figure 6.5C).

A

Top-20 previously validated genes encoding secreted factors up-regulated by KLF1-WT activation	Genes encoding secreted factors up-regulated by KLF1-WT activation identified by differential expression analysis in our dataset	Genes encoding secreted factors up-regulated by KLF1-WT activation by normalised counts in our dataset
FDSCP	FDCSP	
PI16		
ANGPTL7	ANGPTL7	
IL33	IL33	
SERPINB2		
ODAM		
PTHLH		
TNFAIP6		
CFP		
PI3		
TRH		
NRG1		
SERPINA1		
ABI3BP	ABI3BP	
NTNG1		
CST2		
NOV		
IGFBP6		IGFBP6
CCL13		
TNFSF10		
Not identified in our data set	Identified by differential expression analysis	Identified by normalised counts

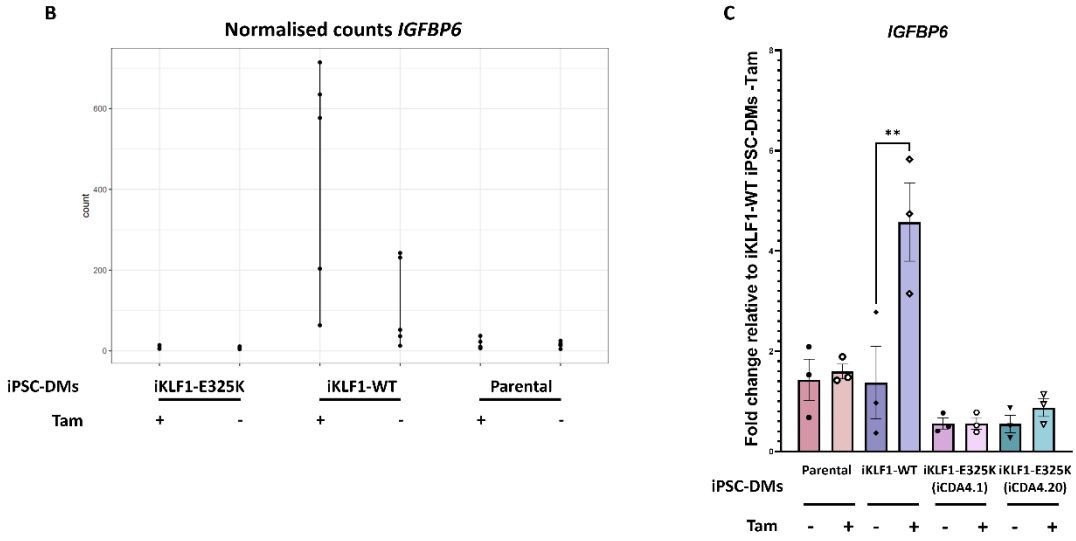

Figure 6.5 IGFBP6 is up-regulated upon KLF1-WT activation and not upon KLF1-E325K activation. Normalised counts shown for all 30 samples sequenced. qRT-PCRs were conducted on RNA extracted from iPSCs from the parental (SFCi55), iKLF1-WT, and both iKLF1-E325K iPSC lines (iCDA4.1 and iCDA4.20).

A: Table showing the previously validated top-20 genes encoding for secreted factors that are up-regulated by KLF1-WT (201). Genes in red were not identified in *my* dataset. Genes in green were identified in my data set by differential gene expression analysis of untreated and 4OH-tamoxifen treated iKLF1-WT iPSC-DMs. Genes in orange were identified in my dataset by normalised counts.

B: Normalised counts for IGFBP6. Datapoints represent individual samples.

C: Gene expression of IGFBP6 assessed by qRT-PCR. Fold change was analysed relative to untreated iKLF1-WT iPSC-DMs. Datapoints represent individual harvests. Error bars represent SEM. One-way ANOVA with Tukey post-test. *$p < 0.05$, **$p < 0.01$.

6.3.1.5 Genes encoding EBI macrophage attachment proteins

In the *in vitro* model of the EBI presented in the previous chapter, fewer erythroid cells matured and enucleated in co-culture with iKLF1-E325K iPSC-DMs compared to iKLF1-WT iPSC-DMs (Figure 5.6). However, there are still significantly more mature enucleated cells in the cultures with iKLF1-E325K iPSC-DMs compared to cultures with no macrophages (Figure 5.6). This demonstrates that iKLF1-E325K iPSC-DMs have a reduced function within the EBI niche, but still retain a significant ability to mature and enucleate erythroid cells. The cell-cell contact of macrophages with erythroblasts within the EBI has been indicated to be more important to promoting erythroid cell maturation and enucleation than the secretion of factors (201, 209). I speculated that this partially retained ability of iKLF1-E325K iPSC-DMs to promote the maturation and enucleation of erythroid cells is due to cell-cell contact mediated by attachment proteins. No genes encoding for EBI attachment proteins were identified to be differentially expressed in my differential expression analyses, therefore I probed my dataset for normalised counts of the following genes encoding EBI macrophage attachment proteins:

- VCAM1: VCAM1 on macrophages binds to α4β1 integrin on erythroblasts (207).
- EMP/MAEA: Erythrocyte macrophage protein, also known as macrophage erythroid attacher (MAEA). EMP/MAEA on macrophages binds both EMP/MAEA on erythroblasts and to a currently unidentified macrophage EMP/MAEA receptor on erythroblasts (211, 213, 214, 216).
- ITGAV. Also known as αv integrin. ITGAV on macrophages binds to ICAM4 on erythroblasts (218, 219).
- CD163. An *in vitro* study in rat EBIs demonstrated that CD163 promotes erythroid cell proliferation (221, 225).
- CD169. Also known as Siglec1. CD169 is extensively expressed by EBI macrophages and has been shown to localise to sites of macrophage-erythroblast contact in EBIs (222).
- PALLADIN: PALLADIN-null macrophages fail to reconstitute EBIs, while PALLADIN-null erythroblasts retain the ability to do so (223, 224).

VCAM1, EMP/MAEA, ITGAV, CD163, CD169 and *PALLADIN* are expressed by iKLF1-E325K, iKLF1-WT and parental line iPSC-DMs irrespective of 4OH-tamoxifen treatment (Figure 6.6).

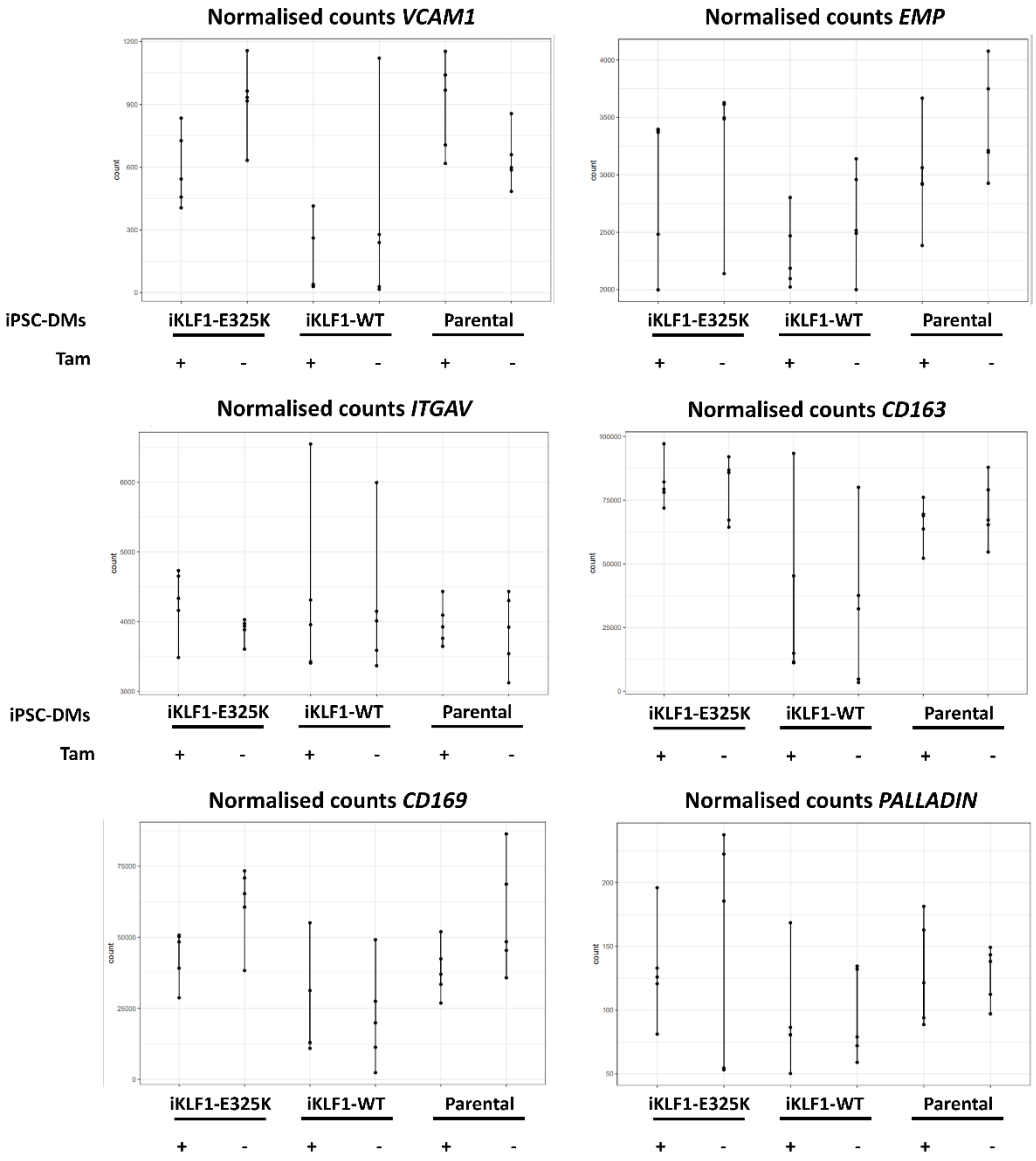

Figure 6.6 iKLF1-E325K and iKLF1-WT iPSC-DMs express comparable levels of EBI macrophage attachment proteins. Normalised counts shown for all 30 samples sequenced for the following genes encoding EBI macrophage attachment proteins: *VCAM1, EMP/MAEA, ITGAV, CD163, CD169* and *PALLADIN.* Datapoints represent individual samples.

6.3.2 Investigation of the effect of IGFBP6 on erythropoiesis

The second aim of this chapter was to use the transcriptomic dataset to identify factors that could be important for erythroid cell maturation and enucleation.

6.3.2.1 IGFBP6 has no effect on erythroid cell maturation and enucleation

The KLF1-WT activation system in iPSC-DMs was previously used to identify up-regulation of the genes encoding the secreted factors IL-33, SERPINB2 and ANGPTL7 upon KLF1-WT activation, which were then demonstrated to promote erythroid cell maturation and enucleation (201). As identified by differential expression analysis, several genes are up-regulated upon KLF1-WT activation that are not up-regulated upon KLF1-E325K activation (Figure 6.3). Functionally, there is a decrease in the percentage of mature enucleated cells in an *in vitro* model of the EBI when cells are cultured with iKLF1-E325K iPSC-DMs compared to iKLF1-WT iPSC-DMs (Figure 5.6). Therefore, it was speculated that a gene up-regulated by KLF1-WT activation and not by KLF1-E325K activation could be important for erythroid cell maturation and enucleation.

One of the genes encoding secreted factors identified by RNA-sequencing that was up-regulated upon KLF1-WT activation and not by KLF1-E325K activation was IGFBP6 (Figure 6.5). The insulin and insulin-like growth factor signalling pathway is highly conserved among multi-cellular organisms and is regulated by Insulin-like growth factor-binding proteins (IGFBPs) (352). Preliminary data from the Forrester lab suggests that IGFBP6 could play a role in erythropoiesis. IGFBP6 was added in combination with NRG1, NOV, CCL13 and TNFSF10 to UCB-derived $CD34^+$ cells under the erythroid cell differentiation conditions. Addition of these 5 factors increased the percentage of mature enucleated erythroid cells present in cultures, and removal of IGFBP6 resulted in a significant decrease in this population. This is unpublished.

I therefore wanted to investigate whether IGFBP6 alone could promote erythroid cell enucleation and maturation. The scaling up of protocols to generate RBCs for therapies need to be cost-effective for wide-spread use. Identifying the key players in promoting RBC differentiation will enable a reduction in the numbers of costly cytokines that need to be added. To assess the effect of IGFBP6 alone on erythroid cell maturation and enucleation, two concentrations of IGFBP6 (100 and 200 nM)

were added to UCB-derived $CD34^+$ cells under erythroid cell differentiation conditions (Chapter 2 Section 2.1.7.3). These concentrations of IGFBP6 were selected based on a previously published study showing that addition of 100 nM IGFBP2 increased proliferation of erythroid progenitors *in vitro* (353). IGFBPs have been demonstrated to compensate for each other *in vitro,* therefore the same 100 nM concentration and a higher 200 nM concentration was deemed appropriate for experiments (352). Erythroid differentiation efficiency, defined as the proportion of mature enucleated erythroid cells in the culture, was assessed by flow cytometry of suspension cells on days 11, 14, 18 and 21. Flow cytometry plots were gated as described in the methods (Chapter 2 Section 2.3.3).

Differentiating UCB-derived $CD34^+$ cells cultured alone or in the presence of two concentrations of IGFBP6 reduced in size across the course of the culture, before expelling their nucleus (Figure 6.7A). There was a progressive increase in the percentage of $CD235a^+$ suspension cells in the cultures and by day 21 over 92% of suspension cells in all conditions expressed CD235a (Figure 6.7B). Addition of IGFBP6 had no effect on the percentage of $CD235a^+$ cells compared to the addition of no factors at all timepoints (Figure 6.7B). There was also a progressive increase in the percentage of mature enucleated ($Hoechst^-CD71^-$) suspension cells in the cultures across the differentiation, however the addition IGFBP6 had no effect on the percentage of mature enucleated cells at each timepoint assayed (Figure 6.7B).

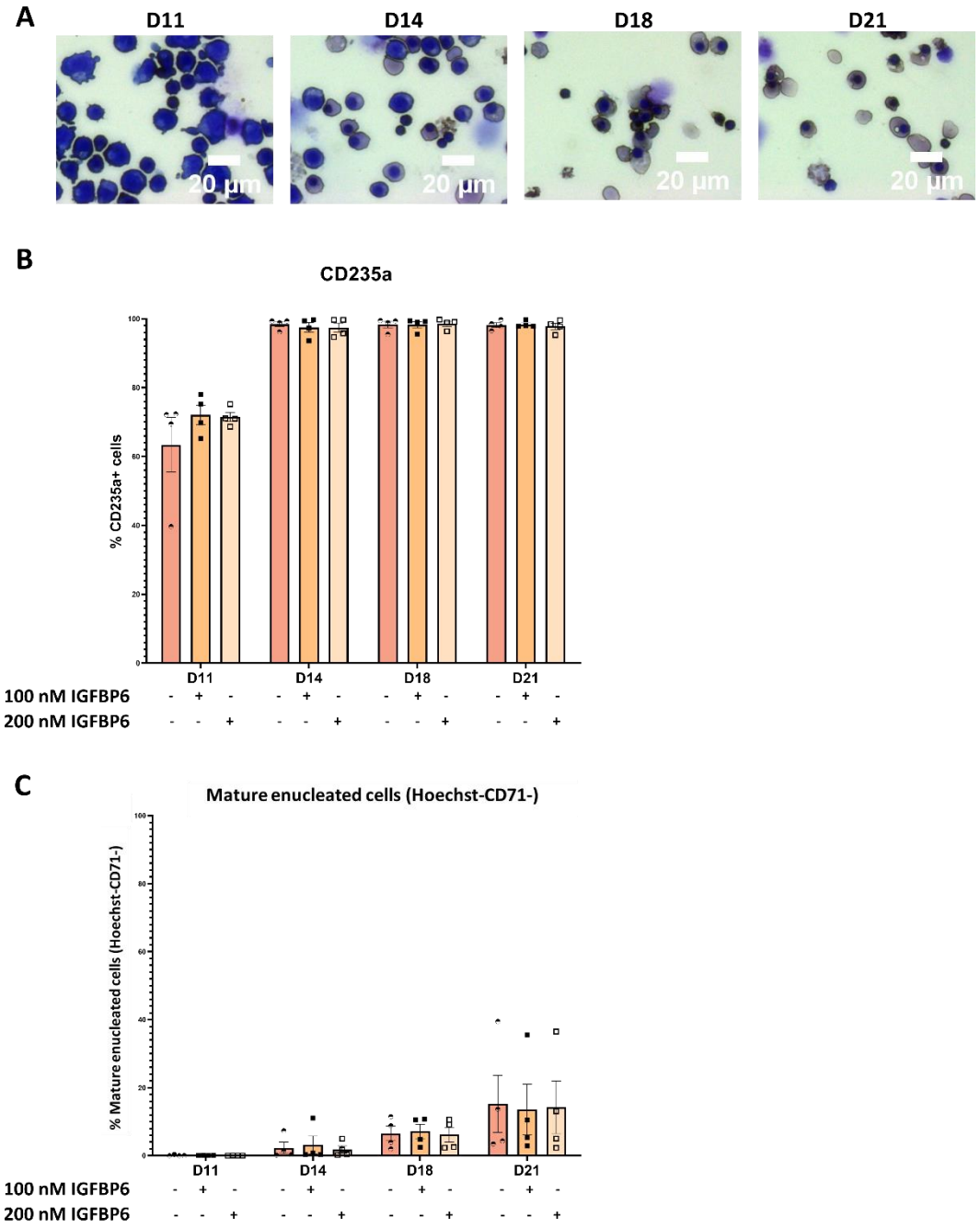

Figure 6.7 IGFBP6 has no effect on erythroid cell maturation and enucleation. IGFBP6 was added to UCB-derived CD34$^+$ cells under erythroid differentiation conditions every 2 days at a concentration of either 100 nM or 200 nM.

A: Representative Kwik-Diff cytospin images of suspension cells for days 11, 14, 18 and 21. 20X magnification.

B: Quantification of flow cytometry analyses of the percentage of CD235a$^+$ suspension cells for days 11, 14, 18 and 21. Datapoints represent individual experiments. Error bars represent SEM. One-way ANOVA with Tukey post-test generated no statistically significant p-values.

C: Quantification of flow cytometry analyses of the percentage of Hoechst$^-$CD71$^-$ suspension cells for days 11, 14, 18 and 21 of the culture. Datapoints represent individual experiments. Error bars represent SEM. One-way ANOVA with Tukey post-test generated no statistically significant p-values.

6.3.2.2 IGFBP6 has no effect on the percentage of cycling UCB-derived $CD34^+$ cells under erythroid differentiation conditions

Several members of the IGFBP family have been identified to have roles in regulating the cell cycle in a diverse range of cell types. IGFBP2 regulates the expression of cell cycle genes in neural stem cells, IGFBP3 and IGFBP5 induce cell cycle arrest in human breast cancer cells, and IGFBP7 acts as a cell cycle repressor in human thyroid cancer (354, 355, 356, 357). IGFBP6 has also been implicated in cell cycle regulation. IGFBP6 knock-down in vascular smooth muscle cells induced S phase arrest during the cell cycle (358). Within the blood system, a role for IGFBP2 in the control of cell cycle progression during EHT has recently been identified (353). Therefore, the effect of IGFBP6 addition on the cell cycle of UCB-derived $CD34^+$ under erythroid cell differentiation conditions was investigated (Chapter 2 Section).

As erythroid cell differentiation progresses from day 12 to day 21, there was a decrease in the percentage of cycling cells from approximately 38% to approximately 7% (Figure 6.7). This corresponds with the increase in mature enucleated cells from day 11-21 of the cultures and is consistent with reports that cell cycle exit is required for erythroblast enucleation (Figure 6.7) (78). The addition of IGFBP6 has no effect on the percentage of cycling cells in the culture (Figure 6.8).

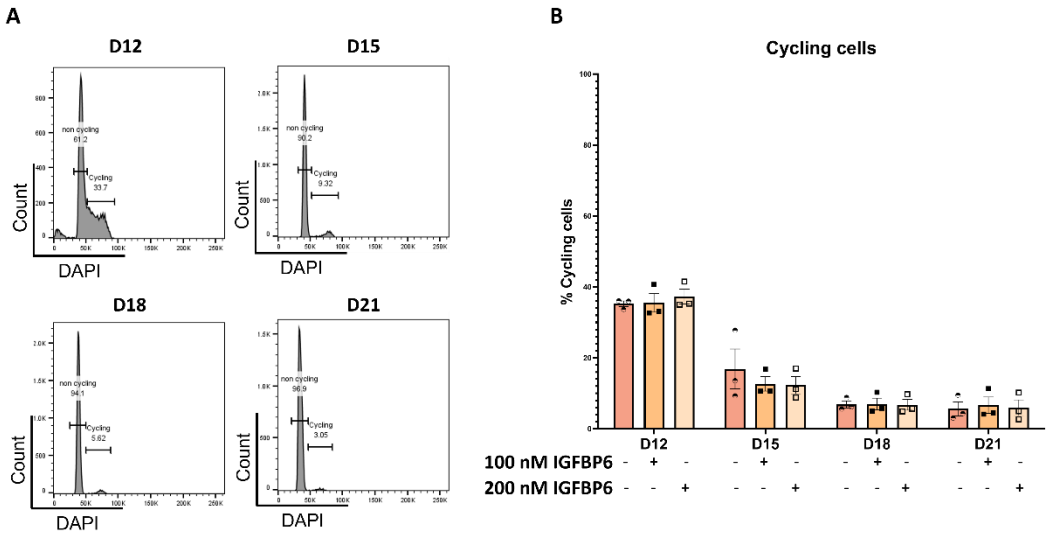

Figure 6.8 IGFBP6 has no effect on the percentage of cycling UCB-derived CD34$^+$ cells under erythroid cell differentiation conditions. IGFBP6 was added to UCB-derived CD34$^+$ cells under erythroid differentiation conditions every 2 days at a concentration of either 100 nM or 200 nM.

A: Representative flow cytometry histogram plots for days 12, 15, 18 and 21 of the differentiation.

B: Quantification of flow cytometry analyses of the percentage of cycling cells in the cultures for days 12, 15, 18 and 21. Datapoints represent individual experiments. Error bars represent SEM. One-way ANOVA with Tukey post-test generated no statistically significant p-values.

6.4 Discussion

I generated a transcriptomic dataset of iKLF1-E325K, iKLF1-WT and parental line iPSC-DMs. I identified significantly fewer genes are regulated by KLF1-E325K (19) compared to KLF1-WT (424). I identified that several KLF1-WT target genes, including *ANGPTL7* and *IGFBP6*, are not KLF1-E325K targets. Taken together with the results presented in Chapter 5 that show that fewer erythroid cells matured and enucleated in co-culture with iKLF1-E325K iPSC-DMs compared to iKLF1-WT iPSC-DMs, these data identify KLF1-E325K as a loss-of-function mutation in iPSC-derived macrophages.

6.4.1 Homozygous vs heterozygous iKLF1-E325K iPSC lines

One limitation I anticipated with myRNA-sequencing data set was that I was comparing iKLF1-WT iPSC-DMs which had two copies of the KLF1-WT-ER^{T2} transgene (homozygous),with iKLF1-E325K iPSC-DMs which had one copy of the KLF1-E325K-ER^{T2} transgene (heterozygous). Validation of expression of *IL-33* and *IGFBP6* by qRT-PCR in iKLF1-E325K iPSC-DMs generated from a homozygous iPSC line which had two copies of the KLF1-E325K-ER^{T2} transgene show expression of both genes consistent with iKLF1-E325K iPSC-DMs generated from the heterozygous line. Validation of further genes in homozygous iKLF1-E325K iPSCs is needed to conclude more broadly that the transcriptomic dataset of iKLF1-E325K iPSC-DMs generated from the heterozygous line are reflective of iKLF1-E325K iPSC-DMs generated from the homozygous line.

6.4.2 Genes encoding for secreted factors

A previous study using iKLF1-WT iPSC-DMs identified that genes encoding the secreted factors IL-33, SERPBINB2, and ANGPTL7, were up-regulated upon KLF1-WT activation, and these factors were then shown to have a role in promoting erythropoiesis (201). Addition of all three of these secreted factors to UCB-derived CD34^{+} cells under erythroid differentiation conditions significantly increased the percentage of mature enucleated erythroid cells in the cultures. Removal of any individual secreted factor resulted in a significant reduction in the number of mature enucleated cells, with removal of IL-33 resulting in the most significant reduction.

Interestingly, addition of IL-33 alone did not increase erythroid cell maturation and enucleation, indicating that IL-33 acts in synergy with other secreted factors (201).

In agreement with this previous study, *IL-33* and *ANGPTL7* were up-regulated in iPSC-DMs upon KLF1-WT activation. In contrast to the previously published dataset, *SERPINB2* was not up-regulated, and was not identified to be expressed in any macrophages in my dataset. This lack of *SERPINB2* expression in iKLF1-WT iPSC-DMs could be responsible for the modest increase in mature enucleated cells I observed in cultures with iKLF1-WT iPSC-DMs compared to 4OH-tamoxifen treated iKLF1-WT iPSC-DMs (Figure 5.6). This increase between untreated and treated iKLF1-WT iPSC-DMs was significant in a previously published experiment (201).

I observed that fewer erythroid cells matured and enucleated in co-culture with iKLF1-E325K iPSC-DMs compared to iKLF1-WT iPSC-DMs, with a decrease of approximately 15% at day 21 of the culture. KLF1-E325K activation in iPSC-DMs up-regulates *IL-33* but not *ANGPTL7*. This loss of *ANPTL7* expression could explain this reduction in the numbers of mature enucleated erythroid cells, as IL-33 has been previously shown to promote erythroid cell maturation and enucleation only in combination with ANPTL7 and/or SERPINB2 (201).

TGFA is the only gene that I identified to be differentially regulated in my dataset. *TGFA* is significantly up-regulated upon KLF1-E325K activation and in contrast is significantly down-regulated upon KLF1-WT activation. In macrophages, TGF-α expression and secretion has only been reported by alveolar macrophages (359, 360). TGF-α addition to avian erythroid progenitors was shown to promote their self-renewal, and removal of TGF-α from erythroid progenitors from chick bone marrow caused them to terminally differentiate (361, 362, 363). It is important to note that avian erythroid cells do not enucleate as part of terminal erythroid differentiation, while human erythroid cells do. Further experiments are needed to investigate whether TGF-α also promotes the self-renewal of human erythroid progenitors, and what if any effect this has on cell cycle exit, which is required for erythroblast enucleation (78). If TGF- α was identified to promote self-renewal in human erythroid progenitors, it is interesting to speculate that its secretion by CDA patient EBI macrophages promotes the self-renewal of nucleated erythroid progenitors,

preventing their terminal differentiation and contributing to the persistence of nucleated erythroid cells in the peripheral blood of CDA patients.

6.4.3 Leakiness of KLF1-E325K-ER^{T2} system in iPSC-DMs hinders identification of differentially expressed genes

I identified *IGFBP6* as a gene up-regulated upon KLF1-WT activation using normalised count data in combination with qPCR data. *IGFBP6* was not identified to be differentially expressed between untreated and treated iKLF1-WT iPSC-DMs in my differential expression analysis. This is likely due to the leakiness of the KLF1-ER^{T2} system, as normalised count data showed that two untreated iKLF1-WT iPSC-DM samples had higher *IGFBP6* counts than two 4OH-tamoxifen treated samples. Therefore, it is possible that other KLF1-WT or KLF1-E325K regulated genes were not identified in my dataset due to the leakiness of the 4OH-tamoxifen ER^{T2} system.

I observed less nuclear translocation in untreated undifferentiated iPSCs compared to untreated iPSC-DMs, and in contrast to iPSC-DMs I did not see a phenotypic effect of this leakiness in cells generated under erythroid differentiation conditions. I therefore speculated that the leakiness in the system was the result of either an aspect of the intrinsic biology of macrophages that induces translocation, or an experimental factor. Untreated iKLF1-WT iPSC-DMs demonstrated less nuclear translocation of KLF1-WT-ER^{T2} fusion protein in previously published data compared with the macrophages used in this chapter, which suggests that a technical rather than a biological factor is inducing translocation. This could be, for example, the presence of a 4OH-tamoxifen analogue in the media used in the differentiation and culture of macrophages.

Interestingly, there does seem to be significant heterogeneity to phenotypic effect of the leakiness in iPSC-DMs. Using *IGFBP6* as an example, there is a range between almost 0 and over 200 counts for *IGFBP6* between untreated iKLF1-WT iPSC-DM samples. I have observed harvest-specific effects in iPSC-DMs, for example CD93 expression decreases with each sequential harvest (unpublished data). While parental, iKLF1-WT and iKLF1-E325K iPSC-DMs were harvested at the same time as each other, all 5 harvests for each of the 5 samples generated per line were conducted over a period of 5 weeks. It is therefore possible that variability between

harvests is responsible for the heterogeneity in expression data, and possibly the heterogeneity in leakiness.

6.4.4 Genes encoding for EBI attachment proteins

I observed a reduced number of mature and enucleated erythroid cells in *in vitro* EBI cultures with iKLF1-E325K iPSC-DMs compared to iKLF1-WT iPSC-DMs, iKLF1-E325K iPSC-DMs were still able to support the maturation of a significant number of cells. I probed my transcriptomic dataset for expression of genes encoding proteins that have been identified or implicated with a role in macrophage-erythroblast attachments within the EBI. I found that *VCAM1*, *EMP/MAEA*, *ITGAV*, *CD163*, *CD169* and *PALLADIN* were expressed by iKLF1-E325K, iKLF1-WT and parental line iPSC-DMs irrespective of 4OH-tamoxifen treatment. I speculate that the unaltered expression of these genes in iKLF1-E325K macrophages is largely responsible for their partially retained ability to mature and enucleate erythroid cells.

6.4.5 A role for exosomes within the EBI?

A recent study observed the transfer of mitochondria from EBI macrophages to erythroblasts, and this transfer enhanced erythroid recovery from stress in a phenylhydrazine-induced model of acute hemolytic anemia (364). A mechanism for this mitochondrial transfer has not yet been elucidated. Other macrophage types have been implicated in mitochondrial transfer, and mitochondria have been previously observed to be transferred between cells via exosomes (365, 366). Therefore, it is interesting to speculate that mitochondria could be transferred from EBI macrophages to erythroblasts within exosomes. *RAB27B* was one of the top up-regulated genes identified in differential gene expression analysis of iKLF1-WT iPSC-DMs, and is significantly up-regulated upon KLF1-WT activation. *RAB27B* is widely expressed in secretory cells, neurons and cells involved in surface protection, and encodes for a protein that has been identified to promote exosome secretion (367, 368). Additionally, *RAB27B* is not up-regulated by KLF1-E325K. It is interesting to speculate that if exosomes do have a role within the EBI, lack of exosomes could be contributing to the erythroid defects of CDA type IV patients

Chapter 7: Summary and Perspectives

7.1 Summary

In summary, I have shown that cells generated from a CDA patient iPSC line under erythroid differentiation conditions were able to recapitulate the disease phenotype of CDA type IV patient erythroid cells. There was a significant decrease in the percentage of $CD235a^+$ cells and $CD71^+$ cells generated from CDA patient iPSCs under erythroid differentiation conditions compared to those generated from two control iPSC lines. Additionally, *GYPA, TFRC, SLC4A1, HBA1* and *ICAM4* were expressed at a lower level in CDA patient iPSC-derived cells compared to controls. This is consistent with findings in a previous study that identified downregulation of several key erythroid genes in CDA type IV patient erythroid cells (131).

CDA type IV patient-derived iPSC line-derived macrophages expressed very low levels of endogenous KLF1, and I concluded that these would not be a faithful model of an EBI macrophage. Therefore, a KLF1-E325K inducible activation system was generated and employed. I confirmed expression of *KLF1-E325K* consistent with CAG promotor activity in a heterozygous line in which the KLF1-E325K-ER^{T2} construct is integrated into one *AAVS1* allele, and a homozygous line in which the KLF1-E325K-ER^{T2} construct is integrated into both AAVS1 alleles. I also confirmed nuclear translocation of the KLF1-E325K-ER^{T2} fusion protein upon the addition of 4OH-tamoxifen in both lines. As proof of principle, I showed that KLF1-E325K activation in cells generated from both iKLF1-E325K iPSC lines under erythroid differentiation conditions recapitulated CDA patient erythroid cell phenotype, generating significantly fewer $CD235^+$ and $CD71^+$ cells.

Macrophages were then generated from both KLF1-E325K iPSC lines. I have shown that E325K impedes the maturation of macrophages induced by KLF1-WT. In an *in vitro* model of the erythroblastic island, fewer erythroid cells matured and enucleated in co-culture with iKLF1-E325K iPSC-DMs compared to iKLF1-WT iPSC-DMs. Overall, these data show that the E325K mutation impedes phenotypic and functional changes induced by KLF1 in iPSC-DMs.

Bulk RNA-sequencing revealed that activation of KLF1-E325K induced the expression of significantly fewer genes compared to KLF1-WT activation. I identified that several KLF1-WT target genes, including *ANGPTL7* and *IGFBP6*, are not KLF1-E325K targets Taken together with the results of *in vitro* EBI assays, the data presented in this thesis identify KLF1-E325K as a loss-of-function mutation in iPSC-derived macrophages

7.2 Perspectives

7.2.1 Generation of human genetically modified iPSC-derived cells to model rare RBC disorders

Of the 9 patients worldwide reported with the rare disease congenital dyserythropoietic anemia type IV, 6 are reported to carry the KLF1-E325K mutation (116, 121, 122, 123, 124, 125, 127, 130, 131, 315, 331). I hypothesised that the production of cell types associated with the EBI niche from iPSCs would provide a powerful tool to model the diseased EBI niche *in vitro*. This would be especially useful for rare diseases such as CDA type IV in which the sourcing of primary tissue is difficult, and in which animal models do not exactly recapitulate the human disease.

I have shown that the integration of a KLF1-E325K-ER^{T2} construct into iPSCs is able to generate a platform to derive erythroid cells that recapitulate the erythroid cell disease pathology of these patients. I did identify challenges to using iPSCs to model erythroid cells of RBC disorders, as these disorders often have pathologies that compound the difficulties in generating RBCs from iPSCs. For example, CDA type IV erythroid cells have a defect in terminal erythropoiesis, during which erythroid cells enucleate. This is difficult to model using iPSC-derived erythroid cells which already do not enucleate at physiological levels. Additionally, I generated macrophages using these iKLF1-E325K-iPSCs and utilised them to identify previously uncharacterised phenotypic and transcriptional changes in KLF1-E325K macrophages.

This study has demonstrated that *in vitro* modelling of the human EBI niche in disease can be used to investigate a contribution of EBI macrophages to pathologies associated with RBC disorders. The KLF1-E325K-ER^{T2} system used in this thesis could be easily mutated to investigate other disease-causing KLF1 mutations, but also to study other genes entirely.

7.2.2 Evaluation of the contribution of secreted factors to iKLF1-E325K function within the EBI niche

I identified that iKLF1-E325K macrophages express the following genes encoding proteins that have been identified or implicated with a role in macrophage-erythroblast attachments within the EBI, *VCAM1*, *EMP/MAEA*, *ITGAV*, *CD163*, *CD169* and *PALLADIN.* I speculated that the expression of these genes in iKLF1-E325K macrophages is responsible for their partly retained ability to mature and enucleate a significant number of erythroid cells in an *in vitro* model of the EBI niche.

Significantly fewer erythroid cells matured and enucleated in culture with iKLF1-E325K iPSC-DMs compared to iKLF1-WT iPSC-DMs. I speculated that this reduction in function within the EBI could be the result of a lack of expression of the secreted factor *ANGPTL7*, which has shown to be required in addition to IL-33 to promote erythroid cell maturation and enucleation. Both *IL-33* and *ANGPTL7* are up-regulated upon KLF1-WT activation. The addition of a transwell to the *in vitro* EBI assay, which prevents the interaction of macrophages with erythroblasts, has been previously used to investigate the contribution of secreted factors only to erythroid cell maturation and enucleation (201, 209). The addition of a transwell to *in vitro* EBI assays with iKLF1-E325K iPSC-DMs would be useful to confirm whether the reduced function of iKLF1-E325K iPSC-DMs is the sole result of secreted factors, and not any unidentified macrophage-erythroblast attachment proteins or other factors.

It is interesting to speculate that ANGPTL7 treatment could be used in patients with CDA type IV to increase the terminal maturation of their erythroid cells. Reducing the nucleated RBCs in the peripheral blood of CDA patients could help to alleviate symptoms such as splenomegaly, which are likely the result of increased removal of RBCs from the blood stream. ANGPTL7 is the least studied member of the angiopoietin-like family of cytokines, for which 8 members have been identified (369). ANGPTL7 has been demonstrated to promote angiogenesis *in vitro* by stimulating the proliferation, motility and invasiveness of endothelial cells, and has been identified to be essential for HSC repopulation (369, 370).

However, it is evident that ANGPTL7 could be a difficult factor to target therapeutically due to its diverse roles and context dependent nature. Modulation of

ANGPTL7 has been previously suggested therapeutic target for increased intraocular pressure (IOP) and glaucoma (371). Current glaucoma medications work by lowering IOP, and *Angptl7* knockout mice were identified to have lower IOP compared to WT mice (371). Injection of ANGPTL7 into mouse eyes increased OAP, suggesting that modulation of ANGPTL7 could help to maintain healthy IOP and prevent the onset or progression of glaucoma (371). ANPTL7 has also been identified to promote insulin resistance and type 2 diabetes mellitus (372). Therefore, ANGPTL7 treatment could increase terminal maturation of CDA patient erythroid cells, at the expense of increasing patients glaucoma risk, insulin sensitivity and risk of type 2 diabetes mellitus.

7.3.3 A role for TGF-α in human erythroid progenitor renewal

TGF-α has been previously demonstrated to promote the self-renewal of chick erythroid progenitors, with removal of TGF-α inducing terminal differentiation of chick erythroid progenitors *in vitro* (361, 362, 363). It is interesting to speculate that TGF-α may also have a role in the self-renewal of human erythroid progenitors. It would also be interesting to investigate whether TGF-α has any effect on cell cycle exit, which is required for erythroblast enucleation (78). To test both of these questions *in vitro*, TGF-α could be added to UCB-derived $CD34^+$ progenitors under erythroid differentiation conditions to investigate whether these cells proliferate more, and whether fewer of these cells exit the cell cycle to enucleate.

TGFA was the only differentially expressed gene that I identified in my transcriptomic dataset. *TGFA* is up-regulated by KLF1-E325K activation, and down-regulated by KLF1-WT activation. It is interesting to speculate that, if TGF-α does indeed promote human erythroid progenitor renewal, its secretion by CDA patient EBI macrophages could promote the self-renewal of nucleated erythroid progenitors, preventing their terminal differentiation and contributing to the persistence of nucleated erythroid cells in the peripheral blood of CDA patients. The mechanism by which CDA patient erythroid cells fail to enucleate has not yet been elucidated.

References

1. Doubek M. [Discovery of blood cells in the 17th century]. Vnitr Lek. 2001;47(7):496-9.
2. Davis IM. "Round, red globules floating in a crystalline fluid" - Antoni van Leeuwenhoek's observations of red blood cells and hemocytes. Micron. 2022;157:103249.
3. Migliaccio G, Migliaccio AR, Petti S, Mavilio F, Russo G, Lazzaro D, et al. Human embryonic hemopoiesis. Kinetics of progenitors and precursors underlying the yolk sac----liver transition. J Clin Invest. 1986;78(1):51-60.
4. Sheng G. Primitive and definitive erythropoiesis in the yolk sac: a bird's eye view. Int J Dev Biol. 2010;54(6-7):1033-43.
5. Yamane T. Mouse Yolk Sac Hematopoiesis. Front Cell Dev Biol. 2018;6:80.
6. Schulz C, Gomez Perdiguero E, Chorro L, Szabo-Rogers H, Cagnard N, Kierdorf K, et al. A lineage of myeloid cells independent of Myb and hematopoietic stem cells. Science. 2012;336(6077):86-90.
7. Palis J, Robertson S, Kennedy M, Wall C, Keller G. Development of erythroid and myeloid progenitors in the yolk sac and embryo proper of the mouse. Development. 1999;126(22):5073-84.
8. Palis J, Chan RJ, Koniski A, Patel R, Starr M, Yoder MC. Spatial and temporal emergence of high proliferative potential hematopoietic precursors during murine embryogenesis. Proc Natl Acad Sci U S A. 2001;98(8):4528-33.
9. McGrath KE, Frame JM, Fegan KH, Bowen JR, Conway SJ, Catherman SC, et al. Distinct Sources of Hematopoietic Progenitors Emerge before HSCs and Provide Functional Blood Cells in the Mammalian Embryo. Cell Rep. 2015;11(12):1892-904.
10. Tober J, Koniski A, McGrath KE, Vemishetti R, Emerson R, de Mesy-Bentley KK, et al. The megakaryocyte lineage originates from hemangioblast precursors and is an integral component both of primitive and of definitive hematopoiesis. Blood. 2007;109(4):1433-41.
11. de Bruijn MF, Speck NA, Peeters MC, Dzierzak E. Definitive hematopoietic stem cells first develop within the major arterial regions of the mouse embryo. Embo j. 2000;19(11):2465-74.
12. Müller AM, Medvinsky A, Strouboulis J, Grosveld F, Dzierzak E. Development of hematopoietic stem cell activity in the mouse embryo. Immunity. 1994;1(4):291-301.
13. Medvinsky A, Dzierzak E. Definitive hematopoiesis is autonomously initiated by the AGM region. Cell. 1996;86(6):897-906.
14. Chen MJ, Li Y, De Obaldia ME, Yang Q, Yzaguirre AD, Yamada-Inagawa T, et al. Erythroid/myeloid progenitors and hematopoietic stem cells originate from distinct populations of endothelial cells. Cell Stem Cell. 2011;9(6):541-52.
15. Julien E, El Omar R, Tavian M. Origin of the hematopoietic system in the human embryo. FEBS Lett. 2016;590(22):3987-4001.
16. Morrison SJ, Scadden DT. The bone marrow niche for haematopoietic stem cells. Nature. 2014;505(7483):327-34.
17. Huisjes R, Bogdanova A, van Solinge WW, Schiffelers RM, Kaestner L, van Wijk R. Squeezing for Life - Properties of Red Blood Cell Deformability. Front Physiol. 2018;9:656.

18. Schechter AN. Hemoglobin research and the origins of molecular medicine. Blood. 2008;112(10):3927-38.
19. Palis J. Primitive and definitive erythropoiesis in mammals. Front Physiol. 2014;5:3.
20. Palis J, Yoder MC. Yolk-sac hematopoiesis: the first blood cells of mouse and man. Exp Hematol. 2001;29(8):927-36.
21. Kingsley PD, Malik J, Fantauzzo KA, Palis J. Yolk sac-derived primitive erythroblasts enucleate during mammalian embryogenesis. Blood. 2004;104(1):19-25.
22. McGrath KE, Kingsley PD, Koniski AD, Porter RL, Bushnell TP, Palis J. Enucleation of primitive erythroid cells generates a transient population of "pyrenocytes" in the mammalian fetus. Blood. 2008;111(4):2409-17.
23. Isern J, Fraser ST, He Z, Baron MH. The fetal liver is a niche for maturation of primitive erythroid cells. Proc Natl Acad Sci U S A. 2008;105(18):6662-7.
24. Fraser ST, Isern J, Baron MH. Maturation and enucleation of primitive erythroblasts during mouse embryogenesis is accompanied by changes in cell-surface antigen expression. Blood. 2007;109(1):343-52.
25. Anifandis G, Sutovsky P, Turek PJ, Chavez SL, Kunej T, Messini CI, et al. Bioethics in human embryology: the double-edged sword of embryo research. Syst Biol Reprod Med. 2022;68(3):169-79.
26. Van Handel B, Prashad SL, Hassanzadeh-Kiabi N, Huang A, Magnusson M, Atanassova B, et al. The first trimester human placenta is a site for terminal maturation of primitive erythroid cells. Blood. 2010;116(17):3321-30.
27. McGrath KE, Frame JM, Fromm GJ, Koniski AD, Kingsley PD, Little J, et al. A transient definitive erythroid lineage with unique regulation of the β-globin locus in the mammalian embryo. Blood. 2011;117(17):4600-8.
28. Frame JM, McGrath KE, Palis J. Erythro-myeloid progenitors: "definitive" hematopoiesis in the conceptus prior to the emergence of hematopoietic stem cells. Blood Cells Mol Dis. 2013;51(4):220-5.
29. Kingsley PD, Malik J, Emerson RL, Bushnell TP, McGrath KE, Bloedorn LA, et al. "Maturational" globin switching in primary primitive erythroid cells. Blood. 2006;107(4):1665-72.
30. Edvardsson L, Dykes J, Olofsson T. Isolation and characterization of human myeloid progenitor populations--TpoR as discriminator between common myeloid and megakaryocyte/erythroid progenitors. Exp Hematol. 2006;34(5):599-609.
31. Akashi K, Traver D, Miyamoto T, Weissman IL. A clonogenic common myeloid progenitor that gives rise to all myeloid lineages. Nature. 2000;404(6774):193-7.
32. Gregory CJ, Eaves AC. Three stages of erythropoietic progenitor cell differentiation distinguished by a number of physical and biologic properties. Blood. 1978;51(3):527-37.
33. Gregory CJ, Eaves AC. Human marrow cells capable of erythropoietic differentiation in vitro: definition of three erythroid colony responses. Blood. 1977;49(6):855-64.
34. Stephenson JR, Axelrad AA, McLeod DL, Shreeve MM. Induction of colonies of hemoglobin-synthesizing cells by erythropoietin in vitro. Proc Natl Acad Sci U S A. 1971;68(7):1542-6.

35. McLeod DL, Shreeve MM, Axelrad AA. Improved plasma culture system for production of erythrocytic colonies in vitro: quantitative assay method for CFU-E. Blood. 1974;44(4):517-34.
36. Broudy VC, Lin N, Brice M, Nakamoto B, Papayannopoulou T. Erythropoietin receptor characteristics on primary human erythroid cells. Blood. 1991;77(12):2583-90.
37. Spivak JL. The mechanism of action of erythropoietin. Int J Cell Cloning. 1986;4(3):139-66.
38. Granick S, Levere RD. HEME SYNTHESIS IN ERYTHROID CELLS. Prog Hematol. 1964;4:1-47.
39. Chen K, Liu J, Heck S, Chasis JA, An X, Mohandas N. Resolving the distinct stages in erythroid differentiation based on dynamic changes in membrane protein expression during erythropoiesis. Proc Natl Acad Sci U S A. 2009;106(41):17413-8.
40. Yeo JH, Lam YW, Fraser ST. Cellular dynamics of mammalian red blood cell production in the erythroblastic island niche. Biophys Rev. 2019;11(6):873-94.
41. Chasis JA, Prenant M, Leung A, Mohandas N. Membrane assembly and remodeling during reticulocyte maturation. Blood. 1989;74(3):1112-20.
42. Skutelsky E, Danon D. An electron microscopic study of nuclear elimination from the late erythroblast. J Cell Biol. 1967;33(3):625-35.
43. Ganzoni A, Hillman RS, Finch CA. Maturation of the macroreticulocyte. Br J Haematol. 1969;16(1):119-35.
44. Gronowicz G, Swift H, Steck TL. Maturation of the reticulocyte in vitro. J Cell Sci. 1984;71:177-97.
45. Paulson RF, Shi L, Wu DC. Stress erythropoiesis: new signals and new stress progenitor cells. Curr Opin Hematol. 2011;18(3):139-45.
46. Socolovsky M. Molecular insights into stress erythropoiesis. Curr Opin Hematol. 2007;14(3):215-24.
47. Paulson RF, Hariharan S, Little J. Stress erythropoiesis: definitions and models for its study. Exp Hematol. 2020.
48. Blanchard KL, Fandrey J, Goldberg MA, Bunn HF. Regulation of the erythropoietin gene. Stem Cells. 1993;11 Suppl 1:1-7.
49. Porayette P, Paulson RF. BMP4/Smad5 dependent stress erythropoiesis is required for the expansion of erythroid progenitors during fetal development. Dev Biol. 2008;317(1):24-35.
50. Adelman CA, Chattopadhyay S, Bieker JJ. The BMP/BMPR/Smad pathway directs expression of the erythroid-specific EKLF and GATA1 transcription factors during embryoid body differentiation in serum-free media. Development. 2002;129(2):539-49.
51. Lohmann F, Bieker JJ. Activation of Eklf expression during hematopoiesis by Gata2 and Smad5 prior to erythroid commitment. Development. 2008;135(12):2071-82.
52. Hattangadi SM, Wong P, Zhang L, Flygare J, Lodish HF. From stem cell to red cell: regulation of erythropoiesis at multiple levels by multiple proteins, RNAs, and chromatin modifications. Blood. 2011;118(24):6258-68.
53. Yasuda Y, Fujita Y, Musha T, Tanaka H, Shiokawa S, Nakamatsu K, et al. Expression of erythropoietin in human female reproductive organs. Ital J Anat Embryol. 2001;106(2 Suppl 2):215-22.

54. Jacobson LO, Goldwasser E, Fried W, Plzak L. Role of the kidney in erythropoiesis. Nature. 1957;179(4560):633-4.
55. Bunn HF. Erythropoietin. Cold Spring Harb Perspect Med. 2013;3(3):a011619.
56. Koury MJ, Bondurant MC. Erythropoietin retards DNA breakdown and prevents programmed death in erythroid progenitor cells. Science. 1990;248(4953):378-81.
57. Malik J, Kim AR, Tyre KA, Cherukuri AR, Palis J. Erythropoietin critically regulates the terminal maturation of murine and human primitive erythroblasts. Haematologica. 2013;98(11):1778-87.
58. Mullally A, Lane SW, Ball B, Megerdichian C, Okabe R, Al-Shahrour F, et al. Physiological Jak2V617F expression causes a lethal myeloproliferative neoplasm with differential effects on hematopoietic stem and progenitor cells. Cancer Cell. 2010;17(6):584-96.
59. Zhao R, Xing S, Li Z, Fu X, Li Q, Krantz SB, et al. Identification of an acquired JAK2 mutation in polycythemia vera. J Biol Chem. 2005;280(24):22788-92.
60. Zhan H, Spivak JL. The diagnosis and management of polycythemia vera, essential thrombocythemia, and primary myelofibrosis in the JAK2 V617F era. Clin Adv Hematol Oncol. 2009;7(5):334-42.
61. Dzierzak E, Philipsen S. Erythropoiesis: development and differentiation. Cold Spring Harb Perspect Med. 2013;3(4):a011601.
62. Brannan CI, Lyman SD, Williams DE, Eisenman J, Anderson DM, Cosman D, et al. Steel-Dickie mutation encodes a c-kit ligand lacking transmembrane and cytoplasmic domains. Proc Natl Acad Sci U S A. 1991;88(11):4671-4.
63. Barminko J, Reinholt B, Baron MH. Development and differentiation of the erythroid lineage in mammals. Dev Comp Immunol. 2016;58:18-29.
64. Sawada K, Krantz SB, Dessypris EN, Koury ST, Sawyer ST. Human colony-forming units-erythroid do not require accessory cells, but do require direct interaction with insulin-like growth factor I and/or insulin for erythroid development. J Clin Invest. 1989;83(5):1701-9.
65. Miller IJ, Bieker JJ. A novel, erythroid cell-specific murine transcription factor that binds to the CACCC element and is related to the Kruppel family of nuclear proteins. Mol Cell Biol. 1993;13(5):2776-86.
66. McConnell BB, Yang VW. Mammalian Krüppel-like factors in health and diseases. Physiol Rev. 2010;90(4):1337-81.
67. Frontelo P, Manwani D, Galdass M, Karsunky H, Lohmann F, Gallagher PG, et al. Novel role for EKLF in megakaryocyte lineage commitment. Blood. 2007;110(12):3871-80.
68. Xue L, Galdass M, Gnanapragasam MN, Manwani D, Bieker JJ. Extrinsic and intrinsic control by EKLF (KLF1) within a specialized erythroid niche. Development. 2014;141(11):2245-54.
69. Kang YJ, Shin JW, Yoon JH, Oh IH, Lee SP, Kim SY, et al. Inhibition of erythropoiesis by Smad6 in human cord blood hematopoietic stem cells. Biochem Biophys Res Commun. 2012;423(4):750-6.
70. Southwood CM, Downs KM, Bieker JJ. Erythroid Kruppel-like factor exhibits an early and sequentially localized pattern of expression during mammalian erythroid ontogeny. Dev Dyn. 1996;206(3):248-59.

71. Southwood CM, Downs KM, Bieker JJ. Erythroid Krüppel-like factor exhibits an early and sequentially localized pattern of expression during mammalian erythroid ontogeny. Dev Dyn. 1996;206(3):248-59.
72. Nuez B, Michalovich D, Bygrave A, Ploemacher R, Grosveld F. Defective haematopoiesis in fetal liver resulting from inactivation of the EKLF gene. Nature. 1995;375(6529):316-8.
73. Perkins AC, Sharpe AH, Orkin SH. Lethal beta-thalassaemia in mice lacking the erythroid CACCC-transcription factor EKLF. Nature. 1995;375(6529):318-22.
74. Perkins AC, Peterson KR, Stamatoyannopoulos G, Witkowska HE, Orkin SH. Fetal expression of a human Agamma globin transgene rescues globin chain imbalance but not hemolysis in EKLF null mouse embryos. Blood. 2000;95(5):1827-33.
75. Drissen R, von Lindern M, Kolbus A, Driegen S, Steinlein P, Beug H, et al. The erythroid phenotype of EKLF-null mice: defects in hemoglobin metabolism and membrane stability. Mol Cell Biol. 2005;25(12):5205-14.
76. Siatecka M, Bieker JJ. The multifunctional role of EKLF/KLF1 during erythropoiesis. Blood. 2011;118(8):2044-54.
77. Tallack MR, Keys JR, Perkins AC. Erythroid Kruppel-like factor regulates the G1 cyclin dependent kinase inhibitor p18INK4c. J Mol Biol. 2007;369(2):313-21.
78. Gnanapragasam MN, McGrath KE, Catherman S, Xue L, Palis J, Bieker JJ. EKLF/KLF1-regulated cell cycle exit is essential for erythroblast enucleation. Blood. 2016;128(12):1631-41.
79. Alhashem YN, Vinjamur DS, Basu M, Klingmüller U, Gaensler KM, Lloyd JA. Transcription factors KLF1 and KLF2 positively regulate embryonic and fetal beta-globin genes through direct promoter binding. J Biol Chem. 2011;286(28):24819-27.
80. Hodge D, Coghill E, Keys J, Maguire T, Hartmann B, McDowall A, et al. A global role for EKLF in definitive and primitive erythropoiesis. Blood. 2006;107(8):3359-70.
81. Tallack MR, Whitington T, Yuen WS, Wainwright EN, Keys JR, Gardiner BB, et al. A global role for KLF1 in erythropoiesis revealed by ChIP-seq in primary erythroid cells. Genome Res. 2010;20(8):1052-63.
82. Pilon AM, Nilson DG, Zhou D, Sangerman J, Townes TM, Bodine DM, et al. Alterations in expression and chromatin configuration of the alpha hemoglobin-stabilizing protein gene in erythroid Kruppel-like factor-deficient mice. Mol Cell Biol. 2006;26(11):4368-77.
83. Pilon AM, Ajay SS, Kumar SA, Steiner LA, Cherukuri PF, Wincovitch S, et al. Genome-wide ChIP-Seq reveals a dramatic shift in the binding of the transcription factor erythroid Kruppel-like factor during erythrocyte differentiation. Blood. 2011;118(17):e139-48.
84. Tallack MR, Magor GW, Dartigues B, Sun L, Huang S, Fittock JM, et al. Novel roles for KLF1 in erythropoiesis revealed by mRNA-seq. Genome Res. 2012;22(12):2385-98.
85. Vinjamur DS, Wade KJ, Mohamad SF, Haar JL, Sawyer ST, Lloyd JA. Krüppel-like transcription factors KLF1 and KLF2 have unique and coordinate roles in regulating embryonic erythroid precursor maturation. Haematologica. 2014;99(10):1565-73.

86. Singleton BK, Burton NM, Green C, Brady RL, Anstee DJ. Mutations in EKLF/KLF1 form the molecular basis of the rare blood group In(Lu) phenotype. Blood. 2008;112(5):2081-8.
87. Borg J, Papadopoulos P, Georgitsi M, Gutiérrez L, Grech G, Fanis P, et al. Haploinsufficiency for the erythroid transcription factor KLF1 causes hereditary persistence of fetal hemoglobin. Nat Genet. 2010;42(9):801-5.
88. Gallienne AE, Dréau HM, Schuh A, Old JM, Henderson S. Ten novel mutations in the erythroid transcription factor KLF1 gene associated with increased fetal hemoglobin levels in adults. Haematologica. 2012;97(3):340-3.
89. Zhou D, Liu K, Sun CW, Pawlik KM, Townes TM. KLF1 regulates BCL11A expression and gamma- to beta-globin gene switching. Nat Genet. 2010;42(9):742-4.
90. Tefferi A, Barbui T. Polycythemia vera and essential thrombocythemia: 2019 update on diagnosis, risk-stratification and management. Am J Hematol. 2019;94(1):133-43.
91. Socie G, Mary JY, de Gramont A, Rio B, Leporrier M, Rose C, et al. Paroxysmal nocturnal haemoglobinuria: long-term follow-up and prognostic factors. French Society of Haematology. Lancet. 1996;348(9027):573-7.
92. Muncie HL, Jr., Campbell J. Alpha and beta thalassemia. Am Fam Physician. 2009;80(4):339-44.
93. Williams TN, Thein SL. Sickle Cell Anemia and Its Phenotypes. Annu Rev Genomics Hum Genet. 2018;19:113-47.
94. Miller JL. Iron deficiency anemia: a common and curable disease. Cold Spring Harb Perspect Med. 2013;3(7).
95. Fibach E, Rachmilewitz EA. Pathophysiology and treatment of patients with beta-thalassemia - an update. F1000Res. 2017;6:2156.
96. Buttarello M. Laboratory diagnosis of anemia: are the old and new red cell parameters useful in classification and treatment, how? Int J Lab Hematol. 2016;38 Suppl 1:123-32.
97. McLean E, Cogswell M, Egli I, Wojdyla D, de Benoist B. Worldwide prevalence of anaemia, WHO Vitamin and Mineral Nutrition Information System, 1993-2005. Public Health Nutr. 2009;12(4):444-54.
98. Kassebaum NJ, Jasrasaria R, Naghavi M, Wulf SK, Johns N, Lozano R, et al. A systematic analysis of global anemia burden from 1990 to 2010. Blood. 2014;123(5):615-24.
99. Jimenez K, Kulnigg-Dabsch S, Gasche C. Management of Iron Deficiency Anemia. Gastroenterol Hepatol (N Y). 2015;11(4):241-50.
100. Eschbach JW, Egrie JC, Downing MR, Browne JK, Adamson JW. Correction of the anemia of end-stage renal disease with recombinant human erythropoietin. Results of a combined phase I and II clinical trial. N Engl J Med. 1987;316(2):73-8.
101. Debeljak N, Sytkowski AJ. Erythropoietin and erythropoiesis stimulating agents. Drug Test Anal. 2012;4(11):805-12.
102. Glaspy J, Bukowski R, Steinberg D, Taylor C, Tchekmedyian S, Vadhan-Raj S. Impact of therapy with epoetin alfa on clinical outcomes in patients with nonmyeloid malignancies during cancer chemotherapy in community oncology practice. Procrit Study Group. J Clin Oncol. 1997;15(3):1218-34.

103. Hillmen P, Young NS, Schubert J, Brodsky RA, Socie G, Muus P, et al. The complement inhibitor eculizumab in paroxysmal nocturnal hemoglobinuria. N Engl J Med. 2006;355(12):1233-43.
104. Debureaux P-E, Cacace F, Silva BGP, Barone F, Calado RT, Fontbrune FSd, et al. Hematological Response to Eculizumab in Paroxysmal Nocturnal Hemoglobinuria: Application of a Novel Classification to Identify Unmet Clinical Needs and Future Clinical Goals. *Blood*; 2019.
105. Saso R, Marsh J, Cevreska L, Szer J, Gale RP, Rowlings PA, et al. Bone marrow transplants for paroxysmal nocturnal haemoglobinuria. Br J Haematol. 1999;104(2):392-6.
106. Locasciulli A, Oneto R, Bacigalupo A, Socie G, Korthof E, Bekassy A, et al. Outcome of patients with acquired aplastic anemia given first line bone marrow transplantation or immunosuppressive treatment in the last decade: a report from the European Group for Blood and Marrow Transplantation (EBMT). Haematologica. 2007;92(1):11-8.
107. Mohty M, Apperley JF. Long-term physiological side effects after allogeneic bone marrow transplantation. Hematology Am Soc Hematol Educ Program. 2010;2010:229-36.
108. Iolascon A, Andolfo I, Russo R. Congenital dyserythropoietic anemias. Blood. 2020;136(11):1274-83.
109. Roy NBA, Babbs C. The pathogenesis, diagnosis and management of congenital dyserythropoietic anaemia type I. Br J Haematol. 2019;185(3):436-49.
110. Dgany O, Avidan N, Delaunay J, Krasnov T, Shalmon L, Shalev H, et al. Congenital dyserythropoietic anemia type I is caused by mutations in codanin-1. Am J Hum Genet. 2002;71(6):1467-74.
111. Babbs C, Roberts NA, Sanchez-Pulido L, McGowan SJ, Ahmed MR, Brown JM, et al. Homozygous mutations in a predicted endonuclease are a novel cause of congenital dyserythropoietic anemia type I. Haematologica. 2013;98(9):1383-7.
112. Schwarz K, Iolascon A, Verissimo F, Trede NS, Horsley W, Chen W, et al. Mutations affecting the secretory COPII coat component SEC23B cause congenital dyserythropoietic anemia type II. Nat Genet. 2009;41(8):936-40.
113. Liljeholm M, Irvine AF, Vikberg AL, Norberg A, Month S, Sandström H, et al. Congenital dyserythropoietic anemia type III (CDA III) is caused by a mutation in kinesin family member, KIF23. Blood. 2013;121(23):4791-9.
114. Singleton BK, Fairweather VSS, Lau W, Parsons SF, Burton NM, Frayne J, et al. A Novel EKLF Mutation in a Patient with Dyserythropoietic Anemia: The First Association of EKLF with Disease in Man. Blood. 2009;114(22):162-.
115. Nichols KE, Crispino JD, Poncz M, White JG, Orkin SH, Maris JM, et al. Familial dyserythropoietic anaemia and thrombocytopenia due to an inherited mutation in GATA1. Nat Genet. 2000;24(3):266-70.
116. Arnaud L, Saison C, Helias V, Lucien N, Steschenko D, Giarratana MC, et al. A dominant mutation in the gene encoding the erythroid transcription factor KLF1 causes a congenital dyserythropoietic anemia. Am J Hum Genet. 2010;87(5):721-7.
117. Wickramasinghe SN, Illum N, Wimberley PD. Congenital dyserythropoietic anaemia with novel intra-erythroblastic and intra-erythrocytic inclusions. Br J Haematol. 1991;79(2):322-30.

118. Parsons SF, Jones J, Anstee DJ, Judson PA, Gardner B, Wiener E, et al. A novel form of congenital dyserythropoietic anemia associated with deficiency of erythroid CD44 and a unique blood group phenotype [In(a-b-), Co(a-b-)]. Blood. 1994;83(3):860-8.
119. Tang W, Cai SP, Eng B, Poon MC, Waye JS, Illum N, et al. Expression of embryonic zeta-globin and epsilon-globin chains in a 10-year-old girl with congenital anemia. Blood. 1993;81(6):1636-40.
120. Feng WC, Southwood CM, Bieker JJ. Analyses of beta-thalassemia mutant DNA interactions with erythroid Kruppel-like factor (EKLF), an erythroid cell-specific transcription factor. J Biol Chem. 1994;269(2):1493-500.
121. Jaffray JA, Mitchell WB, Gnanapragasam MN, Seshan SV, Guo X, Westhoff CM, et al. Erythroid transcription factor EKLF/KLF1 mutation causing congenital dyserythropoietic anemia type IV in a patient of Taiwanese origin: review of all reported cases and development of a clinical diagnostic paradigm. Blood Cells Mol Dis. 2013;51(2):71-5.
122. Bird AR, Karabus CD, Hartley PS. Type IV congenital dyserythropoietic anemia with an unusual response to splenectomy. Am J Pediatr Hematol Oncol. 1985;7(2):196-9.
123. Benjamin JT, Rosse WF, Daldorf FG, McMillan CW. Congential dyserythropoietic anemia--type IV. J Pediatr. 1975;87(2):210-6.
124. Ortolano R, Forouhar M, Warwick A, Harper D. A Case of Congenital Dyserythropoeitic Anemia Type IV Caused by E325K Mutation in Erythroid Transcription Factor KLF1. J Pediatr Hematol Oncol. 2018;40(6):e389-e91.
125. de-la-Iglesia-Iñigo S, Moreno-Carralero MI, Lemes-Castellano A, Molero-Labarta T, Méndez M, Morán-Jiménez MJ. A case of congenital dyserythropoietic anemia type IV. Clin Case Rep. 52017. p. 248-52.
126. Ravindranath Y, Goyette G, Buck S, Gadgeel M, Dombkowski A, Boxer LA, et al.
127. Belgemen-Ozer T, Gorukmez O. A Very Rare Congenital Dyserythropoietic Anemia Variant-Type IV in a Patient With a Novel Mutation in the KLF1 Gene: A Case Report and Review of the Literature. J Pediatr Hematol Oncol. 2020;42(6):e536-e40.
128. Nébor D, Graber JH, Ciciotte SL, Robledo RF, Papoin J, Hartman E, et al. Mutant KLF1 in Adult Anemic Nan Mice Leads to Profound Transcriptome Changes and Disordered Erythropoiesis. Sci Rep. 2018;8(1):12793.
129. Siatecka M, Sahr KE, Andersen SG, Mezei M, Bieker JJ, Peters LL. Severe anemia in the Nan mutant mouse caused by sequence-selective disruption of erythroid Kruppel-like factor. Proc Natl Acad Sci U S A. 2010;107(34):15151-6.
130. Kohara H, Utsugisawa T, Sakamoto C, Hirose L, Ogawa Y, Ogura H, et al. KLF1 mutation E325K induces cell cycle arrest in erythroid cells differentiated from congenital dyserythropoietic anemia patient-specific induced pluripotent stem cells. Exp Hematol. 2019;73:25-37.e8.
131. Varricchio L, Planutis A, Manwani D, Jaffray J, Mitchell WB, Migliaccio AR, et al. Genetic disarray follows mutant KLF1-E325K expression in a congenital dyserythropoietic anemia patient. Haematologica. 2019;104(12):2372-80.
132. Cross AR. Facts About Blood Supply In The US. 2022.
133. Jones JM, Sapiano MRP, Mowla S, Bota D, Berger JJ, Basavaraju SV. Has the trend of declining blood transfusions in the United States ended? Findings of the

2019 National Blood Collection and Utilization Survey. Transfusion. 2021;61 Suppl 2(Suppl 2):S1-s10.
134. Sahu S, Hemlata, Verma A. Adverse events related to blood transfusion. Indian J Anaesth. 2014;58(5):543-51.
135. Hendrickson JE, Hillyer CD. Noninfectious serious hazards of transfusion. Anesth Analg. 2009;108(3):759-69.
136. Transplant NBa. Amber alert issued on blood stocks. 2022.
137. Eder AF, Chambers LA. Noninfectious complications of blood transfusion. Arch Pathol Lab Med. 2007;131(5):708-18.
138. Salinas Cisneros G, Thein SL. Recent Advances in the Treatment of Sickle Cell Disease. Front Physiol. 2020;11:435.
139. Giarratana MC, Rouard H, Dumont A, Kiger L, Safeukui I, Le Pennec PY, et al. Proof of principle for transfusion of in vitro-generated red blood cells. Blood. 2011;118(19):5071-9.
140. Devlin H. New hope for sickle cell patients as UK trial of lab grown red blood cells begins. The Guardian2022.
141. Giarratana MC, Kobari L, Lapillonne H, Chalmers D, Kiger L, Cynober T, et al. Ex vivo generation of fully mature human red blood cells from hematopoietic stem cells. Nat Biotechnol. 2005;23(1):69-74.
142. Miharada K, Hiroyama T, Sudo K, Nagasawa T, Nakamura Y. Efficient enucleation of erythroblasts differentiated in vitro from hematopoietic stem and progenitor cells. Nat Biotechnol. 2006;24(10):1255-6.
143. Fujimi A, Matsunaga T, Kobune M, Kawano Y, Nagaya T, Tanaka I, et al. Ex vivo large-scale generation of human red blood cells from cord blood CD34+ cells by co-culturing with macrophages. Int J Hematol. 2008;87(4):339-50.
144. Zhang Y, Wang C, Wang L, Shen B, Guan X, Tian J, et al. Large-Scale Ex Vivo Generation of Human Red Blood Cells from Cord Blood CD34(+) Cells. Stem Cells Transl Med. 2017;6(8):1698-709.
145. Baek EJ, Kim HS, Kim S, Jin H, Choi TY, Kim HO. In vitro clinical-grade generation of red blood cells from human umbilical cord blood CD34+ cells. Transfusion. 2008;48(10):2235-45.
146. Boehm D, Murphy WG, Al-Rubeai M. The potential of human peripheral blood derived CD34+ cells for ex vivo red blood cell production. J Biotechnol. 2009;144(2):127-34.
147. Kupzig S, Parsons SF, Curnow E, Anstee DJ, Blair A. Superior survival of ex vivo cultured human reticulocytes following transfusion into mice. Haematologica. 2017;102(3):476-83.
148. Nimgaonkar MT, Roscoe RA, Persichetti J, Rybka WB, Winkelstein A, Ball ED. A unique population of CD34+ cells in cord blood. Stem Cells. 1995;13(2):158-66.
149. Sutherland DR, Anderson L, Keeney M, Nayar R, Chin-Yee I. The ISHAGE guidelines for CD34+ cell determination by flow cytometry. International Society of Hematotherapy and Graft Engineering. J Hematother. 1996;5(3):213-26.
150. Trakarnsanga K, Griffiths RE, Wilson MC, Blair A, Satchwell TJ, Meinders M, et al. An immortalized adult human erythroid line facilitates sustainable and scalable generation of functional red cells. Nat Commun. 2017;8:14750.

151. Pereira Daoud AM, Popovic M, Dondorp WJ, Trani Bustos M, Bredenoord AL, Chuva de Sousa Lopes SM, et al. Modelling human embryogenesis: embryo-like structures spark ethical and policy debate. Hum Reprod Update. 2020;26(6):779-98.
152. Kurita R, Suda N, Sudo K, Miharada K, Hiroyama T, Miyoshi H, et al. Establishment of immortalized human erythroid progenitor cell lines able to produce enucleated red blood cells. PLoS One. 2013;8(3):e59890.
153. Hirose S, Takayama N, Nakamura S, Nagasawa K, Ochi K, Hirata S, et al. Immortalization of erythroblasts by c-MYC and BCL-XL enables large-scale erythrocyte production from human pluripotent stem cells. Stem Cell Reports. 2013;1(6):499-508.
154. Huang X, Shah S, Wang J, Ye Z, Dowey SN, Tsang KM, et al. Extensive ex vivo expansion of functional human erythroid precursors established from umbilical cord blood cells by defined factors. Mol Ther. 2014;22(2):451-63.
155. Ebrahimi M, Forouzesh M, Raoufi S, Ramazii M, Ghaedrahmati F, Farzaneh M. Differentiation of human induced pluripotent stem cells into erythroid cells. Stem Cell Res Ther. 2020;11(1):483.
156. Lu SJ, Feng Q, Park JS, Vida L, Lee BS, Strausbauch M, et al. Biologic properties and enucleation of red blood cells from human embryonic stem cells. Blood. 2008;112(12):4475-84.
157. Ma F, Ebihara Y, Umeda K, Sakai H, Hanada S, Zhang H, et al. Generation of functional erythrocytes from human embryonic stem cell-derived definitive hematopoiesis. Proc Natl Acad Sci U S A. 2008;105(35):13087-92.
158. Acosta ND, Golub SH. The New Federalism: State Policies Regarding Embryonic Stem Cell Research. J Law Med Ethics. 2016;44(3):419-36.
159. Olivier EN, Marenah L, McCahill A, Condie A, Cowan S, Mountford JC. High-Efficiency Serum-Free Feeder-Free Erythroid Differentiation of Human Pluripotent Stem Cells Using Small Molecules. Stem Cells Transl Med. 2016;5(10):1394-405.
160. Takahashi K, Tanabe K, Ohnuki M, Narita M, Ichisaka T, Tomoda K, et al. Induction of pluripotent stem cells from adult human fibroblasts by defined factors. Cell. 2007;131(5):861-72.
161. Takahashi K, Yamanaka S. Induction of pluripotent stem cells from mouse embryonic and adult fibroblast cultures by defined factors. Cell. 2006;126(4):663-76.
162. Chambers SM, Fasano CA, Papapetrou EP, Tomishima M, Sadelain M, Studer L. Highly efficient neural conversion of human ES and iPS cells by dual inhibition of SMAD signaling. Nat Biotechnol. 2009;27(3):275-80.
163. Takayama K, Inamura M, Kawabata K, Katayama K, Higuchi M, Tashiro K, et al. Efficient generation of functional hepatocytes from human embryonic stem cells and induced pluripotent stem cells by HNF4α transduction. Mol Ther. 2012;20(1):127-37.
164. Moradi S, Mahdizadeh H, Šarić T, Kim J, Harati J, Shahsavarani H, et al. Research and therapy with induced pluripotent stem cells (iPSCs): social, legal, and ethical considerations. Stem Cell Res Ther. 2019;10(1):341.
165. Bernecker C, Ackermann M, Lachmann N, Rohrhofer L, Zaehres H, Araúzo-Bravo MJ, et al. Enhanced Ex Vivo Generation of Erythroid Cells from Human Induced Pluripotent Stem Cells in a Simplified Cell Culture System with Low Cytokine Support. Stem Cells Dev. 2019;28(23):1540-51.

166. Lapillonne H, Kobari L, Mazurier C, Tropel P, Giarratana MC, Zanella-Cleon I, et al. Red blood cell generation from human induced pluripotent stem cells: perspectives for transfusion medicine. Haematologica. 2010;95(10):1651-9.
167. Dorn I, Klich K, Arauzo-Bravo MJ, Radstaak M, Santourlidis S, Ghanjati F, et al. Erythroid differentiation of human induced pluripotent stem cells is independent of donor cell type of origin. Haematologica. 2015;100(1):32-41.
168. Hockemeyer D, Jaenisch R. Induced Pluripotent Stem Cells Meet Genome Editing. Cell Stem Cell. 2016;18(5):573-86.
169. Hockemeyer D, Soldner F, Beard C, Gao Q, Mitalipova M, DeKelver RC, et al. Efficient targeting of expressed and silent genes in human ESCs and iPSCs using zinc-finger nucleases. Nat Biotechnol. 2009;27(9):851-7.
170. Ackermann M, Kuhn A, Kunkiel J, Merkert S, Martin U, Moritz T, et al. Ex vivo Generation of Genetically Modified Macrophages from Human Induced Pluripotent Stem Cells. Transfus Med Hemother. 2017;44(3):135-42.
171. Kuhn A, Ackermann M, Mussolino C, Cathomen T, Lachmann N, Moritz T. TALEN-mediated functional correction of human iPSC-derived macrophages in context of hereditary pulmonary alveolar proteinosis. Sci Rep. 2017;7(1):15195.
172. Yang CT, Ma R, Axton RA, Jackson M, Taylor AH, Fidanza A, et al. Activation of KLF1 Enhances the Differentiation and Maturation of Red Blood Cells from Human Pluripotent Stem Cells. Stem Cells. 2017;35(4):886-97.
173. De Masi C, Spitalieri P, Murdocca M, Novelli G, Sangiuolo F. Application of CRISPR/Cas9 to human-induced pluripotent stem cells: from gene editing to drug discovery. Hum Genomics. 2020;14(1):25.
174. Raya A, Rodríguez-Pizà I, Guenechea G, Vassena R, Navarro S, Barrero MJ, et al. Disease-corrected haematopoietic progenitors from Fanconi anaemia induced pluripotent stem cells. Nature. 2009;460(7251):53-9.
175. Lee KY, Fong BS, Tsang KS, Lau TK, Ng PC, Lam AC, et al. Fetal stromal niches enhance human embryonic stem cell-derived hematopoietic differentiation and globin switch. Stem Cells Dev. 2011;20(1):31-8.
176. Dias J, Gumenyuk M, Kang H, Vodyanik M, Yu J, Thomson JA, et al. Generation of red blood cells from human induced pluripotent stem cells. Stem Cells Dev. 2011;20(9):1639-47.
177. Chang KH, Nelson AM, Cao H, Wang L, Nakamoto B, Ware CB, et al. Definitive-like erythroid cells derived from human embryonic stem cells coexpress high levels of embryonic and fetal globins with little or no adult globin. Blood. 2006;108(5):1515-23.
178. Salvagiotto G, Burton S, Daigh CA, Rajesh D, Slukvin, II, Seay NJ. A defined, feeder-free, serum-free system to generate in vitro hematopoietic progenitors and differentiated blood cells from hESCs and hiPSCs. PLoS One. 2011;6(3):e17829.
179. Merryweather-Clarke AT, Tipping AJ, Lamikanra AA, Fa R, Abu-Jamous B, Tsang HP, et al. Distinct gene expression program dynamics during erythropoiesis from human induced pluripotent stem cells compared with adult and cord blood progenitors. BMC Genomics. 2016;17(1):817.
180. Trakarnsanga K, Wilson MC, Griffiths RE, Toye AM, Carpenter L, Heesom KJ, et al. Qualitative and quantitative comparison of the proteome of erythroid cells differentiated from human iPSCs and adult erythroid cells by multiplex TMT labelling and nanoLC-MS/MS. PLoS One. 2014;9(7):e100874.

181. Bessis M. [Erythroblastic island, functional unity of bone marrow]. Rev Hematol. 1958;13(1):8-11.
182. Berman I. The ultrastructure of erythroblastic islands and reticular cells in mouse bone marrow. J Ultrastruct Res. 1967;17(3):291-313.
183. Manwani D, Bieker JJ. The erythroblastic island. Curr Top Dev Biol. 2008;82:23-53.
184. May A, Forrester LM. The erythroblastic island niche: modeling in health, stress, and disease. Exp Hematol. 2020;91:10-21.
185. Mohandas N, Prenant M. Three-dimensional model of bone marrow. Blood. 1978;51(4):633-43.
186. Sonoda Y, Sasaki K. Hepatic extramedullary hematopoiesis and macrophages in the adult mouse: histometrical and immunohistochemical studies. Cells Tissues Organs. 2012;196(6):555-64.
187. Yokoyama T, Etoh T, Kitagawa H, Tsukahara S, Kannan Y. Migration of erythroblastic islands toward the sinusoid as erythroid maturation proceeds in rat bone marrow. J Vet Med Sci. 2003;65(4):449-52.
188. Lee SH, Crocker PR, Westaby S, Key N, Mason DY, Gordon S, et al. Isolation and immunocytochemical characterization of human bone marrow stromal macrophages in hemopoietic clusters. J Exp Med. 1988;168(3):1193-8.
189. Yokoyama T, Kitagawa H, Takeuchi T, Tsukahara S, Kannan Y. No apoptotic cell death of erythroid cells of erythroblastic islands in bone marrow of healthy rats. J Vet Med Sci. 2002;64(10):913-9.
190. Giger KM, Kalfa TA. Phylogenetic and Ontogenetic View of Erythroblastic Islands. Biomed Res Int. 2015;2015:873628.
191. Villolobos M, Leon P, Sessions SK, Kezer J. Enucleated Erythrocytes in Plethodontid Salamanders. Herpetologica. 1988;44(2):243-50.
192. Cohen WD. The cytomorphic system of anucleate non-mammalian erythrocytes. Protoplasma. 1982;113(1):23-32.
193. Mueller RL, Gregory TR, Gregory SM, Hsieh A, Boore JL. Genome size, cell size, and the evolution of enucleated erythrocytes in attenuate salamanders. Zoology (Jena). 2008;111(3):218-30.
194. Lo Celso C, Fleming HE, Wu JW, Zhao CX, Miake-Lye S, Fujisaki J, et al. Live-animal tracking of individual haematopoietic stem/progenitor cells in their niche. Nature. 2009;457(7225):92-6.
195. Sugiyama T, Kohara H, Noda M, Nagasawa T. Maintenance of the hematopoietic stem cell pool by CXCL12-CXCR4 chemokine signaling in bone marrow stromal cell niches. Immunity. 2006;25(6):977-88.
196. Kiel MJ, Yilmaz OH, Iwashita T, Terhorst C, Morrison SJ. SLAM family receptors distinguish hematopoietic stem and progenitor cells and reveal endothelial niches for stem cells. Cell. 2005;121(7):1109-21.
197. Romano L, Seu KG, Papoin J, Muench DE, Konstantinidis D, Olsson A, et al. Erythroblastic islands foster granulopoiesis in parallel to terminal erythropoiesis. Blood. 2022;140(14):1621-34.
198. Winkler IG, Sims NA, Pettit AR, Barbier V, Nowlan B, Helwani F, et al. Bone marrow macrophages maintain hematopoietic stem cell (HSC) niches and their depletion mobilizes HSCs. Blood. 2010;116(23):4815-28.

199. Bessis MC, Breton-Gorius J. Iron metabolism in the bone marrow as seen by electron microscopy: a critical review. Blood. 1962;19:635-63.
200. Porcu S, Manchinu MF, Marongiu MF, Sogos V, Poddie D, Asunis I, et al. Klf1 affects DNase II-alpha expression in the central macrophage of a fetal liver erythroblastic island: a non-cell-autonomous role in definitive erythropoiesis. Mol Cell Biol. 2011;31(19):4144-54.
201. Lopez-Yrigoyen M, Yang CT, Fidanza A, Cassetta L, Taylor AH, McCahill A, et al. Genetic programming of macrophages generates an in vitro model for the human erythroid island niche. Nat Commun. 2019;10(1):881.
202. Policard A, Bessis M. Micropinocytosis and rhopheocytosis. Nature. 1962;194:110-1.
203. Allen TD, Dexter TM. Ultrastructural aspects of erythropoietic differentiation in long-term bone marrow culture. Differentiation. 1982;21(2):86-94.
204. Leimberg MJ, Prus E, Konijn AM, Fibach E. Macrophages function as a ferritin iron source for cultured human erythroid precursors. J Cell Biochem. 2008;103(4):1211-8.
205. Seu KG, Papoin J, Fessler R, Hom J, Huang G, Mohandas N, et al. Unraveling Macrophage Heterogeneity in Erythroblastic Islands. Front Immunol. 2017;8:1140.
206. Morris L, Crocker PR, Fraser I, Hill M, Gordon S. Expression of a divalent cation-dependent erythroblast adhesion receptor by stromal macrophages from murine bone marrow. J Cell Sci. 1991;99 (Pt 1):141-7.
207. Sadahira Y, Yoshino T, Monobe Y. Very late activation antigen 4-vascular cell adhesion molecule 1 interaction is involved in the formation of erythroblastic islands. J Exp Med. 1995;181(1):411-5.
208. Crocker PR, Gordon S. Isolation and characterization of resident stromal macrophages and hematopoietic cell clusters from mouse bone marrow. J Exp Med. 1985;162(3):993-1014.
209. Chow A, Huggins M, Ahmed J, Hashimoto D, Lucas D, Kunisaki Y, et al. CD169(+) macrophages provide a niche promoting erythropoiesis under homeostasis and stress. Nat Med. 2013;19(4):429-36.
210. Li W, Wang Y, Zhao H, Zhang H, Xu Y, Wang S, et al. Identification and transcriptome analysis of erythroblastic island macrophages. Blood. 2019;134(5):480-91.
211. Hanspal M, Hanspal JS. The association of erythroblasts with macrophages promotes erythroid proliferation and maturation: a 30-kD heparin-binding protein is involved in this contact. Blood. 1994;84(10):3494-504.
212. Rhodes MM, Kopsombut P, Bondurant MC, Price JO, Koury MJ. Adherence to macrophages in erythroblastic islands enhances erythroblast proliferation and increases erythrocyte production by a different mechanism than erythropoietin. Blood. 2008;111(3):1700-8.
213. Hanspal M, Smockova Y, Uong Q. Molecular identification and functional characterization of a novel protein that mediates the attachment of erythroblasts to macrophages. Blood. 1998;92(8):2940-50.
214. Soni S, Bala S, Gwynn B, Sahr KE, Peters LL, Hanspal M. Absence of erythroblast macrophage protein (Emp) leads to failure of erythroblast nuclear extrusion. J Biol Chem. 2006;281(29):20181-9.

215. Soni S, Bala S, Hanspal M. Requirement for erythroblast-macrophage protein (Emp) in definitive erythropoiesis. Blood Cells Mol Dis. 2008;41(2):141-7.
216. Wei Q, Boulais PE, Zhang D, Pinho S, Tanaka M, Frenette PS. Maea expressed by macrophages, but not erythroblasts, maintains postnatal murine bone marrow erythroblastic islands. Blood. 2019;133(11):1222-32.
217. Lee JC, Gimm JA, Lo AJ, Koury MJ, Krauss SW, Mohandas N, et al. Mechanism of protein sorting during erythroblast enucleation: role of cytoskeletal connectivity. Blood. 2004;103(5):1912-9.
218. Spring FA, Parsons SF, Ortlepp S, Olsson ML, Sessions R, Brady RL, et al. Intercellular adhesion molecule-4 binds alpha(4)beta(1) and alpha(V)-family integrins through novel integrin-binding mechanisms. Blood. 2001;98(2):458-66.
219. Lee G, Lo A, Short SA, Mankelow TJ, Spring F, Parsons SF, et al. Targeted gene deletion demonstrates that the cell adhesion molecule ICAM-4 is critical for erythroblastic island formation. Blood. 2006;108(6):2064-71.
220. Kingsley PD, Greenfest-Allen E, Frame JM, Bushnell TP, Malik J, McGrath KE, et al. Ontogeny of erythroid gene expression. Blood. 2013;121(6):e5-e13.
221. Fabriek BO, Polfliet MM, Vloet RP, van der Schors RC, Ligtenberg AJ, Weaver LK, et al. The macrophage CD163 surface glycoprotein is an erythroblast adhesion receptor. Blood. 2007;109(12):5223-9.
222. Li W, Guo R, Song Y, Jiang Z. Erythroblastic Island Macrophages Shape Normal Erythropoiesis and Drive Associated Disorders in Erythroid Hematopoietic Diseases. Front Cell Dev Biol. 2020;8:613885.
223. Parast MM, Otey CA. Characterization of palladin, a novel protein localized to stress fibers and cell adhesions. J Cell Biol. 2000;150(3):643-56.
224. Liu XS, Li XH, Wang Y, Shu RZ, Wang L, Lu SY, et al. Disruption of palladin leads to defects in definitive erythropoiesis by interfering with erythroblastic island formation in mouse fetal liver. Blood. 2007;110(3):870-6.
225. Chasis JA, Mohandas N. Erythroblastic islands: niches for erythropoiesis. Blood. 2008;112(3):470-8.
226. Kurtz A, Härtl W, Jelkmann W, Zapf J, Bauer C. Activity in fetal bovine serum that stimulates erythroid colony formation in fetal mouse livers is insulinlike growth factor I. J Clin Invest. 1985;76(4):1643-8.
227. Rich IN, Vogt C, Pentz S. Erythropoietin gene expression in macrophages detected by in situ hybridization. Behring Inst Mitt. 1988(83):202-6.
228. Matsushima T, Nakashima M, Oshima K, Abe Y, Nishimura J, Nawata H, et al. Receptor binding cancer antigen expressed on SiSo cells, a novel regulator of apoptosis of erythroid progenitor cells. Blood. 2001;98(2):313-21.
229. Angelillo-Scherrer A, Burnier L, Lambrechts D, Fish RJ, Tjwa M, Plaisance S, et al. Role of Gas6 in erythropoiesis and anemia in mice. J Clin Invest. 2008;118(2):583-96.
230. Tordjman R, Delaire S, Plouët J, Ting S, Gaulard P, Fichelson S, et al. Erythroblasts are a source of angiogenic factors. Blood. 2001;97(7):1968-74.
231. Heideveld E, Hampton-O'Neil LA, Cross SJ, van Alphen FPJ, van den Biggelaar M, Toye AM, et al. Glucocorticoids induce differentiation of monocytes towards macrophages that share functional and phenotypical aspects with erythroblastic island macrophages. Haematologica. 2018;103(3):395-405.

232. Yoffey JM, Yaffe P. The phagocytic central reticular cell of the erythroblastic island in rat bone marrow: changes in hypoxia and rebound. J Reticuloendothel Soc. 1980;28(1):37-47.
233. Toda S, Segawa K, Nagata S. MerTK-mediated engulfment of pyrenocytes by central macrophages in erythroblastic islands. Blood. 2014;123(25):3963-71.
234. Yoshida H, Kawane K, Koike M, Mori Y, Uchiyama Y, Nagata S. Phosphatidylserine-dependent engulfment by macrophages of nuclei from erythroid precursor cells. Nature. 2005;437(7059):754-8.
235. Kawane K, Fukuyama H, Kondoh G, Takeda J, Ohsawa Y, Uchiyama Y, et al. Requirement of DNase II for definitive erythropoiesis in the mouse fetal liver. Science. 2001;292(5521):1546-9.
236. Yoshida H, Okabe Y, Kawane K, Fukuyama H, Nagata S. Lethal anemia caused by interferon-beta produced in mouse embryos carrying undigested DNA. Nat Immunol. 2005;6(1):49-56.
237. Leimberg JM, Konijn AM, Fibach E. Macrophages promote development of human erythroid precursors in transferrin-free culture medium. Hematology. 2005;10(1):73-6.
238. Harandi OF, Hedge S, Wu DC, McKeone D, Paulson RF. Murine erythroid short-term radioprotection requires a BMP4-dependent, self-renewing population of stress erythroid progenitors. J Clin Invest. 2010;120(12):4507-19.
239. Lenox LE, Perry JM, Paulson RF. Extramedullary Erythropoiesis in the Adult Liver Requires BMP-4/Smad5-dependent Signaling. Blood. 2005;105(7):2741-8.
240. Hentze MW, Muckenthaler MU, Andrews NC. Balancing acts: molecular control of mammalian iron metabolism. Cell. 2004;117(3):285-97.
241. Sadahira Y, Mori M, Kimoto T. Participation of radioresistant Forssman antigen-bearing macrophages in the formation of stromal elements of erythroid spleen colonies. Br J Haematol. 1989;71(4):469-74.
242. Sadahira Y, Yasuda T, Yoshino T, Manabe T, Takeishi T, Kobayashi Y, et al. Impaired splenic erythropoiesis in phlebotomized mice injected with CL2MDP-liposome: an experimental model for studying the role of stromal macrophages in erythropoiesis. J Leukoc Biol. 2000;68(4):464-70.
243. Miyake Y, Asano K, Kaise H, Uemura M, Nakayama M, Tanaka M. Critical role of macrophages in the marginal zone in the suppression of immune responses to apoptotic cell-associated antigens. J Clin Invest. 2007;117(8):2268-78.
244. Liao C, Prabhu KS, Paulson RF. Monocyte-derived macrophages expand the murine stress erythropoietic niche during the recovery from anemia. Blood. 2018;132(24):2580-93.
245. Ramos P, Casu C, Gardenghi S, Breda L, Crielaard BJ, Guy E, et al. Macrophages support pathological erythropoiesis in polycythemia vera and beta-thalassemia. Nat Med. 2013;19(4):437-45.
246. Ciavatta DJ, Ryan TM, Farmer SC, Townes TM. Mouse model of human beta zero thalassemia: targeted deletion of the mouse beta maj- and beta min-globin genes in embryonic stem cells. Proc Natl Acad Sci U S A. 1995;92(20):9259-63.
247. Hume DA, Robinson AP, MacPherson GG, Gordon S. The mononuclear phagocyte system of the mouse defined by immunohistochemical localization of antigen F4/80. Relationship between macrophages, Langerhans cells, reticular cells,

and dendritic cells in lymphoid and hematopoietic organs. J Exp Med. 1983;158(5):1522-36.
248. Breton-Gorius J, Guichard J, Vainchenker W. Absence of erythroblastic islands in plasma clot culture and their possible reconstitution after clot lysis. Blood Cells. 1979;5(3):461-9.
249. Xiang J, Wu DC, Chen Y, Paulson RF. In vitro culture of stress erythroid progenitors identifies distinct progenitor populations and analogous human progenitors. Blood. 2015;125(11):1803-12.
250. Hao S, Xiang J, Wu DC, Fraser JW, Ruan B, Cai J, et al. Gdf15 regulates murine stress erythroid progenitor proliferation and the development of the stress erythropoiesis niche. Blood Adv. 2019;3(14):2205-17.
251. Belay E, Hayes BJ, Blau CA, Torok-Storb B. Human Cord Blood and Bone Marrow CD34+ Cells Generate Macrophages That Support Erythroid Islands. PLoS One. 2017;12(1):e0171096.
252. Belay E, Miller CP, Kortum AN, Torok-Storb B, Blau CA, Emery DW. A hyperactive Mpl-based cell growth switch drives macrophage-associated erythropoiesis through an erythroid-megakaryocytic precursor. Blood. 2015;125(6):1025-33.
253. Wynn TA, Chawla A, Pollard JW. Macrophage biology in development, homeostasis and disease. Nature. 2013;496(7446):445-55.
254. Lopez-Yrigoyen M, Fidanza A, Cassetta L, Axton RA, Taylor AH, Meseguer-Ripolles J, et al. A human iPSC line capable of differentiating into functional macrophages expressing ZsGreen: a tool for the study and in vivo tracking of therapeutic cells. Philos Trans R Soc Lond B Biol Sci. 2018;373(1750).
255. Smith TD, Nagalla RR, Chen EY, Liu WF. Harnessing macrophage plasticity for tissue regeneration. Adv Drug Deliv Rev. 2017;114:193-205.
256. Shapouri-Moghaddam A, Mohammadian S, Vazini H, Taghadosi M, Esmaeili SA, Mardani F, et al. Macrophage plasticity, polarization, and function in health and disease. J Cell Physiol. 2018;233(9):6425-40.
257. Bachiller S, Jiménez-Ferrer I, Paulus A, Yang Y, Swanberg M, Deierborg T, et al. Microglia in Neurological Diseases: A Road Map to Brain-Disease Dependent-Inflammatory Response. Front Cell Neurosci. 2018;12:488.
258. McNamara NB, Miron VE. Microglia in developing white matter and perinatal brain injury. Neurosci Lett. 2020;714:134539.
259. Nguyen-Lefebvre AT, Horuzsko A. Kupffer Cell Metabolism and Function. J Enzymol Metab. 2015;1(1).
260. Bertrand JY, Jalil A, Klaine M, Jung S, Cumano A, Godin I. Three pathways to mature macrophages in the early mouse yolk sac. Blood. 2005;106(9):3004-11.
261. McGrath KE, Frame JM, Palis J. Early hematopoiesis and macrophage development. Semin Immunol. 2015;27(6):379-87.
262. Stremmel C, Schuchert R, Wagner F, Thaler R, Weinberger T, Pick R, et al. Yolk sac macrophage progenitors traffic to the embryo during defined stages of development. Nat Commun. 2018;9(1):75.
263. Ginhoux F, Greter M, Leboeuf M, Nandi S, See P, Gokhan S, et al. Fate mapping analysis reveals that adult microglia derive from primitive macrophages. Science. 2010;330(6005):841-5.

264. Gomez Perdiguero E, Klapproth K, Schulz C, Busch K, Azzoni E, Crozet L, et al. Tissue-resident macrophages originate from yolk-sac-derived erythro-myeloid progenitors. Nature. 2015;518(7540):547-51.
265. Bain CC, Hawley CA, Garner H, Scott CL, Schridde A, Steers NJ, et al. Long-lived self-renewing bone marrow-derived macrophages displace embryo-derived cells to inhabit adult serous cavities. Nat Commun. 2016;7:ncomms11852.
266. Bain CC, Bravo-Blas A, Scott CL, Perdiguero EG, Geissmann F, Henri S, et al. Constant replenishment from circulating monocytes maintains the macrophage pool in the intestine of adult mice. Nat Immunol. 2014;15(10):929-37.
267. Molawi K, Wolf Y, Kandalla PK, Favret J, Hagemeyer N, Frenzel K, et al. Progressive replacement of embryo-derived cardiac macrophages with age. J Exp Med. 2014;211(11):2151-8.
268. McKendrick JG, Jones G-R, Elder SS, Mercer E, Magalhaes MS, Rocchi C, et al. CSF1R-dependent macrophages in the salivary gland are essential for epithelial regeneration following radiation-induced injury. bioRxiv. 2022:2022.06.12.495803.
269. Buchrieser J, James W, Moore MD. Human Induced Pluripotent Stem Cell-Derived Macrophages Share Ontogeny with MYB-Independent Tissue-Resident Macrophages. Stem Cell Reports. 2017;8(2):334-45.
270. Fogg DK, Sibon C, Miled C, Jung S, Aucouturier P, Littman DR, et al. A clonogenic bone marrow progenitor specific for macrophages and dendritic cells. Science. 2006;311(5757):83-7.
271. Liu K, Victora GD, Schwickert TA, Guermonprez P, Meredith MM, Yao K, et al. In vivo analysis of dendritic cell development and homeostasis. Science. 2009;324(5925):392-7.
272. Watanabe S, Alexander M, Misharin AV, Budinger GRS. The role of macrophages in the resolution of inflammation. J Clin Invest. 2019;129(7):2619-28.
273. Soehnlein O, Lindbom L. Phagocyte partnership during the onset and resolution of inflammation. Nat Rev Immunol. 2010;10(6):427-39.
274. Kono H, Rock KL. How dying cells alert the immune system to danger. Nat Rev Immunol. 2008;8(4):279-89.
275. Roh JS, Sohn DH. Damage-Associated Molecular Patterns in Inflammatory Diseases. Immune Netw. 2018;18(4):e27.
276. Mukhopadhyay S, Plüddemann A, Gordon S. Macrophage pattern recognition receptors in immunity, homeostasis and self tolerance. Adv Exp Med Biol. 2009;653:1-14.
277. Hirayama D, Iida T, Nakase H. The Phagocytic Function of Macrophage-Enforcing Innate Immunity and Tissue Homeostasis. Int J Mol Sci. 2017;19(1).
278. Qian BZ, Pollard JW. Macrophage diversity enhances tumor progression and metastasis. Cell. 2010;141(1):39-51.
279. Kurowska-Stolarska M, Alivernini S. Synovial tissue macrophages: friend or foe? RMD Open. 2017;3(2):e000527.
280. Alivernini S, MacDonald L, Elmesmari A, Finlay S, Tolusso B, Gigante MR, et al. Distinct synovial tissue macrophage subsets regulate inflammation and remission in rheumatoid arthritis. Nat Med. 2020;26(8):1295-306.
281. Shand FH, Ueha S, Otsuji M, Koid SS, Shichino S, Tsukui T, et al. Tracking of intertissue migration reveals the origins of tumor-infiltrating monocytes. Proc Natl Acad Sci U S A. 2014;111(21):7771-6.

282. Bentzen SM. Preventing or reducing late side effects of radiation therapy: radiobiology meets molecular pathology. Nat Rev Cancer. 2006;6(9):702-13.
283. Firestein GS, McInnes IB. Immunopathogenesis of Rheumatoid Arthritis. Immunity. 2017;46(2):183-96.
284. Takimoto CH, Chao MP, Gibbs C, McCamish MA, Liu J, Chen JY, et al. The Macrophage 'Do not eat me' signal, CD47, is a clinically validated cancer immunotherapy target. Ann Oncol. 2019;30(3):486-9.
285. Zhang C, Yang M, Ericsson AC. Function of Macrophages in Disease: Current Understanding on Molecular Mechanisms. Front Immunol. 2021;12:620510.
286. Cavaliere G. A 14-day limit for bioethics: the debate over human embryo research. BMC Med Ethics. 2017;18(1):38.
287. Strober W. Obtaining human peripheral blood cells. Curr Protoc Immunol. 2001;Appendix 3:Appendix 3F.
288. Moore JK, Mackinnon AC, Wojtacha D, Pope C, Fraser AR, Burgoyne P, et al. Phenotypic and functional characterization of macrophages with therapeutic potential generated from human cirrhotic monocytes in a cohort study. Cytotherapy. 2015;17(11):1604-16.
289. Heideveld E, Masiello F, Marra M, Esteghamat F, Yagci N, von Lindern M, et al. CD14+ cells from peripheral blood positively regulate hematopoietic stem and progenitor cell survival resulting in increased erythroid yield. Haematologica. 2015;100(11):1396-406.
290. Chometon TQ, Siqueira MDS, Sant Anna JC, Almeida MR, Gandini M, Martins de Almeida Nogueira AC, et al. A protocol for rapid monocyte isolation and generation of singular human monocyte-derived dendritic cells. PLoS One. 2020;15(4):e0231132.
291. Fraser AR, Pass C, Burgoyne P, Atkinson A, Bailey L, Laurie A, et al. Development, functional characterization and validation of methodology for GMP-compliant manufacture of phagocytic macrophages: A novel cellular therapeutic for liver cirrhosis. Cytotherapy. 2017;19(9):1113-24.
292. Nielsen MC, Andersen MN, Møller HJ. Monocyte isolation techniques significantly impact the phenotype of both isolated monocytes and derived macrophages in vitro. Immunology. 2020;159(1):63-74.
293. Abrink M, Gobl AE, Huang R, Nilsson K, Hellman L. Human cell lines U-937, THP-1 and Mono Mac 6 represent relatively immature cells of the monocyte-macrophage cell lineage. Leukemia. 1994;8(9):1579-84.
294. Sundström C, Nilsson K. Establishment and characterization of a human histiocytic lymphoma cell line (U-937). Int J Cancer. 1976;17(5):565-77.
295. Naldini A, Sower L, Bocci V, Meyers B, Carney DH. Thrombin receptor expression and responsiveness of human monocytic cells to thrombin is linked to interferon-induced cellular differentiation. J Cell Physiol. 1998;177(1):76-84.
296. Passmore JS, Lukey PT, Ress SR. The human macrophage cell line U937 as an in vitro model for selective evaluation of mycobacterial antigen-specific cytotoxic T-cell function. Immunology. 2001;102(2):146-56.
297. Ziegler-Heitbrock HW, Thiel E, Fütterer A, Herzog V, Wirtz A, Riethmüller G. Establishment of a human cell line (Mono Mac 6) with characteristics of mature monocytes. Int J Cancer. 1988;41(3):456-61.

298. Tsuchiya S, Yamabe M, Yamaguchi Y, Kobayashi Y, Konno T, Tada K. Establishment and characterization of a human acute monocytic leukemia cell line (THP-1). Int J Cancer. 1980;26(2):171-6.
299. Chanput W, Mes JJ, Wichers HJ. THP-1 cell line: an in vitro cell model for immune modulation approach. Int Immunopharmacol. 2014;23(1):37-45.
300. Tsuchiya S, Kobayashi Y, Goto Y, Okumura H, Nakae S, Konno T, et al. Induction of maturation in cultured human monocytic leukemia cells by a phorbol diester. Cancer Res. 1982;42(4):1530-6.
301. Daigneault M, Preston JA, Marriott HM, Whyte MK, Dockrell DH. The identification of markers of macrophage differentiation in PMA-stimulated THP-1 cells and monocyte-derived macrophages. PLoS One. 2010;5(1):e8668.
302. Madhvi A, Mishra H, Leisching GR, Mahlobo PZ, Baker B. Comparison of human monocyte derived macrophages and THP1-like macrophages as in vitro models for M. tuberculosis infection. Comp Immunol Microbiol Infect Dis. 2019;67:101355.
303. van Wilgenburg B, Browne C, Vowles J, Cowley SA. Efficient, long term production of monocyte-derived macrophages from human pluripotent stem cells under partly-defined and fully-defined conditions. PLoS One. 2013;8(8):e71098.
304. Bosshart H, Heinzelmann M. THP-1 cells as a model for human monocytes. Ann Transl Med. 2016;4(21):438.
305. Lopez-Yrigoyen M, May A, Ventura T, Taylor H, Fidanza A, Cassetta L, et al. Production and Characterization of Human Macrophages from Pluripotent Stem Cells. J Vis Exp. 2020(158).
306. Tippett E, Cheng WJ, Westhorpe C, Cameron PU, Brew BJ, Lewin SR, et al. Differential expression of CD163 on monocyte subsets in healthy and HIV-1 infected individuals. PLoS One. 2011;6(5):e19968.
307. Lee CZW, Kozaki T, Ginhoux F. Studying tissue macrophages in vitro: are iPSC-derived cells the answer? Nat Rev Immunol. 2018;18(11):716-25.
308. Chun YS, Byun K, Lee B. Induced pluripotent stem cells and personalized medicine: current progress and future perspectives. Anat Cell Biol. 2011;44(4):245-55.
309. Park IH, Arora N, Huo H, Maherali N, Ahfeldt T, Shimamura A, et al. Disease-specific induced pluripotent stem cells. Cell. 2008;134(5):877-86.
310. Ebert AD, Yu J, Rose FF, Jr., Mattis VB, Lorson CL, Thomson JA, et al. Induced pluripotent stem cells from a spinal muscular atrophy patient. Nature. 2009;457(7227):277-80.
311. Mack DL, Guan X, Wagoner A, Walker SJ, Childers MK. Disease-in-a-dish: the contribution of patient-specific induced pluripotent stem cell technology to regenerative rehabilitation. Am J Phys Med Rehabil. 2014;93(11 Suppl 3):S155-68.
312. Martin M. Cutadapt removes adapter sequences from high-throughput sequencing reads.
313. Dobin A, Davis CA, Schlesinger F, Drenkow J, Zaleski C, Jha S, et al. STAR: ultrafast universal RNA-seq aligner. Bioinformatics. 2013;29(1):15-21.
314. Tefferi A, Pardanani A. Myeloproliferative Neoplasms: A Contemporary Review. JAMA Oncol. 2015;1(1):97-105.
315. Singleton BK, Fairweather VSS, Lau W, Parsons SF, Burton NM, Frayne J, et al.

316. Caminal M, Labrozzi JP, Oliver-Vila I, Alzaga-Gragera M, Marín-Gallén S, Pla A, et al. Ex vivo production of red blood cells from human cord blood.
317. Vodyanik MA, Thomson JA, Slukvin, II. Leukosialin (CD43) defines hematopoietic progenitors in human embryonic stem cell differentiation cultures. Blood. 2006;108(6):2095-105.
318. Kessel KU, Bluemke A, Schöler HR, Zaehres H, Schlenke P, Dorn I. Emergence of CD43-Expressing Hematopoietic Progenitors from Human Induced Pluripotent Stem Cells. Transfus Med Hemother. 2017;44(3):143-50.
319. Eisenwort G, Jurkin J, Yasmin N, Bauer T, Gesslbauer B, Strobl H. Identification of TROP2 (TACSTD2), an EpCAM-like molecule, as a specific marker for TGF-β1-dependent human epidermal Langerhans cells. J Invest Dermatol. 2011;131(10):2049-57.
320. Lammers R, Giesert C, Grünebach F, Marxer A, Vogel W, Bühring HJ. Monoclonal antibody 9C4 recognizes epithelial cellular adhesion molecule, a cell surface antigen expressed in early steps of erythropoiesis. Exp Hematol. 2002;30(6):537-45.
321. Fidanza A, Stumpf PS, Ramachandran P, Tamagno S, Babtie A, Lopez-Yrigoyen M, et al. Single-cell analyses and machine learning define hematopoietic progenitor and HSC-like cells derived from human PSCs. Blood. 2020;136(25):2893-904.
322. Mao B, Huang S, Lu X, Sun W, Zhou Y, Pan X, et al. Early Development of Definitive Erythroblasts from Human Pluripotent Stem Cells Defined by Expression of Glycophorin A/CD235a, CD34, and CD36. Stem Cell Reports. 2016;7(5):869-83.
323. Aisen P. Transferrin receptor 1. Int J Biochem Cell Biol. 2004;36(11):2137-43.
324. Marsee DK, Pinkus GS, Yu H. CD71 (transferrin receptor): an effective marker for erythroid precursors in bone marrow biopsy specimens. Am J Clin Pathol. 2010;134(3):429-35.
325. Nakahata T, Okumura N. Cell surface antigen expression in human erythroid progenitors: erythroid and megakaryocytic markers. Leuk Lymphoma. 1994;13(5-6):401-9.
326. Furthmayr H, Marchesi VT. Subunit structure of human erythrocyte glycophorin A. Biochemistry. 1976;15(5):1137-44.
327. Giger K, Habib I, Ritchie K, Low PS. Diffusion of glycophorin A in human erythrocytes. Biochim Biophys Acta. 2016;1858(11):2839-45.
328. Bennett V, Stenbuck PJ. The membrane attachment protein for spectrin is associated with band 3 in human erythrocyte membranes. Nature. 1979;280(5722):468-73.
329. Reithmeier RA, Casey JR, Kalli AC, Sansom MS, Alguel Y, Iwata S. Band 3, the human red cell chloride/bicarbonate anion exchanger (AE1, SLC4A1), in a structural context. Biochim Biophys Acta. 2016;1858(7 Pt A):1507-32.
330. Sankaran VG, Orkin SH. The switch from fetal to adult hemoglobin. Cold Spring Harb Perspect Med. 2013;3(1):a011643.
331. Ravindranath Y, Johnson RM, Goyette G, Buck S, Gadgeel M, Gallagher PG. KLF1 E325K-associated Congenital Dyserythropoietic Anemia Type IV: Insights Into the Variable Clinical Severity. J Pediatr Hematol Oncol. 2018;40(6):e405-e9.

332. Nakano A, Harada T, Morikawa S, Kato Y. Expression of leukocyte common antigen (CD45) on various human leukemia/lymphoma cell lines. Acta Pathol Jpn. 1990;40(2):107-15.
333. Bohlson SS, Silva R, Fonseca MI, Tenner AJ. CD93 is rapidly shed from the surface of human myeloid cells and the soluble form is detected in human plasma. J Immunol. 2005;175(2):1239-47.
334. Pilling D, Fan T, Huang D, Kaul B, Gomer RH. Identification of markers that distinguish monocyte-derived fibrocytes from monocytes, macrophages, and fibroblasts. PLoS One. 2009;4(10):e7475.
335. Kristiansen M, Graversen JH, Jacobsen C, Sonne O, Hoffman HJ, Law SK, et al. Identification of the haemoglobin scavenger receptor. Nature. 2001;409(6817):198-201.
336. Backé E, Schwarting R, Gerdes J, Ernst M, Stein H. Ber-MAC3: new monoclonal antibody that defines human monocyte/macrophage differentiation antigen. J Clin Pathol. 1991;44(11):936-45.
337. Pulford K, Micklem K, McCarthy S, Cordell J, Jones M, Mason DY. A monocyte/macrophage antigen recognized by the four antibodies GHI/61, Ber-MAC3, Ki-M8 and SM4. Immunology. 1992;75(4):588-95.
338. Crocker PR, Gordon S. Properties and distribution of a lectin-like hemagglutinin differentially expressed by murine stromal tissue macrophages. J Exp Med. 1986;164(6):1862-75.
339. Ghosh Z, Wilson KD, Wu Y, Hu S, Quertermous T, Wu JC. Persistent donor cell gene expression among human induced pluripotent stem cells contributes to differences with human embryonic stem cells. PLoS One. 2010;5(2):e8975.
340. Hu S, Zhao MT, Jahanbani F, Shao NY, Lee WH, Chen H, et al. Effects of cellular origin on differentiation of human induced pluripotent stem cell-derived endothelial cells. JCI Insight. 2016;1(8).
341. Smith JR, Maguire S, Davis LA, Alexander M, Yang F, Chandran S, et al. Robust, persistent transgene expression in human embryonic stem cells is achieved with AAVS1-targeted integration. Stem Cells. 2008;26(2):496-504.
342. Alexopoulou AN, Couchman JR, Whiteford JR. The CMV early enhancer/chicken beta actin (CAG) promoter can be used to drive transgene expression during the differentiation of murine embryonic stem cells into vascular progenitors. BMC Cell Biol. 2008;9:2.
343. Lepper C, Fan CM. Generating tamoxifen-inducible Cre alleles to investigate myogenesis in mice. Methods Mol Biol. 2012;798:297-308.
344. Seime T, Kolind M, Mikulec K, Summers MA, Cantrill L, Little DG, et al. Inducible cell labeling and lineage tracking during fracture repair. Dev Growth Differ. 2015;57(1):10-23.
345. Berner D, Amrhein V. Why and how we should join the shift from significance testing to estimation. J Evol Biol. 2022;35(6):777-87.
346. Amrhein V, Greenland S, McShane B. Scientists rise up against statistical significance. Nature. 2019;567(7748):305-7.
347. Perkins A, Xu X, Higgs DR, Patrinos GP, Arnaud L, Bieker JJ, et al. Krüppeling erythropoiesis: an unexpected broad spectrum of human red blood cell disorders due to KLF1 variants. Blood. 2016;127(15):1856-62.

348. Sheng Q, Vickers K, Zhao S, Wang J, Samuels DC, Koues O, et al. Multi-perspective quality control of Illumina RNA sequencing data analysis. Brief Funct Genomics. 2017;16(4):194-204.
349. Schroeder A, Mueller O, Stocker S, Salowsky R, Leiber M, Gassmann M, et al. The RIN: an RNA integrity number for assigning integrity values to RNA measurements. BMC Mol Biol. 2006;7:3.
350. Lin X, Chang W, Wang Y, Tian M, Yu Z. SRPX2, an independent prognostic marker, promotes cell migration and invasion in hepatocellular carcinoma. Biomed Pharmacother. 2017;93:398-405.
351. Coffey RJ, Gangarosa LM, Damstrup L, Dempsey PJ. Basic actions of transforming growth factor-alpha and related peptides. Eur J Gastroenterol Hepatol. 1995;7(10):923-7.
352. Allard JB, Duan C. IGF-Binding Proteins: Why Do They Exist and Why Are There So Many? Front Endocrinol (Lausanne). 2018;9:117.
353. Petazzi P, Ventura T, Luongo FP, May A, Taylor HA, Romanò N, et al. Arterial cells support the development of human hematopoietic progenitors in vitro via secretion of IGFBP2. bioRxiv. 2022:2022.10.04.510611.
354. Shen F, Song C, Liu Y, Zhang J, Wei Song S. IGFBP2 promotes neural stem cell maintenance and proliferation differentially associated with glioblastoma subtypes. Brain Res. 2019;1704:174-86.
355. Kim HS, Lee WJ, Lee SW, Chae HW, Kim DH, Oh Y. Insulin-like growth factor binding protein-3 induces G1 cell cycle arrest with inhibition of cyclin-dependent kinase 2 and 4 in MCF-7 human breast cancer cells. Horm Metab Res. 2010;42(3):165-72.
356. Butt AJ, Dickson KA, McDougall F, Baxter RC. Insulin-like growth factor-binding protein-5 inhibits the growth of human breast cancer cells in vitro and in vivo. J Biol Chem. 2003;278(32):29676-85.
357. Zhang L, Lian R, Zhao J, Feng X, Ye R, Pan L, et al. IGFBP7 inhibits cell proliferation by suppressing AKT activity and cell cycle progression in thyroid carcinoma. Cell Biosci. 2019;9:44.
358. Wang Z, Qi Y, Wang R, Wu W, Li Z, Wang M, et al. IGFBP6 regulates vascular smooth muscle cell proliferation and morphology via cyclin E-CDK2. J Cell Physiol. 2020;235(12):9538-56.
359. Madtes DK, Raines EW, Sakariassen KS, Assoian RK, Sporn MB, Bell GI, et al. Induction of transforming growth factor-alpha in activated human alveolar macrophages. Cell. 1988;53(2):285-93.
360. Wagner CL, Ryan RM, Forsythe DE, Keenan A, Finkelstein JN. Secretion of transforming growth factor-alpha (TGF alpha) by postnatal rabbit alveolar macrophages. Pediatr Res. 1995;38(1):49-54.
361. Hayman MJ, Meyer S, Martin F, Steinlein P, Beug H. Self-renewal and differentiation of normal avian erythroid progenitor cells: regulatory roles of the TGF alpha/c-ErbB and SCF/c-kit receptors. Cell. 1993;74(1):157-69.
362. Gandrillon O, Schmidt U, Beug H, Samarut J. TGF-beta cooperates with TGF-alpha to induce the self-renewal of normal erythrocytic progenitors: evidence for an autocrine mechanism. Embo j. 1999;18(10):2764-81.

363. Schroeder C, Gibson L, Nordström C, Beug H. The estrogen receptor cooperates with the TGF alpha receptor (c-erbB) in regulation of chicken erythroid progenitor self-renewal. Embo j. 1993;12(3):951-60.
364. Yang C, Yokomori R, Chua LH, Tan SH, Tan DQ, Miharada K, et al. Mitochondria transfer mediates stress erythropoiesis by altering the bioenergetic profiles of early erythroblasts through CD47. J Exp Med. 2022;219(12).
365. Hough KP, Trevor JL, Strenkowski JG, Wang Y, Chacko BK, Tousif S, et al. Exosomal transfer of mitochondria from airway myeloid-derived regulatory cells to T cells. Redox Biol. 2018;18:54-64.
366. Pang Y, Zhang C, Gao J. Macrophages as Emerging Key Players in Mitochondrial Transfers. Front Cell Dev Biol. 2021;9:747377.
367. Ostrowski M, Carmo NB, Krumeich S, Fanget I, Raposo G, Savina A, et al. Rab27a and Rab27b control different steps of the exosome secretion pathway. Nat Cell Biol. 2010;12(1):19-30; sup pp 1-13.
368. Gomi H, Mori K, Itohara S, Izumi T. Rab27b is expressed in a wide range of exocytic cells and involved in the delivery of secretory granules near the plasma membrane. Mol Biol Cell. 2007;18(11):4377-86.
369. Carbone C, Piro G, Merz V, Simionato F, Santoro R, Zecchetto C, et al. Angiopoietin-Like Proteins in Angiogenesis, Inflammation and Cancer. Int J Mol Sci. 2018;19(2).
370. Xiao Y, Wei X, Jiang Z, Wang X, Ye W, Liu X, et al. Loss of Angiopoietin-like 7 diminishes the regeneration capacity of hematopoietic stem and progenitor cells. J Hematol Oncol. 8. England2015. p. 7.
371. Praveen K, Patel GC, Gurski L, Ayer AH, Persaud T, Still MD, et al. ANGPTL7, a therapeutic target for increased intraocular pressure and glaucoma. Commun Biol. 2022;5(1):1051.
372. Xu T, Xu L, Meng P, Ma X, Yang X, Zhou Y, et al. Angptl7 promotes insulin resistance and type 2 diabetes mellitus by multiple mechanisms including SOCS3-mediated IRS1 degradation. Faseb j. 2020;34(10):13548-60.